Modeling of the Heat Transfer in Cables Using Analogies to the Electrical Transmission Line Theory

by

M.Sc. Anika Henke

Dortmund, Germany, 10 March 2023

A Thesis Submitted to the

Faculty of Electrical Engineering and Information Technology
of the TU Dortmund University

in Partial Fulfillment of the Requirements for the Degree of

Doctor of Engineering (Dr.-Ing.)

Supervisor:	Prof. Dr.-Ing. Stephan Frei
External Examiner:	Prof. Dr. rer. nat. Ludwig Brabetz
	(University of Kassel)

Henke, Anika: Modeling of the Heat Transfer in Cables Using Analogies to the Electrical Transmission Line Theory
Genehmigte Dissertation zur Erlangung des akademischen Grades Doktor der Ingenieurwissenschaften (Dr.-Ing.) der Fakultät für Elektrotechnik und Informationstechnik der Technischen Universität Dortmund.
Hauptreferent: Prof. Dr.-Ing. Stephan Frei, Technische Universität Dortmund
Korreferent: Prof. Dr. rer. nat. Ludwig Brabetz, Universität Kassel
Ort und Tag der Einreichung: Dortmund, 14.09.2022
Ort und Tag der mündlichen Prüfung: Dortmund, 08.03.2023

Abstract

In this thesis, the adaption of models and methods known from the electrical **t**ransmission **l**ine (TL) theory to thermal heat transfer problems in cables is analyzed. Possibilities and limitations are presented.

Based on the consequent usage of analogies between electrical and thermal domains, a thermal analog to the electrical TL theory is derived for a single wire cable. The necessary assumptions and simplifications are discussed. For more complex cable arrangements, a general modeling approach is presented, which allows setting up an **e**quivalent **c**ircuit **d**iagram (ECD) and the corresponding system of **p**artial **d**ifferential **e**quations (PDEs) directly based on the physical cable properties. The electrical and thermal models are compared.

The PDEs are solved using different simplifications. At first, basic linear analytical solution approaches for constant excitations are calculated beginning with solutions of the PDEs for special cases (neglection of time and/or spatial dependence). In addition, for relevant cables (single wire cable, system consisting of axially combined single wire cables, two single wire cables, coaxial cable, N identical single wire cables, and a general form), analytical calculation approaches of the complete PDE or system of PDEs are given. Approaches for the consideration of time and spatial varying initial and boundary conditions and inhomogeneity are discussed. For the nonlinear parameter dependence, a fast converging fixed-point iteration is proposed.

The solutions are validated by comparison with measurement results (indirect temperature measurement based on resistance measurement and thermocouple temperature measurement) and numerical reference solutions. An approach for determining some cable parameters that are extremely difficult to be measured directly from the physical arrangement is presented, for example, the coupling conductance between the conductors of a twisted pair cable. Overall, very good accordance between numerically and analytically calculated temperatures is observed. For a cable bundle consisting of 33 cables, the general applicability of the presented methods to complex problems is shown.

The results are discussed with regard to the model and solution accuracy. In addition, the new models are compared to literature approaches for the single wire cable. For multiconductor arrangements, the influence of the bundle on the individual cable temperatures is discussed using the example of a twisted pair cable. Also, the influence of the assumption of a solid conductor in contrast to a stranded conductor is analyzed. Finally, as an application example, a protection strategy for a twisted pair cable for **p**ower **o**ver **d**ata **l**ine (PoDL) applications is developed based on the presented calculation approaches and implemented on a microcontroller. The setup is tested in a laboratory environment which shows the applicability of cable protection strategies directly based on the cable temperature.

Contents

List of Abbreviations

abbreviation	meaning
0 D	zero-**d**imensional
1 D	one-**d**imensional
2 D	two-**d**imensional
3 D	three-**d**imensional
AC	**a**lternating **c**urrent
BEM	**b**oundary **e**lement **m**ethod
const.	constant
DTS	**d**istributed **t**emperature **s**ensing
ECD	**e**quivalent **c**ircuit **d**iagram
e.g.	for example
FDM	**f**inite **d**ifference **m**ethod
FEM	**f**inite **e**lement **m**ethod
FVM	**f**inite **v**olume **m**ethod
HV	**h**igh **v**oltage
IEEE	**I**nstitute of **E**lectrical and **E**lectronics **E**ngineers
LV	**l**ow **v**oltage
MOL	**m**ethod **o**f **l**ines
ODE	**o**rdinary **d**ifferential **e**quation
PDE	**p**artial **d**ifferential **e**quation
PDU	**p**ower **d**istribution **u**nit
PoDL	**p**ower **o**ver **d**ata **l**ine
PVC	**p**oly**v**inyl **c**hloride
RMS	**r**oot **m**ean **s**quare
SMU	**s**ource **m**easurement **u**nit
TEM	**t**ransverse **e**lectro**m**agnetic
TL	**t**ransmission **l**ine

List of Mathematical Symbols

variable	meaning
a	abbreviation in formulas
A	parameter of the partial differential equation
$\mathcal{A}$	area
b	abbreviation in formulas
B	parameter of the partial differential equation
$\mathcal{B}$	magnetic flux density
c	specific heat capacity
C	parameter of the partial differential equation
$\mathcal{C}$	capacitance
cond	condition
d	diameter/distance
D	eigenvalue
$\mathcal{D}$	electric flux density
$\mathbf{D}$	diagonal matrix
e	constant, Euler's number
e	calculation effort
$\boldsymbol{e}$	unit vector
E	energy
$\mathcal{E}$	electric field strength
$\mathbf{E}$	transformation matrix
f	function (in general formulas)
F	abbreviation in solutions
g	gravitational acceleration
G	conductance
Gr	Grashof number
H	magnetic field strength
i	running index
I	electrical current
j	running index
J	current density
k	correction factor
K	number of nodes
l	segment length
L	inductance

variable	meaning
$\mathcal{L}$	cable length
l_α	characteristic length
m	node
n	running index, abbreviation in solutions
$\boldsymbol{n}$	normal vector
N	number of conductors
$\mathcal{N}$	number of particles
Nu	Nusselt number
p	pressure
P	heat flow
Pr	Prandtl number
q	charge
Q	heat
r	radius
R	resistance
Ra	Rayleigh number
res	residual
RMS	root mean square value
s	Laplace variable
t	time
T	temperature
T_0	initial cable temperature
T_1, T_2	cable termination temperature
u	variable for general formulas, basis function in FEM
U	voltage
$\mathbf{U}$	identity matrix
$\boldsymbol{v}$	eigenvector
V	volume
w	weight
W	abbreviation in solutions
$\mathcal{W}$	work
x	abbreviation in solutions
X	abbreviation in solutions
z	coordinate in space
α	heat transfer coefficient
β	angle

variable	meaning
$\Gamma(\cdot)$	Heaviside step function
$\delta(\cdot)$	Dirac delta distribution
Δ	difference, uncertainty
ϵ	permittivity
ε	emissivity
η_T	linear temperature coefficient for the conductor's conductivity
θ	abbreviation in solutions
κ	integration constant
λ	conductivity
Λ	abbreviation in solutions
μ	magnetic permeability
ν	kinematic viscosity
ξ	chemical potential
π	circular ratio
ρ	mass density
σ	Stefan-Boltzmann constant
τ	window width
ϕ	scalar potential
$\mathbf{\Phi}$	state-transition matrix
φ	coordinate (cylindrical coordinates)
χ	decision variable
$\dot{\omega}$	(external) heat source density

notation	meaning
X	scalar
$\boldsymbol{X}$	vector
$\mathbf{X}$	matrix

operator	meaning
$(\cdot)'$	per unit length quantity / spatial derivative
$\dot{(\cdot)}$	time derivative
$\mathrm{d}\cdot$	differential
$\mathrm{div}(\cdot)$	divergence
$\mathrm{grad}(\cdot)$	gradient
$\mathrm{rot}(\cdot)$	rotation
$\partial\cdot$	partial differential
$\delta\cdot$	inexact differential

subscript	meaning
1 it	one **it**eration
abs	**abs**olute
air	**air**
app	**app**roximate
b	**b**efore
bc	**b**oundary **c**ondition
c	**c**onductor
char	**char**acteristic
co	**co**axial cable
cond	**cond**uctor
conv	**conv**ection
corr	**corr**ected
coup	**coup**ling
crit	**crit**ical
e	**e**nvironment
eff	**eff**ective
el	**el**ectrical
em	**em**ergency
end	**end**
f	**f**illing
fi	**fi**eld
flat	**flat** area at the cable center
G	**G**reen's functions time domain
geom	**geom**etrical
GL	**G**reen's functions **L**aplace domain
hom	**hom**ogeneous
hys	**hys**teresis
i	**i**nsulation
ic	**i**nitial **c**ondition
id	**id**entical
ii	**i**nner **i**nsulation
in	**in**ner
inh	**inh**omogeneity
insu	**insu**lation
it	**it**erative
K	**K**elvin
l	**l**inear

subscript	meaning
last	**last**
lim	**lim**it
lo	**lo**ng
La	**L**aplace transform and **a**pproximation
m	**m**ean
max	**max**imum
meas	**meas**urement
mid	**mid**dle
no	**no**rmal
node	**node**
num	**num**erical
oi	**o**uter **i**nsulation
out	**out**er
part	**part**iculate
plot	**plot**
preset	**preset**
r	**r**adial
rad	**rad**iation
rect	**rect**angular
ref	**ref**erence
rel	**rel**ative
rs	**r**adial **s**teady state
rt	**r**adial **t**ransient
s	**s**urface
semi	**semi**-infinite
sh	**sh**ield
she	**she**ath
simp	**simp**lified
strand	**strand**
stst	axial **st**eady **st**ate
sw	**s**ingle **w**ire cable
t	**t**otal
tc	**t**hermo**c**ouple
tsw	**t**wo **s**ingle **w**ire cables
v	**v**ariant
vo	**vo**ltage
w/o it	**w**ith**o**ut **it**eration

List of Figures

List of Tables

1 Introduction

The technical development of electrical and electronic components is proceeding at a rapid pace. More powerful and at the same time smaller components are taking on more complex functions. These also include safety-relevant features that lead to new demands concerning reliability - safety-relevant functions should not simply be switched off in critical cases because this can result in potentially dangerous situations for the end user. Overall, these developments lead to new challenges and requirements concerning diagnosis functions as well as architectures [1]. In this context, heat generation and dissipation play an important role. In addition to the individual functional elements, the consideration of the interconnecting conductor structures is gaining importance due to the increasing power levels. The thermal behavior must therefore always be taken into account when cables, busbars, or conductor traces that are used to supply individual functions are dimensioned [2].

In this thesis, the focus is put on cables. During operation, the cable has to be protected from damage to the temperature-sensitive insulation and, in the worst case, a cable fire. Classically, melting fuses are used for this safety-relevant purpose. Those cannot fulfill the ever-rising requirements of flexibility and their tripping behavior only partly depends on the relevant cable temperature. That is why electronic fuses are developed, that consist of a (software) controlled switch and therefore allow very flexible switching strategies. As the temperature of the cable that has to be protected is the relevant parameter, strategies for continuous cable temperature monitoring are necessary. For high power transmission cables, various approaches for online temperature monitoring already exist. One example of such an approach is **d**istributed **t**emperature **s**ensing (DTS) [3], where the response of a thin optical fiber to laser pulses is analyzed. Overall, this procedure is quite complex, so it is only economical for special applications (especially very long, large and expensive cables such as submarine cables).

In practice, however, thinner and shorter cables are often used and the cost pressure on cable systems is high. Simple single cables are necessary for various application fields to supply a wide range of elements. In some cases, shielded single (coaxial) or multiconductor cables are also used to reduce interference emissions. Twisted pair cables are applied, for example, to supply low-power consumers via communication lines (**p**ower **o**ver **d**ata **l**ine, PoDL, [4]). Systems constructed from three identical cables are particularly used for power supply. In general, conductor bundles of any complexity can appear, for example, in the main wiring harness of vehicles.

For all these applications of comparatively thin and short cables, thermal considerations play an increasing role. Direct temperature measurements are too complex and expensive. Thus, indirect model-based approaches based on current measurements are necessary. Until now, in addition to the application of elaborate measurements, the thermal behavior of

those cables has been described almost exclusively by numerical approaches, primarily **f**inite **e**lement **m**ethods (FEMs) [2]. However, since these numerical calculation approaches are associated with a high effort (in form of computing capacity and runtime), these approaches are usually not real-time capable. The aim of this thesis is therefore to determine analytical calculation rules for the current-based cable temperature estimation for selected, particularly relevant conductor arrangements.

In chapter 2, an overview of different cable protection approaches is given with a focus on automotive applications. Besides classical (melting) fuses, also approaches based on controlled switches are shown. A current-based and a temperature-based decision are discussed and the different protection strategies are compared. In the next step, an overview of the theoretical basics and the state of the art concerning thermal effects on cables is briefly summarized in chapter 3. In addition, electrical effects on cables are presented in the form of the electrical **t**ransmission **l**ine (TL) theory.

In chapter 4, the basic modeling approach that is used in this thesis for the thermal cable models is introduced, which is the usage of analogies between electrical and thermal domains. This is followed by the development of a thermal analog to the electrical TL theory, i.e., a kind of thermal TL theory in chapter 5. After preliminary considerations concerning the general similarities and differences between the electrical and thermal domain, formulations for a single wire cable and more complex cable arrangements are derived. The electrical and thermal TL models are critically compared.

The resulting system of nonlinear **p**artial **d**ifferential **e**quations (PDEs) cannot directly be solved analytically. That is why in chapter 6, at first analytical solutions for the linearized PDE system with constant excitations are derived, mostly based on the solution approaches known from the electrical domain as the solution in the Laplace domain or Green's function approaches. Solutions for a single wire cable, a system of axially connected single wire cables, two single wire cables, a coaxial cable, N identical single wire cables, and a general solution approach are described. In the next step, approaches for the consideration of time and spatial varying initial and boundary conditions and inhomogeneity as well as the nonlinear parameter dependence are discussed. The calculation approaches are validated in chapter 7 using measurements and numerical reference solutions.

The results are analyzed in chapter 8: The model and solution accuracies are discussed and the new models are compared to previous literature approaches. Typical simplifying assumptions such as the neglect of cable bundles or branded conductors are evaluated. In addition, an application example is shown: A protection strategy for a twisted pair cable is developed, implemented on a simple microcontroller, and tested to show the practical applicability of the approaches. This thesis concludes with a summary.

2 Cable Protection

Overload scenarios can lead to critical situations in electrical circuits, which on the one hand can endanger users, but on the other hand potentially damage or destroy sensitive components. For more than a century [5, p. 2], protection strategies have therefore been used to minimize the risks for people and components. Various approaches have been developed for this purpose. In this thesis, the focus is put on cable protection.

2.1 Overview

When an electric current flows through a cable, the finite conductivity of the conductor material causes electrical power losses. These losses are converted into heat, which heats the cable. The insulation material reacts more sensitively to temperature increases than the inner (metal) conductor: When the insulation material heats up, initially its aging process is massively accelerated. Further heating can also lead to (plastic) deformation and, in the worst case, to a cable fire. These undesirable consequences of an excessively high insulation temperature have to be avoided. The cables must therefore be protected from overcurrent-induced overtemperatures. If only the cable heating due to the ohmic losses plays a role and the environment cools the cable, the hottest point of the insulation is found at the transition between the inner conductor and the insulation. Accordingly, the inner conductor temperature is relevant for the insulation status.

The most popular and widespread devices concerning cable protection are (melting) fuses [5, p. 1], in which a wire melts during overload operation and thus interrupts the circuit, and circuit breakers, which interrupt the circuit by the thermally induced deformation of a bimetal [6]. For more specialized applications, also many other protection devices were developed in the past, which include, for example, resettable fuses [5, 6]. Those typically consist of positive temperature coefficient devices (for example polymers [7, 8] or ceramic materials [6]) that show a very large resistance in case of an overcurrent, thus limiting the current flow [5, p. 15]. Permanent power fuses, or sodium fuses, use the phase transition of sodium from solid to plasma to dramatically increase the resistance in case of a fault [9, 10]. Electronically controlled systems represent another group of protection devices, in which, for example, a tripping decision is made based on a current or temperature estimation and the circuit is interrupted using some kind of switch (e.g., field effect transistor or relay) [5, 6].

Overall, many possible protection methods and elements exist for different applications and a complete overview would be beyond the scope of this thesis. Therefore, exemplarily, the development of cable protection strategies for application in automotive vehicles from (melting) fuses to modern flexible strategies is motivated in the following.

2.2 Melting Fuses

Melting fuses, or shortly fuses, are widely used in many applications. The worldwide production was estimated to be over 10 billion fuses annually in 2004 [5, p. 16]. The history of fuses goes back to the 19th century [5, p. 2]. According to [11], the first design specifications for fuses were patented by Thomas Edison in 1881. The basic principle has remained the same throughout this time: A comparatively short (and thus inexpensive) piece of wire is sacrificed in case of an overload to protect the rest of the circuit from damage [5, p. 1]. Thus, the geometrical and/or physical properties of this short piece must differ from those of the rest of the circuit in such a way that a predetermined breaking point is created here, which is destroyed by an overload before the other elements suffer serious damage. Usually, this is ensured by a comparatively thin wire made of a material with a low melting temperature.

Basically, a melting fuse behaves like a controlled resistor (see figure 2.1): Before tripping, the (time-dependent) resistance $R(t)$ is comparatively low, after tripping, the resistance is very high. The exact triggering time of the melting fuse is influenced by the temperature of the melting wire. In addition to the geometrical and physical fuse properties and the current, this depends in particular on the ambient conditions such as the ambient temperature or the type of installation. Overall, there is a complex dependence on the load current I, but also on many other influencing variables such as the ambient temperature T_e, the initial temperature T_0, or the connected cables.

The tripping behavior can be realized by different types of melting fuses. Those are subdivided into three categories [5, p. 11]. **H**igh **v**oltage (HV) fuses and **l**ow **v**oltage (LV) fuses differ in terms of voltage (limit $1000\,\mathrm{V}$ **a**lternating **c**urrent (AC)). The third category, miniature fuses, is primarily determined by the geometrical dimensions. Typical automotive fuses belong to this category. Fuses can also be classified in terms of their spatial structure into enclosed fuses and semi-enclosed fuses [5, p. 11]. Thermal models for different fuse types can be found for example in [12–18].

Fuses play a major role in automotive applications. Already in 2004, each vehicle was equipped with 30 to 75 fuses, depending on the price category [5, p. 134]. Due to increasing automation and electrification in the vehicle, the number of consumers, the complexity

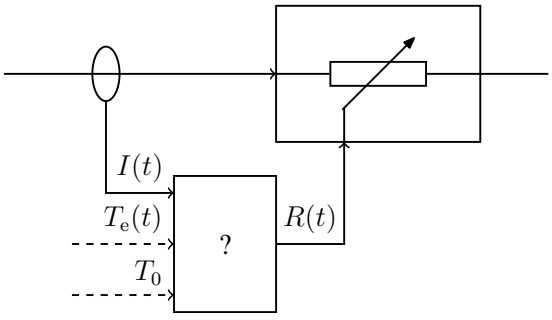

Figure 2.1: Function of a melting fuse as a controlled resistor.

of the wiring harness, and thus the number of elements to be protected from overcurrents continues to increase [19]. At the end of the 1970s, blade-type fuses (see, for example, [20]) were developed primarily for use in automobiles [5, pp. 134-137], which quickly became established and today represent the typical fuse form in automotive vehicles. They are used to protect circuits with rated currents of up to 100 A, typically with voltages of up to 32 V.

The design process for cable and fuse is now briefly outlined. Current-time characteristics as given in figure 2.2 are used to illustrate the typical behavior of the individual elements (see e.g. [6, 20]): In the normal load characteristic, the typical time is shown that a certain current flows in normal operation. For a fuse, the characteristic shows, depending on the load current, after what time the fuse operates. For a cable, the characteristic typically indicates the time a given constant current has to flow to heat up the cable to a certain temperature. First of all, the basis is the supplied load. Based on its current-time characteristic (yellow curve in figure 2.2) a fuse is designed which can permanently tolerate the standard load. The tripping characteristic of this fuse (green curve in figure 2.2) then indicates the time the wire needs to melt as a function of the current and is typically chosen to be higher than the load characteristic by a factor of 1.25 to two [5, pp. 141-142]. The cable, which is used for supply and has to be protected against overtemperatures, must have a destruction characteristic (blue curve in figure 2.2) that is even higher to ensure that the fuse breaks the circuit before the cable suffers irreversible damage. Typically, the cable and fuse show a comparable behavior regarding low overcurrents, but at high overcurrents, the fuse (which is thin compared to the cable) reacts much faster than the cable [21]. So, there can be significant distances between the characteristic curves (red area in figure 2.2).

Fuses are widely used, established, and trusted. In [22], a list of advantages for LV fuses is given, many of which also apply to HV fuses and miniature fuses [5, p. 140]. Among them are the following advantages: Generally, no complicated short-circuit calculations are required for the use. Fuses are simple, reliable, and overall inexpensive components. Because they cannot be reset, the user is encouraged to take a closer look at the problem that caused

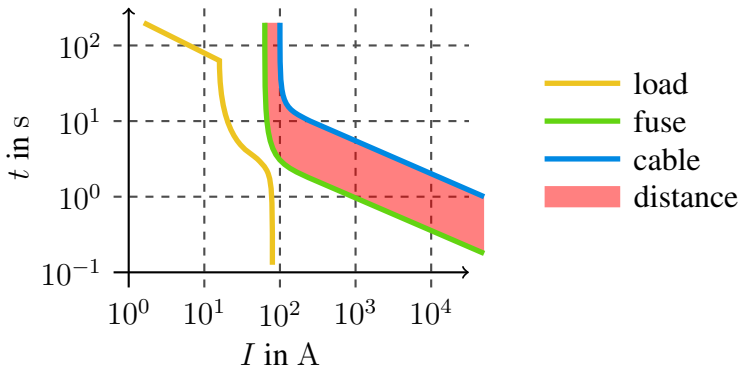

Figure 2.2: Characteristics of load, melting fuse, and cable.

the overload to identify and correct the fault. Fuses reliably switch off even high currents and minimize supply voltage drops because of the short tripping times.

There are also some disadvantages associated with fuses. Using melting fuses implicitly assumes homogeneous cables and cable environments, so variations along the cables cannot be considered. The real cable temperature is not known in this approach. Fuse and cable ideally are exposed to the same environmental and initial conditions, nevertheless, both react differently to them, so the influence of those conditions on the real cable temperature is only partly considered in the triggering decision. Safety distances must be included: The minimum fusing current always has to be lower than the current that the cables and other elements can tolerate. Conversely, cables need to be selected that withstand, for example, a $50\,\%$ higher continuous current than the fuse rating (if the fusing factor is 1.5), which increases the cable price and weight. In addition, depending on the chosen fuse, different cables are necessary [5, p. 153], so the fusing strategy must already be known in detail when selecting the cable. This reduces the flexibility of the entire wiring system. In addition, the fuse must be replaced after operating (reset is not possible), so all fuses have to be placed in easily accessible locations in the wiring system, which further limits the possible arrangements. Overall, fuses are very unflexible as the switching behavior of an installed fuse cannot be adapted. Many fuses do not allow full-range protection over the entire current range [5, p. 142]. Also, there are critical cases and current loads in which the fuse has not tripped but plastic deformation has already occurred [5, p. 141]. Then, when a new load is applied, the fusing behavior is unspecified and it usually operates much earlier than expected. These critical cases form a narrow band in the current-time diagram, which should be avoided if possible. Another critical aspect regarding the characteristic curves for fuses is that they do not depend on the fuse alone, but for comparatively small overcurrents also on the ambient conditions and the connected cables [5, p. 33]. The specification of “the” fuse characteristic for a specific fuse is therefore not possible. So, again, safety margins are inevitably necessary. Quantifying these precisely is not trivial, so usually, significantly over-dimensioned designs are the result. Because of these disadvantages, other protection strategies are developed. An overview of advantages and disadvantages in comparison with the other protection strategies presented in the following is given in table 2.1.

2.3 Controlled Switches

In the case of fuses, a large safety margin is required between the tripping characteristic of the fuse and the cable characteristic due to the different behaviors of fuses and cables, resulting in over-dimensioned cables and unusable cable reserves. Smart fuse protection strategies allow better adaption of the tripping characteristic to the actual physical conditions. In principle, a software-controlled switch is used for disconnecting the circuit [23], whereby a wide variety of approaches can be considered for the specific implementation of the tripping rule.

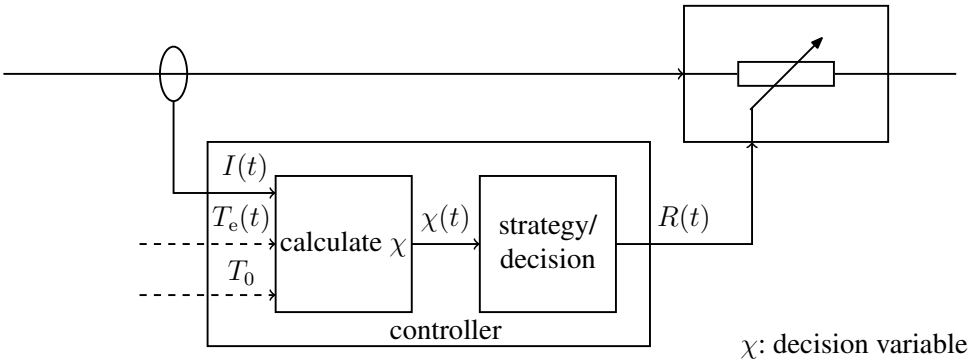

Figure 2.3: Function of a controlled switch as a controlled resistor.

The underlying setup is shown in figure 2.3: The input variables serve as the basis for the decision. Those typically include the time-dependent measured current $I(t)$ and can be supplemented by other variables such as the ambient temperature T_e or the initial temperature T_0. From these input variables, the development of the decision variable χ is first calculated in a controller. Based on this decision variable, the tripping decision is then made and the current is switched, which can be understood as equivalent to the control of a variable resistor. In contrast to the simple (melting) fuse (see figure 2.1), the entire decision process in the controller is freely programmable and thus much more flexible. Resetting or switching on is also possible.

The time-depending input variables have to be measured. On the one hand, more information enables a more precise assessment of the cable situation and thus a more accurate switching behavior, on the other hand, it also causes an increased measurement effort. A compromise must therefore be found between these two effects: The overall goal is to enable a safe decision with as little (measurement) effort as possible. Compared to the melting fuse, more different components are now involved in the decision-making process. Each of these components can fail and thus cause the failure of the protection strategy so the overall failure probability increases.

In the general approach, the decision variable is not specified in detail - a wide variety of variables can be chosen here. Two prominent approaches are presented below.

2.3.1 Current-Based Decision

One possibility is to directly use the cable characteristic. In this current-time characteristic, the permissible load duration of the cable until the selected maximum temperature is reached is given as a function of the electrical current. When determining these curves, the axial heat flow is neglected, i.e. long cables are assumed. In addition, a constant current pulse, as well as an initially cold cable, are assumed and the ambient temperature is set to a fixed value.

In practically relevant applications, single constant current pulses only rarely occur. Nevertheless, the current-time characteristics that are usually given by the manufacturer are often

used for cable protection. To relate continuous transient currents with the cable characteristics, moving **r**oot **m**ean **s**quare (RMS) windows are therefore used [24, A.1].

The procedure is as follows: First, a point (I, τ) is chosen on the current-time characteristic. Then, at each time t, the question is whether an unacceptably high load (i.e., greater than I) has occurred in the time window of width τ ending at time t. Therefore, the RMS value

$$\mathrm{RMS}_\tau(t) = \sqrt{\frac{1}{\tau}\int_{t-\tau}^{t} I^2(\tilde{t})\,\mathrm{d}\tilde{t}} = \chi(t) \tag{2.1}$$

for the window of width τ is used as decision variable $\chi(t)$ and compared with the allowed value from the characteristic I. The RMS value is continuously updated during operation. In total, such a dynamic approach is carried out in parallel for different points on the characteristic curve (typically between six and ten points) to reproduce the entire bandwidth of the characteristic curve as far as possible. Overall, the decision variables are here the RMS values that are continuously calculated from the measured current and compared to the maximum permissible values for the switching decision (see figure 2.4).

However, problems can also arise with this approach. These are discussed in the following.

By selecting specific points on the characteristic curve, it is reproduced in discretized form. In the next step, the RMS values for window widths between the explicitly selected and considered widths are analyzed. For this purpose, it is first assumed that two window widths τ_1 and τ_2 were selected for the fuse protection and that the permissible limit values I_1 and I_2 are not exceeded by the associated RMS values for a current waveform not defined in more detail. Mathematically this means for all $\hat{t} \leq t$:

$$\mathrm{RMS}_{\tau_1}(\hat{t}) = \sqrt{\frac{1}{\tau_1}\int_{\hat{t}-\tau_1}^{\hat{t}} I^2(\tilde{t})\,\mathrm{d}\tilde{t}} \leq I_1, \quad \mathrm{RMS}_{\tau_2}(\hat{t}) = \sqrt{\frac{1}{\tau_2}\int_{\hat{t}-\tau_2}^{\hat{t}} I^2(\tilde{t})\,\mathrm{d}\tilde{t}} \leq I_2. \tag{2.2}$$

Without a restriction of generality, $I_1 \geq I_2$ and $\tau_1 \leq \tau \leq \tau_2$ are assumed. Then, the following worst-case estimation holds for the RMS for window width τ:

$$\mathrm{RMS}_\tau(t) \leq \sqrt{\frac{1}{\tau}\left[\tau_2 I_2^2 - \int_{t-\tau_2}^{t-\tau} I^2(\tilde{t})\,\mathrm{d}\tilde{t}\right]} \leq \sqrt{\frac{\tau_2}{\tau}} I_2. \tag{2.3}$$

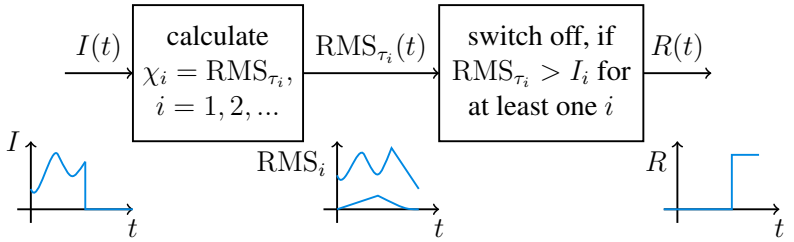

Figure 2.4: Controller function for a current-based switching decision using RMS values.

Explicitly, no statement of form $\mathrm{RMS}_\tau(t) \leq I_1$ is possible, so an estimation against the smaller of the two considered windows is not directly possible.

Based on this approach, using a given cable characteristic, windows can be chosen left of the characteristic which ensures that for all possible current developments, the moving RMS value does not exceed the characteristic. The area with high currents for short times is uncritical here, as there, the worst case and the characteristic show the same behavior. Heat conduction and all kind of interaction with the environment do not play any role in this adiabatic case. Unlike, for comparatively low overcurrents, critical cases can occur.

Due to the worst case, higher values can appear for longer windows than for short windows. An example of such a problematic case is shown in the following. The current-time characteristic for a $6\,\mathrm{mm}^2$ cable with the initial and ambient temperature of $60\,^\circ\mathrm{C}$ and the maximum permissible temperature of $105\,^\circ\mathrm{C}$ (black curve in figure 2.5) is analyzed. The green and black points of this characteristic curve are now used for protection. The worst-case curve between the selected window widths is given. The current development shown in figure 2.6 is assumed: Three single, comparatively high pulses occur. In figure 2.6, the time evolution of some of the selected windows is shown together with the maximum allowed values (green). At all these windows, the allowed values are not exceeded. Also, the development of the maximum occurring RMS values as a function of the window width is shown continuously in yellow in figure 2.5. It can be seen that in some cases the permissible values are exceeded in the areas between the windows for protection, which would not be noticed by the protection strategy. An example of a particularly critical window width is shown in yellow in figures 2.5 and 2.6. There, an RMS value is reached that is about $7.5\,\mathrm{A}$ above the allowable current value for this window.

In addition to the RMS values for different window widths, the actual temperature development is also calculated (see figure 2.6, blue). It can be seen that the first pulse raises the temperature close to the permissible limit, as also expected based on the RMS value for the window width of $55\,\mathrm{s}$. Between the pulses, the cable cools down again, yet the starting temperature at the beginning of the second pulse is already $80\,^\circ\mathrm{C}$ so the characteristic curve can actually no longer be applied. Thus, within the second pulse, the permissible temperature of $105\,^\circ\mathrm{C}$ is exceeded.

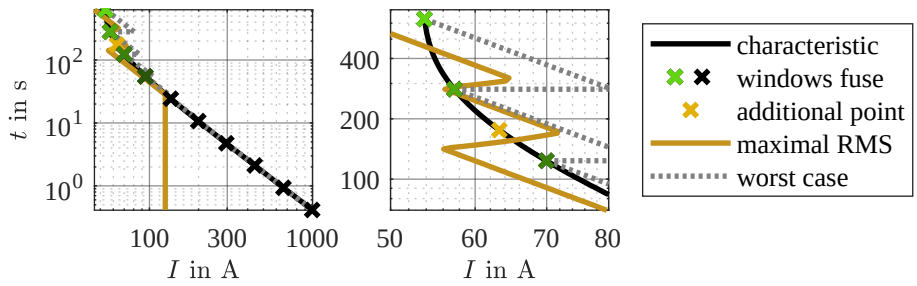

Figure 2.5: Cable characteristic and chosen windows for an exemplary protection strategy.

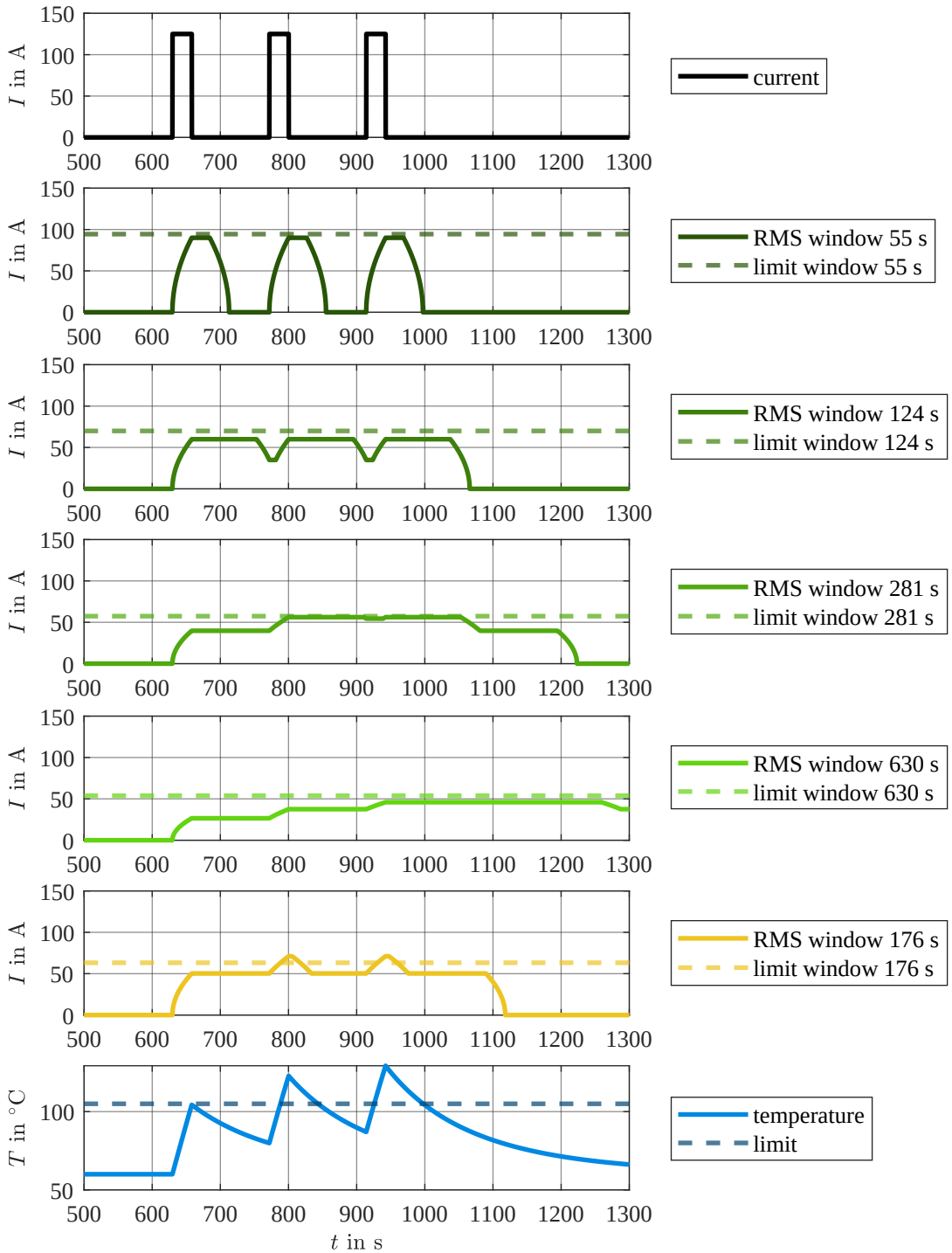

Figure 2.6: Exemplary critical load current that leads to an overheating cable but is not detected by the protection strategy.

Here another problem of the described approach becomes apparent: The given characteristic curve is based on the assumption of a starting temperature of $60\,^{\circ}\mathrm{C}$ and therefore cannot be used already for the second pulse. However, the actual cable temperature is not known in this approach. It could be continuously measured in parallel, but due to the high effort of this approach, it is not practically relevant. Worst-case assumptions would be necessary, but the question arises of which cable temperature should be used: After all, during operation, temperatures can occur right up to the permissible limit temperature, so this would represent the formal worst case. However, the specification of a characteristic curve for heating starting at the maximum permissible temperature up to the same temperature is not reasonable. Thus, the initial conditions are not sufficiently continuously considered in this approach. To be able to track the initial temperature and thus the characteristic curve, a temperature monitoring system running in parallel would be necessary. However, if the actual cable temperature is known, it is also possible to trigger directly on this basis and the entire RMS approach is no longer needed. For the ambient temperature, worst-case assumptions or additional measurements are also necessary for the selection of the characteristic curve. Implicitly, constant values are assumed by choosing a characteristic curve here. Nevertheless, the possibility of choosing an appropriate cable characteristic allows more flexible strategies than the simple melting fuse.

With the use of controlled switches, controlled overload and switching on is possible. Nevertheless, because of the unknown cable temperature in the RMS-based approach, both of those functions cannot be used directly based on the physical cable status but can only be implemented based on assumptions or rough approximations.

In principle, the discretization of the current sampling can also lead to further problems. Maxima of the RMS values can thus possibly no longer be resolved. However, this problem also occurs in other protection strategies, so it is assumed here and in the following that the actual current waveform is known with sufficient accuracy not to cause any additional problems.

A very relevant question is to what extent the RMS value is at all directly related to the evolving conductor temperature. The underlying idea here is that the squared current influences the injected power and therefore the RMS value corresponds to the temperature. However, nonlinear effects are not taken into account: In particular, the heat dissipation from the cable surface to the environment is highly nonlinear. In the literature, therefore, the actual exponent for the current influence on the temperature is given overall between 1.5 and 2 (depending on the emissivity of the surface) [25] or between 1.5 and 1.85 [26]. Various factors influence this behavior. Therefore, the pure RMS value does not reproduce the occurring effects well enough and is thus not always suitable for a sufficiently accurate estimation of the conductor temperature.

Overall, some difficulties arise in the application of this algorithm. Therefore, cables are

usually significantly oversized in practice and switched off far before reaching critical temperatures, so reserves can often not be utilized. Many windows and/or significant cable reserves have to be taken into account. The necessary reserves vary depending on the selected window width. Good protection strategies can only be found for the special case where ambient and initial temperatures are constant and only individual current pulses occur between which the cable cools down completely. All conditions that differ from these strict assumptions can lead to significant problems.

2.3.2 Temperature-Based Decision

The two previous approaches had in common that the actual cable temperature was not known and therefore could not be taken into account. Based on this, various difficulties arose. To avoid these, the cable temperature T itself is required as decision variable χ and therefore has to be continuously monitored. In the ideal case, both the time and spatial temperature development along the complete cable are known.

On the one hand, this can be achieved via measurement. For example, the DTS [3] can be applied: Here, a thin optical fiber is placed directly in the cable, and the response of this fiber to laser pulses is analyzed, so the conductor temperature can be determined with a spatial and temporal resolution. This procedure needs a rather complex technique for measuring and processing the recorded data. Typical resolutions are in the range of meters, but special techniques also allow higher spatial resolutions for shorter cables (e.g. [27, 28]). The optical fiber itself should not relevantly distort the measured temperature curve, so this method is only partly suitable for thin cables. Because of the complexity of this procedure, it is only economical if the optical fiber is laid directly with the cable and very long, large, and expensive cables (e.g. underground cables or submarine cables) are to be monitored.

Alternatively, the cable temperature can be calculated using appropriate thermal cable models. Typically, based on the current measurement (and possible additional inputs) the time-dependent temperature development is calculated. Then, the current can be switched off if the maximum permissible temperature T_{lim} is exceeded and switched on again if the cable temperature falls below the lower temperature T_{hys}, thus using hysteresis to avoid permanent

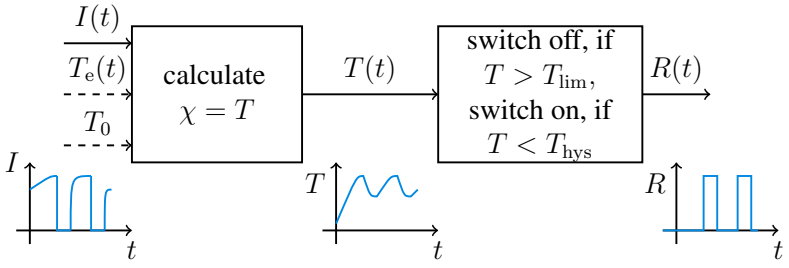

Figure 2.7: Controller function for a temperature-based switching decision using thermal cable models.

switching. An overview of this approach is given in figure 2.7. On the one hand, appropriate models must describe the physical conditions reliably and with sufficient accuracy, but on the other hand, they must not become too complex to remain competitive compared to the very cheap fuse protection. This thesis aims to contribute to such protection strategies in the form of simple (therefore analytical) models for cable temperature calculation.

2.4 Comparison of Different Protection Strategies

Finally, in table 2.1, the properties of the presented protection approaches (melting fuse, controlled switch with RMS-based and temperature-based decision) are directly compared to highlight the advantages of controlled switches with temperature-based protection strategies.

In the first two approaches, the cable temperature is not known: The melting fuse is chosen to fit the thermal behavior of the cable, but cannot reproduce its behavior under varying conditions or give any information about the real cable temperature. Therefore, high safety margins are necessary. With the RMS-based approach, the aim is to know whether the maximum permissible cable temperature is exceeded or not – but the real cable temperature is not known in detail, which causes again safety margins. The three approaches also differ in terms of their consideration of the environmental temperature, the initial cable temperature, and earlier loads. Using the melting fuse, this is partly considered as the fuse is on the one hand exposed to the same conditions and loads, but on the other hand, reacts differently than the cable. In the RMS-based approach, the consideration of the environmental temperature is possible via measurement, although implicitly a constant environmental temperature is assumed when choosing a cable characteristic. Nevertheless, slow changes in the environmental temperature can be considered by choosing the appropriate characteristic. For the initial characteristic choice, an initial cable temperature is necessary, which has to be measured or assumed. The continuous update of this initial temperature for the choice of the appropriate characteristic for each window is highly problematic in this approach, as the cable temperature is unknown. Using the thermal cable model, again, via measurement the environmental temperature can be determined and used as input for the calculation. An initial cable temperature has to be known as in the previous case but then, at each moment the temperature calculation is performed based on the earlier results which directly allows the consideration of earlier loads. In addition, also spatial varying temperatures can be taken into account by appropriate models, which is not supported for the melting fuse and the RMS-based approach. In contrast to the other two approaches, also the safety margin can be reduced. Overall, the usage of a thermal cable model directly provides the temperature information, so in this case, thinner cables can be chosen, which reduces the cable weight.

A melting fuse cannot be switched on again but has to be replaced after operating once. Therefore, it has to be placed at a well-accessible fuse box in the final setup, which limits possible boardnet architectures. Also, controlled overload is not possible and the switching

strategy cannot be influenced after the installation of the fuse. Unlike, the controlled switches can flexibly change their strategy during operation, be switched off later to allow controlled overload, or be switched on again, although in the case of the RMS-based approach this procedure has to be predetermined without knowledge of the cable temperature, so it is uncontrolled to some extend. As the switch does not have to be replaced after an operation, no central and accessible fuse box is necessary any longer, which allows new architectures of the overall boardnet. All in all, the melting fuse is very unflexible in comparison with the other two alternatives.

A melting fuse is a very simple protection device that can directly be integrated into the circuit. Therefore, only this single element is necessary for protection without additional supply or calculation, which is why high reliability is achieved. Unlike, the usage of controlled switches causes calculation effort (which also goes ahead with a necessary power supply), implementation effort, and memory requirements depending on the chosen algorithm. Each of the involved elements or steps can fail and therefore, result in reduced reliability. A higher effort has to be put into the implementation.

Table 2.1: Comparison between different cable protection strategies.

	(melting) fuse	controlled switch (RMS)	controlled switch (thermal model)
cable temperature	unknown	unknown	known
consideration of environmental temperature	partly	possible (not continuous)	possible
initial cable temperature	partly	has to be known	has to be known
consideration of earlier loads	partly	highly problematic	possible
consideration of spatial temperature distribution	not possible	not possible	possible
cable weight	high	medium	low
safety margin	**high**	**high**	**low**
reset/switch-on	not possible	possible (partly controlled)	possible
controlled overload	not possible	possible (partly controlled)	possible
fuse positions	well accessible	flexible	flexible
flexibility	**low**	**partly**	**high**
implementation effort	none	low	high
calculation effort	none	low	medium/high
memory requirements	none	medium/high	medium
reliability	very good	medium	medium
effort	**low**	**high**	**high**

3 Fundamentals of Thermal and Electrical Effects on Transmission Lines

In this chapter, the fundamentals of thermal and electrical effects on TLs are discussed. Some considerations of this chapter were already published in [A.2].

3.1 Thermal Effects on Transmission Lines

Thermal issues for a wide variety of structures and elements play an important role in many different disciplines. The focus of this thesis is on the thermal modeling of current-carrying cables. Also in this field, many modeling approaches were developed and many investigations were performed. For example, a large number of dissertations (e.g., [2, 29–39]) already dealt with this topic. Numerous publications, review papers, and basic literature (e.g., [40–45]) have presented and systematized the diverse investigations. Selected methods have also been standardized (e.g., [46–52]) and, accordingly, are widely used commercially. An overview of the historical development of thermal cable modeling can be found in [53]. Many important approaches and developments are addressed there. Due to the long development of thermal cable models (first considerations go back to the 19th century [53]) and the resulting number of investigations (a search of the database of the **I**nstitute of **E**lectrical and **E**lectronics **E**ngineers, IEEE, with the keyword “thermal cable model” returns more than 1200 entries), an overview of all approaches cannot be given in the following. Instead, a classification according to different criteria is suggested for already existing approaches. The mentioned sources in each case are meant as examples and do not claim to be complete.

3.1.1 Heat Flow Directions

Many round cables can be considered cylindrical structures. Therefore, cylindrical coordinates are appropriate, as shown in figure 3.1. Two prominent transport directions for the heat can be distinguished, the current flow direction (z-direction, axial) and the directions in the plane transverse to the current flow, which sum up φ- and r-directions (radial direction).

Different modeling approaches can be distinguished concerning their treatment of the different heat flow directions: First, all three spatial directions can be considered (see, e.g., [54–56]). Thus, arbitrary arrangements of cables can be described without the need for rotational symmetry. For example, the complete heat flow along a bundle of cables [57] can

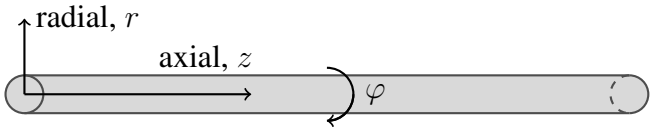

Figure 3.1: Coordinates, axial and radial direction along a cable.

be considered in this way. However, the resulting models are very complex and usually can only be solved with great effort, so simplifications are sought wherever possible. One widely used simplification is the neglection of axial heat flow: In the case of long, homogeneous conductors whose ends are at non-critical temperatures, only the heat transport processes in the transverse direction are relevant for the maximum conductor temperature, especially if the internal ohmic losses in the conductor are the only heat source to be considered. The heat flux in the current flow direction in the cable middle, where the highest temperatures are expected, is then negligible, so it is sufficient to consider any cross-section of the conductor, obtaining a two-**d**imensional (2 D) radial model (see, e.g., [55, 58–67]). If, in addition, the arrangement is also symmetrical in the φ-direction (the typical case for this is a single cable), the model order can be further reduced, leaving only a one-**d**imensional (1 D) radial model (see, e.g., [68–77]). If, in addition to the heat flux in the r-direction, the axial cable direction is also taken into account (z-direction), the result is again a 2 D model in which the rotational symmetry of the arrangement is considered. Examples of such approaches can be found in [57, 78, 79]. Also in this thesis, basically the heat flux in φ-direction is not considered. Based on this, approximations for the description of rotationally unsymmetrical cable arrangements (multiconductor cable arrangements) are also proposed.

3.1.2 Time Dependence

Thermal models can also be classified with respect to their consideration of transient effects. In steady-state models, thermal equilibrium is assumed: Here, the long-term state after all adjustment processes is described. Such models without consideration of time dependence are widely used (see e.g. [58, 60, 61, 63–65, 67, 78–80]), but reach their limits in practically relevant problems. For example, cables can tolerate much higher currents in the short term than in the long term. To describe this behavior, transient models are needed (see, e.g., [54, 57, 68–77, 81–86]). However, fully accounting for all transient effects is very challenging due to retroactive effects (e.g., temperature-dependent thermal cable parameters, see section 5.2.2), so limiting assumptions are almost always made. For example, it is implicitly assumed that temporal changes occur slowly, so a quasi-static approach can be used and the separation of cable heating and heat conduction is a good approximation. This assumption is also made in this thesis. Furthermore, for most of the presented solutions, it is assumed that the instantaneous parameter values have already existed since the beginning of the investigation and thus, did not change during a transient calculation.

3.1.3 Basic Modeling Approach

For the description of thermal phenomena on conductors, on the one hand, the basic physical equations can directly be used. Here, the heat conduction equation plays a special role, which is based on the conservation of energy. This approach is widely used (see, e.g., [60, 62, 64, 75, 78, 80, 81]) and directly provides a differential equation describing the problem.

Together with appropriate initial, boundary, and transition conditions, an overall mathematical description can be found. A drawback of this approach is that the formulations are not very descriptive and interrelationships and influences can sometimes be difficult to discern. An alternative approach is given by using the equivalence between electrical and thermal domains (see also chapter 4). This approach allows using **e**quivalent **c**ircuit **d**iagrams (ECDs) known from electrical engineering also for the description of thermal problems. The individual effects are separated from each other and represented in concentrated elements. The result is a descriptive formulation, which, however, is also accompanied by approximations due to the separation of effects. This approach is widely used (see e.g. [57, 59, 68–74, 76, 82, 84]) and is also used in this thesis.

3.1.4 Cable Environment

In liquids and gases, all three heat transfer mechanisms, conduction, radiation, and convection, occur. In contrast, only heat conduction occurs in solids [87, p. 1]. Thus, for the thermal behavior of current-carrying cables, heat conduction within the cable dominates. However, since interaction with the environment also occurs, radiation and convection have to be taken into account for a complete description, depending on the type of installation. In the case of air installation (see e.g. [66]), for example, the interaction between cable and environment occurs primarily via convection and radiation - heat conduction plays only a subordinate role here due to the comparatively low density of the air. Practically relevant examples of cables laying freely in the air are overhead lines, for which transient models are needed to account for the influence of weather on temperature development [45, 88–95]. At the other extreme, cables may be surrounded by solids, so coupling with the environment primarily occurs via thermal conduction. Typical examples are cables surrounded by soil (e.g. underground cables [62, 63, 71, 76, 82, 96] or buried submarine cables [56]). Determining the thermal parameters of the earth is particularly challenging since these depend on variables that are difficult to predict, such as humidity [71]. Laying in water [97] or combinations of laying in air and solids are also possible (e.g., cable laying in a pipe [62, 64, 98–101] or cable bundles [23, 58–61, 81, 85, 102–107]). Often, the highest temperatures are expected for installation freely in the air (worst case) [36]. This assumption is reasonable if surrounding elements cool the cables, but can lead to problems if, for example, there is a current through several cables in a bundle and thus they are heated at the same time (see section 8.4.1) or close to the cable additional heated elements appear [79].

3.1.5 Modeled Area

Thermal models can be further distinguished in terms of their spatial scope: What exactly is covered by the model? In the general case, both the cable and the transition to the environment as well as the environment itself in a selected area around the cable are directly modeled (see e.g. [55, 56, 63, 66, 84]). However, especially for the consideration of air as

an ambient material, this approach leads to very complex models due to the different effects that occur. Alternatively, as a simplification, only the cable itself is modeled directly and the transition to the environment is defined in terms of boundary conditions (see e.g. [57, 60]). In this context, a constant ambient temperature is assumed (see e.g. [59, 61]), so the heating of the environment via the cable itself is not directly modeled. Rather, the ambient temperature is measured, for example, and serves as an input variable for the model (see e.g. [60]). It is assumed that the ambient temperature changes comparatively slowly, so these changes can be taken into account via quasi-static approaches (using the current ambient temperature for each time). This approach is also used in this thesis. Another possibility is to only model the effects in the cable itself. In this case, the coupling to the environment is no longer modeled, but the surface temperature of the cable is measured and used as an input variable for the model (see e.g. [74, 76, 82, 108]). This simplifies the model itself considerably, but temperature measurements on the cable can be comparatively expensive and time-consuming, depending on the application.

3.1.6 Numerical vs. Analytical Solution Approaches

Due to the complex nonlinear parameter dependencies that occur in the thermal domain, numerical methods for temperature calculation (e.g., [70, 77]) are widely used. With the help of commercial computer programs for thermal simulations, complex three-**d**imensional (3 D) models of cable structures can be built up and calculated. Mostly FEMs are used (e.g. [54–56, 58, 62–64, 66, 67, 83, 96]), but also other approaches such as **f**inite **d**ifference **m**ethods (FDMs) [69, 77, 83] or **f**inite **v**olume **m**ethods (FVMs) [30, 81, 104] appear. Using numerical methods, the transient temperature distributions can be calculated even for complex conductive structures with inhomogeneous environmental conditions. In principle, however, these methods are associated with considerable numerical effort, although a reduction of the computational effort can be achieved by neglecting the time dependence (see e.g. [58]). Since the steady state is often not sufficient for practical problems, the practical applicability of such calculations is significantly limited. In contrast, analytical descriptions [61, 75, 76, 80, 85, 86, 98, 109] are computationally faster but mostly rely on simplifications. A combination of both approaches is proposed, for example, in [60]: Analytical relations are used to describe the problem with constant parameters, and the nonlinear parameter dependence is taken into account via a superimposed fixed-point iteration. This approach is also used in this thesis.

3.2 Electrical Transmission Line Theory

For many decades, electrical cable behavior has been deeply investigated [110, p. 2]. Over time, the knowledge and understanding of the appearing effects grew, leading from the first basic models for simple conductive structures to more and more detailed models for more complex cable arrangements. For several parallel cables, the multiconductor TL theory was

established, e.g. [110–112]. Today, a huge variety of methods is known, allowing current and voltage calculations along conductive structures. Special cases lead to simplified formulations for several applications.

3.2.1 Equivalent Circuit Diagrams and Partial Differential Equations

Often, ECDs for infinitesimally short cable segments are used. For a field excited system consisting of a reference conductor and a second parallel conductor, oriented in the direction of the coordinate z, the ECD in figure 3.2 is found for a segment of the infinitesimal length $\mathrm{d}z$ [110, p. 584]. The cable elements (resistance R'_{el}, inductance L'_{el}, capacitance[1] $\mathcal{C}'_{\mathrm{el}}$, and conductance G'_{el}) and the sources that are used to model the coupling of external magnetic (voltage source U'_{fi}) and electrical (current source I'_{fi}) fields are given as per unit length parameters, which means that they are normalized to the length, which is a (spatial) derivative. In this thesis, per unit length parameters are marked with an upstroke. In the ECDs in this whole thesis, all per unit length quantities formally have to be multiplied by the length, which is neglected due to the clarity of the figures. Using Kirchhoff's laws, a system of coupled PDEs relating the current I and voltage U of the segment is derived with the time t:

$$\begin{aligned} \frac{\partial U(z,t)}{\partial z} + L'_{\mathrm{el}}\frac{\partial I(z,t)}{\partial t} + R'_{\mathrm{el}} I(z,t) &= U'_{\mathrm{fi}}, \\ \frac{\partial I(z,t)}{\partial z} + \mathcal{C}'_{\mathrm{el}}\frac{\partial U(z,t)}{\partial t} + G'_{\mathrm{el}} U(z,t) &= I'_{\mathrm{fi}}. \end{aligned} \tag{3.1}$$

This system, which couples voltage and current, can be reduced to a single PDE for the voltage in the case of $\partial U'_{\mathrm{fi}}/\partial z = 0$ and $\partial I'_{\mathrm{fi}}/\partial t = 0$:

$$\frac{\partial^2 U(z,t)}{\partial z^2} - L'_{\mathrm{el}}\mathcal{C}'_{\mathrm{el}}\frac{\partial^2 U(z,t)}{\partial t^2} - (L'_{\mathrm{el}}G'_{\mathrm{el}} + R'_{\mathrm{el}}\mathcal{C}'_{\mathrm{el}})\frac{\partial U(z,t)}{\partial t} - R'_{\mathrm{el}}G'_{\mathrm{el}}U(z,t) = -R'_{\mathrm{el}}I'_{\mathrm{fi}}. \tag{3.2}$$

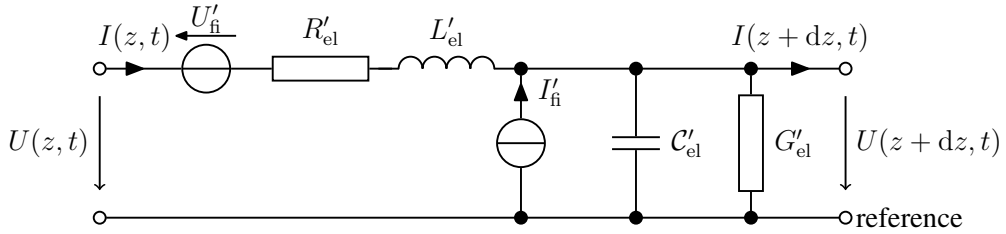

Figure 3.2: Electrical ECD for an infinitesimally long segment of a single conductor and a reference conductor.

[1] In this thesis, some mathematical symbols (A, B, C, D, E, L, N, W, ε, φ) are used to describe different quantities. To distinguish between them, one (typically the more rarely occurring) quantity is therefore written in a different font ($\mathcal{A}$, $\mathcal{B}$, $\mathcal{C}$, $\mathcal{D}$, $\mathcal{E}$, $\mathcal{L}$, $\mathcal{N}$, $\mathcal{W}$, ϵ, ϕ). This sometimes results in an unusual appearance of widely known relationships, which is why this distinction is briefly pointed out again when the corresponding quantities are introduced. The corresponding assignments can be found in the list of mathematical symbols. $\mathcal{C}$ describes electrical or thermal capacitances, whereas C is a parameter of the partial differential equations.

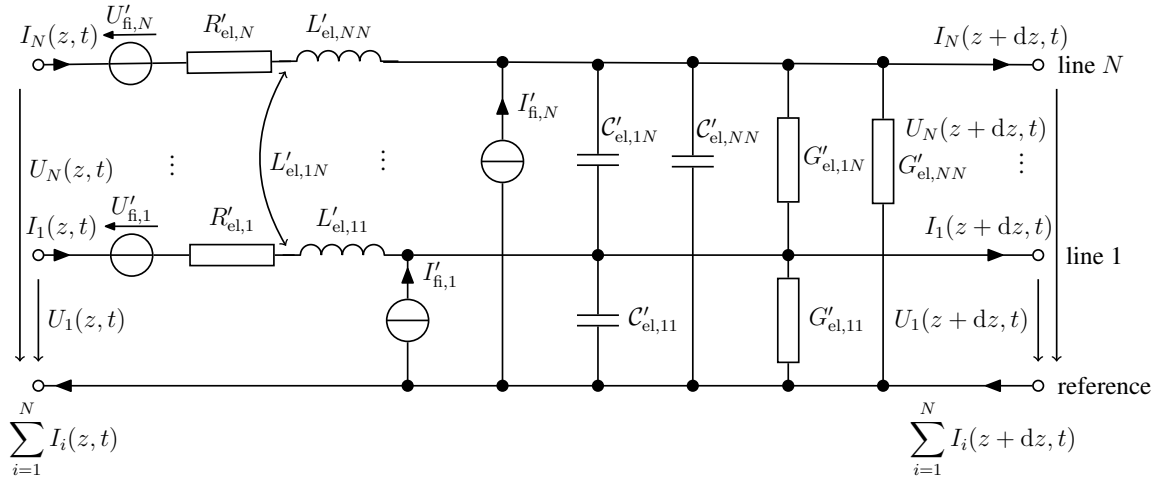

Figure 3.3: Electrical ECD for an infinitesimally long segment of a multiconductor arrangement.

To model not only a single conductor with a reference conductor but $N+1$ parallel conductors (one of which is again the reference conductor) and their interaction, the ECD in figure 3.3 is used for the case of an ideal reference conductor (resistance is equal to zero). The interaction between the different conductors leads to matrix-vector expressions, that relate currents and voltages on the analyzed conductors to each other:

$$\begin{aligned} \frac{\partial \boldsymbol{U}(z,t)}{\partial z} + \mathbf{L}'_{\mathrm{el}} \frac{\partial \boldsymbol{I}(z,t)}{\partial t} + \mathbf{R}'_{\mathrm{el}} \boldsymbol{I}(z,t) &= \boldsymbol{U}'_{\mathrm{fi}}, \\ \frac{\partial \boldsymbol{I}(z,t)}{\partial z} + \boldsymbol{\mathcal{C}}'_{\mathrm{el}} \frac{\partial \boldsymbol{U}(z,t)}{\partial t} + \mathbf{G}'_{\mathrm{el}} \boldsymbol{U}(z,t) &= \boldsymbol{I}'_{\mathrm{fi}}. \end{aligned} \tag{3.3}$$

Again, an expression only for the voltage can be derived equivalently to equation (3.2) with $\partial \boldsymbol{U}'_{\mathrm{fi}} / \partial z = \mathbf{0}$, $\partial \boldsymbol{I}'_{\mathrm{fi}} / \partial t = \mathbf{0}$ and $\boldsymbol{U} = \boldsymbol{U}(z,t)$:

$$\frac{\partial^2 \boldsymbol{U}}{\partial z^2} - \mathbf{L}'_{\mathrm{el}} \boldsymbol{\mathcal{C}}'_{\mathrm{el}} \frac{\partial^2 \boldsymbol{U}}{\partial t^2} - (\mathbf{L}'_{\mathrm{el}} \mathbf{G}'_{\mathrm{el}} + \mathbf{R}'_{\mathrm{el}} \boldsymbol{\mathcal{C}}'_{\mathrm{el}}) \frac{\partial \boldsymbol{U}}{\partial t} - \mathbf{R}'_{\mathrm{el}} \mathbf{G}'_{\mathrm{el}} \boldsymbol{U} = -\mathbf{R}'_{\mathrm{el}} \boldsymbol{I}'_{\mathrm{fi}}. \tag{3.4}$$

To sum up, the scalar parameters from the single conductor now become matrices. The entries in the different per unit length matrices depend on the geometry and material parameters. All of those matrices are in general fully occupied and symmetrical. A system of coupled PDEs is formulated.

3.2.2 Solution Approaches

Generally, the solution of the previously presented systems of PDEs is not trivial. In the electrical TL theory, many methods were developed to solve these equations for different applications. Because of the variety of methods, here, only a little proportion can be presented shortly.

Often, transformations [110–114] are used to solve the differential equations. Especially

the Laplace domain or the frequency domain play important roles. The basic idea in the use of transformations is to convert derivatives to algebraic operations to reduce the PDEs to **o**rdinary **d**ifferential **e**quations (ODEs) or even algebraic equations [110, p. 241]. Often, those simplified formulations can be solved for example using similarity transformations [110–112] directly in the image domain. In many cases, the complex structure of the result prevents the transformation back into the time domain. Then, numerical solutions (see for example [115]) can be used for the inverse transformation or model order reduction approaches [110, 111, 116] are applied, that enable an analytical inverse transformation even for complex arrangements. Another approach for the solution of the PDE is the use of Green's functions (see for example [117–122]) in the time domain or the image domain. The basic idea here is to find a characteristic function for the differential equation ("kernel") that is used as the basis for the consideration of stimuli, initial, and boundary conditions. When applied in combination with a transformation, choosing an appropriate approach for Green's function can help to avoid problems with the inverse transformation.

To describe the current and voltage signals, macromodels can be applied (see for example [110, pp. 450-453]). The aim is to transfer the PDEs to a set of ODEs via some kind of discretization to enable the implementation in given circuit simulators. One prominent approach (see for example [110, pp. 265-269] and [123]) is to divide the conductive structure into segments with a length that is short compared to the typical wavelength of the system. Each of those segments is modeled using an ECD with lumped elements. Then, numerical solutions can be used for the solution. A problem with this approach is that especially for high frequencies, a huge number of segments is necessary. That is why also different techniques for a more efficient discretization were developed for example the method of characteristics (delayed controlled sources), developments in basic function, or approximations for special expressions [111].

In the general case, the cable parameters are nonlinear (see for example [124–126]), typically frequency-dependent. Then, also the corresponding PDE is nonlinear. For the solution considering this behavior, for example, the harmonic balance method [127], the waveform relaxation [128], or iterations [129] are used.

All in all, the complexity and solvability of the different problems vary. For general conductor arrangements, very complex systems can result, that sometimes can only be solved with a high effort by numerical approaches [110, 111, 130] as finite differences or recursive approaches. Nevertheless, the amount of methods and approaches is huge and continuously increasing. Current research is, for example, focused on inhomogeneous or bent conductors [131] and the analysis of statistical influences on the conductor arrangement (see for example [132]).

4 Thermo-Electrical Analogy

Over the years, a huge variety of methods was developed to describe electrical cable behavior (electrical TL theory). A comparably well-established thermal TL theory has not been derived so far. A fundamental question, therefore, is whether methods from the electrical domain can be used for the description of thermal processes as well. That is why in this section, the analogy between thermal and electrical domains is analyzed. This chapter is based on [A.2].

Electrical charges q_{el} form the fundamental basis for observable electromagnetic effects. Charges of equal sign repel each other. Electrical charges are discretized on the elementary level as multiples of the elementary charge. However, since this elementary charge is extremely small, this discretization no longer plays a role on the macroscopic level. There, the spatial charge distribution can often be described very precisely by a continuous charge density ρ_{el}. Without further external influences, electrical charges strive towards a spatial uniform distribution, which manifests itself in a constant volume charge density. A completely analog behavior can be observed in the thermal domain: Here, a temperature difference induces a balancing process, which eventually leads to a uniform temperature distribution. On a molecular level, the temperature of a medium characterizes the average of the kinetic energy, rotation energy, and oscillation energy of the molecules. Analog to the electrical volume charge density, which strives for an equal distribution, an energy density ρ is used in the thermal sense.

In the thermal and electrical domain, the charge (or energy) in a given volume is calculated by integration over this density. A thermal charge

$$q = \int_V \rho \, \mathrm{d}V \tag{4.1}$$

thus represents a certain amount of energy. In the electrical domain, this charge

$$q_{\mathrm{el}} = \int_V \rho_{\mathrm{el}} \, \mathrm{d}V \tag{4.2}$$

is carried by particles, for example, electrons, and is a characteristic property of the particle that cannot be easily transferred from one particle to another. In the thermal domain, the energy is also carried by molecules but can be exchanged between them by collision and radiation. Thus, molecules in the thermal domain cannot initially be understood as being equivalent to electrons in the electrical domain. Instead, however, it is possible to understand quasiparticles as carriers of the energy portions, which are the thermal charges q. A fundamental difference between the electrical and thermal charges consists of the fact that there are no negative energies - and thus no negative thermal charges and no negative thermal charge

densities.

The charge quantity that passes a given cross-section per time defines the electrical current

$$I = \frac{\mathrm{d}q_{\mathrm{el}}}{\mathrm{d}t} = \int_{\mathcal{A}} \boldsymbol{J}_{\mathrm{el}} \, \mathrm{d}\boldsymbol{n}_{\mathcal{A}} \tag{4.3}$$

which is an effect or through quantity. $\boldsymbol{J}_{\mathrm{el}}$ is the electrical current density. In the thermal domain, the heat flow

$$P = \frac{\mathrm{d}q}{\mathrm{d}t} = \int_{\mathcal{A}} \boldsymbol{J} \, \mathrm{d}\boldsymbol{n}_{\mathcal{A}} \tag{4.4}$$

fulfills an equivalent role and is also defined accordingly (energy that passes a given cross-section per time) with the thermal current density $\boldsymbol{J}$.

The electrical scalar potential[2] ϕ_{el} describes the ability of the conservative (electrical) force field to relocate charge carriers and therefore, to perform work. This electrical scalar potential is a property that is assigned to the space itself and thus, does not depend on the presence of matter or charges at the evaluated point, because the charges causing the potential can be far away due to the infinite range of the Coulomb interaction. Constant offsets in the potential do not change the physical behavior, which allows the definition of a reference potential. Generally, the electrical scalar potential can have any value. The corresponding (potential) quantity in the thermal domain is the temperature T and therefore, is always coupled to appearing matter and energy stored in it. Equivalently to the electrical domain, a reference temperature can be chosen. But, in contrast to the electrical domain, an overall absolute temperature scale exists that is especially characterized by the absolute zero point (thermal energy is zero). Temperatures below this value (and strictly speaking also the zero point itself) cannot be reached. To sum up, in both domains, a potential quantity can be found (electrical scalar potential respectively temperature), but their properties differ between the electrical and thermal domains. The potential is related to the current density via

$$\boldsymbol{J}_{\mathrm{el}} = -\lambda_{\mathrm{el}} \operatorname{grad}(\phi_{\mathrm{el}}), \qquad \boldsymbol{J} = -\lambda \operatorname{grad}(T) \tag{4.5}$$

with the corresponding conductivities λ_{el} (electrical) and λ (thermal), respectively. The conservation of electrical charge is equivalent to energy conservation in the thermal domain, both of which are described via a continuity equation:

$$\operatorname{div}(\boldsymbol{J}_{\mathrm{el}}) = -\frac{\partial \rho_{\mathrm{el}}}{\partial t}, \qquad \operatorname{div}(\boldsymbol{J}) = -\frac{\partial \rho}{\partial t}. \tag{4.6}$$

From the electrical scalar potential, the electrical voltage U between two points in space can be found as their potential difference. This voltage is the cause or across quantity corresponding to the through quantity of the current. Equivalently, a temperature difference

[2] ϕ is the scalar potential, whereas φ is a coordinate.

between two points causes a heat flow between these points.

(Negative) electrical charges at points with lower potential have lower potential energy than charges at points with higher potential. Due to energy minimization, therefore, a force exists that pulls positive charges to points with lower potential. Therefore, a voltage between two points induces a charge movement and thus a current as long as an appropriate path is provided (without potential barriers, which especially means that a finite resistance between the two points is necessary). A very typical case is a current through a conductor. For different materials, the same voltage typically leads to different currents. This dependence is described via the resistance

$$R_{\mathrm{el}} = \frac{U}{I} \tag{4.7}$$

which is defined as the ratio between the voltage and the current. In the thermal domain, a directly parallel formulation can be found: Energy minimization here causes energy (thermal charges) to move from higher temperatures (potentials) to lower temperatures. The ratio between temperature difference and heat flow again defines the (thermal) resistance

$$R = \frac{\Delta T}{P}. \tag{4.8}$$

The similarity of this formulation of the resistance manifests in the calculation formulas for the resistances for identical geometries: For a cylinder (length l, cross-section $\mathcal{A}$), the axial resistances R_{el} (electrical) and R (thermal) are

$$R_{\mathrm{el}} = \frac{l}{\lambda_{\mathrm{el}}\mathcal{A}}, \quad R = \frac{l}{\lambda\mathcal{A}}. \tag{4.9}$$

For a cylindrical shell (inner radius r_{in}, outer radius r_{out}), the radial resistances are

$$R_{\mathrm{el}} = \frac{\ln\left(\frac{r_{\mathrm{out}}}{r_{\mathrm{in}}}\right)}{2\pi\lambda_{\mathrm{el}}l}, \quad R = \frac{\ln\left(\frac{r_{\mathrm{out}}}{r_{\mathrm{in}}}\right)}{2\pi\lambda l}. \tag{4.10}$$

Heat can also be stored in the medium. To model this, a thermal capacitance $\mathcal{C}$ is necessary:

$$P = \mathcal{C}\frac{\mathrm{d}(\Delta T)}{\mathrm{d}t} \Rightarrow \mathcal{C} = \frac{q}{\Delta T}. \tag{4.11}$$

Mathematically, $\mathcal{C}$ connects the time derivative of the temperature difference with the heat flow analog to the electrical domain (capacitance $\mathcal{C}_{\mathrm{el}}$):

$$I = \mathcal{C}_{\mathrm{el}}\frac{\mathrm{d}U}{\mathrm{d}t} \Rightarrow \mathcal{C}_{\mathrm{el}} = \frac{q_{\mathrm{el}}}{U}. \tag{4.12}$$

There is no thermal equivalent to the electrical inductance because a thermal equivalent to the magnetic field does not exist.

Based on these equivalences between the electrical and thermal domain, also, the often neglected thermal propagation processes along the longitudinal cable direction show analogies to electrical propagation processes on cables. So far, only isolated modeling approaches have been proposed that are directly based on the electrical TL theory (e.g., [133]). This analogy is also mentioned in [134], but not consequently used to find new solution approaches for the thermal problem. The potential of this analogy was not systematically evaluated in the past. In this thesis, selected approaches from the electrical domain are used to describe thermal effects on cables.

5 Thermal Cable Modeling Based on the Electrical Transmission Line Theory

In the previous chapter, correlations between the electrical and thermal domains were observed. Based on these results, in this chapter, a modeling approach for electrical propagation processes on homogeneous cables (see chapter 3 in [110]) is analyzed concerning its applicability to thermal processes. First, a detailed comparison between the two domains is performed for this purpose. Subsequently, approaches for a thermal TL theory are developed for a single cable and a multiconductor system. The results are compared to the formulations in the electrical domain.

5.1 Preliminary Considerations - Comparison Between Electrical and Thermal Effects on Cables

Before the potentials of a thermal analogy to the electrical TL theory are evaluated, electrical and thermal effects on cables are compared. Some parts of those considerations are based on [A.2].

5.1.1 Basic Physical Equations

In this section, the physical relationships that characterize the electrical and thermal domains, respectively, are compared. For this purpose, the basic equations are analyzed.

The following paragraph is based on the discussion in [135, pp. 521-522]. Electrical and magnetic processes can be described time-dependently via Maxwell's equations[3]

$$\begin{aligned} \mathrm{rot}(\boldsymbol{\mathcal{E}}) &= -\frac{\partial}{\partial t}\boldsymbol{\mathcal{B}}, & \mathrm{div}(\boldsymbol{\mathcal{D}}) &= \rho_{\mathrm{el}}, \\ \mathrm{rot}(\boldsymbol{H}) &= \boldsymbol{J}_{\mathrm{el}} + \frac{\partial}{\partial t}\boldsymbol{\mathcal{D}}, & \mathrm{div}(\boldsymbol{\mathcal{B}}) &= 0 \end{aligned} \tag{5.1}$$

together with the material equations for the linear case[4]

$$\boldsymbol{\mathcal{D}} = \epsilon\boldsymbol{\mathcal{E}}, \boldsymbol{\mathcal{B}} = \mu\boldsymbol{H}, \boldsymbol{J}_{\mathrm{el}} = \lambda_{\mathrm{el}}\boldsymbol{\mathcal{E}}. \tag{5.2}$$

Here, $\boldsymbol{\mathcal{E}}$ and $\boldsymbol{H}$ represent the electric and magnetic fields, respectively, and $\boldsymbol{\mathcal{D}}$ and $\boldsymbol{\mathcal{B}}$ are the associated flux densities. μ is the magnetic permeability and ϵ is the permittivity. Using the Lorenz gauge condition, a hyperbolic PDE (wave equation) follows for the electrical scalar

[3] In this thesis, $\mathcal{E}$ describes the electric field strength, whereas E is the energy. $\mathcal{D}$ is the electric flux density. In contrast, D is a parameter of the PDEs. $\mathcal{B}$ describes the magnetic flux density, and B is a parameter of the PDEs.

[4] ϵ is the permittivity, whereas ε is the emissivity.

potential ϕ_{el}:

$$\operatorname{div}\left(\operatorname{grad}\left(\phi_{\mathrm{el}}\right)\right) - \mu\epsilon\frac{\partial^2}{\partial t^2}\phi_{\mathrm{el}} = -\frac{\rho_{\mathrm{el}}}{\epsilon}. \tag{5.3}$$

Thermally, no similarly compact closed formulation can be found. This is because there are three basic heat transport mechanisms, which are based on different physical effects. Thus, thermal conduction, radiation, and convection are described by different mathematical relationships. Heat conduction is mediated at the microscopic level by collisions between particles. Macroscopic, the associated energy transfer is described mathematically by the heat conduction differential equation [136, p. 85], i.e., a parabolic PDE for the temperature T (analog to the hyperbolic PDE for the electrical scalar potential, see equation (5.3)):

$$\operatorname{div}\left(\operatorname{grad}\left(T\right)\right) - \frac{c}{\lambda}\frac{\partial T}{\partial t} = -\frac{\dot{\omega}}{\lambda}. \tag{5.4}$$

Here, c represents the specific heat capacity and $\dot{\omega}$ is the (external) heat source density. λ is the thermal conductivity, which, according to Fourier's law [136, 137] (see also equation (4.5), thermal formulation) describes the relationship between the heat flux density $\boldsymbol{J}$ and the temperature gradient. Thus, it is an analog of the material equation for the electrical current density (see equation (4.5), electrical formulation).

Thermal radiation is based on a fundamentally different mechanism. Here, heat is transferred by electromagnetic radiation [136, 137] which is emitted by accelerated charges in the molecules. In contrast to the other heat transfer mechanisms, this effect also occurs without an intermediary medium and can therefore take place in a vacuum [136, 137]. The heat flow P passing a radiating surface is linearly dependent on the fourth power of the temperature T of this surface[5] $\mathcal{A}$ [136, p. 737]:

$$P = \varepsilon\sigma\mathcal{A}T^4. \tag{5.5}$$

$\sigma = 5.67 \cdot 10^{-8}\,\mathrm{W/m^2K^4}$ is the Stefan-Boltzmann constant and ε is the surface emissivity.

Convection, on the other hand, is a flow effect in a liquid or gas and describes a combination of diffusion and a macroscopic motion [136, p. 378]. Typically, it is presented as a third individual heat transfer mechanism, nevertheless, heat conduction is a part of this effect [136, p. 378]. In addition, the fluid dynamics of the surrounding material are important here. A distinction is made between free and forced convection. In the case of free convection, the flow is caused only by density differences in the fluid as a result of heating and the associated temperature differences [136, 137]. In the case of forced convection, there is a forced external flow [136, 137]. In the general case, the calculation of all effects is very complicated. In many cases, no exact analytical closed-form expression can be found [137, p. 17]. However, for special geometrical arrangements, approaches are given in [138, pp. 27-29] which can be used to describe the relationship between heat flow and temperature. For free convection

[5] $\mathcal{A}$ describes areas, and A is a parameter of the PDEs.

around a horizontally oriented cylinder, the relationship is given in section 5.2.2.

Thus, in contrast to the electrical domain, the processes in the thermal domain are more diverse and more difficult to accommodate in a common formulation. In the cables under consideration, all three propagation processes, heat conduction, radiation, and convection, play a role. Radiation and convection occur at the surface of the cable, while thermal conduction occurs primarily in the interior. Assuming that the cables are located in the air, the heat conduction in the surroundings is neglected, since the thermal conductivity is assumed to be very low, so radiation and convection dominate at the cable surface.

To find a comparable formulation in the thermal domain, despite the very dominant differences between the electrical and thermal domains, the focus is now put on the heat conduction inside the cable. There, structural similarities to the electrical domain can be found (PDE of second order, equivalent material equation). Nevertheless, the differential equations also show differences: In the electrical domain, hyperbolic equations describe an oscillating system with wave propagation effects (see equation (5.3)). The second time derivative corresponds to an oscillating behavior. Unlike, in the thermal domain, the differential equation is parabolic (see equation (5.4)). Therefore, wave phenomena such as reflections, standing waves, and resonances do not appear in the thermal domain. Nevertheless, based on the underlying similarities, a similar formulation in the thermal domain is searched. The idea is now to set the model boundary to the cable surface, and thus, describe a purely thermal conduction system. However, since this system is not closed (because there are heat fluxes beyond the system boundaries), appropriate boundary conditions are necessary. First, the ohmic heating of the cable is chosen as input variable. To describe the heat flow through the cable surface to the environment via convection and radiation, (rather complicated and nonlinear) boundary conditions are defined at this surface. The model itself only describes the cable itself, because only up to this point the modeling can be applied purely via heat conduction.

5.1.2 Modeling Goal

In the electrical domain, cables are often primarily an unwanted interference factor. Ideally, for many applications, current and voltage should transfer from the input to the output without loss and delay [110, p. xviii] (of course, there are also exceptions, in which, for example, cable inductances are used quite specifically to influence the oscillation behavior of the overall circuit). Since current and voltage at the input and output of real cables are generally not identical, often, the connection behavior of cables is searched. Therefore, two-port networks or chain matrices for the direct connection of the currents and voltages at the cable terminations are typically used [110, pp. 269-278]. However, there are applications where the pure connection behavior is not sufficient. An example from the field of electromagnetic compatibility is the determination of the radiated fields of a conductor arrangement, which

are potential interference sources for other elements.

In the thermal domain, one of the main motivations for temperature calculation is the protection of the cables themselves and nearby installed components. For this purpose, the decisive variable is usually the maximum (possibly only locally appearing) cable temperature. That is why not only the connection behavior but explicitly the entire temperature development along the cable is decisive here.

5.1.3 Basic Modeling Approaches

a) TEM Assumption and Fields

The following paragraph is based on the explanations in [110, pp. 4-5]. In the electrical domain, the assumption that only **t**ransverse **e**lectro**m**agnetic (TEM) fields are present plays a major role, which means that only the TEM mode is capable of propagation, i.e., no field components in the axial cable direction appear. This ensures that current and voltage are uniquely defined for the case of frequencies not equal to $0\,\mathrm{Hz}$. Theoretically, there are also higher modes. However, these are strongly attenuated below a cutoff frequency (typically low GHz range), so their influence becomes negligible. The TEM mode, on the other hand, has a cutoff frequency of $0\,\mathrm{Hz}$ and is therefore always capable of propagation. The assumption that only transverse electromagnetic fields occur is no longer accurate for lossy conductors and/or inhomogeneous surrounding materials. However, assuming that the effects occurring due to the additional modes are small, they can be incorporated into the formulation for ideal TEM modes (quasi-TEM). An important consequence of the TEM assumption is that the current sum becomes zero in any cross-section of the conductor arrangement. Therefore, one conductor can be thought of as a reference or return conductor through which the current flows back. For this central assumption to be valid, as mentioned above, the frequency has to be low enough, which corresponds to electrically short structures. Then, the modeling approach via an ECD can be applied. If this circuit is built up for a cable segment of infinitesimal length (which is, obviously, electrically short), an overall electrically long cable length does not cause any problems. Unlike, in the radial direction, electrically short structures are mandatory.

The concept of the reference conductor and TEM fields cannot be applied to the thermal domain. At first, in the thermal domain, the field concept is only partially applicable. Here the modeling ends at the cable surface, the environment is only considered by boundary conditions. That is why no fields can meaningfully be defined or even calculated in the space between the two conductors. An equivalent to magnetic fields does not appear in the thermal domain at all. An analog to the electric field can be defined in the conductor itself as a gradient of the temperature, but not in a vacuum - a temperature is always necessary and therefore, so is a medium. Also, there is no physically closed circuit in the thermal domain - heat flows from places of higher temperature to places of lower temperature, but

not back again. Therefore, there is no physical thermal equivalent for the reference conductor from the electrical domain. Nevertheless, it is possible and necessary to define a common reference in the thermal domain as well, to which the different effects refer. However, this reference then has no physical equivalent. This becomes clear also by the consideration that electrically, typically, charge conservation is assumed in a closed circuit. So there is a closed system. However, the thermal equivalent to the charge, the energy, is always supplied by the ohmic losses in the inner conductor - so there is no closed system. The interaction with the environment (which is only taken into account by the boundary conditions) ensures that an energy flow beyond the system boundary can also be observed at the outer model termination. Nevertheless, the thermal effects in the model refer to one shared reference which is why the ECD can be closed via this reference path, even though there is no physical equivalent and thus, the heat flow through this reference does not physically exist.

Fields mediate long-distance effects in the electrical domain: Even if two structures do not touch each other, they can interact. Thermally this happens with radiation. In the following models, however, only heat conduction is explicitly considered mathematically as only the cable itself is directly modeled - and the basic prerequisite for heat conduction is that there is direct contact. For thermal conduction, therefore, there is no long-distance effect.

b) Closed System Assumption

Thermally, a spatially closed system is necessary to find a comparable formulation to the electrical domain, since radiation and convection at the conductor surface mathematically follow fundamentally different relationships than thermal conduction (which, comparable to the wave effects in the electrical domain, also follows a PDE of second order). A thermal insulation material, which is placed around thermal conductors and in which therefore no thermal conduction takes place, thus also directly prevents the coupling between these conductors via thermal conduction. Therefore, it is rather to be understood as a boundary condition for single conductor considerations but is not suitable to build up a multiconductor problem equivalent to the electrical domain. These observations can be traced back to the different meanings that capacitance fulfills in the thermal and electrical domains.

c) Capacitances

In the electrical domain, a capacitance is not directly assignable to a point in space but is a property between two mutually insulated conductive structures. This capacitance then crucially depends on what material is placed in the space between them. Knowledge of the field in the insulating material alone is sufficient to determine the capacitance [110, pp. 26-27]; the material properties of the conductor are irrelevant. The geometrical arrangement of the conductors, on the other hand, plays a major role. A capacitance is thus usefully defined independently of electrical conduction between these two conductive structures.

In the thermal domain, a fundamentally different situation is observed. There, capacitances

describe a local property. The governing quantity is the specific heat capacity. The capacitance of a conductor against reference does not depend at all on the surrounding material and only from the surroundings no conclusions about the capacitance are possible. Only the material properties of the conductor determine the capacitance, the geometrical arrangement is not relevant - the total heat capacitance remains the same for an element of constant volume (or constant mass) even if it is transformed into a different shape. The heat capacitance is always related to the reference [52, 134, 139] - it is a local property, so there is no physical equivalent for the second node. In this respect, however, there is also no thermal capacitance between two conductive structures, as is the case (the only one occurring) in the electrical domain. Thus, in thermal models that directly aim to describe the physical properties, only capacitances against reference occur.

The underlying fundamental difference is that in the thermal domain, heat conduction and heat capacitance cannot be separated. This can be seen directly in the heat conduction differential equation, where both effects occur together. To each infinitesimal volume element a resistance can be assigned, which it opposes a directed heat flow, but also a heat capacitance, which relates the supplied energy and the resulting temperature increase. In the later modeling for conduction, this is exactly what becomes a critical point - because there, heat conduction and heat radiation have to be separated. This is one of the key approximations necessary to find a formulation similar to the electrical domain. However, a direct physical arrangement, where thermal conduction and capacitance naturally occur separately, does not exist. In this respect, there is no thermal equivalent to an electrical insulator. Therefore, it is also not possible to find an example in which a transferability between the electrical and thermal domain can be found directly without approximations.

5.2 Single Conductor Transmission Line Theory

In the electrical TL theory, a typical basic arrangement consists of two parallel conductors, one of which is selected as the reference conductor. Equivalently, in the thermal domain, a single conductor with an insulation layer is the basic arrangement. The cross-section of this cable is shown in figure 5.1: Around the solid conductor with radius r_c, there is an insulation

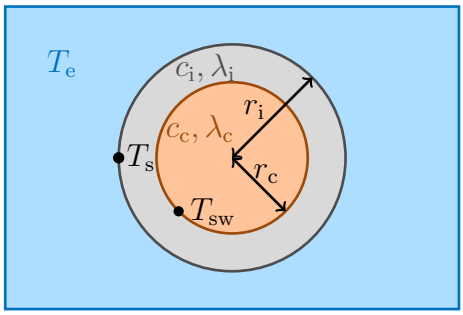

Figure 5.1: Cross-section of the analyzed single wire cable.

layer with outer radius r_i. The specific volume-related heat capacities of the conductor and insulation material are c_c and c_i, respectively. The corresponding thermal conductivities are λ_c and λ_i. The temperature at the junction between the conductor and insulation is T_sw (**s**ingle **w**ire), and the cable **s**urface temperature is T_s. The **e**nvironment has a constant temperature of T_e.

5.2.1 Partial Differential Equation

For many applications, the temperature development between T_sw and T_s is not relevant, so only the temperatures at specific nodal points are necessary. That is why a description of the dependence of those nodal temperatures on each other is searched. So, a differential equation depending only on one spatial coordinate z and the time t is derived in this section, which describes the behavior of the relevant nodal temperatures (in this case primarily the conductor temperature). First, the heat equation is derived as the basic description of the physical behavior. Assuming constant material parameters, individual differential equations for the conductor and the insulation layer are found. Then, boundary and transition conditions are defined that are necessary to couple the conductor and insulation temperatures. After that, the equations for the conductor and the insulation are integrated separately to get rid of the radial dependence. Finally, the PDE for the conductor temperature is derived.

a) Heat Equation

The heat equation describes heat conduction in a medium. This equation is derived in the following. According to the first law of thermodynamics, an extended form of the conservation of energy applies to changes in the energy E, the heat Q, and the work[6] $\mathcal{W}$:

$$\mathrm{d}E = \delta Q + \delta \mathcal{W}. \tag{5.6}$$

Here it has to be distinguished between total differentials (d) and inexact or incomplete differentials (δ). For the total differential $\mathrm{d}E$, an associated potential can be given and the integral (i.e. E) does not depend on the path of state changes. In contrast, for δQ and $\delta \mathcal{W}$, in general, no associated potential can be given. Thus, there is no state variable "heat" or "work" and the integral depends on the path. In thermodynamics, $\delta \mathcal{W}$ can be described as

$$\delta \mathcal{W} = -p\mathrm{d}V + \xi \mathrm{d}\mathcal{N} \tag{5.7}$$

with pressure p and chemical potential ξ. Therefore, for a closed system (constant number of particles[7] $\mathcal{N}$) with no volume work (constant volume V), the work has to vanish:

$$\delta \mathcal{W} = 0 \Rightarrow \mathrm{d}E = \delta Q. \tag{5.8}$$

[6] In this thesis, $\mathcal{W}$ describes the work, whereas W is an abbreviation in some solutions.
[7] $\mathcal{N}$ is the number of particles. In contrast, N describes the number of conductors.

Due to conservation of energy, in this case, also conservation of heat applies. Generally, a continuity equation can be determined from a conservation variable. In general, the temporal change of the density belonging to this conservation variable (here: heat density $\partial Q/\partial V$) is related to the spatial change of the corresponding current density. The current density here is the heat flux density

$$\boldsymbol{J} = \frac{1}{\mathcal{A}} \frac{\partial Q}{\partial t} \boldsymbol{n}_{\mathcal{A}} \tag{5.9}$$

across the edge of the volume, where $\boldsymbol{n}_{\mathcal{A}}$ points in the direction of the energy propagation, indicating the direction of the heat flow, and $\mathcal{A}$ is the area through which the heat flows. Thus, the continuity equation becomes

$$\frac{\partial^2 Q}{\partial t \, \partial V} + \operatorname{div}(\boldsymbol{J}) = \dot{\omega}. \tag{5.10}$$

$\dot{\omega}$ is an additional heat source density in the volume. Via Fourier's law (see equation (4.5), thermal formulation, analog to Ohm's law), the heat flux density can be expressed via the temperature. The heat capacitance $\mathcal{C}_V$ is defined as follows, assuming a constant volume and a constant number of particles:

$$\mathcal{C}_V = \left.\frac{\partial Q}{\partial T}\right|_{V,\mathcal{N}}. \tag{5.11}$$

Inserting the volumetric specific heat capacity c with

$$\frac{\partial \mathcal{C}_V}{\partial V} = c = \left.\frac{\partial \left(\partial Q/\partial V\right)}{\partial T}\right|_{V,\mathcal{N}} \Rightarrow \frac{\partial Q}{\partial V} = cT \tag{5.12}$$

and equation (4.5) into equation (5.10) leads to

$$\frac{\partial (cT)}{\partial t} - \operatorname{div}(\lambda \operatorname{grad}(T)) = \dot{\omega}. \tag{5.13}$$

With $\partial c/\partial t = 0$ and $\operatorname{grad}(\lambda) = \mathbf{0}$ the heat equation follows:

$$c\frac{\partial T}{\partial t} - \lambda \operatorname{div}(\operatorname{grad}(T)) = \dot{\omega}. \tag{5.14}$$

For application to radially symmetric cables, this is formulated in cylindrical coordinates:

$$\dot{\omega} = c\frac{\partial T}{\partial t} - \lambda \left(\frac{1}{r}\frac{\partial}{\partial r}\left(r\frac{\partial T}{\partial r}\right) + \frac{1}{r^2}\frac{\partial^2 T}{\partial \varphi^2} + \frac{\partial^2 T}{\partial z^2} \right) \tag{5.15}$$

with radius r, axial coordinate z, and angle φ. Due to the symmetry of the analyzed cable, it is

$$\frac{\partial^2 T}{\partial \varphi^2} = 0. \tag{5.16}$$

b) Boundary and Transition Conditions

The temperatures in the different cable areas are linked by boundary and transition conditions. These are used later to determine the special solutions for the problem from the general solutions, i.e. to calculate the constants. First of all, a steady temperature curve is required at the transition between the conductor (radial temperature distribution $T_{\mathrm{cond}}(r)$) and the insulation (radial temperature distribution $T_{\mathrm{insu}}(r)$):

$$T_{\mathrm{cond}}(r = r_{\mathrm{c}}) = T_{\mathrm{insu}}(r = r_{\mathrm{c}}). \tag{5.17}$$

Fourier's law in cylindrical coordinates leads to

$$\boldsymbol{J} = -\lambda \left(\frac{\partial T}{\partial r}\boldsymbol{e}_r + \frac{1}{r}\frac{\partial T}{\partial \varphi}\boldsymbol{e}_\varphi + \frac{\partial T}{\partial z}\boldsymbol{e}_z \right). \tag{5.18}$$

The heat flow in the radial direction is therefore

$$J_r(r) = \boldsymbol{J}\boldsymbol{e}_r = -\lambda \frac{\partial T}{\partial r}. \tag{5.19}$$

This heat flow has to be continuous at the junction between conductor ($J_{r,\mathrm{c}}(r)$) and insulation ($J_{r,\mathrm{i}}(r)$):

$$J_{r,\mathrm{c}}(r = r_{\mathrm{c}}) = J_{r,\mathrm{i}}(r = r_{\mathrm{c}}) \Leftrightarrow -\lambda_{\mathrm{c}} \frac{\partial T_{\mathrm{cond}}}{\partial r}(r = r_{\mathrm{c}}) = -\lambda_{\mathrm{i}} \frac{\partial T_{\mathrm{insu}}}{\partial r}(r = r_{\mathrm{c}}). \tag{5.20}$$

In the conductor, there should be no kinks in the temperature curve, because this would represent an unphysical behavior. Due to the radial symmetry, the following condition must therefore apply in the center of the conductor:

$$\frac{\partial T_{\mathrm{cond}}}{\partial r}(r = 0) = 0. \tag{5.21}$$

At a surface, the heat flux density

$$\boldsymbol{J} = \frac{1}{\mathcal{A}} P \boldsymbol{n}_{\mathcal{A}} = \alpha (T_{\mathrm{s},1} - T_{\mathrm{s},2}) \boldsymbol{n}_{\mathcal{A}} \tag{5.22}$$

depends on the heat transfer coefficient α as well as the area $\mathcal{A}$ and the temperatures $T_{\mathrm{s},1}$ and $T_{\mathrm{s},2}$ of the media involved, where $\boldsymbol{n}_{\mathcal{A}}$ indicates the direction of the heat flux. Thus, at the surface of the insulation, the heat flux density in the radial direction is

$$J_{r,\mathrm{i}}(r = r_{\mathrm{i}}) = \boldsymbol{J}\boldsymbol{e}_r = \alpha \left(T_{\mathrm{insu}}(r = r_{\mathrm{i}}) - T_{\mathrm{e}} \right) = \alpha (T_{\mathrm{s}} - T_{\mathrm{e}}). \tag{5.23}$$

Here, $T_{\mathrm{insu}}(r)$ is the insulation temperature, so at the surface ($r = r_{\mathrm{i}}$) it just gives the cable surface temperature $T_{\mathrm{s}} = T_{\mathrm{insu}}(r = r_{\mathrm{i}})$. On the other hand, this heat flux density can also be

calculated from the derivative of the insulation temperature:

$$J_{r,\mathrm{i}}(r = r_\mathrm{i}) = -\lambda_\mathrm{i} \frac{\partial T_\mathrm{insu}}{\partial r}(r = r_\mathrm{i}) = \alpha(T_\mathrm{s} - T_\mathrm{e}). \tag{5.24}$$

c) Conductor

For the conductor the heat equation is

$$c_\mathrm{c} \frac{\partial T_\mathrm{cond}(r)}{\partial t} - \lambda_\mathrm{c} \left(\frac{1}{r} \frac{\partial}{\partial r} \left(r \frac{\partial T_\mathrm{cond}(r)}{\partial r} \right) + \frac{\partial^2 T_\mathrm{cond}(r)}{\partial z^2} \right) = \dot{\omega}_\mathrm{cond}. \tag{5.25}$$

A positive value of $\dot{\omega}_\mathrm{cond}$ corresponds to heat input. Formally, heat conduction (mediated by the thermal conductivity of the conductor λ_c) and the heating of the material (capacitance, mediated by the specific heat capacity per volume of the conductor c_c) in the conductor are coupled. Modeling in an ECD would therefore require an infinite sequence of infinitesimal RC elements in the radial direction. Here, however, a reduction to one resistor and one capacitance only is searched, which effectively equals a separation of the two effects. Since only the temperature at the junction between the conductor and the insulation, i.e. at the point $r = r_\mathrm{c}$, is considered later, it is assumed that the complete capacitance of the conductor becomes effective at this point. Moreover, due to the high thermal conductivity of the conductor material, the resistance in the radial direction becomes very small. For vanishing resistance, the assumption of an equivalent capacitance at the junction between conductor and insulation is even exact. Therefore,

$$\frac{\partial T_\mathrm{cond}(r)}{\partial t} \approx \frac{\partial T_\mathrm{sw}}{\partial t}, \quad T_\mathrm{sw} = T_\mathrm{cond}(r = r_\mathrm{c}) \tag{5.26}$$

is assumed. An analog procedure can also be applied for the derivative in z-direction: For the case of very high conductivity in the conductor material, an almost uniform temperature distribution will occur radially and stronger temperature variations will be observed in the axial direction due to the significantly different size ratios (conductor length[8] $\mathcal{L} \gg$ conductor radius r_c). As an approximation, the z-dependence can thus be evaluated at an arbitrary but fixed position in the radial direction. Since only the position $r = r_\mathrm{c}$ is of interest later, i.e. the transition between conductor and insulation, this position is directly used here as an approximation:

$$\frac{\partial^2 T_\mathrm{cond}(r)}{\partial z^2} \approx \frac{\partial^2 T_\mathrm{sw}}{\partial z^2}. \tag{5.27}$$

Thus, in this case, the heat equation becomes

$$\lambda_\mathrm{c} \frac{\partial}{\partial r} \left(r \frac{\partial T_\mathrm{cond}(r)}{\partial r} \right) = r c_\mathrm{c} \frac{\partial T_\mathrm{sw}}{\partial t} - r \lambda_\mathrm{c} \frac{\partial^2 T_\mathrm{sw}}{\partial z^2} - r \dot{\omega}_\mathrm{cond}. \tag{5.28}$$

[8] In this thesis, $\mathcal{L}$ describes the cable length, whereas L is an inductance.

Applying separation of variables and the assumption that $\dot{\omega}_{\mathrm{cond}}$ is constant over the conductor cross-section, it follows for the derivative of the conductor temperature in radial direction:

$$\lambda_{\mathrm{c}} \frac{\partial T_{\mathrm{cond}}(r)}{\partial r} = \frac{\kappa_{1,\mathrm{c}}}{r} + \frac{c_{\mathrm{c}}}{2} r \frac{\partial T_{\mathrm{sw}}}{\partial t} - \frac{\lambda_{\mathrm{c}}}{2} r \frac{\partial^2 T_{\mathrm{sw}}}{\partial z^2} - \frac{1}{2} r \dot{\omega}_{\mathrm{cond}} \tag{5.29}$$

with the integration constant $\kappa_{1,\mathrm{c}}$. Performing a second integration leads to

$$\lambda_{\mathrm{c}} T_{\mathrm{cond}}(r) = \kappa_{2,\mathrm{c}} + \kappa_{1,\mathrm{c}} \ln(r) + \frac{c_{\mathrm{c}}}{4} r^2 \frac{\partial T_{\mathrm{sw}}}{\partial t} - \frac{\lambda_{\mathrm{c}}}{4} r^2 \frac{\partial^2 T_{\mathrm{sw}}}{\partial z^2} - \frac{1}{4} r^2 \dot{\omega}_{\mathrm{cond}} \tag{5.30}$$

with the second integration constant $\kappa_{2,\mathrm{c}}$. With equation (5.21) it follows

$$\kappa_{1,\mathrm{c}} = 0. \tag{5.31}$$

In addition, equation (5.26) leads to

$$\kappa_{2,\mathrm{c}} = \lambda_{\mathrm{c}} T_{\mathrm{sw}} + \frac{1}{4} r_{\mathrm{c}}^2 \dot{\omega}_{\mathrm{cond}} - \frac{c_{\mathrm{c}}}{4} r_{\mathrm{c}}^2 \frac{\partial T_{\mathrm{sw}}}{\partial t} + \frac{\lambda_{\mathrm{c}}}{4} r_{\mathrm{c}}^2 \frac{\partial^2 T_{\mathrm{sw}}}{\partial z^2}. \tag{5.32}$$

In total, the radially dependent conductor temperature is

$$T_{\mathrm{cond}}(r) = T_{\mathrm{sw}} + \frac{1}{4\lambda_{\mathrm{c}}} \left(r_{\mathrm{c}}^2 - r^2\right) \dot{\omega}_{\mathrm{cond}} - \frac{c_{\mathrm{c}}}{4\lambda_{\mathrm{c}}} \left(r_{\mathrm{c}}^2 - r^2\right) \frac{\partial T_{\mathrm{sw}}}{\partial t} + \frac{1}{4} \left(r_{\mathrm{c}}^2 - r^2\right) \frac{\partial T_{\mathrm{sw}}}{\partial z^2} \tag{5.33}$$

and its derivative is

$$\frac{\partial T_{\mathrm{cond}}(r)}{\partial r} = \frac{c_{\mathrm{c}}}{2\lambda_{\mathrm{c}}} r \frac{\partial T_{\mathrm{sw}}}{\partial t} - \frac{r}{2} \frac{\partial^2 T_{\mathrm{sw}}}{\partial z^2} - \frac{1}{2\lambda_{\mathrm{c}}} r \dot{\omega}_{\mathrm{cond}}. \tag{5.34}$$

d) Insulation

In contrast to the conductor, no heat source is assumed in the insulation, so the heat equation for the radially dependent insulation temperature $T_{\mathrm{insu}}(r)$ is reduced to

$$c_{\mathrm{i}} \frac{\partial T_{\mathrm{insu}}(r)}{\partial t} - \lambda_{\mathrm{i}} \left(\frac{1}{r} \frac{\partial}{\partial r} \left(r \frac{\partial T_{\mathrm{insu}}(r)}{\partial r} \right) + \frac{\partial^2 T_{\mathrm{insu}}(r)}{\partial z^2} \right) = 0. \tag{5.35}$$

c_{i} is the specific heat capacity per volume of the insulation material. Due to the low thermal conductivity λ_{i} of the insulation compared to the conductor, the heat flow in the insulation in the z direction is neglected:

$$\frac{\partial^2 T_{\mathrm{insu}}(r)}{\partial z^2} \approx 0. \tag{5.36}$$

Similar to the conductor, heat conduction and heating of the material are formally coupled in the insulation. For a reduction to a single resistor and a single capacitance, these two effects must be decoupled. Because later the temperature at the transition between conductor and

insulation is particularly relevant, the assumption is made that the entire capacitance of the insulation is already effective at the transition between conductor and insulation. Thus,

$$\frac{\partial T_{\mathrm{insu}}(r)}{\partial t} \approx \frac{\partial T_{\mathrm{sw}}}{\partial t} \tag{5.37}$$

is used. Then, from the heat equation, it follows

$$c_{\mathrm{i}} \frac{\partial T_{\mathrm{sw}}}{\partial t} - \lambda_{\mathrm{i}} \frac{1}{r} \frac{\partial}{\partial r} \left(r \frac{\partial T_{\mathrm{insu}}(r)}{\partial r} \right) = 0. \tag{5.38}$$

In the first step, an expression for the derivative of the insulation temperature can be determined by applying the separation of variables:

$$\lambda_{\mathrm{i}} \frac{\partial T_{\mathrm{insu}}(r)}{\partial r} = \frac{\kappa_{1,\mathrm{i}}}{r} + \frac{c_{\mathrm{i}}}{2} r \frac{\partial T_{\mathrm{sw}}}{\partial t}. \tag{5.39}$$

With equation (5.24) the integration constant $\kappa_{1,\mathrm{i}}$ is determined:

$$\kappa_{1,\mathrm{i}} = r_{\mathrm{i}} \alpha (T_{\mathrm{e}} - T_{\mathrm{s}}) - \frac{c_{\mathrm{i}}}{2} r_{\mathrm{i}}^2 \frac{\partial T_{\mathrm{sw}}}{\partial t}. \tag{5.40}$$

Inserting this leads to

$$\lambda_{\mathrm{i}} \frac{\partial T_{\mathrm{insu}}(r)}{\partial r} = \frac{r_{\mathrm{i}}}{r} \alpha (T_{\mathrm{e}} - T_{\mathrm{s}}) + \frac{c_{\mathrm{i}}}{2} \left(r - \frac{r_{\mathrm{i}}^2}{r} \right) \frac{\partial T_{\mathrm{sw}}}{\partial t}. \tag{5.41}$$

Using again that the complete insulation capacitance is already effective at the inner insulation radius ($r = r_{\mathrm{c}}$) allows the following simplification:

$$\frac{c_{\mathrm{i}}}{2} \left(r - \frac{r_{\mathrm{i}}^2}{r} \right) \frac{\partial T_{\mathrm{sw}}}{\partial t} \approx \frac{c_{\mathrm{i}}}{2} \left(r_{\mathrm{c}} - \frac{r_{\mathrm{i}}^2}{r_{\mathrm{c}}} \right) \frac{\partial T_{\mathrm{sw}}}{\partial t}. \tag{5.42}$$

After a second integration, it follows for the insulation temperature:

$$\lambda_{\mathrm{i}} T_{\mathrm{insu}}(r) = \kappa_{2,\mathrm{i}} + r_{\mathrm{i}} \alpha \ln(r) (T_{\mathrm{e}} - T_{\mathrm{s}}) + \frac{c_{\mathrm{i}}}{2} \left(r_{\mathrm{c}} - \frac{r_{\mathrm{i}}^2}{r_{\mathrm{c}}} \right) r \frac{\partial T_{\mathrm{sw}}}{\partial t} \tag{5.43}$$

with the integration constant $\kappa_{2,\mathrm{i}}$. Using $r = r_{\mathrm{c}}$ for the capacitance-related term leads to

$$T_{\mathrm{insu}}(r) = \frac{\kappa_{2,\mathrm{i}}}{\lambda_{\mathrm{i}}} + \frac{r_{\mathrm{i}} \alpha}{\lambda_{\mathrm{i}}} \ln(r) (T_{\mathrm{e}} - T_{\mathrm{s}}) + \frac{c_{\mathrm{i}}}{2\lambda_{\mathrm{i}}} \left(r_{\mathrm{c}}^2 - r_{\mathrm{i}}^2 \right) \frac{\partial T_{\mathrm{sw}}}{\partial t}. \tag{5.44}$$

Therefore, the surface temperature T_{s} is

$$T_{\mathrm{s}} = T_{\mathrm{insu}}(r = r_{\mathrm{i}}) = \frac{\kappa_{2,\mathrm{i}}}{\lambda_{\mathrm{i}}} + \frac{r_{\mathrm{i}} \alpha}{\lambda_{\mathrm{i}}} (T_{\mathrm{e}} - T_{\mathrm{s}}) \ln(r_{\mathrm{i}}) + \frac{c_{\mathrm{i}}}{2\lambda_{\mathrm{i}}} \left(r_{\mathrm{c}}^2 - r_{\mathrm{i}}^2 \right) \frac{\partial T_{\mathrm{sw}}}{\partial t} \tag{5.45}$$

and the temperature at the transition to the conductor is

$$T_{\mathrm{sw}} = T_{\mathrm{insu}}(r = r_{\mathrm{c}}) = \frac{\kappa_{2,\mathrm{i}}}{\lambda_{\mathrm{i}}} + \frac{r_{\mathrm{i}}\alpha}{\lambda_{\mathrm{i}}}(T_{\mathrm{e}} - T_{\mathrm{s}})\ln(r_{\mathrm{c}}) + \frac{c_{\mathrm{i}}}{2\lambda_{\mathrm{i}}}\left(r_{\mathrm{c}}^2 - r_{\mathrm{i}}^2\right)\frac{\partial T_{\mathrm{sw}}}{\partial t}. \tag{5.46}$$

Using equation (5.46), $\kappa_{2,\mathrm{i}}$ is calculated:

$$\kappa_{2,\mathrm{i}} = \lambda_{\mathrm{i}} T_{\mathrm{sw}} - r_{\mathrm{i}}\alpha(T_{\mathrm{e}} - T_{\mathrm{s}})\ln(r_{\mathrm{c}}) - \frac{c_{\mathrm{i}}}{2}\left(r_{\mathrm{c}}^2 - r_{\mathrm{i}}^2\right)\frac{\partial T_{\mathrm{sw}}}{\partial t}. \tag{5.47}$$

The difference between surface and conductor temperature then results in a linear relationship between the two temperatures:

$$T_{\mathrm{s}} = \frac{1}{1 + \frac{r_{\mathrm{i}}\alpha}{\lambda_{\mathrm{i}}}\ln\left(\frac{r_{\mathrm{i}}}{r_{\mathrm{c}}}\right)} T_{\mathrm{sw}} + \frac{\frac{r_{\mathrm{i}}\alpha}{\lambda_{\mathrm{i}}}\ln\left(\frac{r_{\mathrm{i}}}{r_{\mathrm{c}}}\right)}{1 + \frac{r_{\mathrm{i}}\alpha}{\lambda_{\mathrm{i}}}\ln\left(\frac{r_{\mathrm{i}}}{r_{\mathrm{c}}}\right)} T_{\mathrm{e}}, \tag{5.48}$$

which leads to a formulation for the insulation temperature and its derivative as a function of the conductor temperature rather than the surface temperature:

$$T_{\mathrm{insu}}(r) = \frac{1 + \frac{r_{\mathrm{i}}\alpha}{\lambda_{\mathrm{i}}}\ln\left(\frac{r_{\mathrm{i}}}{r}\right)}{1 + \frac{r_{\mathrm{i}}\alpha}{\lambda_{\mathrm{i}}}\ln\left(\frac{r_{\mathrm{i}}}{r_{\mathrm{c}}}\right)} T_{\mathrm{sw}} + \frac{\frac{r_{\mathrm{i}}\alpha}{\lambda_{\mathrm{i}}}\ln\left(\frac{r}{r_{\mathrm{c}}}\right)}{1 + \frac{r_{\mathrm{i}}\alpha}{\lambda_{\mathrm{i}}}\ln\left(\frac{r_{\mathrm{i}}}{r_{\mathrm{c}}}\right)} T_{\mathrm{e}}, \tag{5.49}$$

$$\frac{\partial T_{\mathrm{insu}}(r)}{\partial r} = \frac{1}{r}\frac{\frac{r_{\mathrm{i}}\alpha}{\lambda_{\mathrm{i}}}}{1 + \frac{r_{\mathrm{i}}\alpha}{\lambda_{\mathrm{i}}}\ln\left(\frac{r_{\mathrm{i}}}{r_{\mathrm{c}}}\right)}(T_{\mathrm{e}} - T_{\mathrm{sw}}) - \frac{c_{\mathrm{i}}}{2\lambda_{\mathrm{i}}}\left(\frac{r_{\mathrm{i}}^2}{r} - r\right)\frac{\partial T_{\mathrm{sw}}}{\partial t}. \tag{5.50}$$

e) Thermal Transmission Line Equation

In the remaining condition for the continuity of the heat flow at the transition between the conductor and the insulation (see equation (5.20)), the expressions derived above for the derivative of the temperatures (see equations (5.34) and (5.50)) are inserted. Rearranging then provides the differential equation for the present case:

$$\begin{aligned} &\frac{1}{R'}\frac{\partial^2 T_{\mathrm{sw}}(z,t)}{\partial z^2} - \mathcal{C}'\frac{\partial T_{\mathrm{sw}}(z,t)}{\partial t} - G' T_{\mathrm{sw}}(z,t) = -\left(G' T_{\mathrm{e}} + P'_{\mathrm{el}}\right) \\ \Leftrightarrow\ &\frac{\partial^2 T_{\mathrm{sw}}(z,t)}{\partial z^2} - A_{\mathrm{sw}}\frac{\partial T_{\mathrm{sw}}(z,t)}{\partial t} - B_{\mathrm{sw}} T_{\mathrm{sw}}(z,t) = C_{\mathrm{sw}}. \end{aligned} \tag{5.51}$$

Here, the cable parameters $\mathcal{C}'$, R', G', and P'_{el}, which are explained in detail in the following subsection, and the following substitutes are introduced:

$$A_{\mathrm{sw}} = R'\mathcal{C}', \qquad B_{\mathrm{sw}} = R'G', \qquad C_{\mathrm{sw}} = -R'\left(P'_{\mathrm{el}} + G' T_{\mathrm{e}}\right). \tag{5.52}$$

An equivalent formulation for this PDE connects the axial heat flow $P(z,t)$ with the temperature:

$$\begin{aligned} \frac{\partial T_{\mathrm{sw}}(z,t)}{\partial z} + R' P(z,t) &= 0, \\ \frac{\partial P(z,t)}{\partial z} + \mathcal{C}' \frac{\partial T_{\mathrm{sw}}(z,t)}{\partial t} + G' T_{\mathrm{sw}}(z,t) &= P'_{\mathrm{el}} + G' T_{\mathrm{e}}. \end{aligned} \tag{5.53}$$

5.2.2 Parameter Calculation

By inserting equations (5.34) and (5.50) into equation (5.20) and comparing them with the differential equation (5.51), the parameters $\mathcal{C}'$, R', G', and P'_{el} can directly be identified. The following presentation of the corresponding calculation formulas is based on the presentation in [A.3].

Using the specific heat capacities per volume of the conductor (c_{c}) and insulation (c_{i}) material and the volume filled with the materials, the thermal per unit length capacitances for the conductor ($\mathcal{C}'_{\mathrm{c}}$) and the insulation ($\mathcal{C}'_{\mathrm{i}}$) are calculated:

$$\mathcal{C}'_{\mathrm{c}} = c_{\mathrm{c}} \pi r_{\mathrm{c}}^2, \quad \mathcal{C}'_{\mathrm{i}} = c_{\mathrm{i}} \pi \left(r_{\mathrm{i}}^2 - r_{\mathrm{c}}^2 \right). \tag{5.54}$$

Both of those capacitances are summed up in one complete cable capacitance $\mathcal{C}'$:

$$\mathcal{C}' = \mathcal{C}'_{\mathrm{c}} + \mathcal{C}'_{\mathrm{i}}. \tag{5.55}$$

The thermal per unit length resistance

$$R'_{\mathrm{i}} = \frac{\ln\left(\frac{r_{\mathrm{i}}}{r_{\mathrm{c}}}\right)}{2\pi\lambda_{\mathrm{i}}} \tag{5.56}$$

is used to model the heat flow through the insulation. The thermal per unit length resistance

$$R'_{\alpha}(T_{\mathrm{s}}) = \frac{1}{2\pi r_{\mathrm{i}} \alpha(T_{\mathrm{s}})} \tag{5.57}$$

models the heat transfer between the cable surface and the environment. The necessary heat transfer coefficient

$$\alpha(T_{\mathrm{s}}) = \alpha_{\mathrm{rad}}(T_{\mathrm{s}}) + \alpha_{\mathrm{conv}}(T_{\mathrm{s}}) \tag{5.58}$$

consists of a part to mention radiation (α_{rad}) and a second part for convection (α_{conv}). The heat transfer coefficient for free convection in the air is calculated via

$$\alpha_{\mathrm{conv}}(T_{\mathrm{s}}) = \frac{\mathrm{Nu}(T_{\mathrm{s}}) \cdot \lambda_{\mathrm{air}}(T_{\mathrm{s}})}{l_{\alpha}} \tag{5.59}$$

with the thermal conductivity of air λ_{air}, the characteristic length of the cable $l_{\alpha} = 2r_{\mathrm{i}}$, and

the Nusselt number for a horizontal cylinder freely in the air [140]

$$\mathrm{Nu}(T_\mathrm{s}) = \left(0.6 + \frac{0.387 \cdot \mathrm{Ra}(T_\mathrm{s})^{\frac{1}{6}}}{\left(1 + \left(\frac{0.559}{\mathrm{Pr}(T_\mathrm{s})}\right)^{\frac{9}{16}}\right)^{\frac{8}{27}}} \right)^2 . \tag{5.60}$$

Here, Pr is the Prandtl number and

$$\mathrm{Ra}(T_\mathrm{s}) = \mathrm{Gr}(T_\mathrm{s}) \cdot \mathrm{Pr}(T_\mathrm{s}) \tag{5.61}$$

is the Rayleigh number. The Grashof number Gr is calculated via

$$\mathrm{Gr}(T_\mathrm{s}) = \frac{g l_\alpha^3 \left|T_\mathrm{s} - T_\mathrm{e}\right|}{T_\mathrm{e,K} \nu_\mathrm{air}^2(T_\mathrm{s})} \tag{5.62}$$

using the environmental air temperature (T_e in $^\circ\mathrm{C}$ and $T_\mathrm{e,K}$ in K), the gravity of earth $g = 9.81\,\mathrm{m/s^2}$, and the kinematic viscosity ν_air [140].

Values for the material parameters λ_air, ν_air, and Pr are given in form of tables for example in [138, pp. 197-198]. In this thesis, the following fourth-degree polynomial approximations of those table data for dry air and pressure of $1\,\mathrm{bar}$ are used:

$$\frac{\nu_\mathrm{air}}{1\,\frac{\mathrm{m^2}}{\mathrm{s}}} = 1.77 \cdot 10^{-17} T_\mathrm{m}^4 - 4.83 \cdot 10^{-14} T_\mathrm{m}^3 + 1.14 \cdot 10^{-10} T_\mathrm{m}^2 + 8.81 \cdot 10^{-8} T_\mathrm{m} + 1.35 \cdot 10^{-5}, \tag{5.63}$$

$$\mathrm{Pr} = 2.23 \cdot 10^{-13} T_\mathrm{m}^4 - 6.27 \cdot 10^{-10} T_\mathrm{m}^3 + 5.91 \cdot 10^{-7} T_\mathrm{m}^2 - 1.58 \cdot 10^{-4} T_\mathrm{m} + 0.711, \tag{5.64}$$

$$\frac{\lambda_\mathrm{air}}{1\,\frac{\mathrm{W}}{\mathrm{Km}}} = -1.35 \cdot 10^{-14} T_\mathrm{m}^4 + 3.64 \cdot 10^{-11} T_\mathrm{m}^3 - 4.33 \cdot 10^{-8} T_\mathrm{m}^2 + 7.7 \cdot 10^{-5} T_\mathrm{m} + 2.43 \cdot 10^{-2}. \tag{5.65}$$

T_m is the value of the mean temperature of the cable surface temperature and the environmental temperature:

$$T_\mathrm{m}(T_\mathrm{s}) = \frac{0.5(T_\mathrm{s} + T_\mathrm{e})}{1\,^\circ\mathrm{C}}. \tag{5.66}$$

For the calculation of the heat transfer coefficient for radiation

$$\alpha_\mathrm{rad}(T_\mathrm{s}) = \varepsilon\sigma \left(T_\mathrm{s,K} + T_\mathrm{e,K}\right) \cdot \left(T_\mathrm{s,K}^2 + T_\mathrm{e,K}^2\right) \tag{5.67}$$

the absolute cable surface temperature in Kelvin $T_{\mathrm{s,K}}$ and the emissivity of the insulation surface ε (the value 0.95 is used in this thesis [141]) are needed. $\sigma \approx 5.6704{\cdot}10^{-8}\,\mathrm{W/(m^2K^4)}$ is the Stefan-Boltzmann constant. The conductance G' is calculated via

$$G'(T_{\mathrm{s}}) = \frac{1}{R'_{\mathrm{i}} + R'_{\alpha}(T_{\mathrm{s}})} \tag{5.68}$$

and thus depends on the cable surface temperature. For the calculation of the heat source P'_{el}, due to the relatively small temperature rises that are assumed in this thesis, a linearly temperature-dependent electrical conductor resistance [142, p. 99] is assumed:

$$P'_{\mathrm{el}}(T_{\mathrm{sw}}) = \pi r_{\mathrm{c}}^2 \dot{\omega}_{\mathrm{cond}} = I^2 R'_{\mathrm{ref}} \left(1 + \eta_T \left(T_{\mathrm{sw}} - T_{\mathrm{ref}}\right)\right). \tag{5.69}$$

η_T is the linear temperature coefficient for the conductor's conductivity and R'_{ref} is the electrical per unit length resistance at the reference temperature T_{ref}. The axial thermal per unit length resistance R' is calculated via

$$R' = \frac{1}{\lambda_{\mathrm{c}} \pi r_{\mathrm{c}}^2}. \tag{5.70}$$

5.2.3 Thermal Equivalent Circuit Diagram

In the electrical domain, an ECD for an infinitesimally short cable segment (length $\mathrm{d}z \to 0$) can be found that directly corresponds to the differential equation and provides the same information. This ECD can be regarded as an alternate descriptive representation form of the mathematical model (differential equation). Equivalently, in the thermal domain, based on the PDE a corresponding thermal ECD can be found that also allows a more intuitive interpretation of the basic model. Comparing equation (3.2) from the electrical domain with the thermal formulation (see equation (5.53)) directly leads from the electrical ECD (see figure 3.2) to the corresponding thermal ECD shown in figure 5.2. All per unit length quantities, marked with an upstroke, have to be multiplied by the segment length. Here and in the following, this multiplication is neglected in the ECDs for the sake of clarity.

In this circuit, the assumptions from the theoretical derivation of the PDE can be found again. In addition, the influence of the different physical layers can directly be observed in

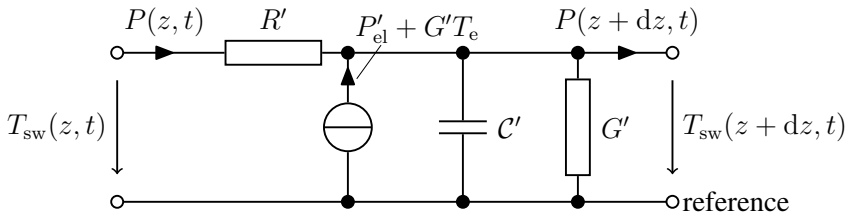

Figure 5.2: ECD for an infinitesimally short segment of a single wire cable.

this representation: Due to the finite electrical cable resistance, an electrical current flowing through the cable will always cause electrical losses in form of heat. This heat is impressed on the conductor and modeled by the heat source P'_{el}. All parts of the cable, in this case, conductor and insulation material, can store heat and thus, heat up. The heat storage capacity of the cable is represented using the thermal capacitances $\mathcal{C}'_{\mathrm{c}}$ and $\mathcal{C}'_{\mathrm{i}}$, which are summed up to the capacitance $\mathcal{C}'$. This complete capacitance is connected to the conductor temperature node, which shows again the assumption from above: The complete insulation capacitance is assumed directly at the connection between conductor and insulation. The insulation sets the resistance R'_{i} against a radial heat flow. This resistance causes different inner and outer insulation surface temperatures. For the conductor, typically, the thermal conductivity is significantly higher (three orders) than the thermal conductivity of the insulation [73]. That is why the appearing radial temperature differences in the conductor are very small and thus, neglected in this thesis. So, there is no radial resistance for the conductor in the ECD. The heat flow between the cable surface and the environment (here: air) is represented in the resistance R'_{α}. R'_{i} and R'_{α} are combined to find the conductance G'. The resistance R' describes the axial heat flow in the conductor (which is not negligible unlike the radial heat flow in the conductor due to the much higher cable length in comparison with the cable radius). Due to the already mentioned relationship between the thermal conductivities, the axial heat flow in the insulation material is not directly considered (infinite resistance), but only indirectly modeled via the path through the conductor.

5.3 Multiconductor Transmission Line Theory

In this section, more complex cable arrangements are analyzed. In the first step, the formulation known from the electrical domain is used to set up an ECD as well as the corresponding system of PDEs in the thermal domain. In the next step, the limitations of this analogy are discussed and an expansion is presented to find a more general thermal formulation.

5.3.1 Analogy to the Electrical Domain

In the electrical domain, the corresponding ECD for an arrangement of multiple cables is given in figure 3.3. From this, the thermal ECD in figure 5.3 is derived by setting the inductances as well as the voltage sources to zero. Furthermore, the capacitances between the individual cables are zero, as thermal capacitances always refer to the reference temperature [139]. Analogously, the associated differential equations are set up. In analogy to equation (3.3), the system of coupled PDEs for the temperatures $\boldsymbol{T}$ and heat flows $\boldsymbol{P}$ is

$$\begin{aligned} \frac{\partial \boldsymbol{T}(z,t)}{\partial z} + \mathbf{R}'\boldsymbol{P}(z,t) &= \mathbf{0}, \\ \frac{\partial \boldsymbol{P}(z,t)}{\partial z} + \mathbf{C}'\frac{\partial \boldsymbol{T}(z,t)}{\partial t} + \mathbf{G}'\boldsymbol{T}(z,t) &= \boldsymbol{P}'_{\mathrm{el}} + \mathbf{G}'\left(T_{\mathrm{e}} \dots T_{\mathrm{e}}\right)^{T}. \end{aligned} \tag{5.71}$$

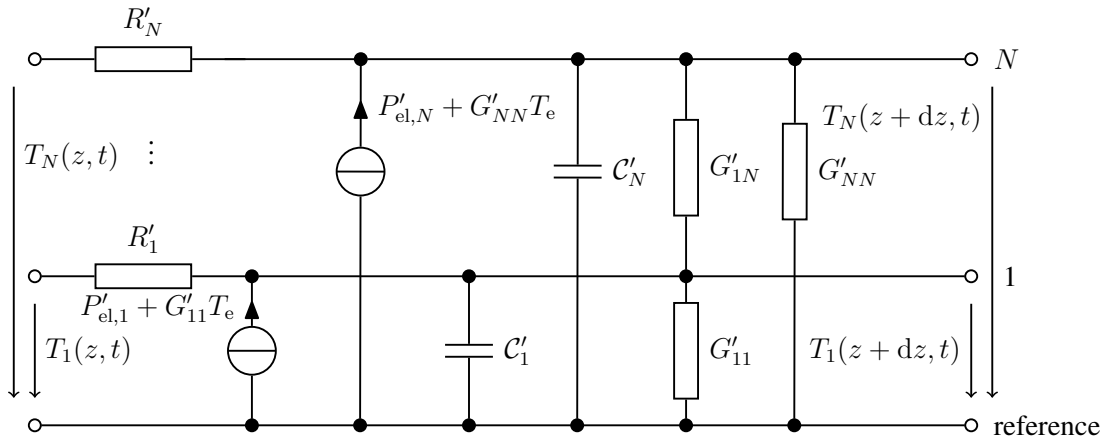

Figure 5.3: Electrical ECD for an infinitesimally short segment of a multiconductor arrangement (N conductors).

The cable properties are described by the matrices $\mathbf{R}'$, $\mathbf{C}'$, $\mathbf{G}'$, and the vector $\boldsymbol{P}'_\mathrm{el}$. The corresponding formulation only for the cable temperatures (as in equation (3.4) for the electrical domain) is as follows:

$$\begin{aligned} &\frac{\partial^2 \boldsymbol{T}(z,t)}{\partial z^2} - \mathbf{R}'\mathbf{C}'\frac{\partial \boldsymbol{T}(z,t)}{\partial t} - \mathbf{R}'\mathbf{G}'\boldsymbol{T}(z,t) = -\mathbf{R}'\left(\boldsymbol{P}'_\mathrm{el} + \mathbf{G}'\begin{pmatrix} T_\mathrm{e} \\ \vdots \\ T_\mathrm{e} \end{pmatrix}\right) \\ &\Leftrightarrow \frac{\partial^2 \boldsymbol{T}(z,t)}{\partial z^2} - \mathbf{A}\frac{\partial \boldsymbol{T}(z,t)}{\partial t} - \mathbf{B}\boldsymbol{T}(z,t) = \boldsymbol{C}. \end{aligned} \tag{5.72}$$

In the electrical domain, the matrix $\mathbf{C}'_\mathrm{el}$ has diagonal and non-diagonal entries. In contrast, in the thermal domain, the matrix $\mathbf{C}'$ is diagonal because as mentioned already thermal capacitances always refer to the reference temperature, and the individual conductors only couple via a resistance, not via a capacitance. So the thermal matrix shows a simpler overall structure than the general electrical matrix.

5.3.2 Limitations of the Analogy and General Problem Formulation

The problem formulation from the previous section describes the cable temperatures at specific cross-sectional points (“nodes”). At those temperature nodes, the axial heat conduction is considered and, in addition, a thermal capacitance is placed. This leads to the appearance of both derivatives (time and spatial). Nevertheless, for example, the coupling between a cable and the environment depends on the cable surface temperature, which does not appear in the above formulation until now. Thus, an expansion is proposed here that allows the consideration of additional temperatures:

$$\tilde{\mathbf{D}}\frac{\partial^2 \tilde{\boldsymbol{T}}(z,t)}{\partial z^2} - \tilde{\mathbf{A}}\frac{\partial \tilde{\boldsymbol{T}}(z,t)}{\partial t} - \tilde{\mathbf{B}}\tilde{\boldsymbol{T}}(z,t) = \tilde{\boldsymbol{C}}. \tag{5.73}$$

It has to be mentioned, that both, $\tilde{\mathbf{A}}$ and $\tilde{\mathbf{D}}$ are diagonal matrices. For a problem that can be formulated equivalently to the electrical domain only two types of equations appear in this system: On the one hand, PDEs that include both, the first time derivative and the second spatial derivative, and on the other hand, linear equations without any derivatives arise. Then, the temperature vector $\tilde{\boldsymbol{T}}(z,t)$ can be split up into a part with derivatives (**v**ariant, $\boldsymbol{T}$) and a part without derivatives (**l**inear, $\boldsymbol{T}_\mathrm{l}$) by using appropriate matrices (consisting only of zeros and ones) $\mathbf{E}_\mathrm{v}$ for $\boldsymbol{T}$ and $\mathbf{E}_\mathrm{l}$ for $\boldsymbol{T}_\mathrm{l}$:

$$\tilde{\boldsymbol{T}} = \mathbf{E}_\mathrm{v}\boldsymbol{T} + \mathbf{E}_\mathrm{l}\boldsymbol{T}_\mathrm{l}. \tag{5.74}$$

Inserting this into equation (5.73) and multiplying with $\mathbf{E}_\mathrm{l}^T$ leads to a formulation for the linear part:

$$\boldsymbol{T}_\mathrm{l} = -\left(\mathbf{E}_\mathrm{l}^T\tilde{\mathbf{B}}\mathbf{E}_\mathrm{l}\right)^{-1}\mathbf{E}_\mathrm{l}^T\left(\tilde{\mathbf{B}}\mathbf{E}_\mathrm{v}\boldsymbol{T} + \tilde{\boldsymbol{C}}\right). \tag{5.75}$$

Inserting this into $\mathbf{E}_\mathrm{v}^T$ multiplied with equation (5.73) leads to a formulation only for the variant parts equivalent to equation (5.72):

$$\begin{aligned}
\boldsymbol{C} &= \frac{\partial^2\boldsymbol{T}(z,t)}{\partial z^2} - \mathbf{A}\frac{\partial\boldsymbol{T}(z,t)}{\partial t} - \mathbf{B}\boldsymbol{T}(z,t), \\
\hat{\mathbf{D}} &= \mathbf{E}_\mathrm{v}^T\tilde{\mathbf{D}}\mathbf{E}_\mathrm{v}, \quad \mathbf{A} = \hat{\mathbf{D}}^{-1}\mathbf{E}_\mathrm{v}^T\tilde{\mathbf{A}}\mathbf{E}_\mathrm{v}, \\
\mathbf{B} &= \hat{\mathbf{D}}^{-1}\mathbf{E}_\mathrm{v}^T\tilde{\mathbf{B}}\left[\mathbf{E}_\mathrm{v} - \mathbf{E}_\mathrm{l}\left(\mathbf{E}_\mathrm{l}^T\tilde{\mathbf{B}}\mathbf{E}_\mathrm{l}\right)^{-1}\mathbf{E}_\mathrm{l}^T\tilde{\mathbf{B}}\mathbf{E}_\mathrm{v}\right], \\
\boldsymbol{C} &= \hat{\mathbf{D}}^{-1}\mathbf{E}_\mathrm{v}^T\left[-\tilde{\mathbf{B}}\mathbf{E}_\mathrm{l}\left(\mathbf{E}_\mathrm{l}^T\tilde{\mathbf{B}}\mathbf{E}_\mathrm{l}\right)^{-1}\mathbf{E}_\mathrm{l}^T + \mathbf{U}_N\right]\tilde{\boldsymbol{C}}.
\end{aligned} \tag{5.76}$$

The matrix $\hat{\mathbf{D}}$ is diagonal without any zeros at the main diagonal, so $\hat{\mathbf{D}}^{-1}$ can be calculated easily.

This rearranging only works, if zero rows appear simultaneously in $\tilde{\mathbf{A}}$ and $\tilde{\mathbf{D}}$. This is not always the case. As seen before, thermal storage capacitance and thermal conductivity are separated in the model by evaluating only specific radial points. For example, for the insulation layer of a single wire cable, the complete thermal capacitance was positioned at the inner insulation radius. This is an approximation that can only be applied for comparatively slow thermal effects. A better approximation can be found for example by placing one part of the capacitance on the inner side and the rest on the outside, as proposed by Van Wormer [143]. The known ECD from figure 5.2 is rearranged to a new version, see figure 5.4. At the conductor temperature node (green), an axial resistance and a conductance are connected, but at the cable surface (red node), a capacitance is placed, but no axial heat flow is considered. This leads to an entry in the corresponding line in matrix $\tilde{\mathbf{A}}$ but there is no entry in the corresponding line of $\tilde{\mathbf{D}}$. Then, the above-presented reduction would not work any longer and no ECD and PDE directly analog to the electrical domain can be found.

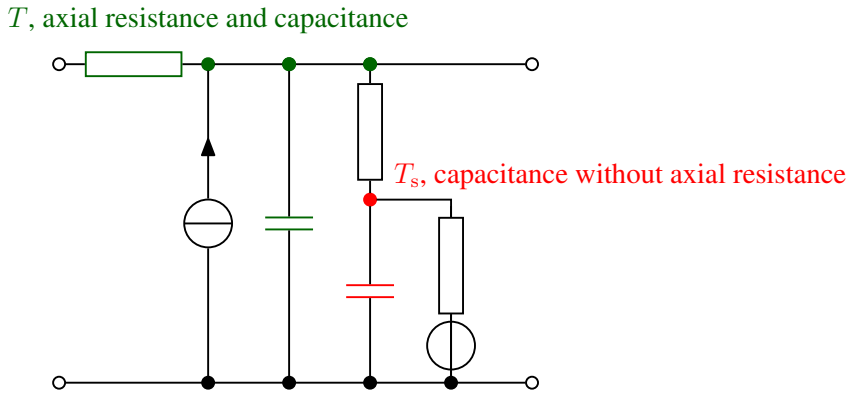

Figure 5.4: Exemplary ECD that cannot be treated equivalently to the electrical domain.

5.3.3 Thermal Equivalent Circuit Diagrams, Partial Differential Equations, and Parameter Calculation

Using a single wire cable, the basic procedure for deriving the thermal TL equation with the necessary assumptions was presented in section 5.2. The approach can be divided into the following steps:

1. Nodal points in the radial direction are defined at which the temperature is to be determined.

2. For all homogeneous layers, the heat conduction equation is integrated twice about r. Assumptions have to be introduced regarding negligible or vanishing dependencies. For example, symmetry considerations or knowledge of the magnitude of the material parameters can be used for this purpose. For the derivatives with regard to z and t, values at specific nodal points are chosen as an approximation. Thus, heat conduction and heat storage capacitance are separated in the radial direction and each is modeled by a concentrated element.

3. Transition and boundary conditions for the elements under consideration are established.

4. Based on these additional conditions, the still unknown constants in the formulation from step 2 are determined and the differential equation is derived.

In principle, this procedure can be transferred to other conductor arrangements. For more complex conductor arrangements, there are more areas for which the temperature is calculated individually. In addition, a higher number of transition and boundary conditions occurs, more assumptions are necessary, and altogether more complex calculations result. In the case of non-concentric structures (e.g. several conductors, an example is shown in figure 5.5), formally, the assumption of symmetry in the φ-direction is no longer tenable and becomes a rough approximation. In this case, additional resistances or conductances are added

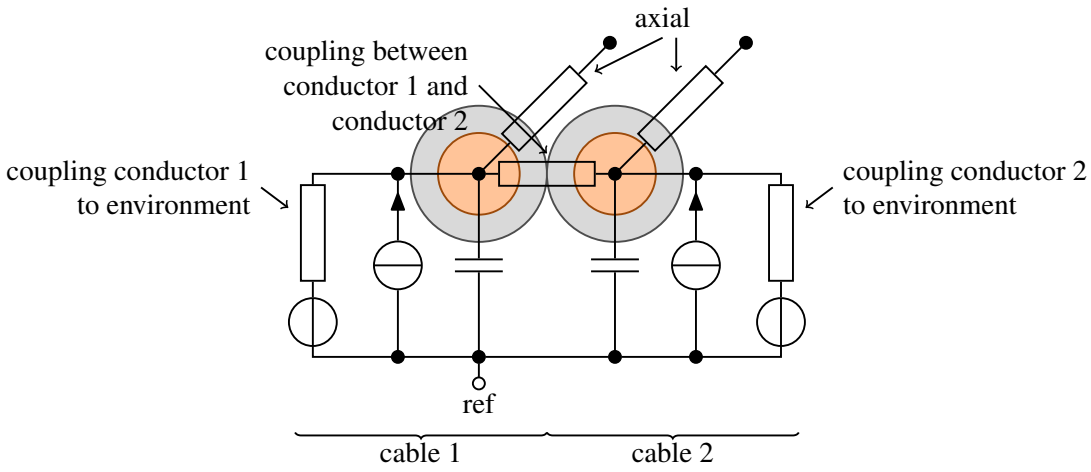

Figure 5.5: Exemplary ECD for the visualization of the treatment of unconcentric cable structures.

to model the coupling between the conductors. These can be understood as integral quantities between both conductors. To avoid a double consideration, an appropriate scaling of some resistances can be used in a later step. This requires assumptions for the area over which the coupling occurs. Overall, the formal mathematical derivation of these coupling resistances is very complex and depends on parameters that are difficult to determine in reality, such as the contact pressure. It is therefore advisable to determine these parameters metrologically for specific arrangements using test measurements. Some approaches for specific cable arrangements are presented in chapter 7.

All in all, the formal mathematical derivation of the PDE for complex conductor arrangements requires many assumptions and a lot of complex calculations. That is why a simpler approach is searched. Remembering the results from the single wire structure, an equivalent presentation form of the PDE was the corresponding ECD, in which the necessary elements could directly be linked to the physical properties of the different cable layers. Extending this understanding of the basic physical properties of the different cable layers, here, a more intuitive approach is presented: Instead of the formal evaluation and integration of the heat equation, the relevant nodes are defined based on the geometrical arrangement for the individual layers and partial ECD diagrams are set up. Via a formalism, that shows similarities with the stamp formalism known from the (modified) nodal analysis from the electrical domain, a system of coupled PDEs is set up, which has the form known from equation (5.73). In the following, for different physical layers, the corresponding formulations are presented. A shielded two-conductor cable is used to exemplarily highlight the modeled nodes.

a) Conductive Layer

The three conductive layers of the exemplary cable are sketched in green in figure 5.6. Such a conductive layer is characterized radially via its per unit length heat capacitance

$$\mathcal{C}'_{\mathrm{c}} = c_{\mathrm{c}} \mathcal{A}_{\mathrm{c}}. \tag{5.77}$$

Here, c_{c} is the specific volumetric heat capacitance of the conductor and $\mathcal{A}_{\mathrm{c}}$ is the cross-section area of the conductor layer. Due to the typically high thermal conductivity compared to typical insulation material conductivities, the thermal resistance in the radial direction is neglected. So, the complete conductor is represented by one radial node m_{c}. Furthermore, an electrical current I_{c} in this conductive structure induces losses that heat the conductor, which is modeled via the heat source

$$P'_{\mathrm{el,c}} = I_{\mathrm{c}}^2 \cdot R'_{\mathrm{ref,c}} \cdot \left(1 + \eta_T \cdot \left(T_{\mathrm{c}} - T_{\mathrm{ref,c}}\right)\right). \tag{5.78}$$

$R'_{\mathrm{ref,c}}$ is the reference resistance, i.e. the electrical resistance of the conductor in the unloaded state at reference temperature $T_{\mathrm{ref,c}}$. η_T is the linear temperature coefficient of the conductor material. A typical value for copper is $\eta_T = 3.93 \cdot 10^{-3}\,1/\mathrm{K}$, which is used throughout this complete thesis. In the axial direction, on the other hand, heat conduction is modeled via the resistance

$$R'_{\mathrm{c}} = \frac{1}{\lambda_{\mathrm{c}} \mathcal{A}_{\mathrm{c}}} \tag{5.79}$$

with the specific thermal conductivity of the conductor material λ_{c}. Combining these three elements provides an ECD component as shown in figure 5.7. The described node m_{c} in the radial direction is split up into two nodes $m_{\mathrm{c},z}$ and $m_{\mathrm{c},z+\mathrm{d}z}$ at different axial positions. As $\mathrm{d}z \to 0$, this reduces to just one radial node m_{c}. Thus, to describe such a layer, the conductor temperature $T_{\mathrm{c}}(z,t)$ is introduced as a variable. In the nodal equation, this yields an expression of the form

$$\frac{1}{R'_{\mathrm{c}}} \frac{\partial^2 T_{\mathrm{c}}}{\partial z^2} = \mathcal{C}'_{\mathrm{c}} \frac{\partial}{\partial t} T_{\mathrm{c}} + P'_{\mathrm{el,c}}. \tag{5.80}$$

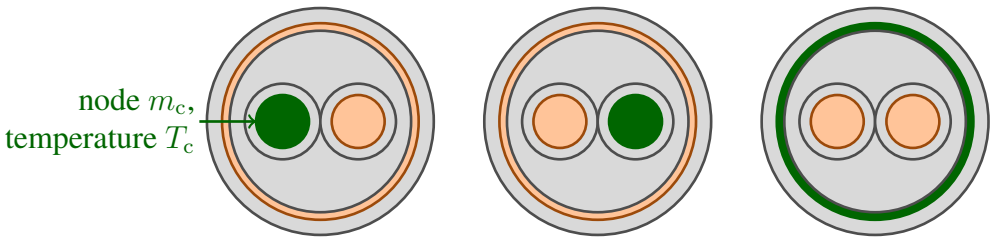

Figure 5.6: Exemplary conductive layers (cross-section, green).

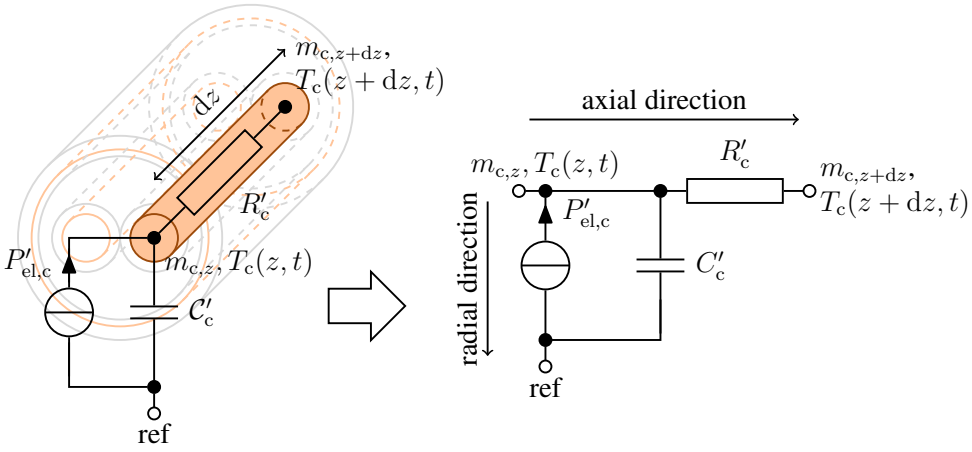

Figure 5.7: ECD for a conductive layer.

b) Concentric Insulation Layer

In contrast to a conductor layer, for a concentric insulation layer, as exemplarily sketched in figure 5.8, the heat conduction and thus the temperature difference between the inside and outside of the insulation plays a role that can no longer be neglected due to the low thermal conductivity. Physically, heat conduction and heat storage cannot be separated. Nevertheless, a modeling approach is chosen in which individual discrete elements are used to describe those two physical effects. Additional correction factors can be necessary to avoid a double consideration of physical effects (see chapter 7). Those are not considered in this section.

Single RC-Structure Usually, it is assumed that the entire capacitance of the insulation structure is already effective on its inner side. Then a single resistance and a single capacitance are sufficient for the description. The total capacitance of the insulation layer can be calculated from the cross-section area $\mathcal{A}_\mathrm{i}$ and the specific heat capacity of the insulation material c_i:

$$\mathcal{C}'_\mathrm{i} = c_\mathrm{i}\mathcal{A}_\mathrm{i} = c_\mathrm{i}\pi\left(r^2_\mathrm{i,out} - r^2_\mathrm{i,in}\right). \tag{5.81}$$

Here $r_\mathrm{i,out}$ represents the outer radius of the considered layer, and $r_\mathrm{i,in}$ is the inner radius. The conductance for the description of the radial heat conduction through this layer is given

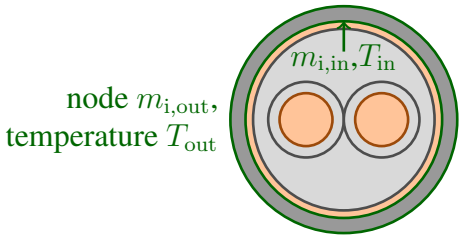

Figure 5.8: Exemplary insulation layer (cross-section).

by

$$G'_{\mathrm{i}} = \frac{2\pi\lambda_{\mathrm{i}}}{\ln\left(\frac{r_{\mathrm{i,out}}}{r_{\mathrm{i,in}}}\right)}, \tag{5.82}$$

where λ_{i} is the specific thermal conductivity of the insulation material. The combination of these two elements provides an ECD component as shown in figure 5.9(a). Thus, to describe such a layer, the temperatures on the inside and outside of the layer are needed as variables. If one or both temperatures are already used as variables (conductor temperatures), correspondingly fewer new unknowns are needed. In the nodal equation for node $m_{\mathrm{i,in}}$, the temperature at the inner side results in an additional expression of the form

$$+ G'_{\mathrm{i}}(T_{\mathrm{in}} - T_{\mathrm{out}}) + \mathcal{C}'_{\mathrm{i}}\frac{\partial T_{\mathrm{in}}}{\partial t}. \tag{5.83}$$

For the outside (node $m_{\mathrm{i,out}}$) a term of the following form results:

$$- G'_{\mathrm{i}}(T_{\mathrm{in}} - T_{\mathrm{out}}). \tag{5.84}$$

Transient processes are partly not modeled accurately due to the drastic assumption of only one equivalent capacitance. For more accurate modeling, the finer modeling proposed in [143] can be used here, in which the capacitance is divided among several positions in the radial direction. Long- and short-term transients are distinguished, depending on whether the transient duration times are greater or lower than

$$\frac{1}{3}R'_{\mathrm{t}}C'_{\mathrm{t}}, \tag{5.85}$$

where C'_{t} is the total thermal per unit length capacitance of the complete cable and R'_{t} is the sum of the radial per unit length resistances of the cable [144].

Van Wormer Capacitances for Long-Term Transients For long-term transients, [143] proposes a division of the capacitances between the inner and outer insulation boundaries, so the portion $p_{\mathrm{i,lo}}\mathcal{C}'_{\mathrm{i}}$ is applied on the inside and the portion $(1 - p_{\mathrm{i,lo}})\mathcal{C}'_{\mathrm{i}}$ is applied on the outside with

$$p_{\mathrm{i,lo}} = \frac{1}{2\ln\left(\frac{r_{\mathrm{i,out}}}{r_{\mathrm{i,in}}}\right)} - \frac{1}{\left(\frac{r_{\mathrm{i,out}}}{r_{\mathrm{i,in}}}\right)^2 - 1}. \tag{5.86}$$

The corresponding ECD is shown in figure 5.9(b). The expression for the nodal equation for the temperature on the inside is then given as

$$+ p_{\mathrm{i,lo}}\mathcal{C}'_{\mathrm{i}}\frac{\partial T_{\mathrm{in}}}{\partial t} + G'_{\mathrm{i}}\left(T_{\mathrm{in}} - T_{\mathrm{out}}\right). \tag{5.87}$$

For the outside, there is a term of the form

$$+ G'_{\mathrm{i}}(T_{\mathrm{out}} - T_{\mathrm{in}}) + (1 - p_{\mathrm{i,lo}})\mathcal{C}'_{\mathrm{i}} \frac{\partial T_{\mathrm{out}}}{\partial t}. \tag{5.88}$$

Van Wormer Capacitances for Short Term Transients For short-time transients, according to [143], an additional node is introduced in the insulation layer and the division known from the last section is implemented individually for the inner and outer cylinder shell, resulting in three capacitances. The resistance for heat conduction through the entire insulation layer is divided between the two sublayers accordingly. With

$$\mathcal{C}'_{\mathrm{i,1}} = c_{\mathrm{i}}\pi \left(r_{\mathrm{i,in}} r_{\mathrm{i,out}} - r^2_{\mathrm{i,in}}\right), \tag{5.89}$$

$$\mathcal{C}'_{\mathrm{i,2}} = c_{\mathrm{i}}\pi \left(r^2_{\mathrm{i,out}} - r_{\mathrm{i,in}} r_{\mathrm{i,out}}\right), \tag{5.90}$$

$$p_{\mathrm{i}} = \frac{1}{2\ln\left(\dfrac{r_{\mathrm{i,out}}}{r_{\mathrm{i,in}}}\right)} - \frac{1}{\dfrac{r_{\mathrm{i,out}}}{r_{\mathrm{i,in}}} - 1}, \tag{5.91}$$

the ECD shown in figure 5.9(c) results. All three node temperatures are then required as variables in the representation. For the newly introduced intermediate temperature T_{mid}, the nodal equation is

$$0 = 2G'_{\mathrm{i}}(2T_{\mathrm{mid}} - T_{\mathrm{out}} - T_{\mathrm{in}}) + \left((1 - p_{\mathrm{i}})\mathcal{C}'_{\mathrm{i,1}} + p_{\mathrm{i}}\mathcal{C}'_{\mathrm{i,2}}\right) \frac{\partial T_{\mathrm{mid}}}{\partial t}. \tag{5.92}$$

For the internal insulation temperature T_{in}, the additional expression is

$$+ p_{\mathrm{i}}\mathcal{C}'_{\mathrm{i,1}} \frac{\partial T_{\mathrm{in}}}{\partial t} + 2G'_{\mathrm{i}}(T_{\mathrm{in}} - T_{\mathrm{mid}}), \tag{5.93}$$

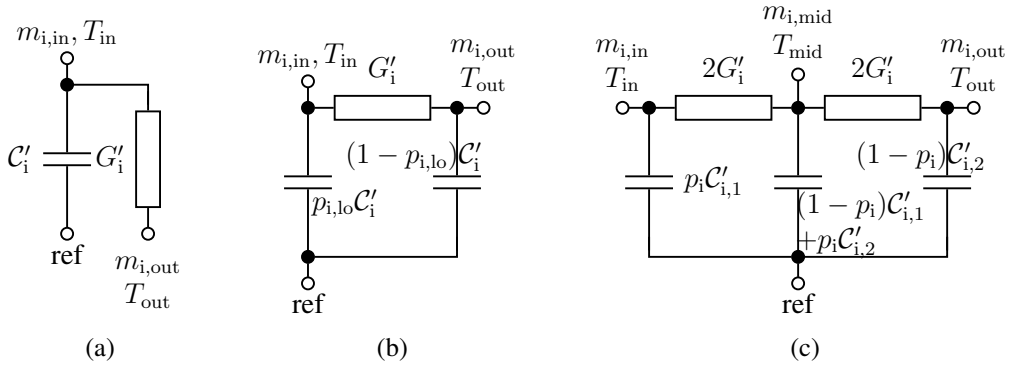

Figure 5.9: ECDs for a concentric insulation layer. (a) Simple RC structure. (b) Van Wormer capacitances for long-term transients. (c) Van Wormer capacitances for short-term transients.

and for the external temperature T_{out}, the necessary expression is

$$+ 2G'_{\mathrm{i}}(T_{\mathrm{out}} - T_{\mathrm{mid}}) + (1 - p_{\mathrm{i}})\mathcal{C}'_{\mathrm{i},2}\frac{\partial T_{\mathrm{out}}}{\partial t}. \tag{5.94}$$

c) Common Filling (Insulation) Around Several Structures

For a common filling around several structures as shown in figure 5.10(a), the assumption of radial symmetry is a rough approximation. In contrast to the previous considerations, it does not make sense here to place the capacitance on the inside, since the total capacitance must play a role for all enclosed structures. Therefore, the total capacitance of the filler material

$$\mathcal{C}'_{\mathrm{f}} = c_{\mathrm{f}}\mathcal{A}_{\mathrm{f}} \tag{5.95}$$

is placed at the surface node of the filling. c_{f} is the specific volume-related heat capacity of the filling and $\mathcal{A}_{\mathrm{f}}$ is the cross-section area of the filling. Again, the assumption of a uniform surface temperature is not always justifiable. But, in particular, if the filling is followed by a conductive layer that has high thermal conductivity, it is expected that the approximation of a uniform temperature at the transition between this conductor and the insulation only leads to small errors.

As shown in figure 5.10(b), additional conductances are assumed between the enclosed structures and the surface of the filler material to model heat conduction. Again, the temperatures at the surfaces of the enclosed structures $T_{\mathrm{in},i}$ and additionally the temperature at the surface of the filling T_{out} are needed as variables. For the nodal equations at the inner nodes, a new term of the form

$$+ G'_{\mathrm{f},i}\left(T_{\mathrm{in},i} - T_{\mathrm{out}}\right),\ i = 1, \ldots, N \tag{5.96}$$

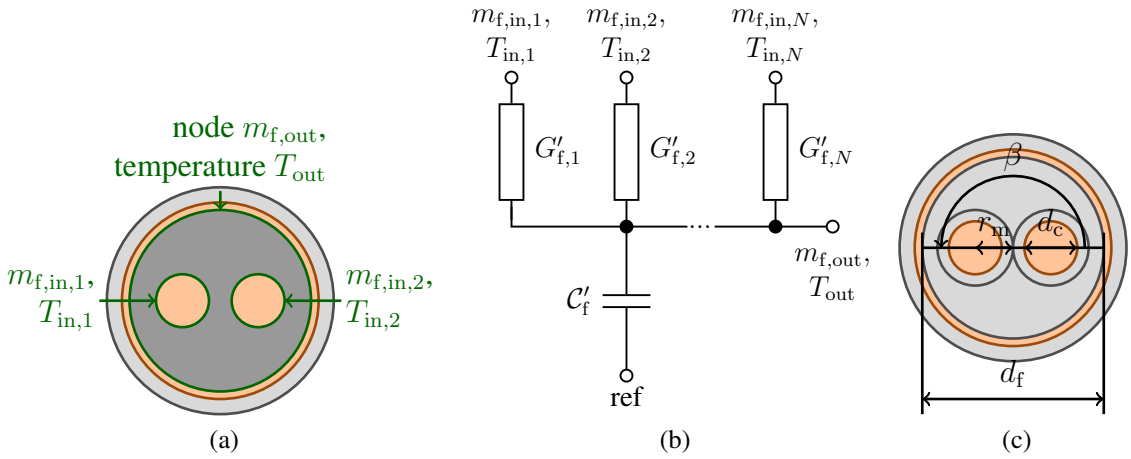

Figure 5.10: Exemplary filling layer. (a) Cross-section. (b) ECD. (c) Filling geometry for parameter calculation.

results, for the nodal equation at the surface the term

$$+ \mathcal{C}'_{\mathrm{f}} \frac{\partial T_{\mathrm{out}}}{\partial t} + \sum_{i=1}^{N} G'_{\mathrm{f},i} \left(T_{\mathrm{out}} - T_{\mathrm{in},i} \right) \tag{5.97}$$

is added. The determination of the resistances is non-trivial in the general case. According to [145], for the thermal conduction between the inner conductor and the surface of the filling, the same conductance

$$G'_{\mathrm{f},i} = \frac{1}{2\pi\lambda_{\mathrm{f}}} \operatorname{arcosh}\left(\frac{d_{\mathrm{f}}^2 + d_{\mathrm{c}}^2 - 4r_{\mathrm{m}}^2}{2 d_{\mathrm{f}} d_{\mathrm{c}}} \right), \quad i = 1, \ldots, N \tag{5.98}$$

can be used for all inner conductors analog to the characteristic impedance of an eccentric coaxial cable. This approach is valid for the assumption that the enclosed structures are identical conductors having the same distance from the center of the cable and being uniformly distributed. λ_{f} represents the specific thermal conductivity of the filling material, d_{f} is the outer diameter of the filling and d_{c} is the outer diameter of the enclosed inner conductors. r_{m} is the distance of the center of the inner conductors from the center of the filling, as sketched in figure 5.10(c).

d) Interaction Between Surface and Environment

The cable surface (see figure 5.11(a)) interacts with the environment via convection and radiation in the case of a cable surrounded by air, which is assumed in this complete thesis. This is modeled via a conductance

$$G'_{\mathrm{s}} = (\alpha_{\mathrm{conv}} + \alpha_{\mathrm{rad}}) 2\pi r_{\mathrm{s}} \tag{5.99}$$

which links the surface (radius r_{s}) with the ambient temperature T_{e} (given as the difference from the reference temperature). Here, convection and radiation are taken into account via the heat transfer coefficients α_{conv} and α_{rad} (for their calculation see section 5.2.2) and multiplied by the surface perimeter $2\pi r_{\mathrm{s}}$. Additional correction factors, again, are not considered in this section. The resulting ECD can be found in figure 5.11(b). In the nodal equation for the

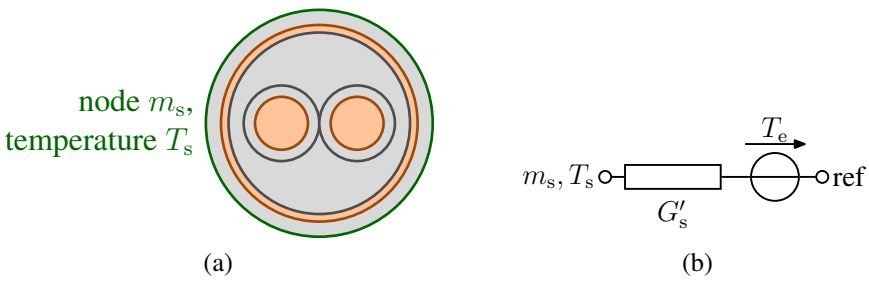

Figure 5.11: Exemplary surface. (a) Cross-section. (b) ECD.

surface temperature, the new expression is as follows:

$$+ G'_{\mathrm{s}}(T_{\mathrm{s}} - T_{\mathrm{e}}). \tag{5.100}$$

e) Coupling Between Conductors

The coupling between two conductors (nodes $m_{\mathrm{c},1}$ and $m_{\mathrm{c},2}$, see figure 5.12(a)) is modeled via a resistor as shown in figure 5.12(b). In the nodal equation for the first conductor, an expression of the form

$$+ R'_{\mathrm{c},1} G'_{12} (T_{\mathrm{c},1} - T_{\mathrm{c},2}) \tag{5.101}$$

is added. For the second conductor, the necessary expression is

$$+ R'_{\mathrm{c},2} G'_{12} (T_{\mathrm{c},2} - T_{\mathrm{c},1}). \tag{5.102}$$

The calculation of the needed resistor is non-trivial and only for special cases, analytical estimations are possible. One example of such a special case is the direct coupling of adjacent identical conductors via a common filling under the assumption that the total arrangement consists of identical and uniformly distributed conductors at the same distance from the cable center. Then, the resistance can be calculated analog to the characteristic impedance of an eccentric coaxial cable according to [145]:

$$G'_{12} = \frac{1}{\pi \lambda_{\mathrm{f}}} \operatorname{arcosh}\left(\frac{a_{\mathrm{f}}}{d_{\mathrm{c}}} \frac{d_{\mathrm{f}}^2 - a_{\mathrm{f}}^2 + d_{\mathrm{c}}^2}{d_{\mathrm{f}}^2 + a_{\mathrm{f}}^2 - d_{\mathrm{c}}^2} \right), \quad a_{\mathrm{f}} = 2 r_{\mathrm{m}} \sin\left(\frac{\beta}{2} \right). \tag{5.103}$$

Here, β is the angle between two inner conductors as shown in figure 5.10(c).

In the general case, the coupling is very complex and can only be determined numerically or via measurements. By directly modeling the coupling between the two conductors, part of the material located between these conductors is already taken into account. Accordingly, a correction of the resistances describing this area is necessary. Convection and radiation are typically also restricted, so a correction is necessary here as well. Approaches for these parameter determinations from measurement results for specific cable arrangements are presented in chapter 7.

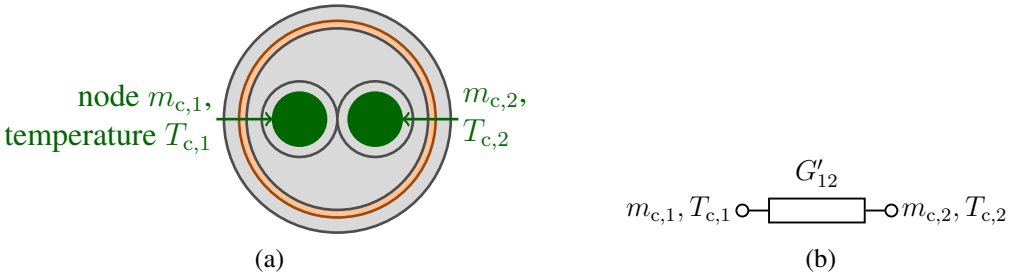

Figure 5.12: Exemplary coupling between two conductors. (a) Cross-section. (b) ECD.

From those different approaches, the complete system of partial differential equations is set up. For all of the presented elements, the corresponding entries for the matrices $\tilde{\mathbf{A}}$ to $\tilde{\mathbf{D}}$ are shown in table A.1.

f) Algorithm

All in all, the following steps, which are also presented in figure A.1, are necessary to set up the differential equation: First, the necessary nodes and thus the relevant temperatures must be determined from the geometry. A node is provided for each conductive layer. For insulating layers, one node is provided on the inside and one on the outside. For several concentric radial layers, a continuous temperature curve at the transition is assumed. For example, if a conductive solid inner conductor is directly surrounded by an insulation layer, two nodes or relevant temperatures are defined for this arrangement: The conductor temperature, which also is the temperature on the inside of the insulation, and the temperature on the outside of the insulation. Using the defined nodes, the general form of the PDE is set up.

In the next step, individual ECDs are now set up for each of the different geometrical elements (concentric conductor layer, concentric insulation layer, common filling) as well as physical effects (interaction between surface and environment, coupling between conductors) as summed up in figure A.1. These are linked at the defined nodes, resulting in an overall ECD. If this ECD is not explicitly searched, this step can also be omitted. In addition, stamps are used to directly define the corresponding nodal equations. Based on the material parameters and geometrical dimensions of the individual layers, the associated parameters are calculated. Especially for non-radial symmetric effects, this parameter determination can be challenging. In some cases, the parameters have to be found by measurement.

Finally, the calculated parameters are inserted into the previously defined PDE system. All in all, with this formalism, the differential equations can directly be formulated in the notation presented in equation (5.73), even without an explicit evaluation of the ECD.

5.4 Comparison Between Electrical and Thermal Transmission Line Models

In this section, the derived thermal models are compared with approaches from the electrical domain. The necessary assumptions are discussed first, followed by a direct comparison of the PDEs and ECDs and a discussion on the model classification.

5.4.1 Assumptions

As already mentioned in section 5.1.3, in the electrical domain, the TEM field assumption is decisive. As there is no physical equivalent to the reference conductor in the thermal domain, this assumption does not hold there.

However, some approximations and assumptions are also necessary for the thermal do-

main. First, a constant ambient temperature is assumed: The heating of the environment is not taken into account here. The ambient air is not covered by the model whose boundaries are at the cable surface. At this termination, boundary conditions are specified to consider radiation and convection. Heat conduction in the surrounding air is explicitly not considered here. The assumption of a constant ambient temperature is a good approximation if it changes slowly or only slightly compared to the other thermal processes in the system. Then, for each time, the ambient temperature at that time is assumed as an approximation in the later calculations.

Nonlinear effects appear widely in the thermal domain. In the derivation of the differential equation, the temperature dependence of the material parameters was not considered. Consequently, already the PDE is an approximation. To take into account the temperature-dependent behavior in the second step, the temperature dependences of the electrical losses that heat the cable and radiation and convection at the cable surface are included in the parameter calculation. In the electrical domain, such self-consistent problems do not typically appear. There, frequency-dependent parameters are common, but not voltage-dependent parameters. That is why the methods from the electrical domain can be transferred, especially if the parameters are assumed to be constant in the thermal domain as well. For the solution in the next chapter exactly this approach is used. Later, an iterative procedure is used to adjust the parameters to the conductor temperature. Implicitly, however, constant parameters are still assumed in the solution - so this approach only leads to good results if the conductor temperature changes slowly.

Since the thermal conductivity of the conductor material is much higher than that of the insulation, segments adjacent to each other in the axial direction are assumed to couple to each other much stronger in the inner conductor than in the insulation. As an approximation, the direct coupling in the insulation is therefore neglected, so the insulation temperatures at adjacent segments are only indirectly coupled to each other via the inner conductor temperature. In the radial direction, the temperature drop across the insulation layer is much higher than across the inner conductor due to the size ratios of the thermal conductivities, which is why the entire inner conductor is regarded as a single node with a radially constant temperature. This consideration is based on the assumption that the radial expansion of the inner conductor is considerably smaller than its axial expansion (along which temperature changes are indeed taken into account). This requirement is thus quite comparable to the requirement for electrically short cross-sections in the electrical domain, which is needed there to allow the TEM assumption.

5.4.2 Partial Differential Equations and Equivalent Circuit Diagrams

Comparing the PDE (5.51) with the corresponding equation (3.2) in the electrical domain shows a very similar form. Setting $L'_{\mathrm{el}} = 0$ directly leads to an equivalent formulation with

$I'_{\mathrm{f}} = -\left(G'T_{\mathrm{e}} + P'_{\mathrm{el}}\right)$. The same changes are necessary to transform the ECDs from the electrical to the thermal domain. But there are also differences: As already mentioned in section 5.1, the final differential equations in the electrical domain are hyperbolic and describe an oscillating system, whereas, in the thermal domain, the differential equations are parabolic. An equivalent to the electrical inductance cannot be found.

The choice of a physically existing conductor as the electrical reference conductor provides an additional degree of freedom, so to speak: If only one conductor differs from the other conductors, then it is still possible to exploit certain symmetries in the equations and the ECD, which may result in a quite simple formulation. In particular, for the solution of the resulting equations, this can have significant advantages. Also in the thermal ECD, there is a common reference node, which seems to lead back the heat flow to the inner conductor. However, since there is no physical equivalent to this reference node, this is a modeling artifact. The heat does not flow back into the conductor.

Applying the general approach for thermal modeling of different cable structures from section 5.3.3 can result in an equivalent circuit or PDE, respectively, that cannot be treated analog to the electrical domain. Then, methods known from the electrical TL theory cannot be directly transferred to the thermal problem. That is why in the following, the focus is on thermal models analog to the electrical domain.

5.4.3 Model Classification

In the electrical domain, cable models can be classified in different ways according to [110, pp. 33-37]. First, a distinction can be made between uniform and nonuniform lines: In the general case of nonuniform lines, the cable parameters change along the line and thus depend on the coordinate z. This violates the TEM assumption. For the important case of uniform lines, i.e., constant cross-sections through the entire setup along z, on the other hand, these parameters are independent of z. Another widely spread dependence in the electrical domain is the frequency dependence of the cable parameters. Often, solutions are found using approaches in the frequency domain together with a superposition approach based on the linearity of the problem. In the thermal domain, this frequency dependence does not appear in a comparable form. Instead, here, the cable parameters are partially dependent on the cable temperature. As the temperature changes along the cable, the parameters also vary with z, resulting in a nonuniform cable. This implicit temperature dependence leads to a self-consistent problem in the thermal domain - the differential equation is nonlinear. Approaches based on superposition and uniform lines are thus formally not directly applicable. Nevertheless, in the remainder of this thesis, exactly such procedures will be used to determine an approximate solution in the thermal domain, since they form the basis of the classical TL theory. The nonlinear implicit temperature dependence is initially excluded for the solution of the differential equation and later approximately taken into account via an iterative

approach.

In the electrical domain, a further distinction can be made between homogeneous and inhomogeneous surrounding materials. For inhomogeneous environments (e.g., combinations of insulation material and air), the velocities of the propagating waves are not identical. The TEM assumption is formally no longer exact, but can still be used as an approximation for many cases (quasi-TEM). Primarily, there are changes in the calculation of the cable parameters in contrast to the homogeneous case. In the thermal domain, the model does not cover the environment. That is why inhomogeneity is not considered in an equivalent way as in the electrical domain. Within the cable, however, homogeneity is often assumed for the determination of the cable parameters.

A special but important case in the electrical domain is the presence of perfect conductors and lossless surrounding materials. The cable parameters G'_{el} and R'_{el} then vanish. This eliminates the damping terms in the wave equation and simplifies the solution. Some methods have been developed specifically for this idealized case. However, if the losses in the conductor are considered ($R'_{\mathrm{el}} \neq 0$), this formally violates the TEM assumption. Nevertheless, the quasi-TEM approximation is typically assumed. In the thermal domain, R' can also be neglected. However, this corresponds directly to the case where the inner conductor is at an axially constant temperature. In general, axial boundary conditions can no longer be fulfilled in a meaningful way. However, the conductance G' cannot be neglected at all, since it represents the heat conduction through the insulation layer (which may become unnecessary in the case of an uninsulated inner conductor) and the transition to the environment (which is always present). In this respect, in the thermal domain, losses always have to be incorporated into the model and the specific approaches for the lossless case from the electrical domain cannot be transferred in a meaningful way.

6 Solutions

In this section, analytical solution methods for selected cable arrangements and thus concrete calculation rules for the temperature profile are developed. Methods known from the electrical TL theory are used to find solutions in the thermal domain. That is why the additional matrix $\tilde{\mathbf{D}}$ from equation (5.73) is not considered here, but the reduced formulation given in equation (5.72) (equivalent to the electrical domain) is analyzed. Then, in general, the following system of coupled differential equations with initial and boundary conditions has to be solved:

$$\tilde{\boldsymbol{C}}(\boldsymbol{T}(z,t),\boldsymbol{T}_\mathrm{s}(z,t),z,t) = \frac{\partial^2 \boldsymbol{T}(z,t)}{\partial z^2} - \mathbf{A}\frac{\partial \boldsymbol{T}(z,t)}{\partial t} - \mathbf{B}(\boldsymbol{T}_\mathrm{s}(z,t))\boldsymbol{T}(z,t), \tag{6.1}$$

$$\boldsymbol{T}_\mathrm{s}(z,t) = \boldsymbol{f}(\boldsymbol{T}(z,t),\boldsymbol{T}_\mathrm{s}(z,t)), \tag{6.2}$$

$$\boldsymbol{T}(z,0) = \tilde{\boldsymbol{T}}_0(z), \quad \boldsymbol{T}(0,t) = \tilde{\boldsymbol{T}}_1(t), \quad \boldsymbol{T}(\mathcal{L},t) = \tilde{\boldsymbol{T}}_2(t). \tag{6.3}$$

Depending on the exact conductor arrangement, the functional (implicit) dependence of the surface temperature on the conductor temperature $\boldsymbol{f}(\boldsymbol{T}(z,t),\boldsymbol{T}_\mathrm{s}(z,t))$ varies. For the single conductor, for example, the required relationship has the following form:

$$T_\mathrm{s,sw}(z,t) = T_\mathrm{sw}(z,t) - R'_\mathrm{i}G'(T_\mathrm{s,sw}(z,t)) \cdot (T_\mathrm{sw}(z,t) - T_\mathrm{e}). \tag{6.4}$$

Overall, on the one hand, spatial and time-dependent initial and boundary conditions can occur. The excitation $\tilde{\boldsymbol{C}}$ also has an explicit spatial and time dependence in the general case. On the other hand, the formulation is implicit because the parameters $\tilde{\boldsymbol{C}}$ and $\mathbf{B}$ in the differential equation depend again on the sought conductor temperature and the surface temperature. The surface temperature itself is a function of the inner conductor temperature. This formulation is also implicit. These two effects (location and time dependences as well as implicitness of the formulation) considerably complicate the solution of the differential equation system. In the following, a formulation for this problem is approached step by step. Two main approximations are used: On the one hand, the explicit location and time dependencies of the initial and boundary conditions as well as the excitation are neglected:

$$\tilde{\boldsymbol{T}}_0(z) = \boldsymbol{T}_0, \quad \tilde{\boldsymbol{T}}_1(t) = \boldsymbol{T}_1, \quad \tilde{\boldsymbol{T}}_2(t) = \boldsymbol{T}_2, \tag{6.5}$$

$$\tilde{\boldsymbol{C}}(\boldsymbol{T}(z,t),\boldsymbol{T}_\mathrm{s}(z,t),z,t) = \boldsymbol{C}(\boldsymbol{T}(z,t),\boldsymbol{T}_\mathrm{s}(z,t)). \tag{6.6}$$

These assumptions are summarized with the term “constant excitations”. Many practically relevant problems can be described approximately or at least investigated concerning their worst-case behavior using this assumption. On the other hand, the implicit parameter dependencies are neglected:

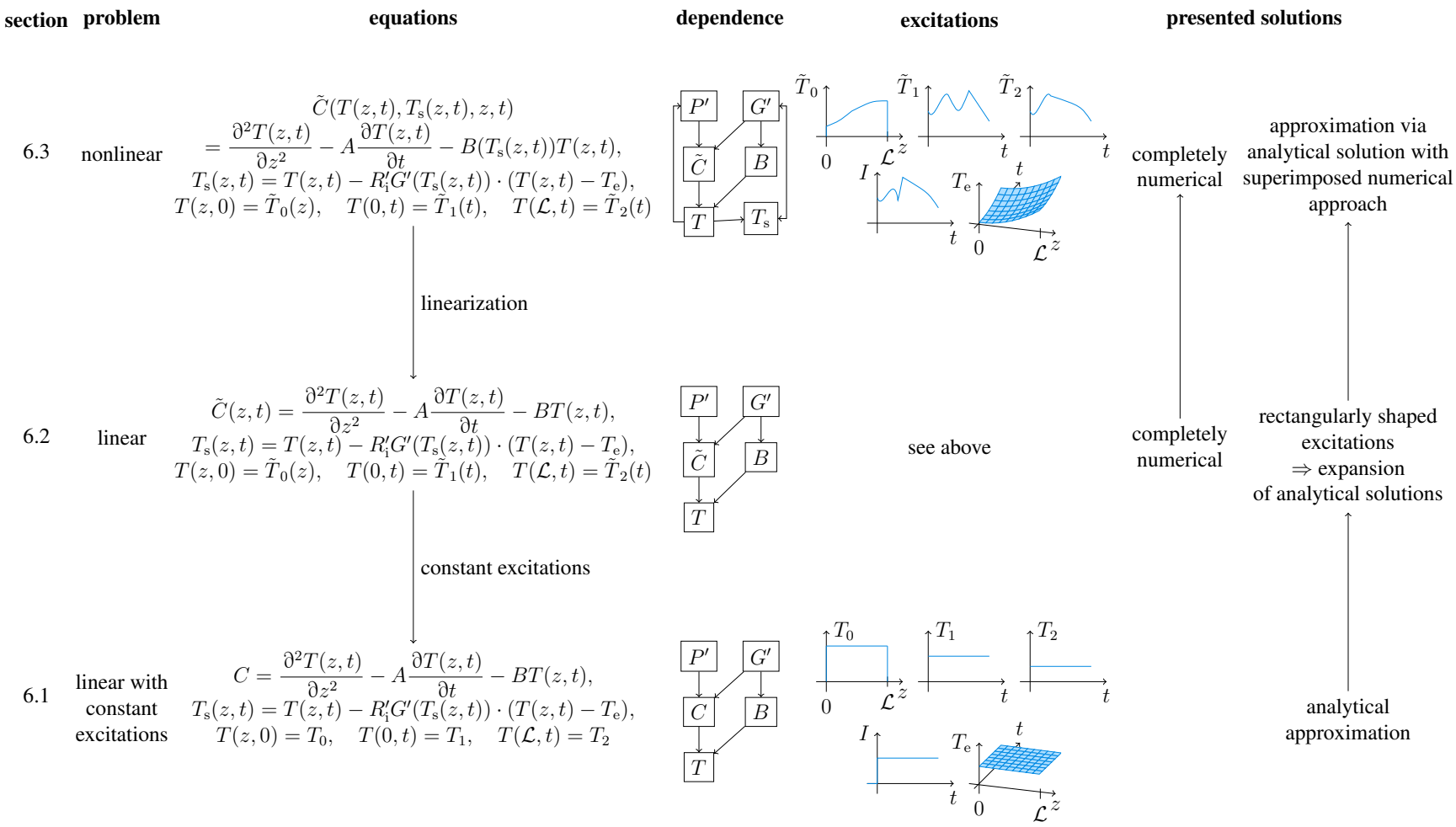

Figure 6.1: Overview of the different problems that have to be solved for the single wire cable. The sections that deal with the different problems are given.

$$\mathbf{B}(\boldsymbol{T}_\mathrm{s}(z,t)) = \mathbf{B} = \text{const.}, \quad \tilde{\boldsymbol{C}}(\boldsymbol{T}(z,t), \boldsymbol{T}_\mathrm{s}(z,t), z, t) = \boldsymbol{C}(z,t). \tag{6.7}$$

These assumptions are described in the following with the expression “linearized”. The surface temperature calculation is then decoupled from the conductor temperature calculation and can thus be excluded from the primary problem formulation. Then, preliminary guesses are necessary to determine the parameters. One possibility is to use initial estimates for the conductor temperature and the cable parameters. In principle, with suitable guesses, the temperature curves can be approximated well. This is discussed in section 7.3.1.a).

In the following section 6.1, both simplifications are used together. Thus, solutions or solution methods of the linearized problem for special cable arrangements and constant excitations are determined. The focus here is on analytical approaches. These form the basis for the further course of this thesis. In the second step (see section 6.2), temporally and spatially varying excitations are then discussed. The implicit nonlinear dependence on the conductor and surface temperatures is again neglected. Finally, in section 6.3, the influence of nonlinearity is investigated. Different solutions to the general problem are discussed. Numerical approaches are needed here due to the non-trivial relationships. An overview of the different (simplified) problems and the corresponding sections and solutions for the example of the single wire cable is given in figure 6.1.

6.1 Basic Linear Analytical Solution Approaches for Special Setups and Constant Excitations

For the solution to the linearized problem with constant excitations,

$$\boldsymbol{C} = \frac{\partial^2 \boldsymbol{T}(z,t)}{\partial z^2} - \mathbf{A}\frac{\partial \boldsymbol{T}(z,t)}{\partial t} - \mathbf{B}\boldsymbol{T}(z,t), \tag{6.8}$$

$$\boldsymbol{T}(z,0) = \boldsymbol{T}_0, \quad \boldsymbol{T}(0,t) = \boldsymbol{T}_1, \quad \boldsymbol{T}(\mathcal{L},t) = \boldsymbol{T}_2, \tag{6.9}$$

a modification of the three-step approach presented in [110, p. 3] for the electrical domain is used. There, in the first step, the general form of the differential equation is adapted to the actual problem by determining the required parameters. The general solution of this problem is found in the second step. The result describes not yet the concrete time development, but the set of all possible time courses. In the third step, the specific searched development is determined from this set of possible developments by the inclusion of the boundary conditions.

In the thermal domain, this procedure can be applied completely analogously. After concretizing the general PDE for the given problem in the first step, the solution is developed in the second step. In the following, different possible approaches for the considered cases (approach via **L**aplace transform with **a**pproximation (index La), via **G**reen’s functions in the

time domain (index G), via **G**reen's functions in the **L**aplace domain (index GL), a **simp**lified form of the ECD (index simp) and an **it**erative approach (index it)) are presented. A general solution results here as well, in which remaining unknown factors are determined by the boundary conditions. However, since this is partially done, e.g., in the Laplace domain, and only the complete solution is transformed back into the time domain, the clear separation between the second and third steps from [110, p. 3] is omitted in the further course. Instead, the boundary conditions are directly used for the solution of the PDE.

First, based on the PDE in matrix-vector form, simplified solutions are derived, which result if the time and/or spatial dependence can be neglected. In the following, a **s**ingle **w**ire cable (index sw), a system of single wire cables, an arrangement of **t**wo **s**ingle **w**ire cables (index tsw), a **co**axial cable (index co), an arrangement of N **id**entical single wire cables (index id) as well as a rather general conductor arrangement analog to the electrical domain are investigated considering the temporal and spatial dependence.

Throughout this complete thesis, many and more indices appear to distinguish, for example, between different temperatures. Often, even several indices are combined, as shown in figure 6.2. That is why a specific index directory can be found within the list of mathematical symbols.

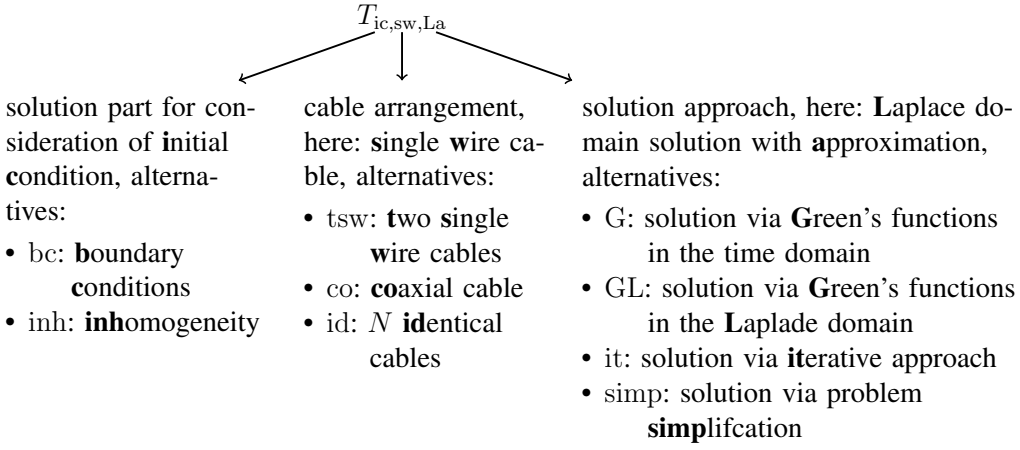

Figure 6.2: Example for multiple indices with a short explanation.

6.1.1 Neglection of Spatial and/or Time Dependence

In the first step, simplified versions of the complete PDE are analyzed neglecting the spatial and/or the time dependence. Under those assumptions, solutions can be found for the general case analog to the electrical domain known from equation (5.72).

a) Radial Steady State

If only the steady-state temperatures $\boldsymbol{T}_{\mathrm{rs}}$ for long cables are searched, the time and spatial dependencies can both be neglected. Then, the system of PDEs is reduced to a simple

algebraic expression, that can directly be solved:

$$-\mathbf{B}\boldsymbol{T}_{\mathrm{rs}} = \boldsymbol{C} \Leftrightarrow \boldsymbol{T}_{\mathrm{rs}} = -\mathbf{B}^{-1}\boldsymbol{C}. \tag{6.10}$$

b) Axial Steady State

If the spatial dependence has to be considered, but only the **st**eady-**st**ate temperature distribution $\boldsymbol{T}_{\mathrm{ststst}}(z)$ along the cable arrangement is searched, the following system of differential equations describes the system:

$$\frac{\partial^2}{\partial z^2}\boldsymbol{T}_{\mathrm{ststst}}(z) - \mathbf{B}\boldsymbol{T}_{\mathrm{ststst}}(z) = \boldsymbol{C} \tag{6.11}$$

with the boundary conditions (assumed constant temperatures at cable terminations)

$$\boldsymbol{T}_{\mathrm{ststst}}(0) = \boldsymbol{T}_1 = \begin{pmatrix} T_{1,1} \\ T_{1,2} \\ \vdots \\ T_{1,N} \end{pmatrix}, \quad \boldsymbol{T}_{\mathrm{ststst}}(\mathcal{L}) = \boldsymbol{T}_2 = \begin{pmatrix} T_{2,1} \\ T_{2,2} \\ \vdots \\ T_{2,N} \end{pmatrix}. \tag{6.12}$$

Those coupled differential equations are decoupled diagonalizing the matrix $\mathbf{B}$:

$$\mathbf{B} = \mathbf{E}_{\mathbf{B}}\mathbf{D}_{\mathbf{B}}\mathbf{E}_{\mathbf{B}}^{-1}, \quad \mathbf{D}_{\mathbf{B}} = \begin{pmatrix} D_{\mathbf{B},1} & 0 & \dots & 0 \\ 0 & D_{\mathbf{B},2} & \ddots & \vdots \\ \vdots & \ddots & \ddots & 0 \\ 0 & \dots & 0 & D_{\mathbf{B},N} \end{pmatrix}. \tag{6.13}$$

Then, the complete solution $\boldsymbol{T}_{\mathrm{ststst}}(z)$ is the superposition of the homogeneous solution

$$\boldsymbol{T}_{\mathrm{hom,ststst}}(z) = \mathbf{E}_{\mathbf{B}}\mathrm{e}^{\sqrt{\mathbf{D}_{\mathbf{B}}}z}\boldsymbol{T}_{\mathrm{ststst},1} + \mathbf{E}_{\mathbf{B}}\mathrm{e}^{-\sqrt{\mathbf{D}_{\mathbf{B}}}z}\boldsymbol{T}_{\mathrm{ststst},2} \tag{6.14}$$

with

$$\mathrm{e}^{\pm\sqrt{\mathbf{D}_{\mathbf{B}}}z} = \begin{pmatrix} \mathrm{e}^{\pm\sqrt{D_{\mathbf{B},1}}z} & 0 & \dots & 0 \\ 0 & \mathrm{e}^{\pm\sqrt{D_{\mathbf{B},2}}z} & \ddots & \vdots \\ \vdots & \ddots & \ddots & 0 \\ 0 & \dots & 0 & \mathrm{e}^{\pm\sqrt{D_{\mathbf{B},N}}z} \end{pmatrix} \tag{6.15}$$

and a particulate solution $\boldsymbol{T}_{\mathrm{part,ststst}} = \boldsymbol{T}_{\mathrm{rs}}$:

$$\boldsymbol{T}_{\mathrm{ststst}}(z) = \boldsymbol{T}_{\mathrm{hom,ststst}}(z) + \boldsymbol{T}_{\mathrm{part,ststst}}. \tag{6.16}$$

Via the evaluation of the boundary conditions, the factors $\boldsymbol{T}_{\mathrm{ststst},1}$ and $\boldsymbol{T}_{\mathrm{ststst},2}$ are determined:

$$\boldsymbol{T}_{\mathrm{stst},1} = \left(\mathrm{e}^{-\sqrt{\mathbf{D_B}}\mathcal{L}} - \mathrm{e}^{\sqrt{\mathbf{D_B}}\mathcal{L}}\right)^{-1} \left[\mathrm{e}^{-\sqrt{\mathbf{D_B}}\mathcal{L}}\mathbf{E}_{\mathbf{B}}^{-1}\left(\boldsymbol{T}_1 - \boldsymbol{T}_{\mathrm{rs}}\right) - \mathbf{E}_{\mathbf{B}}^{-1}\left(\boldsymbol{T}_2 - \boldsymbol{T}_{\mathrm{rs}}\right)\right], \tag{6.17}$$

$$\boldsymbol{T}_{\mathrm{stst},2} = \left(\mathrm{e}^{-\sqrt{\mathbf{D_B}}\mathcal{L}} - \mathrm{e}^{\sqrt{\mathbf{D_B}}\mathcal{L}}\right)^{-1} \left[-\mathrm{e}^{\sqrt{\mathbf{D_B}}\mathcal{L}}\mathbf{E}_{\mathbf{B}}^{-1}\left(\boldsymbol{T}_1 - \boldsymbol{T}_{\mathrm{rs}}\right) + \mathbf{E}_{\mathbf{B}}^{-1}\left(\boldsymbol{T}_2 - \boldsymbol{T}_{\mathrm{rs}}\right)\right]. \tag{6.18}$$

c) Radial Transient Case

If the axial temperature distribution is not relevant, but the transient temperature development has to be considered, the reduced form of the PDE system is

$$-\mathbf{A}\frac{\partial}{\partial t}\boldsymbol{T}_{\mathrm{rt}}(t) - \mathbf{B}\boldsymbol{T}_{\mathrm{rt}}(t) = \boldsymbol{C}. \tag{6.19}$$

This general matrix formulation can directly be solved. Again, the solution is the superposition of the homogeneous solution and a particulate part:

$$\boldsymbol{T}_{\mathrm{rt}}(t) = \mathbf{E}_{\mathbf{A}^{-1}\mathbf{B}}\exp\left(-\mathbf{D}_{\mathbf{A}^{-1}\mathbf{B}}t\right)\boldsymbol{T}_{\mathrm{rt},0} + \boldsymbol{T}_{\mathrm{rs}} \tag{6.20}$$

with the diagonalization of the matrix $\mathbf{A}^{-1}\mathbf{B}$:

$$\mathbf{A}^{-1}\mathbf{B} = \mathbf{E}_{\mathbf{A}^{-1}\mathbf{B}}\mathbf{D}_{\mathbf{A}^{-1}\mathbf{B}}\mathbf{E}_{\mathbf{A}^{-1}\mathbf{B}}^{-1}. \tag{6.21}$$

Evaluating the initial condition $\boldsymbol{T}_{\mathrm{rt}}(0) = \boldsymbol{T}_0$ (assumed constant cable temperature at $t = 0\,\mathrm{s}$) leads to

$$\boldsymbol{T}_{\mathrm{rt},0} = \mathbf{E}_{\mathbf{A}^{-1}\mathbf{B}}^{-1}\left(\boldsymbol{T}_0 - \boldsymbol{T}_{\mathrm{rs}}\right). \tag{6.22}$$

6.1.2 Single Wire Cable

In this section, a single wire cable is analyzed. The thermal ECD for such a cable is given in figure 5.2. As derived in section 5.2, the PDE

$$\frac{\partial^2 T_{\mathrm{sw}}(z,t)}{\partial z^2} - A_{\mathrm{sw}}\frac{\partial T_{\mathrm{sw}}(z,t)}{\partial t} - B_{\mathrm{sw}}T_{\mathrm{sw}}(z,t) = \tilde{C}_{\mathrm{sw}}(z,t), \tag{6.23}$$

with a constant excitation $\tilde{C}_{\mathrm{sw}}(z,t) = C_{\mathrm{sw}}$ and the constant boundary and initial conditions

$$T_{\mathrm{sw}}(0,t) = \tilde{T}_{1,\mathrm{sw}}(t) = T_{1,\mathrm{sw}}, \qquad T_{\mathrm{sw}}(\mathcal{L},t) = \tilde{T}_{2,\mathrm{sw}}(t) = T_{2,\mathrm{sw}}, \tag{6.24}$$

$$T_{\mathrm{sw}}(z,0) = \tilde{T}_{0,\mathrm{sw}}(z) = T_{0,\mathrm{sw}} \tag{6.25}$$

has to be solved. The problem can be classified as an inhomogeneous differential equation with inhomogeneous boundary and initial conditions as generally, C_{sw}, $T_{0,\mathrm{sw}}$, $T_{1,\mathrm{sw}}$, and $T_{2,\mathrm{sw}}$ are not zero. Assuming linearity, according to the principle of superposition, the complete solution results as the superposition of solutions that take into account only one of the different

initial and boundary conditions and the stimulations ($\tilde{C}_{\mathrm{sw}}$) assuming the others to vanish:

$$T_{\mathrm{sw}}(z,t) = T_{\tilde{T}_{0,\mathrm{sw}}}(z,t,T_{0,\mathrm{sw}}) + T_{\tilde{T}_{1,\mathrm{sw}}}(z,t,T_{1,\mathrm{sw}}) + T_{\tilde{T}_{2,\mathrm{sw}}}(z,t,T_{2,\mathrm{sw}}) + T_{\tilde{C},\mathrm{sw}}(z,t,C_{\mathrm{sw}}). \tag{6.26}$$

Due to symmetry considerations, the influence of the cable termination temperatures has to fulfill the following condition:

$$T_{\tilde{T}_{1,\mathrm{sw}}}(z,t,T_{1,\mathrm{sw}}) = T_{\mathrm{bc,sw}}(z,t,T_{1,\mathrm{sw}}), \quad T_{\tilde{T}_{2,\mathrm{sw}}}(z,t,T_{2,\mathrm{sw}}) = T_{\mathrm{bc,sw}}(z_{\mathcal{L}},t,T_{2,\mathrm{sw}}) \tag{6.27}$$

with $z_{\mathcal{L}} = \mathcal{L} - z$. Analogously, also for the **i**nitial **c**onditions and the **inh**omogeneity, explicit functions are introduced:

$$T_{\tilde{T}_{0,\mathrm{sw}}}(z,t,T_{0,\mathrm{sw}}) = T_{\mathrm{ic,sw}}(z,t,T_{0,\mathrm{sw}}), \quad T_{\tilde{C},\mathrm{sw}}(z,t,C_{\mathrm{sw}}) = T_{\mathrm{inh,sw}}(z,t,C_{\mathrm{sw}}). \tag{6.28}$$

The corresponding cable surface temperature is

$$T_{\mathrm{s,sw}}(z,t) = T_{\mathrm{sw}}(z,t) - R_{\mathrm{i}}' G' (T_{\mathrm{sw}}(z,t) - T_{\mathrm{e}}). \tag{6.29}$$

a) Direct Solution in the Laplace Domain and Approximation

In this section, solution approaches based on a Laplace domain solution are presented for a finite and a semi-infinite single wire cable. This section is based on [A.3].

Finite Cable In the first step, the Laplace transform about the time of the PDE together with constant initial and boundary conditions is performed to reduce the complexity of the differential equation: Time derivatives do not appear any longer, so the PDE is reduced to an ODE with the Laplace variable s:

$$\frac{\mathrm{d}^2 T_{\mathrm{sw}}(z,s)}{\mathrm{d}z^2} - (sA_{\mathrm{sw}} + B_{\mathrm{sw}}) T_{\mathrm{sw}}(z,s) = \frac{C_{\mathrm{sw}}}{s} - A_{\mathrm{sw}} T_{0,\mathrm{sw}}, \tag{6.30}$$

$$T_{\mathrm{sw}}(0,s) = \frac{T_{1,\mathrm{sw}}}{s}, \quad T_{\mathrm{sw}}(\mathcal{L},s) = \frac{T_{2,\mathrm{sw}}}{s}. \tag{6.31}$$

Then, in the Laplace domain, the differential equation is directly solved by superpositioning a homogeneous and a particulate term:

$$T_{\mathrm{sw}}(z,s) = T_{\mathrm{sw},1}(s)\mathrm{e}^{z\tilde{a}} + T_{\mathrm{sw},2}(s)\mathrm{e}^{-z\tilde{a}} + T_{\mathrm{part,sw}}(s), \tag{6.32}$$

$$\tilde{a} = \sqrt{sA_{\mathrm{sw}} + B_{\mathrm{sw}}}, \quad T_{\mathrm{part,sw}}(s) = \frac{sA_{\mathrm{sw}}T_{0,\mathrm{sw}} - C_{\mathrm{sw}}}{s(sA_{\mathrm{sw}} + B_{\mathrm{sw}})}.$$

The boundary conditions in the Laplace domain are used to calculate the prefactors $T_{\mathrm{sw},1}(s)$ and $T_{\mathrm{sw},2}(s)$, which results in

$$T_{\mathrm{sw},1}(s) = \frac{T_{1,\mathrm{sw}} - sT_{\mathrm{part,sw}}(s)}{s\left(1+\mathrm{e}^{\mathcal{L}\tilde{a}}\right)} + \frac{(T_{1,\mathrm{sw}} - T_{2,\mathrm{sw}})\mathrm{e}^{-\mathcal{L}\tilde{a}}}{s\left(\mathrm{e}^{-2\mathcal{L}\tilde{a}}-1\right)}, \tag{6.33}$$

$$T_{\mathrm{sw},2}(s) = \frac{T_{2,\mathrm{sw}} - sT_{\mathrm{part,sw}}(s)}{s\left(1+\mathrm{e}^{-\mathcal{L}\tilde{a}}\right)} + \frac{T_{2,\mathrm{sw}} - T_{1,\mathrm{sw}}}{s\left(\mathrm{e}^{-2\mathcal{L}\tilde{a}}-1\right)}. \tag{6.34}$$

As originally the time domain solution was searched, the complete solution has to be transformed from the Laplace domain back to the time domain. For some of the expressions from the prefactors, no corresponding expression in the time domain is known. That is why an alternate formulation is necessary, that allows an analytical transformation back into the time domain. For this purpose, the prefactors are approximated suitably:

$$\mathrm{e}^{-\mathcal{L}\tilde{a}} \pm 1 \approx \pm 1. \tag{6.35}$$

This approximation leads to good results especially for long cables (see also section 7.3.1.d), [A.3, A.4]). The new, reduced form of the prefactors then becomes

$$T_{\mathrm{sw},1}(s) \approx \left(\frac{T_{2,\mathrm{sw}}}{s} - T_{\mathrm{part,sw}}(s)\right)\mathrm{e}^{-\mathcal{L}\tilde{a}}, \quad T_{\mathrm{sw},2}(s) \approx \frac{T_{1,\mathrm{sw}}}{s} - T_{\mathrm{part,sw}}(s). \tag{6.36}$$

This new formulation allows the analytical transformation back into the time domain yielding

$$\begin{aligned} T_{\mathrm{sw,La}}(z,t) = {} & T_{\mathrm{ic,sw,La}}(z,t,T_{0,\mathrm{sw}}) + T_{\mathrm{bc,sw,La}}(z,t,T_{1,\mathrm{sw}}) \\ & + T_{\mathrm{bc,sw,La}}(z_{\mathcal{L}},t,T_{2,\mathrm{sw}}) + T_{\mathrm{inh,sw,La}}(z,t,C_{\mathrm{sw}}) \end{aligned} \tag{6.37}$$

with

$$T_{\mathrm{ic,sw,La}}(z,t,T_{0,\mathrm{sw}}) = -\Gamma(t)T_{0,\mathrm{sw}}\Lambda_3(t)[1-\Lambda_1(z,t)-\Lambda_1(z_{\mathcal{L}},t)], \tag{6.38}$$

$$T_{\mathrm{bc,sw,La}}(z,t,T_{\mathrm{bc}}) = -\Gamma(t)\frac{T_{\mathrm{bc}}}{2}\Lambda_2(z,t), \tag{6.39}$$

$$\begin{aligned} T_{\mathrm{inh,sw,La}}(z,t,C_{\mathrm{sw}}) = {} & -\frac{C_{\mathrm{sw}}}{B_{\mathrm{sw}}}\Gamma(t) + T_{\mathrm{ic,sw,La}}\left(z,t,\frac{C_{\mathrm{sw}}}{B_{\mathrm{sw}}}\right) + T_{\mathrm{bc,sw,La}}\left(z,t,\frac{C_{\mathrm{sw}}}{B_{\mathrm{sw}}}\right) \\ & + T_{\mathrm{bc,sw,La}}\left(z_{\mathcal{L}},t,\frac{C_{\mathrm{sw}}}{B_{\mathrm{sw}}}\right), \end{aligned} \tag{6.40}$$

$$\Lambda_1(z,t) = \mathrm{erf}\left(\frac{z}{2}\sqrt{\frac{A_{\mathrm{sw}}}{t}}\right), \ \Lambda_2(z,t) = \theta_1(z,t) + \theta_2(z,t), \ \Lambda_3(t) = \mathrm{e}^{-\frac{B_{\mathrm{sw}}}{A_{\mathrm{sw}}}t}, \tag{6.41}$$

$$\theta_1(z,t) = -\mathrm{e}^{-z\sqrt{B_{\mathrm{sw}}}}\,\mathrm{erfc}\left(\frac{zA_{\mathrm{sw}} - 2t\sqrt{B_{\mathrm{sw}}}}{2\sqrt{A_{\mathrm{sw}}t}}\right), \tag{6.42}$$

$$\theta_2(z,t) = -\mathrm{e}^{z\sqrt{B_{\mathrm{sw}}}}\,\mathrm{erfc}\left(\frac{zA_{\mathrm{sw}} + 2t\sqrt{B_{\mathrm{sw}}}}{2\sqrt{A_{\mathrm{sw}}t}}\right). \tag{6.43}$$

This solution approach was also discussed in [A.3, A.5, A.6].

Semi-infinite Cable If not a finite cable is described but an infinitely long cable starting at $z = 0\,\mathrm{m}$, the prefactor $T_{\mathrm{sw},1}(s)$ from the above-presented solution has to be set to zero: $T_{\mathrm{sw},1}(s) = 0$. Then, the remaining boundary condition $T_{\mathrm{sw,La,semi}}(0, s) = T_{1,\mathrm{sw}}/s$ is used to calculate the second prefactor:

$$T_{\mathrm{sw},2}(s) = \frac{T_{1,\mathrm{sw}}}{s} - T_{\mathrm{part,sw}}(s). \tag{6.44}$$

The final result is derived via transformation back into the time domain:

$$T_{\mathrm{sw,La,semi}}(z,t) = \frac{C_{\mathrm{sw}}}{B_{\mathrm{sw}}} - \left(\frac{C_{\mathrm{sw}}}{B_{\mathrm{sw}}} - T_{0,\mathrm{sw}}\right)\Lambda_3(t)\Lambda_1(z,t) + \left(\frac{C_{\mathrm{sw}}}{B_{\mathrm{sw}}} - T_{1,\mathrm{sw}}\right)\frac{\Lambda_2(z,t)}{2}. \tag{6.45}$$

b) Solution via Green's Functions in the Time Domain

In this approach, a time domain Green's functions formulation is used to solve the PDE. This approach was earlier presented in [A.4] and can be used to derive the (already known) solutions for an infinitely long or semi-infinite cable but also for the finite cable, for which, in the last approach, an approximation was necessary. For the derivation of the fundamental solutions of the given problem, analog to [146, pp. 150-151], the spatial Fourier transform is used. The Green's function $G_{\mathrm{sw}}(z,t|\tilde{z},\tilde{t})$ for the problem

$$-\frac{1}{A_{\mathrm{sw}}}\frac{\partial^2}{\partial z^2}T_{\mathrm{sw}}(z,t) + \frac{\partial}{\partial t}T_{\mathrm{sw}}(z,t) + \frac{B_{\mathrm{sw}}}{A_{\mathrm{sw}}}T_{\mathrm{sw}}(z,t) = -\frac{C_{\mathrm{sw}}}{A_{\mathrm{sw}}} \tag{6.46}$$

with the boundary and initial conditions from equations (6.24) and (6.25) is

$$\begin{aligned} G_{\mathrm{sw}}(z,t|\tilde{z},\tilde{t}) = {} & \Gamma(t-\tilde{t})\exp\left(-\frac{B_{\mathrm{sw}}}{A_{\mathrm{sw}}}(t-\tilde{t})\right)\sqrt{\frac{A_{\mathrm{sw}}}{4\pi(t-\tilde{t})}} \\ & \cdot \sum_{n=-\infty}^{\infty}\left[\exp\left(-\frac{A_{\mathrm{sw}}(\tilde{n}+z-\tilde{z})^2}{4(t-\tilde{t})}\right) - \exp\left(-\frac{A_{\mathrm{sw}}(\tilde{n}+z+\tilde{z})^2}{4(t-\tilde{t})}\right)\right] \end{aligned} \tag{6.47}$$

with $\tilde{n} = 2n\mathcal{L}$. It is important to mention, that this Green's function only applies for the finite cable. The different solution parts are calculated as follows for constant initial and boundary conditions and excitation:

$$\begin{aligned} T_{\mathrm{ic,sw,G}}(z,t,T_{0,\mathrm{sw}}) &= \int_0^{\mathcal{L}} G_{\mathrm{sw}}(z,t|\tilde{z},0)T_{0,\mathrm{sw}}\,\mathrm{d}\tilde{z} \\ &= -\Gamma(t)T_{0,\mathrm{sw}}\Lambda_3(t)\left\{1 - \Lambda_1(z,t) - \Lambda_1(z_{\mathcal{L}},t) + \sum_{n=1}^{\infty}\left[\Lambda_1(-z_{\mathcal{L}}+\tilde{n},t)\right.\right. \\ &\quad \left.\left. - \Lambda_1(z+\tilde{n},t) + \Lambda_1(-z_{\mathcal{L}}-\tilde{n},t) - \Lambda_1(z-\tilde{n},t)\right]\right\}, \end{aligned} \tag{6.48}$$

$$T_{\mathrm{bc,sw,G}}(z,t,T_{\mathrm{bc}}) = \int_0^t \sqrt{\frac{1}{A_{\mathrm{sw}}\pi\tilde{t}}}\frac{\partial}{\partial z}\sum_{n=-\infty}^{\infty}\exp\left(-\frac{A_{\mathrm{sw}}(\tilde{n}+z)^2}{4\tilde{t}}-\frac{B_{\mathrm{sw}}}{A_{\mathrm{sw}}}\tilde{t}\right)T_{\mathrm{bc}}\,\mathrm{d}\tilde{t}$$
$$= -\Gamma(t)\frac{T_{\mathrm{bc}}}{2}\left\{\Lambda_2(z,t)+\sum_{n=1}^{\infty}[\Lambda_2(z+\tilde{n},t)-\Lambda_2(-z+\tilde{n},t)]\right\}, \quad (6.49)$$

$$T_{\mathrm{inh,sw,G}}(z,t,C_{\mathrm{sw}}) = -\int_0^t\int_0^{\mathcal{L}} G_{\mathrm{sw}}(z,\hat{t}|\tilde{z},0)\frac{C_{\mathrm{sw}}}{A_{\mathrm{sw}}}\,\mathrm{d}\tilde{z}\,\mathrm{d}\hat{t}$$
$$= -\frac{C_{\mathrm{sw}}}{B_{\mathrm{sw}}}\Gamma(t)+T_{\mathrm{ic,sw,G}}\left(z,t,\frac{C_{\mathrm{sw}}}{B_{\mathrm{sw}}}\right)+T_{\mathrm{bc,sw,G}}\left(z,t,\frac{C_{\mathrm{sw}}}{B_{\mathrm{sw}}}\right)$$
$$+T_{\mathrm{bc,sw,G}}\left(z_{\mathcal{L}},t,\frac{C_{\mathrm{sw}}}{B_{\mathrm{sw}}}\right), \quad (6.50)$$

$$T_{\mathrm{sw,G}}(z,t) = T_{\mathrm{ic,sw,G}}(z,t,T_{0,\mathrm{sw}})+T_{\mathrm{bc,sw,G}}(z,t,T_{1,\mathrm{sw}})+T_{\mathrm{bc,sw,G}}(z_{\mathcal{L}},t,T_{2,\mathrm{sw}})$$
$$+T_{\mathrm{inh,sw,G}}(z,t,C_{\mathrm{sw}}). \quad (6.51)$$

All in all, the earlier expression from the solution in the Laplace domain $T_{\mathrm{sw,La}}(z,t)$ appears again in this solution and is extended by new terms. This series formulation covers the complete solution of the partial differential equation, because, unlike the earlier approach, here, approximations were not necessary. If this solution is implemented, nevertheless, the sum has to be stopped after a finite number of addends, which practically also causes an approximation. The convergence behavior of this solution is analyzed in section 7.3.1.c).

c) Solution via Green's Functions in the Laplace Domain

The Laplace domain solution from above could not directly be transformed back into the time domain due to some problematic expressions. In this section, an alternative formulation in the Laplace domain is derived using Green's functions that can directly be transformed back into the time domain. This approach is also known from the electrical TL theory [118]. This section is based on [A.4].

In the Laplace domain, the problem has the form of the Helmholtz equation, so the known Green's function for this problem could be used directly. This way, the above-presented solution is found again and thus, the same problem with the transformation back into the time domain appears again. That is why an alternate formulation for the necessary Green's function is used:

$$G_{\mathrm{sw,L}}(z,\tilde{z},s) = -\frac{2}{\mathcal{L}}\sum_{n=1}^{\infty}\frac{\sin(n_{\mathcal{L}}z)\sin(n_{\mathcal{L}}\tilde{z})}{(sA_{\mathrm{sw}}+B_{\mathrm{sw}})+n_{\mathcal{L}}^2} \quad (6.52)$$

with $n_{\mathcal{L}} = n\pi/\mathcal{L}$. Using the abbreviation $n_{\mathrm{u},\mathcal{L}} = (2n+1)\pi/\mathcal{L}$, the individual solution components are calculated and directly transformed back into the time domain:

$$T_{\mathrm{ic,sw,GL}}(z,s,T_{0,\mathrm{sw}}) = -\int_0^{\mathcal{L}} G_{\mathrm{sw,L}}(z,\tilde{z},s) A_{\mathrm{sw}} T_{0,\mathrm{sw}}\,\mathrm{d}\tilde{z}$$
$$= \frac{4A_{\mathrm{sw}}T_{0,\mathrm{sw}}}{\mathcal{L}} \sum_{n=0}^{\infty} \frac{\sin\left(n_{\mathrm{u},\mathcal{L}} z\right)}{\left(sA_{\mathrm{sw}}+B_{\mathrm{sw}}\right)+n_{\mathrm{u},\mathcal{L}}^2} \frac{1}{n_{\mathrm{u},\mathcal{L}}}$$
$$\downarrow$$
$$T_{\mathrm{ic,sw,GL}}(z,t,T_{0,\mathrm{sw}}) = T_{0,\mathrm{sw}} \frac{4}{\pi} \sum_{n=0}^{\infty} \exp\left(-\frac{t}{A_{\mathrm{sw}}}\left(n_{\mathrm{u},\mathcal{L}}^2 + B_{\mathrm{sw}}\right)\right) \frac{\sin\left(n_{\mathrm{u},\mathcal{L}} z\right)}{2n+1}, \tag{6.53}$$

$$T_{\mathrm{inh,sw,GL}}(z,s,C_{\mathrm{sw}}) = -\int_0^{\mathcal{L}} G_{\mathrm{sw,L}}(z,\tilde{z},s) \frac{C_{\mathrm{sw}}}{s}\,\mathrm{d}\tilde{z} = \frac{4C_{\mathrm{sw}}}{s\mathcal{L}} \sum_{n=0}^{\infty} \frac{\sin(n_{\mathrm{u},\mathcal{L}} z)}{\left(sA_{\mathrm{sw}}+B_{\mathrm{sw}}\right)+n_{\mathrm{u},\mathcal{L}}^2} \frac{1}{n_{\mathrm{u},\mathcal{L}}}$$
$$\downarrow$$
$$T_{\mathrm{inh,sw,GL}}(z,t,C_{\mathrm{sw}}) = -C_{\mathrm{sw}} \frac{4}{\pi} \sum_{n=0}^{\infty} \frac{1-\exp\left(-\frac{t}{A_{\mathrm{sw}}}\left(n_{\mathrm{u},\mathcal{L}}^2 + B_{\mathrm{sw}}\right)\right)}{B_{\mathrm{sw}} + n_{\mathrm{u},\mathcal{L}}^2} \frac{\sin\left(n_{\mathrm{u},\mathcal{L}} z\right)}{2n+1}, \tag{6.54}$$

$$T_{\mathrm{bc,sw,GL}}(z,s,T_{\mathrm{bc}}) = -\frac{T_{\mathrm{bc}}}{s} \frac{\partial}{\partial\tilde{z}} G_{\mathrm{sw,L}}(z,\tilde{z},s)|_{\tilde{z}=0} = \frac{2}{\mathcal{L}}\pi \frac{T_{\mathrm{bc}}}{s} \sum_{n=1}^{\infty} \frac{n_{\mathcal{L}} \sin\left(n_{\mathcal{L}} z\right)}{\left(sA_{\mathrm{sw}}+B_{\mathrm{sw}}\right)+n_{\mathcal{L}}^2}$$
$$\downarrow$$
$$T_{\mathrm{bc,sw,GL}}(z,t,T_{\mathrm{bc}}) = \frac{2}{\mathcal{L}} T_{\mathrm{bc}} \sum_{n=1}^{\infty} \left[1-\exp\left(-\frac{t}{A_{\mathrm{sw}}}\left[n_{\mathcal{L}}^2 + B_{\mathrm{sw}}\right]\right)\right] \frac{n_{\mathcal{L}} \sin\left(n_{\mathcal{L}} z\right)}{n_{\mathcal{L}}^2 + B_{\mathrm{sw}}}, \tag{6.55}$$

$$T_{\mathrm{sw,GL}}(z,t) = T_{\mathrm{ic,sw,GL}}(z,t,T_{0,\mathrm{sw}}) + T_{\mathrm{bc,sw,GL}}(z,t,T_{1,\mathrm{sw}}) + T_{\mathrm{bc,sw,GL}}(z_{\mathcal{L}},t,T_{2,\mathrm{sw}})$$
$$+ T_{\mathrm{inh,sw,GL}}(z,t,C_{\mathrm{sw}}). \tag{6.56}$$

At the cable terminations, the applied boundary conditions are only fulfilled for the limits

$$\lim_{z\to 0} T_{\mathrm{bc,sw,GL}}(z,t,T_{1,\mathrm{sw}}) = T_{1,\mathrm{sw}}, \quad \lim_{z\to 0} T_{\mathrm{bc,sw,GL}}(z_{\mathcal{L}},t,T_{2,\mathrm{sw}}) = T_{2,\mathrm{sw}}, \tag{6.57}$$

but not if the coordinates $z = 0\,\mathrm{m}$ and $z_{\mathcal{L}} = 0\,\mathrm{m}$ are directly inserted. Also, the corresponding solution part $T_{\mathrm{bc,sw,GL}}(z,t,T_{\mathrm{bc}})$ only converges very slowly (see section 7.3.1.c)), so many addends have to be taken into account for a precise result. Overall this limits the applicability of this complete formulation. For the special case of identical cable termination temperatures $T_{1,\mathrm{sw}} = T_{2,\mathrm{sw}}$, setting the reference temperature to this value $T_{1,\mathrm{sw}}$ allows a formulation without the unsteady and slowly converging part.

6.1.3 Systems of Single Wire Cables

In this section, a thermal model for a system of single wire cables that are thermally connected at the cable terminations is developed. This model considers the axial heat exchange between the individual cables and is based on [A.7].

In section 6.1.2.a), an analytical calculation method for the calculation of the temperature of a single cable of length $\mathcal{L}$ oriented in z-direction consisting of conductor and insulation loaded with the current I was presented. From this known temperature distribution, the corresponding heat flow distribution $P(z,t)$ along the cable is calculated, which linearly depends on the cable termination temperatures T_1 and T_2:

$$
\begin{aligned}
P(z,t) &= -\frac{1}{R'}\frac{\partial T(z,t)}{\partial z} = F_1(z,t)T_1 + F_2(z,t)T_2 + F_3(z,t), \qquad (6.58)\\
F_1(z,t) &= \frac{\Lambda_4(z,t)}{2R'}, \quad F_2(z,t) = -\frac{\Lambda_4(z_{\mathcal{L}},t)}{2R'},\\
F_3(z,t) &= \left(\frac{C}{B}+T_0\right)\frac{1}{R'}\sqrt{\frac{A}{t\pi}}\exp\left(-\frac{B}{A}t\right)\left(\exp\left(-\frac{Az_{\mathcal{L}}^2}{4t}\right)-\exp\left(-\frac{Az^2}{4t}\right)\right)\\
&\quad + \frac{C}{B}\left(F_1(z,t)+F_2(z,t)\right),\\
\Lambda_4(z,t) &= 2\sqrt{\frac{A}{t\pi}}\exp\left(-\frac{Az^2}{4t}-\frac{Bt}{A}\right)\cosh\left(\frac{z}{2}\sqrt{B}\right)+\sqrt{B}\left(\theta_1(z,t)-\theta_2(z,t)\right).
\end{aligned}
$$

Based on this, a network of N single wire cables that are thermally connected at K nodes is analyzed. An example of such a system is given in figure 6.3. The axial heat exchange between the cables is calculated, assuming that there is no coupling between the cables transversal to the axial direction.

As in the earlier presented solution, the cable termination temperatures are needed and have to be precalculated. To do that, in the first step, the vectors with the cable end temperatures for all conductors, $\boldsymbol{T}_i,\ i=1,2$, are split up into the **g**iven values $\boldsymbol{T}_{i,\mathrm{g}}$ at the outer boundaries of the network and the **u**nknown values $\boldsymbol{T}_{i,\mathrm{u}}$ at the inner nodes using the matrices $\mathbf{E}_{i,\mathrm{g}}$ and $\mathbf{E}_{i,\mathrm{u}}$:

$$
\boldsymbol{T}_i = (T_{i,1}\ T_{i,2}\ \ldots\ T_{i,N})^T = \mathbf{E}_{i,\mathrm{g}}\boldsymbol{T}_{i,\mathrm{g}} + \mathbf{E}_{i,\mathrm{u}}\boldsymbol{T}_{i,\mathrm{u}}. \qquad (6.59)
$$

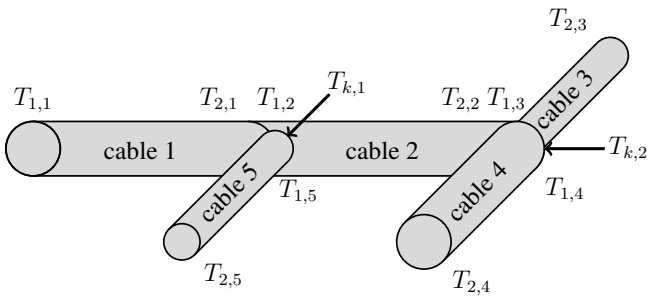

Figure 6.3: Exemplary system of single wire cables.

Perfect thermal connections are assumed. Then, the temperature behaves continuously at the nodes. The unknown cable temperatures are expressed in terms of the nodal temperatures $\boldsymbol{T}_k = (T_{k,1}\ T_{k,2}\ \ldots\ T_{k,K})^T$ using the matrix $\mathbf{E}_{i,k}$ which reduces the number of unknowns:

$$\boldsymbol{T}_i = (T_{i,1}\ T_{i,2}\ \ldots\ T_{i,N})^T = \mathbf{E}_{i,\mathrm{g}}\boldsymbol{T}_{i,\mathrm{g}} + \mathbf{E}_{i,\mathrm{u}}\mathbf{E}_{i,k}\boldsymbol{T}_k = \mathbf{E}_{i,\mathrm{g}}\boldsymbol{T}_{i,\mathrm{g}} + \hat{\mathbf{E}}_i\boldsymbol{T}_k. \tag{6.60}$$

At the nodes, the heat flow fulfills Kirchhoff's law, which means that the incoming heat (cables with local $z = \mathcal{L}$ and T_2 at the node) equals the heat that leaves the node (cables with local $z = 0\,\mathrm{m}$ and T_1 at the node). Using the vector of the heat flow

$$\begin{aligned}\boldsymbol{P}(z_1, z_2, ..., z_N, t) = \mathbf{F}_1(z_1, z_2, ..., z_N, t)\boldsymbol{T}_1 + \mathbf{F}_2(z_1, z_2, ..., z_N, t)\boldsymbol{T}_2 \\ + \boldsymbol{F}_3(z_1, z_2, ..., z_N, t),\end{aligned} \tag{6.61}$$

with

$$\begin{aligned}\mathbf{F}_i(z_1, z_2, ..., z_N, t) &= \mathrm{diag}\left(F_{i,1}(z_1, t), ..., F_{i,N}(z_N, t)\right), \quad i = 1, 2, \\ \boldsymbol{F}_3(z_1, z_2, ..., z_N, t) &= \left(F_{3,1}(z_1, t)\ \ldots\ F_{3,N}(z_N, t)\right)^T,\end{aligned} \tag{6.62}$$

Kirchhoff's laws can be expressed as

$$\hat{\mathbf{E}}_2^T\boldsymbol{P}(\mathcal{L}_1, ..., \mathcal{L}_N, t) - \hat{\mathbf{E}}_1^T\boldsymbol{P}(0, ..., 0, t) = \mathbf{0}. \tag{6.63}$$

Inserting equation (6.60) and equation (6.61) into equation (6.63) and rearranging leads to the system of linear equations that has to be solved to find the unknown nodal temperatures:

$$\begin{aligned}&\left[\hat{\mathbf{E}}_2^T\left(\mathbf{F}_{1,\mathcal{L}}(t)\hat{\mathbf{E}}_1 + \mathbf{F}_{2,\mathcal{L}}(t)\hat{\mathbf{E}}_2\right) - \hat{\mathbf{E}}_1^T\left(\mathbf{F}_{1,0}(t)\hat{\mathbf{E}}_1 + \mathbf{F}_{2,0}(t)\hat{\mathbf{E}}_2\right)\right]\boldsymbol{T}_k \\ &= \left(\hat{\mathbf{E}}_1^T\mathbf{F}_{1,0}(t) - \hat{\mathbf{E}}_2^T\mathbf{F}_{1,\mathcal{L}}(t)\right)\mathbf{E}_{1,\mathrm{g}}\boldsymbol{T}_{1,\mathrm{g}} + \left(\hat{\mathbf{E}}_1^T\mathbf{F}_{2,0}(t) - \hat{\mathbf{E}}_2^T\mathbf{F}_{2,\mathcal{L}}(t)\right)\mathbf{E}_{2,\mathrm{g}}\boldsymbol{T}_{2,\mathrm{g}} \\ &\quad + \hat{\mathbf{E}}_1^T\boldsymbol{F}_{3,0}(t) - \hat{\mathbf{E}}_2^T\boldsymbol{F}_{3,\mathcal{L}}(t)\end{aligned} \tag{6.64}$$

with

$$\begin{aligned}\mathbf{F}_{i,0}(t) &= \mathbf{F}_i(0, ..., 0, t), \quad \mathbf{F}_{i,\mathcal{L}}(t) = \mathbf{F}_i(\mathcal{L}_1, ..., \mathcal{L}_N, t), \quad i = 1, 2, \\ \boldsymbol{F}_{3,0}(t) &= \boldsymbol{F}_3(0, ..., 0, t), \quad \boldsymbol{F}_{3,\mathcal{L}}(t) = \boldsymbol{F}_3(\mathcal{L}_1, ..., \mathcal{L}_N, t).\end{aligned} \tag{6.65}$$

Knowing the nodal temperatures, the axial temperature distribution along the cables is calculated using equation (6.37) (solution for a single wire cable from the Laplace domain with approximation).

6.1.4 Two Single Wire Cables

In this section, an arrangement of two coupled single wire cables is analyzed (cross-section see figure 6.4). In the general case, those two wires do not necessarily have to be identical.

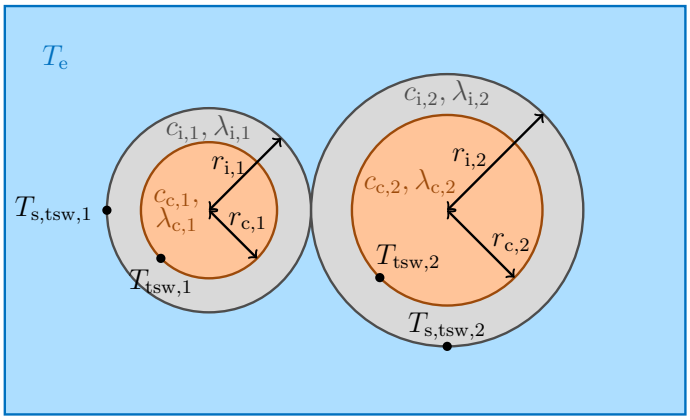

Figure 6.4: Cross-section of the analyzed arrangement of two single wire cables.

a) Partial Differential Equations and Equivalent Circuit Diagram

Using the precede presented in section 5.3.3, the ECD given in figure 6.5 is derived that describes this cable arrangement. The corresponding PDE system is

$$\boldsymbol{C}_\mathrm{tsw} = \frac{\partial^2}{\partial z^2}\boldsymbol{T}_\mathrm{tsw}(z,t) - \mathbf{A}_\mathrm{tsw}\frac{\partial}{\partial t}\boldsymbol{T}_\mathrm{tsw}(z,t) - \mathbf{B}_\mathrm{tsw}\boldsymbol{T}_\mathrm{tsw}(z,t), \tag{6.66}$$

$$\mathbf{A}_\mathrm{tsw} = \begin{pmatrix} A_{11} & 0 \\ 0 & A_{22} \end{pmatrix} = \begin{pmatrix} R'_1\mathcal{C}'_1 & 0 \\ 0 & R'_2\mathcal{C}'_2 \end{pmatrix}, \quad \boldsymbol{C}_\mathrm{tsw} = \begin{pmatrix} C_{\mathrm{tsw},1} \\ C_{\mathrm{tsw},2} \end{pmatrix} = \begin{pmatrix} -R'_1(P'_{\mathrm{el},1} + G'_1 T_\mathrm{e}) \\ -R'_2(P'_{\mathrm{el},2} + G'_2 T_\mathrm{e}) \end{pmatrix},$$

$$\mathbf{B}_\mathrm{tsw} = \begin{pmatrix} B_{11} & B_{12} \\ B_{21} & B_{22} \end{pmatrix} = \begin{pmatrix} R'_1(G'_1 + G'_{12}) & -R'_1 G'_{12} \\ -R'_2 G'_{12} & R'_2(G'_2 + G'_{12}) \end{pmatrix}, \quad \boldsymbol{T}_\mathrm{tsw}(z,t) = \begin{pmatrix} T_{\mathrm{tsw},1}(z,t) \\ T_{\mathrm{tsw},2}(z,t) \end{pmatrix}.$$

The surface temperatures are calculated from the cable temperatures via

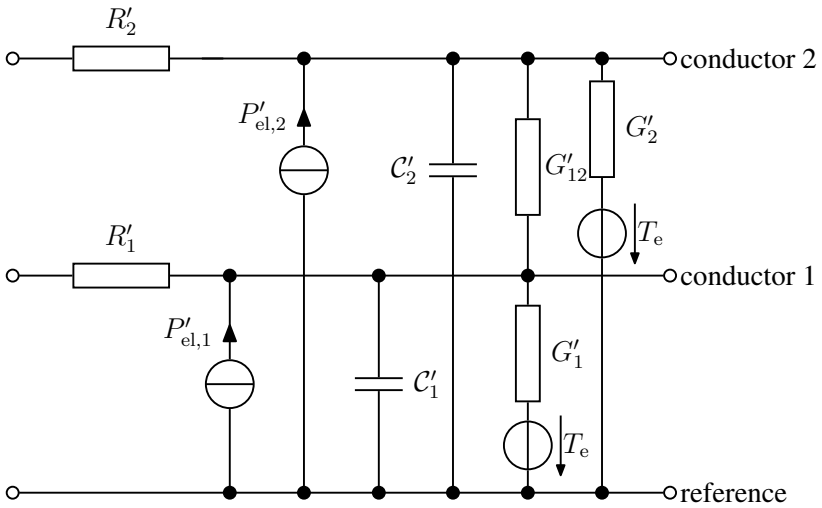

Figure 6.5: ECD for an infinitesimally short cable segment (two single wire cables).

$$\boldsymbol{T}_{\mathrm{s,tsw}}(z,t) = \boldsymbol{T}_{\mathrm{tsw}}(z,t) - \mathbf{R}'_{\mathrm{i,tsw}}\mathbf{G}'_{ii,\mathrm{tsw}}\left(\boldsymbol{T}_{\mathrm{tsw}}(z,t) - T_{\mathrm{e}}\cdot\begin{pmatrix}1\\1\end{pmatrix}\right), \tag{6.67}$$

$$\mathbf{R}'_{\mathrm{i,tsw}} = \begin{pmatrix}R'_{\mathrm{i},1} & 0\\ 0 & R'_{\mathrm{i},2}\end{pmatrix}, \mathbf{G}'_{ii,\mathrm{tsw}} = \begin{pmatrix}G'_{11} & 0\\ 0 & G'_{22}\end{pmatrix}, G'_{ii} = \frac{1}{R'_{\mathrm{i},i} + R'_{\alpha,i}}, i = 1,2.$$

b) Closed Formulation for the Radial Transient Case

In the general solution for the radial transient case known from section 6.1.1.c), a matrix diagonalization is necessary. For the special case of two coupled single wire cables, in the following, an explicit formulation is derived. In the case of this cable arrangement, the matrix formulation of the system of differential equations can be rewritten as two coupled equations:

$$\begin{aligned}-A_{11}\frac{\partial}{\partial t}T_{\mathrm{tsw,rt},1}(t) - B_{11}T_{\mathrm{tsw,rt},1}(t) - B_{12}T_{\mathrm{tsw,rt},2}(t) &= C_{\mathrm{tsw},1},\\ -A_{22}\frac{\partial}{\partial t}T_{\mathrm{tsw,rt},2}(t) - B_{21}T_{\mathrm{tsw,rt},1}(t) - B_{22}T_{\mathrm{tsw,rt},2}(t) &= C_{\mathrm{tsw},2}.\end{aligned} \tag{6.68}$$

Rearranging leads to a differential equation for the temperature $T_{\mathrm{tsw,rt},1}(t)$:

$$\frac{\partial^2}{\partial t^2}T_{\mathrm{tsw,rt},1}(t) + \theta_{\mathrm{tsw},1}\frac{\partial}{\partial t}T_{\mathrm{tsw,rt},1}(t) + \theta_{\mathrm{tsw},2}T_{\mathrm{tsw,rt},1}(t) = \theta_{\mathrm{tsw},3,1}, \tag{6.69}$$

$$\theta_{\mathrm{tsw},1} = \frac{A_{22}B_{11} + A_{11}B_{22}}{A_{11}A_{22}},\ \theta_{\mathrm{tsw},2} = \frac{B_{11}B_{22} - B_{21}B_{12}}{A_{11}A_{22}},\ \theta_{\mathrm{tsw},3,1} = \frac{C_{\mathrm{tsw},2}B_{12} - C_{\mathrm{tsw},1}B_{22}}{A_{11}A_{22}}.$$

This differential equation is solved with

$$T_{\mathrm{tsw,rt},1}(t) = T_{\mathrm{tsw,rt},1,1}\mathrm{e}^{\theta_{\mathrm{tsw},4}t} + T_{\mathrm{tsw,rt},2,1}\mathrm{e}^{\theta_{\mathrm{tsw},5}t} + \frac{\theta_{\mathrm{tsw},3,1}}{\theta_{\mathrm{tsw},2}}, \tag{6.70}$$

$$\theta_{\mathrm{tsw},i} = -\frac{\theta_{\mathrm{tsw},1}}{2} + (-1)^i\sqrt{\frac{\theta_{\mathrm{tsw},1}^2}{4} - \theta_{\mathrm{tsw},2}}, \quad i = 4,5.$$

Using the second conductor temperature

$$T_{\mathrm{tsw,rt},2}(t) = -\frac{A_{11}}{B_{12}}\frac{\partial}{\partial t}T_{\mathrm{tsw,rt},1}(t) - \frac{B_{11}}{B_{12}}T_{\mathrm{tsw,rt},1}(t) - \frac{C_{\mathrm{tsw},1}}{B_{12}} \tag{6.71}$$

and the initial conditions for both temperatures, $T_{\mathrm{tsw,rt},1}(0) = T_{0,\mathrm{tsw},1}$ and $T_{\mathrm{tsw,rt},2}(0) = T_{0,\mathrm{tsw},2}$, it follows with $i = 1,2$:

$$T_{\mathrm{tsw,rt},i,1} = (-1)^i\frac{T_{0,\mathrm{tsw},1}B_{11} + T_{0,\mathrm{tsw},2}B_{12} + C_{\mathrm{tsw},1} + A_{11}\theta_{\mathrm{tsw},6-i}\left(T_{0,\mathrm{tsw},1} - \dfrac{\theta_{\mathrm{tsw},3,1}}{\theta_{\mathrm{tsw},2}}\right)}{A_{11}\sqrt{\theta_{\mathrm{tsw},1}^2 - 4\theta_{\mathrm{tsw},2}}}.$$

So now, the complete temperature development is known for the first conductor. The corresponding temperature of the second conductor is derived using equation (6.71):

$$T_{\mathrm{tsw,rt},2}(t) = T_{\mathrm{tsw,rt},1,2}\mathrm{e}^{\theta_{\mathrm{tsw},4}t} + T_{\mathrm{tsw,rt},2,2}\mathrm{e}^{\theta_{\mathrm{tsw},5}t} + \frac{\theta_{\mathrm{tsw},3,2}}{\theta_{\mathrm{tsw},2}}, \tag{6.72}$$

$$\theta_{\mathrm{tsw},3,2} = \frac{C_{\mathrm{tsw},1}B_{21} - C_{\mathrm{tsw},2}B_{11}}{A_{11}A_{22}}, \quad i = 1, 2,$$

$$T_{\mathrm{tsw,rt},i,2} = (-1)^i \frac{T_{0,\mathrm{tsw},2}B_{22} + T_{0,\mathrm{tsw},1}B_{21} + C_{\mathrm{tsw},2} + A_{22}\theta_{\mathrm{tsw},6-i}\left(T_{0,\mathrm{tsw},2} - \dfrac{\theta_{\mathrm{tsw},3,2}}{\theta_{\mathrm{tsw},2}}\right)}{A_{22}\sqrt{\theta_{\mathrm{tsw},1}^2 - 4\theta_{\mathrm{tsw},2}}}.$$

c) Direct Solution in the Laplace Domain and Approximation

In this section, both, the time and the spatial dependence are considered. In the Laplace domain, the solution of the complete PDE system is

$$\boldsymbol{T}_{\mathrm{tsw}}(z,s) = \mathbf{E}_{\tilde{\mathbf{A}},\mathrm{tsw}}\mathrm{e}^{z\sqrt{\mathbf{D}_{\tilde{\mathbf{A}},\mathrm{tsw}}}}\boldsymbol{T}_{\mathrm{tsw},1}(s) + \mathbf{E}_{\tilde{\mathbf{A}},\mathrm{tsw}}\mathrm{e}^{-z\sqrt{\mathbf{D}_{\tilde{\mathbf{A}},\mathrm{tsw}}}}\boldsymbol{T}_{\mathrm{tsw},2}(s) - \tilde{\mathbf{A}}_{\mathrm{tsw}}^{-1}\hat{\boldsymbol{C}}_{\mathrm{tsw}}, \tag{6.73}$$

$$\begin{aligned}\boldsymbol{T}_{\mathrm{tsw},i}(s) = \mathbf{E}_{\mathcal{L},\mathrm{tsw}} \Bigg\{ &(-1)^{i+1}\mathrm{e}^{(-1)^i\mathcal{L}\sqrt{\mathbf{D}_{\tilde{\mathbf{A}},\mathrm{tsw}}}}\mathbf{E}_{\tilde{\mathbf{A}},\mathrm{tsw}}^{-1}\left[\frac{\boldsymbol{T}_{1,\mathrm{tsw}}}{s} + \tilde{\mathbf{A}}_{\mathrm{tsw}}^{-1}\hat{\boldsymbol{C}}_{\mathrm{tsw}}\right] \\ &+(-1)^i\mathbf{E}_{\tilde{\mathbf{A}},\mathrm{tsw}}^{-1}\left[\frac{\boldsymbol{T}_{2,\mathrm{tsw}}}{s} + \tilde{\mathbf{A}}_{\mathrm{tsw}}^{-1}\hat{\boldsymbol{C}}_{\mathrm{tsw}}\right]\Bigg\},\end{aligned}$$

$$i = 1, 2, \quad \hat{\boldsymbol{C}}_{\mathrm{tsw}} = \frac{\boldsymbol{C}_{\mathrm{tsw}}}{s} - \mathbf{A}_{\mathrm{tsw}}\boldsymbol{T}_{0,\mathrm{tsw}}, \quad \mathbf{E}_{\mathcal{L},\mathrm{tsw}} = \left[\mathrm{e}^{-\mathcal{L}\sqrt{\mathbf{D}_{\tilde{\mathbf{A}},\mathrm{tsw}}}} - \mathrm{e}^{\mathcal{L}\sqrt{\mathbf{D}_{\tilde{\mathbf{A}},\mathrm{tsw}}}}\right]^{-1}$$

with the diagonalization of the matrix $\tilde{\mathbf{A}}_{\mathrm{tsw}}$:

$$\tilde{\mathbf{A}}_{\mathrm{tsw}} = s\mathbf{A}_{\mathrm{tsw}} + \mathbf{B}_{\mathrm{tsw}} = \mathbf{E}_{\tilde{\mathbf{A}},\mathrm{tsw}}\mathbf{D}_{\tilde{\mathbf{A}},\mathrm{tsw}}\mathbf{E}_{\tilde{\mathbf{A}},\mathrm{tsw}}^{-1}, \quad \mathbf{D}_{\tilde{\mathbf{A}},\mathrm{tsw}} = \begin{pmatrix} D_{\tilde{\mathbf{A}},\mathrm{tsw},1} & 0 \\ 0 & D_{\tilde{\mathbf{A}},\mathrm{tsw},2} \end{pmatrix}. \tag{6.74}$$

As $\tilde{\mathbf{A}}_{\mathrm{tsw}}$ and its diagonalization depend on the Laplace variable s, an explicit expression is necessary for the transformation back into the time domain. In the following, for a shorter notation, $\hat{A} = A_{11} - A_{22}$ and $\hat{B} = B_{11} - B_{22}$ are used. Depending on the parameters and exact setup, different cases can occur:

case 1: $B_{12}B_{21} \neq 0$

In this case, the different conductor temperatures couple. Then, in the calculation, a double square root appears. The inner square root is

$$W_{\mathrm{tsw}} = \sqrt{\frac{1}{4}\left(\hat{A}s + \hat{B}\right)^2 + B_{12}B_{21}}, \tag{6.75}$$

which is of the order one with regard to s. To transform this back into the time domain, a Taylor series expansion (order one) is used to find a linear approximation of the square root:

$$W_{\mathrm{tsw}} \approx W_1 s + W_0, \quad W_1 = \frac{\hat{A}\hat{B}}{2\sqrt{\hat{B}^2 + 4B_{12}B_{21}}}, \quad W_0 = \sqrt{\frac{\hat{B}^2}{4} + B_{12}B_{21}}. \tag{6.76}$$

Depending on the different parameters, this approximation changes. It is important to know if W_1 and W_0 become zero or not because this influences the partial fraction decomposition that is performed in the following. That is why two different subcases are necessary. For both of them, the result for the complete solution of the differential equation is a very complicated expression, which can be found in appendix B.

case 2: $(B_{12} = 0 \wedge B_{21} \neq 0) \vee (B_{12} \neq 0 \wedge B_{21} = 0)$

Here, B_{12} and B_{21} are not both equal or both unequal to zero. Physically, this would mean a coupling only in one direction, which is not reasonable. That is why this case is not further evaluated.

case 3: $B_{12} = B_{21} = 0$

In this case, two uncoupled equations are the result. The solution is already known from the solution for a single wire cable. Physically, both conductor temperatures do not influence each other.

As can be seen from those solutions for a finite cable, the results are very complicated and computationally intensive, even though analytical formulations were found. This is due to the decoupling similarity transform, which depends on the Laplace variable s and therefore massively increases the complexity as an explicit formulation is necessary for the transform back into the time domain. Because of this complexity, numerical instabilities become more probable. Therefore, this approach with the solution in the Laplace domain and approximation for the transformation back into the time domain is not usable for real setups. This is the reason why this approach will not be further investigated for more general arrangements. Instead, different approaches are necessary.

d) Solution via Green's Functions in the Laplace Domain

As already presented for the single wire cable, Green's functions can be used in the Laplace domain to find a series formulation for the cable temperatures. The complete calculation formula in the general case is calculated here. In the Laplace domain, the formulation of the general PDE system analog to the electrical domain is

$$\frac{\partial^2}{\partial z^2}\boldsymbol{T}(z,s) - (s\mathbf{A} + \mathbf{B})\boldsymbol{T}(z,s) = \frac{\boldsymbol{C}}{s} - \mathbf{A}\boldsymbol{T}_0 = \hat{\boldsymbol{C}}(s), \tag{6.77}$$

$$\boldsymbol{T}(0,s) = \tilde{\boldsymbol{T}}_1(s) = \frac{\boldsymbol{T}_1}{s}, \quad \boldsymbol{T}(\mathcal{L},s) = \tilde{\boldsymbol{T}}_2(s) = \frac{\boldsymbol{T}_2}{s}. \tag{6.78}$$

So, a differential equation of the following form has to be solved:

$$\frac{\partial^2}{\partial z^2}\boldsymbol{T}(z) - (s\mathbf{A} + \mathbf{B})\boldsymbol{T}(z) = \boldsymbol{f}(z), \quad \boldsymbol{T}(0) = \tilde{\boldsymbol{T}}_1, \quad \boldsymbol{T}(\mathcal{L}) = \tilde{\boldsymbol{T}}_2. \tag{6.79}$$

The corresponding Green's function $\mathbf{G}_{\text{gen}}(z, \tilde{z}, s)$, therefore, has to fulfill the following equations, where N is the number of conductors:

$$\frac{\partial^2}{\partial z^2}\mathbf{G}_{\text{gen}}(z, \tilde{z}, s) - (s\mathbf{A} + \mathbf{B})\mathbf{G}_{\text{gen}}(z, \tilde{z}, s) = \delta(z, \tilde{z})\mathbf{U}_N, \tag{6.80}$$

$$\mathbf{G}_{\text{gen}}(0, \tilde{z}, s) = \mathbf{G}_{\text{gen}}(\mathcal{L}, \tilde{z}, s) = \mathbf{G}_{\text{gen}}(z, 0, s) = \mathbf{G}_{\text{gen}}(z, \mathcal{L}, s) = 0, \tag{6.81}$$

$$\mathbf{G}_{\text{gen}}(z, \tilde{z}, s) = \mathbf{G}_{\text{gen}}(\tilde{z}, z, s). \tag{6.82}$$

Because of the structure of $\mathbf{G}_{\text{gen}}(z, \tilde{z}, s)$, it is also:

$$\frac{\partial^2}{\partial z^2}\mathbf{G}_{\text{gen}}(z, \tilde{z}, s) - \mathbf{G}_{\text{gen}}(z, \tilde{z}, s)(s\mathbf{A} + \mathbf{B}) = \delta(z, \tilde{z})\mathbf{U}_N. \tag{6.83}$$

Generally, applying the product rule leads to

$$\int_0^{\mathcal{L}} \left[\frac{\mathrm{d}^2}{\mathrm{d}\tilde{z}^2}(\mathbf{u}_2) \cdot \boldsymbol{u}_1 - \mathbf{u}_2\frac{\mathrm{d}^2}{\mathrm{d}\tilde{z}^2}\boldsymbol{u}_1\right] \mathrm{d}\tilde{z} = \left[\frac{\mathrm{d}}{\mathrm{d}\tilde{z}}(\mathbf{u}_2) \cdot \boldsymbol{u}_1 - \mathbf{u}_2\frac{\mathrm{d}}{\mathrm{d}\tilde{z}}\boldsymbol{u}_1\right]_{\tilde{z}=0}^{\mathcal{L}}. \tag{6.84}$$

Using

$$\boldsymbol{u}_1 = \boldsymbol{T}(\tilde{z}) \text{ and } \mathbf{u}_2 = \mathbf{G}_{\text{gen}}(z, \tilde{z}, s), \tag{6.85}$$

equation (6.84) can be written as

$$\begin{aligned} &\int_0^{\mathcal{L}} \left[\frac{\mathrm{d}^2}{\mathrm{d}\tilde{z}^2}\left(\mathbf{G}_{\text{gen}}(z, \tilde{z}, s)\right) \cdot \boldsymbol{T}(\tilde{z}) - \mathbf{G}_{\text{gen}}(z, \tilde{z}, s)\frac{\mathrm{d}^2}{\mathrm{d}\tilde{z}^2}\boldsymbol{T}(\tilde{z})\,\mathrm{d}\tilde{z}\right] \\ &= \left[\frac{\mathrm{d}}{\mathrm{d}\tilde{z}}\left(\mathbf{G}_{\text{gen}}(z, \tilde{z}, s)\right) \cdot \boldsymbol{T}(\tilde{z}) - \mathbf{G}_{\text{gen}}(z, \tilde{z}, s)\frac{\mathrm{d}}{\mathrm{d}\tilde{z}}\boldsymbol{T}(\tilde{z})\right]_{\tilde{z}=0}^{\mathcal{L}}. \end{aligned} \tag{6.86}$$

Inserting equations (6.79) and (6.83) leads to the calculation formula for the temperature development:

$$\begin{aligned} \boldsymbol{T}(z) = &\int_0^{\mathcal{L}} \mathbf{G}_{\text{gen}}(z, \tilde{z}, s)\boldsymbol{f}(\tilde{z})\,\mathrm{d}\tilde{z} \\ &+ \frac{\mathrm{d}}{\mathrm{d}\tilde{z}}\left(\mathbf{G}_{\text{gen}}(z, \tilde{z}, s)\right)\Big|_{\tilde{z}=\mathcal{L}} \tilde{\boldsymbol{T}}_2(s) - \frac{\mathrm{d}}{\mathrm{d}\tilde{z}}\left(\mathbf{G}_{\text{gen}}(z, \tilde{z}, s)\right)\Big|_{\tilde{z}=0} \tilde{\boldsymbol{T}}_1(s). \end{aligned} \tag{6.87}$$

Inserting the Green's function

$$\mathbf{G}_{\text{gen}}(z, \tilde{z}, s) = -\sum_{n=1}^{\infty}\left[\mathbf{B} + s\mathbf{A} + n_{\mathcal{L}}^2\mathbf{U}_N\right]^{-1}\frac{2}{\mathcal{L}}\sin\left(n_{\mathcal{L}}z\right)\sin\left(n_{\mathcal{L}}\tilde{z}\right) \tag{6.88}$$

as well as $\boldsymbol{f}(\tilde{z}) = \hat{\boldsymbol{C}}(s)$ and equation (6.78) leads to

$$\begin{aligned}&\boldsymbol{T}_{\mathrm{GL}}(z,s) \\ &= \underbrace{\frac{4}{\pi}\sum_{n=0}^{\infty}\sin\left(n_{\mathrm{u},\mathcal{L}}z\right)\frac{1}{n_{\mathrm{u}}}\boldsymbol{X}_1(s,n_{\mathrm{u}},\boldsymbol{T}_0,\boldsymbol{C})}_{\boldsymbol{T}_{\mathrm{hom}}(z,s)=\boldsymbol{T}_{\tilde{\boldsymbol{T}}_0}(z,s,\boldsymbol{T}_0)+\boldsymbol{T}_{\tilde{\boldsymbol{C}}}(z,s,\boldsymbol{C})} + \underbrace{\sum_{n=1}^{\infty}\frac{2n_{\mathcal{L}}}{\mathcal{L}}\sin\left(n_{\mathcal{L}}z\right)\boldsymbol{X}_2(s,n,\boldsymbol{T}_1-(-1)^n\boldsymbol{T}_2)}_{\boldsymbol{T}_{\mathrm{inh}}(z,s)=\boldsymbol{T}_{\tilde{\boldsymbol{T}}_1}(z,s,\boldsymbol{T}_1)+\boldsymbol{T}_{\tilde{\boldsymbol{T}}_2}(z,s,\boldsymbol{T}_2)},\end{aligned} \tag{6.89}$$

$$\boldsymbol{X}_1(s,n_{\mathrm{u}},\boldsymbol{T}_0,\boldsymbol{C}) = -\left[\mathbf{B}+s\mathbf{A}+n_{\mathrm{u},\mathcal{L}}^2\mathbf{U}_N\right]^{-1}\hat{\boldsymbol{C}}, \tag{6.90}$$

$$\boldsymbol{X}_2(s,n,\boldsymbol{T}_{\mathrm{bc}}) = \frac{1}{s}\left[\mathbf{B}+s\mathbf{A}+n_{\mathcal{L}}^2\mathbf{U}_N\right]^{-1}\boldsymbol{T}_{\mathrm{bc}}. \tag{6.91}$$

The solution part $\boldsymbol{T}_{\mathrm{hom}}(z,s)$ describes the solution for homogeneous boundary conditions. Via $\boldsymbol{T}_{\mathrm{inh}}(z,s)$, inhomogeneous boundary conditions are taken into account. The general solution in the time domain then becomes

$$\begin{aligned}\boldsymbol{T}_{\mathrm{GL}}(z,t) = &\frac{4}{\pi}\sum_{n=0}^{\infty}\sin\left(n_{\mathrm{u},\mathcal{L}}z\right)\frac{1}{n_{\mathrm{u}}}\boldsymbol{x}_1(t,n,\boldsymbol{T}_0,\boldsymbol{C}) \\ &+\sum_{n=1}^{\infty}\frac{2n_{\mathcal{L}}}{\mathcal{L}}\sin\left(n_{\mathcal{L}}z\right)\boldsymbol{x}_2(t,n,\boldsymbol{T}_1-(-1)^n\boldsymbol{T}_2).\end{aligned} \tag{6.92}$$

So, for a specific solution, only $\boldsymbol{x}_1(t,n_{\mathrm{u}},\boldsymbol{T}_0,\boldsymbol{C})$ and $\boldsymbol{x}_2(t,n,\boldsymbol{T}_1-(-1)^n\boldsymbol{T}_2)$ have to be calculated. In the case of an arrangement of two single wire cables, the following matrix inversion can be calculated explicitly:

$$\begin{aligned}\hat{\mathbf{A}} = \left[\mathbf{B}_{\mathrm{tsw}}+s\mathbf{A}_{\mathrm{tsw}}+n_{\mathcal{L}}^2\mathbf{U}_2\right]^{-1} &= \begin{pmatrix}\hat{A}_{11}(s,n) & \hat{A}_{12}\\ \hat{A}_{21} & \hat{A}_{22}(s,n)\end{pmatrix}^{-1} \\ &= \frac{1}{\hat{A}_{11}(s,n)\hat{A}_{22}(s,n)-\hat{A}_{12}\hat{A}_{21}}\begin{pmatrix}\hat{A}_{22}(s,n) & -\hat{A}_{12}\\ -\hat{A}_{21} & \hat{A}_{11}(s,n)\end{pmatrix}.\end{aligned} \tag{6.93}$$

Then, equation (6.89) is reformulated:

$$\begin{aligned}\boldsymbol{X}_1(s,n_{\mathrm{u}},\boldsymbol{T}_0,\boldsymbol{C}) &= \frac{1}{\det(\mathbf{A}_{\mathrm{tsw}})}\frac{\boldsymbol{b}_1s^2+\boldsymbol{b}_2s+\boldsymbol{b}_3}{s(s-a_{\mathrm{tsw},1})(s-a_{\mathrm{tsw},2})}, \\ \boldsymbol{b}_1 &= \det(\mathbf{A}_{\mathrm{tsw}})\boldsymbol{T}_{0,\mathrm{tsw}}, \\ \boldsymbol{b}_2 &= \left(\det(\mathbf{B}_{\mathrm{tsw}})\mathbf{B}_{\mathrm{tsw}}^{-1}+n_{\mathrm{u},\mathcal{L}}^2\mathbf{U}_2\right)\mathbf{A}_{\mathrm{tsw}}\boldsymbol{T}_{0,\mathrm{tsw}}-\det(\mathbf{A}_{\mathrm{tsw}})\mathbf{A}_{\mathrm{tsw}}^{-1}\boldsymbol{C}_{\mathrm{tsw}}, \\ \boldsymbol{b}_3 &= \left(\det(\mathbf{B}_{\mathrm{tsw}})\mathbf{B}_{\mathrm{tsw}}^{-1}+n_{\mathrm{u},\mathcal{L}}^2\mathbf{U}_2\right)\boldsymbol{C}_{\mathrm{tsw}}, \\ a_{\mathrm{tsw},i} &= -\frac{1}{2}\left(\frac{B_{11}+n_{\mathrm{u},\mathcal{L}}^2}{A_{11}}+\frac{B_{22}+n_{\mathrm{u},\mathcal{L}}^2}{A_{22}}\right) \\ &\quad -(-1)^i\sqrt{\frac{1}{4}\left(\frac{B_{11}+n_{\mathrm{u},\mathcal{L}}^2}{A_{11}}-\frac{B_{22}+n_{\mathrm{u},\mathcal{L}}^2}{A_{22}}\right)^2+\frac{B_{12}B_{21}}{\det(\mathbf{A}_{\mathrm{tsw}})}}, \quad i=1,2.\end{aligned} \tag{6.94}$$

The transformation back into the time domain leads to

$$\boldsymbol{x}_1(t, n_\mathrm{u}, \boldsymbol{T}_0, \boldsymbol{C}) = \frac{1}{\det(\mathbf{A}_\mathrm{tsw}) a_{\mathrm{tsw},1} a_{\mathrm{tsw},2} (a_{\mathrm{tsw},2} - a_{\mathrm{tsw},1})} \left\{ \boldsymbol{b}_3 (a_{\mathrm{tsw},2} - a_{\mathrm{tsw},1}) \right. \tag{6.95}$$
$$\left. - a_{\mathrm{tsw},2} \left[a_{\mathrm{tsw},1} \left(\boldsymbol{b}_1 a_{\mathrm{tsw},1} + \boldsymbol{b}_2 \right) + \boldsymbol{b}_3 \right] \mathrm{e}^{a_{\mathrm{tsw},1} t} + a_{\mathrm{tsw},1} \left[a_{\mathrm{tsw},2} \left(\boldsymbol{b}_1 a_{\mathrm{tsw},2} + \boldsymbol{b}_2 \right) + \boldsymbol{b}_3 \right] \mathrm{e}^{a_{\mathrm{tsw},2} t} \right\}.$$

The corresponding expression for $\boldsymbol{X}_2(s, n, \boldsymbol{T}_\mathrm{bc})$ is

$$\begin{aligned}
\boldsymbol{X}_2(s, n, \boldsymbol{T}_\mathrm{bc}) &= - \frac{\boldsymbol{b}_4 s + \boldsymbol{b}_5}{\det(\mathbf{A}_\mathrm{tsw}) s (s - a_{\mathrm{tsw},3}) (s - a_{\mathrm{tsw},4})}, \\
\boldsymbol{b}_4 &= - \det(\mathbf{A}_\mathrm{tsw}) \mathbf{A}_\mathrm{tsw}^{-1} \left(\boldsymbol{T}_{1,\mathrm{tsw}} - (-1)^n \boldsymbol{T}_{2,\mathrm{tsw}} \right), \\
\boldsymbol{b}_5 &= - \left(\det(\mathbf{B}_\mathrm{tsw}) \mathbf{B}_\mathrm{tsw}^{-1} + n_\mathcal{L}^2 \mathbf{U}_2 \right) \left(\boldsymbol{T}_{1,\mathrm{tsw}} - (-1)^n \boldsymbol{T}_{2,\mathrm{tsw}} \right), \\
a_{\mathrm{tsw},i} &= - \frac{1}{2} \left(\frac{B_{11} + n_\mathcal{L}^2}{A_{11}} + \frac{B_{22} + n_\mathcal{L}^2}{A_{22}} \right) \\
&\quad - (-1)^i \sqrt{\frac{1}{4} \left(\frac{B_{11} + n_\mathcal{L}^2}{A_{11}} - \frac{B_{22} + n_\mathcal{L}^2}{A_{22}} \right)^2 + \frac{B_{12} B_{21}}{\det(\mathbf{A}_\mathrm{tsw})}}, \quad i = 3, 4.
\end{aligned} \tag{6.96}$$

In the time domain, this leads to

$$\boldsymbol{x}_2(t, n, \boldsymbol{T}_\mathrm{bc}) = - \frac{1}{\det(\mathbf{A}_\mathrm{tsw}) a_{\mathrm{tsw},3} a_{\mathrm{tsw},4} (a_{\mathrm{tsw},4} - a_{\mathrm{tsw},3})} \left\{ - a_{\mathrm{tsw},4} \left[\boldsymbol{b}_4 a_{\mathrm{tsw},3} + \boldsymbol{b}_5 \right] \mathrm{e}^{a_{\mathrm{tsw},3} t} \right.$$
$$\left. + a_{\mathrm{tsw},3} \left[\boldsymbol{b}_4 a_{\mathrm{tsw},4} + \boldsymbol{b}_5 \right] \mathrm{e}^{a_{\mathrm{tsw},4} t} + \boldsymbol{b}_5 (a_{\mathrm{tsw},4} - a_{\mathrm{tsw},3}) \right\}. \tag{6.97}$$

e) Iterative Approach Based on the Solution for Single Wire Cable

The basic ECD in figure 6.5 can be rearranged to a new version as presented in figure 6.6. Then, it becomes more obvious, that two single cables are coupled in the model only by a single conductance. This shows in the coupled differential equations as well:

$$\begin{aligned}
&\frac{\partial^2}{\partial z^2} T_{\mathrm{tsw,it},1}(z,t) - R'_1 \mathcal{C}'_1 \frac{\partial}{\partial t} T_{\mathrm{tsw,it},1}(z,t) - R'_1 (G'_1 + G'_{12}) T_{\mathrm{tsw,it},1}(z,t) \\
&\qquad = - R'_1 \left(P'_{\mathrm{el},1} + G'_1 T_\mathrm{e} + G'_{12} T_{\mathrm{tsw,it},2}(z,t) \right),
\end{aligned} \tag{6.98}$$

$$\begin{aligned}
&\frac{\partial^2}{\partial z^2} T_{\mathrm{tsw,it},2}(z,t) - R'_2 \mathcal{C}'_2 \frac{\partial}{\partial t} T_{\mathrm{tsw,it},2}(z,t) - R'_2 (G'_2 + G'_{12}) T_{\mathrm{tsw,it},2}(z,t) \\
&\qquad = - R'_2 \left(P'_{\mathrm{el},2} + G'_2 T_\mathrm{e} + G'_{12} T_{\mathrm{tsw,it},1}(z,t) \right).
\end{aligned} \tag{6.99}$$

Comparing this formulation with the differential equation for a single cable known from equation (5.51) shows the equivalence between them if for each cable the temperature of the other cable is treated as a constant. Based on this, an iterative solution approach is proposed as presented in figure 6.7: At first, the solution for a single wire cable is used to calculate the temperature distribution along the first cable using the corresponding value for $T_{\mathrm{tsw,it},2}(z,t)$ at each position. This temperature development is used to calculate the temperature distribu-

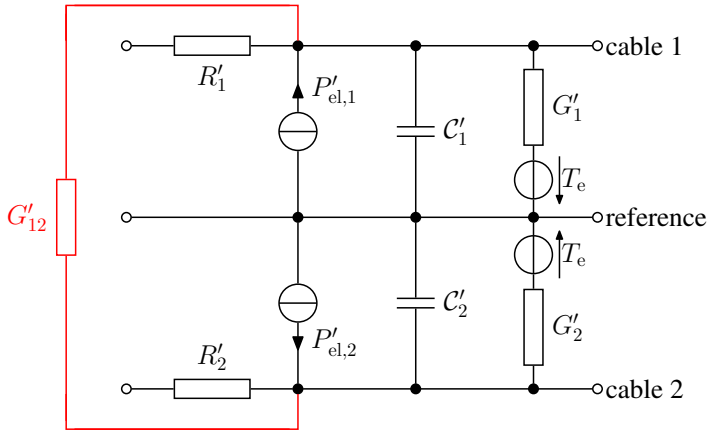

Figure 6.6: Rearranged equivalent circuit for an infinitesimally short segment of a cable arrangement of two single wire cables.

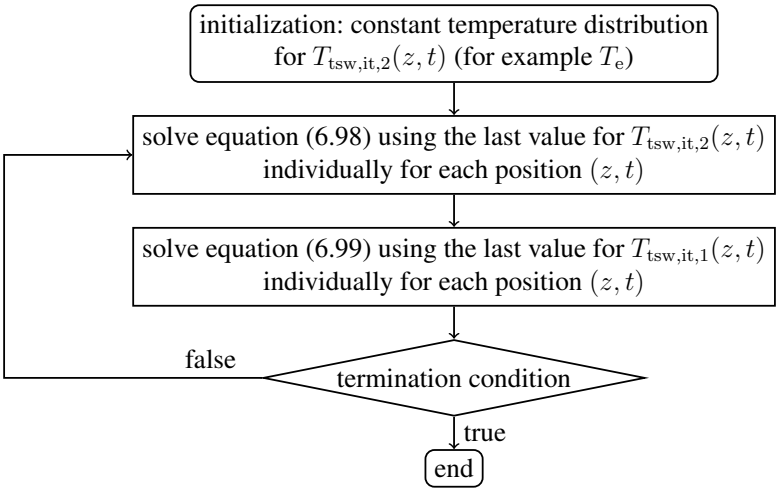

Figure 6.7: Iterative solution scheme for a coupled system of PDEs.

tion along the second cable $T_{\mathrm{tsw,it,2}}(z,t)$. This result is again used to recalculate the first cable temperature. The iteration is stopped when the deviation between two consecutive iterations falls below a given threshold.

f) Simplification of the Equivalent Circuit

As the coupling in the differential equations complicates their solutions, in this section, simplifications of the ECD and the differential equations are discussed. The first idea is to consider the axial heat flow only along one of the two cables and combine both of the capacitances. Then, the solution for a single wire cable can be applied. For better modeling of the transient behavior, a capacitance correction is added: By now, the sum of the capacitances of both cables was used. For the first conductor, however, the capacitance of the second conductor is connected with an additional conductance. To find a suitable estimation to consider this, the radial ECD is first analyzed for the case without current in conductor two as shown in figure 6.8.

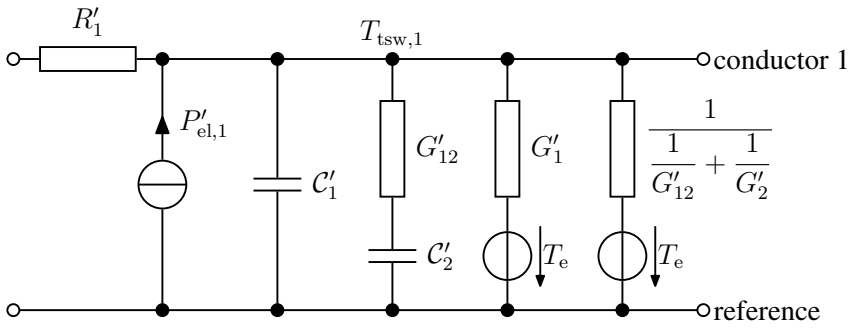

Figure 6.8: ECD without current in conductor 2.

A constant current is impressed. First, the capacitance $\mathcal{C}'_1$ is charged because here no resistance appears. This increases the voltage at the temperature node $T_{\mathrm{tsw},1}$. However, the further charging of the capacitance is opposed by a certain resistance due to the already existing charge with increasing voltage (temperature), so now also the other branches gain importance. As a first approximation, only the resistances of the branches are considered. If the first capacitance is already sufficiently charged, the current will be distributed to the remaining three radial branches (each with only one resistance). The branch with the second capacitance will have the following part:

$$\frac{G'_{12}}{G'_{12}+G'_1+G'_{12}G'_2/(G'_{12}+G'_2)} = p_{\mathrm{tsw,simp}}. \tag{6.100}$$

As the first approach, it is assumed that only this part of the capacitance $\mathcal{C}'_2$ is effective:

$$\mathcal{C}' = \mathcal{C}'_1 + p_{\mathrm{tsw,simp}}\mathcal{C}'_2. \tag{6.101}$$

The first cable temperature is calculated with the single wire approximation from section 6.1.2.a) using

$$A_{\mathrm{sw}} = R'_1\mathcal{C}',\ B_{\mathrm{sw}} = R'_1\left(\frac{G'_{12}G'_2}{G'_{12}+G'_2}+G'_1\right), \tag{6.102}$$

$$C_{\mathrm{sw}} = -R'_1\left(P'_{\mathrm{el},1}+\frac{G'_{12}\left(P'_{\mathrm{el},2}+T_\mathrm{e}G'_2\right)}{G'_{12}+G'_2}+G'_1T_\mathrm{e}\right). \tag{6.103}$$

For a better consideration of the transient behavior of the second conductor, the remaining part of $\mathcal{C}'_2$ has to be charged as well. Therefore, the following calculation rule for $T_{\mathrm{tsw,simp},2}(z,t)$ is proposed:

$$\begin{aligned} T_{\mathrm{tsw,simp},2}(z,t) = T_{0,\mathrm{tsw},2} &+ \left(1-\exp\left(-\frac{tG'_{12}}{\mathcal{C}'_{2,\mathrm{rem}}}\right)\right) \\ &\cdot\left(\frac{G'_{12}}{G'_{12}+G'_2}T_{\mathrm{tsw,simp},1}(z,t)+\frac{T_\mathrm{e}G'_2+P'_{\mathrm{el},2}}{G'_{12}+G'_2}-T_{0,\mathrm{tsw},2}\right), \end{aligned} \tag{6.104}$$

$$\mathcal{C}'_{2,\mathrm{rem}} = (1-p_{\mathrm{tsw,simp}})\mathcal{C}'_2. \tag{6.105}$$

6.1.5 Coaxial Cable

a) Partial Differential Equations and Equivalent Circuit Diagram

For a coaxial cable with the cross-section shown in figure 6.9, the ECD is given in figure 6.10. The corresponding PDE system follows the same structure as the PDE system for the arrangement of two single wire cables (see equation (6.66)):

$$\boldsymbol{C}_{\mathrm{co}} = \frac{\partial^2}{\partial z^2}\boldsymbol{T}_{\mathrm{co}}(z,t) - \mathbf{A}_{\mathrm{co}}\frac{\partial}{\partial t}\boldsymbol{T}_{\mathrm{co}}(z,t) - \mathbf{B}_{\mathrm{co}}\boldsymbol{T}_{\mathrm{co}}(z,t), \tag{6.106}$$

$$\mathbf{A}_{\mathrm{co}} = \begin{pmatrix} A_{11} & 0 \\ 0 & A_{22} \end{pmatrix} = \begin{pmatrix} R'_{\mathrm{c}}(\mathcal{C}'_{\mathrm{c}} + \mathcal{C}'_{\mathrm{ii}}) & 0 \\ 0 & R'_{\mathrm{sh}}(\mathcal{C}'_{\mathrm{sh}} + \mathcal{C}'_{\mathrm{oi}}) \end{pmatrix},$$

$$\mathbf{B}_{\mathrm{co}} = \begin{pmatrix} B_{11} & B_{12} \\ B_{21} & B_{22} \end{pmatrix} = \begin{pmatrix} R'_{\mathrm{c}}G'_{\mathrm{ii}} & -R'_{\mathrm{c}}G'_{\mathrm{ii}} \\ -R'_{\mathrm{sh}}G'_{\mathrm{ii}} & R'_{\mathrm{sh}}(G'_{\mathrm{ii}} + G') \end{pmatrix},$$

$$\boldsymbol{C}_{\mathrm{co}} = \begin{pmatrix} C_{\mathrm{co,c}} \\ C_{\mathrm{co,sh}} \end{pmatrix} = \begin{pmatrix} -R'_{\mathrm{c}}P'_{\mathrm{el,c}} \\ -R'_{\mathrm{sh}}(P'_{\mathrm{el,sh}} + G'T_{\mathrm{e}}) \end{pmatrix}, \quad \boldsymbol{T}_{\mathrm{co}}(z,t) = \begin{pmatrix} T_{\mathrm{co,c}}(z,t) \\ T_{\mathrm{co,sh}}(z,t) \end{pmatrix}.$$

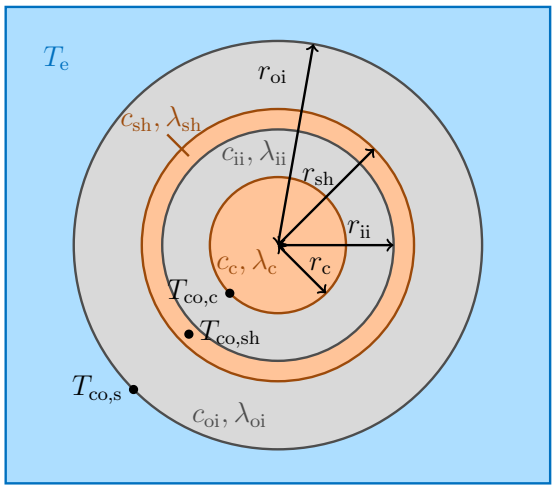

Figure 6.9: Cross-section of the analyzed coaxial cable.

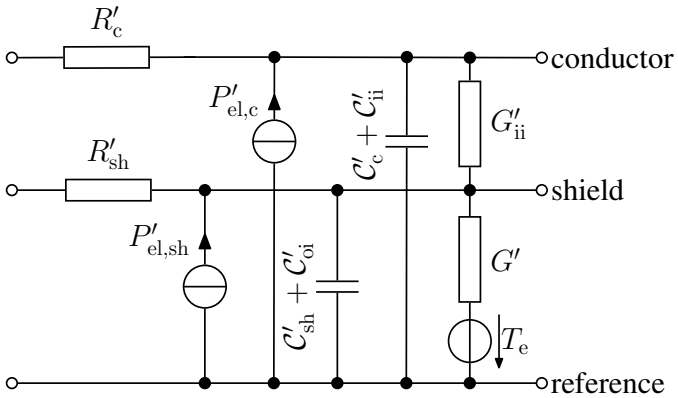

Figure 6.10: ECD for an infinitesimally short segment of a coaxial cable.

That is why most of the solutions presented in section 6.1.4 can also be applied to this problem. The surface temperature is calculated from the shield temperature via

$$T_{\mathrm{co,s}}(z,t) = T_{\mathrm{co,sh}}(z,t) - R'_{\mathrm{oi}} G' (T_{\mathrm{co,sh}}(z,t) - T_{\mathrm{e}}), \tag{6.107}$$

where R'_{oi} describes the radial thermal resistance of the outer insulation.

b) Direct Solution in the Laplace Domain and Approximation

As the system of PDEs has the same appearance as for the arrangement of two single wire cables, the solution that was presented in section 6.1.4.c) can also be applied here. Also, the same numerical stability problems appear due to the complicated formulation of the solution.

c) Solution via Green's Functions in the Laplace Domain

Again, the solution from section 6.1.4.c) for the arrangement of two single wires can directly be used for the temperature calculation of a coaxial cable. Using this, a series formulation of the complete solution without any approximation is given.

d) Iterative Approach Based on the Solution for Single Wire Cable

The solution from section 6.1.4.e) for the arrangement of two single wires can also be applied for the temperature calculation of a coaxial cable: The solution for a single wire cable is used for the temperature calculation of the inner conductor and shield, assuming the other temperature to be constant. An iteration is used to recalculate the conductor temperature based on the known shield temperature, then the shield temperature based on the known conductor temperature, and so on.

e) Simplification of the Equivalent Circuit

In this section, a simplification of the ECD is presented, that allows the calculation of the cable temperature based on the solution for a single wire cable. The axial heat flow along the shield is neglected. In addition, the capacitances for shield and outer insulation are combined with the capacitances for the inner conductor and the inner insulation. This equals

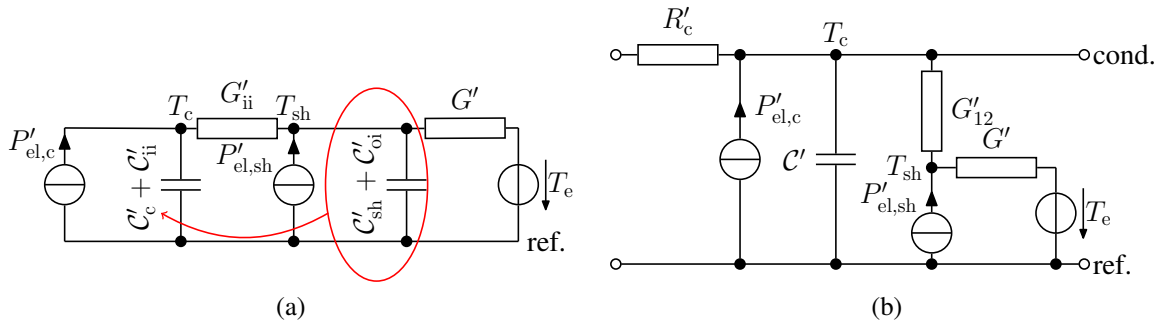

Figure 6.11: (a) Relocation of capacitances for the radial model for a coaxial cable. (b) Simplified axial model for a coaxial cable.

the relocation of the outer capacitances in the circuit, which is presented in figure 6.11(a) for the radial model. As a result, a simplified radial ECD is found. The corresponding axial model (with neglection of the axial heat flow along the shield) is presented in figure 6.11(b) with

$$\mathcal{C}' = \mathcal{C}'_{\mathrm{c}} + \mathcal{C}'_{\mathrm{ii}} + \mathcal{C}'_{\mathrm{sh}} + \mathcal{C}'_{\mathrm{oi}}, \quad G' = \frac{1}{R'_{\mathrm{oi}} + R'_{\alpha}}. \tag{6.108}$$

The corresponding PDE equals the PDE for the single wire cable (see equation (5.51)) with

$$A = R'_{\mathrm{c}}\mathcal{C}', \quad B = R'_{\mathrm{c}}\frac{G'G'_{\mathrm{ii}}}{G' + G'_{\mathrm{ii}}}, \quad C = -R'_{\mathrm{c}}\left(P'_{\mathrm{el,c}} + G'_{\mathrm{ii}}\frac{P'_{\mathrm{el,sh}} + T_{\mathrm{e}}G'}{G' + G'_{\mathrm{ii}}}\right). \tag{6.109}$$

So the solutions for the single wire cable can be applied. The shield temperature is

$$T_{\mathrm{co,simp,sh}}(z,t) = \frac{G'_{\mathrm{ii}}}{G' + G'_{\mathrm{ii}}}T_{\mathrm{co,simp}}(z,t) + \frac{T_{\mathrm{e}}G' + P'_{\mathrm{el,sh}}}{G' + G'_{\mathrm{ii}}}. \tag{6.110}$$

6.1.6 Identical Single Wire Cables

a) Partial Differential Equations and Equivalent Circuit Diagram

The ECD for a cable arrangement consisting of N identical single wire cables (cross-section see figure 6.12) is given in figure 6.13. The corresponding PDE system is as follows:

$$\boldsymbol{C}_{\mathrm{id}} = \frac{\partial^2}{\partial z^2}\boldsymbol{T}_{\mathrm{id}}(z,t) - \mathbf{A}_{\mathrm{id}}\frac{\partial}{\partial t}\boldsymbol{T}_{\mathrm{id}}(z,t) - \mathbf{B}_{\mathrm{id}}\boldsymbol{T}_{\mathrm{id}}(z,t), \tag{6.111}$$

$$\mathbf{A}_{\mathrm{id}} = A_{\mathrm{id}}\mathbf{U}_N = R'\mathcal{C}'\mathbf{U}_N, \quad \mathbf{B}_{\mathrm{id}} = R'\mathbf{G}', \quad \boldsymbol{C}_{\mathrm{id}} = -R'(\boldsymbol{P}'_{\mathrm{el}} + T_{\mathrm{e}}\boldsymbol{G}'_{\mathrm{e}}),$$

$$\mathbf{G}' = \begin{pmatrix} \tilde{G}'_{11} & -G'_{12} & \dots & -G'_{1N} \\ -G'_{12} & \ddots & \ddots & \vdots \\ \vdots & \ddots & \ddots & -G'_{N-1,N} \\ -G'_{1N} & \dots & -G'_{N-1,N} & \tilde{G}'_{NN} \end{pmatrix}, \quad \boldsymbol{T}_{\mathrm{id}} = \begin{pmatrix} T_{\mathrm{id},1} \\ T_{\mathrm{id},2} \\ \vdots \\ T_{\mathrm{id},N} \end{pmatrix},$$

$$\boldsymbol{G}'_{\mathrm{e}} = \begin{pmatrix} G'_{11} \\ G'_{22} \\ \vdots \\ G'_{NN} \end{pmatrix}, \quad \boldsymbol{P}'_{\mathrm{el}} = \begin{pmatrix} P'_{\mathrm{el},1} \\ P'_{\mathrm{el},2} \\ \vdots \\ P'_{\mathrm{el},N} \end{pmatrix}, \quad \tilde{G}'_{ii} = \sum_{j=1}^{N} G'_{ij},\ i = 1, \dots, N.$$

The surface temperatures are calculated from the cable temperatures via

$$\boldsymbol{T}_{\mathrm{id,s}}(z,t) = \boldsymbol{T}_{\mathrm{id}}(z,t) - R'_{\mathrm{i}}\mathbf{G}'_{ii}\left(\boldsymbol{T}_{\mathrm{id}}(z,t) - T_{\mathrm{e}} \cdot \begin{pmatrix} 1 \\ \vdots \\ 1 \end{pmatrix}\right), \quad \mathbf{G}'_{ii} = \begin{pmatrix} G'_{11} & 0 & 0 \\ 0 & \ddots & 0 \\ 0 & 0 & G'_{NN} \end{pmatrix}, \tag{6.112}$$

where R'_{i} describes the resistance against the radial heat flow through the insulation.

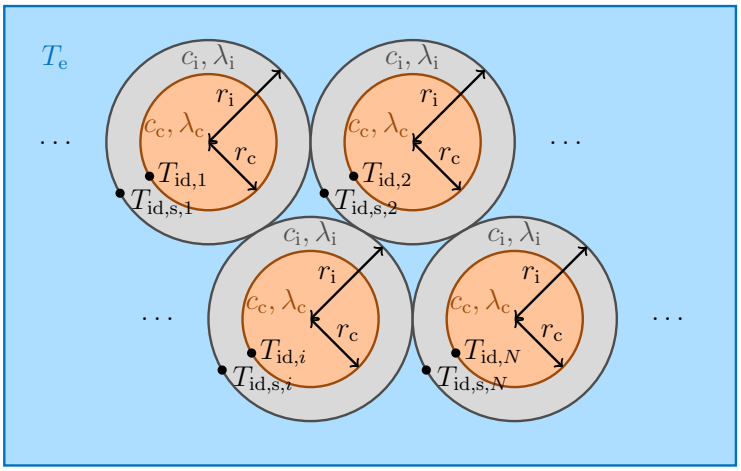

Figure 6.12: Cross-section of the analyzed arrangement of N identical single wire cables.

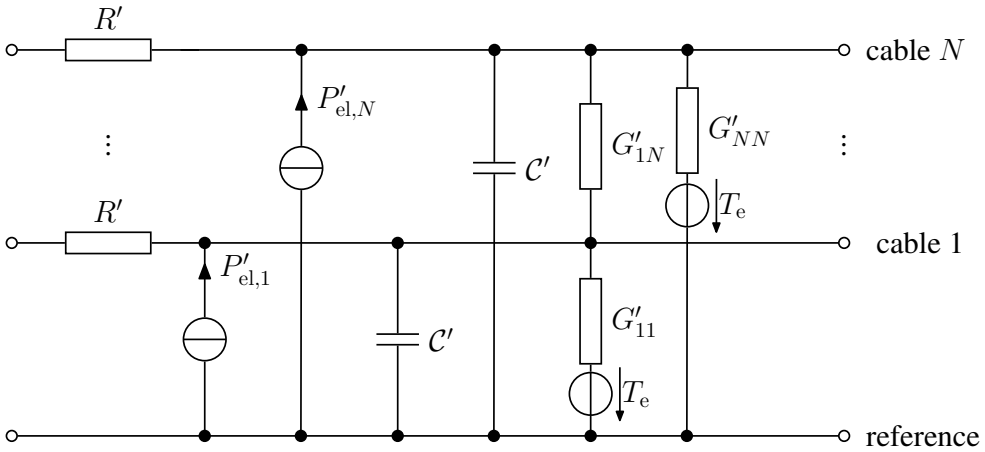

Figure 6.13: ECD for an infinitesimally short segment of an arrangement of N identical single wire cables.

b) Direct Solution in the Laplace Domain and Approximation

This section is based on [A.8]. Transforming the general PDE analog to the electrical domain into the Laplace domain leads to the formulation known from equations (6.77) and (6.78). For the solution, those coupled differential equations have to be decoupled. In the general case, this leads to very complex formulations as exemplarily shown in the comparatively simple case of two conductors in section 6.1.4.c). This is because the matrix $s\mathbf{A} + \mathbf{B}$, which has to be diagonalized, includes the Laplace variable s, which then also appears in the necessary transformation matrices. To find a transformation that is independent of the Laplace variable s, equivalently to the approaches known from the electrical domain (see chapter 9.2.4 in [110]), a special case is investigated: For identical conductors, it is $\mathbf{A}_\mathrm{id} = A_\mathrm{id}\mathbf{U}_N$ as already mentioned before. Then, only the matrix $\mathbf{B}_\mathrm{id}$, which is independent of s, has to be diagonalized:

$$\mathbf{B}_{\mathrm{id}} = \mathbf{E}_{\mathbf{B},\mathrm{id}} \mathbf{D}_{\mathbf{B},\mathrm{id}} \mathbf{E}_{\mathbf{B},\mathrm{id}}^{-1}, \quad \mathbf{D}_{\mathbf{B},\mathrm{id}} = \begin{pmatrix} D_{\mathbf{B},\mathrm{id},1} & 0 & \dots & 0 \\ 0 & D_{\mathbf{B},\mathrm{id},2} & \ddots & \vdots \\ \vdots & \ddots & \ddots & 0 \\ 0 & \dots & 0 & D_{\mathbf{B},\mathrm{id},N} \end{pmatrix}. \tag{6.113}$$

This leads to a decoupled system of PDEs in the Laplace domain for the modal temperatures $\boldsymbol{T}_{\mathrm{id,m}} = \mathbf{E}_{\mathbf{B},\mathrm{id}}^{-1} \boldsymbol{T}_{\mathrm{id}}$:

$$\frac{\partial^2}{\partial z^2} \boldsymbol{T}_{\mathrm{id,m}} - \underbrace{(s A_{\mathrm{id}} \mathbf{U}_N + \mathbf{D}_{\mathbf{B},\mathrm{id}})}_{\tilde{\mathbf{a}}_{\mathrm{id}}^2 \Rightarrow \text{diagonal matrix}} \boldsymbol{T}_{\mathrm{id,m}} = \mathbf{E}_{\mathbf{B},\mathrm{id}}^{-1} \underbrace{\left(\frac{\boldsymbol{C}_{\mathrm{id}}}{s} - A_{\mathrm{id}} \boldsymbol{T}_{0,\mathrm{id}} \right)}_{\hat{\boldsymbol{C}}_{\mathrm{id}}}. \tag{6.114}$$

The solution is the superposition of a homogeneous and a particulate part:

$$\boldsymbol{T}_{\mathrm{id,m}}(z,s) = \mathrm{e}^{-\tilde{\mathbf{a}}_{\mathrm{id}} z} \boldsymbol{T}_{\mathrm{id},1}(s) + \mathrm{e}^{\tilde{\mathbf{a}}_{\mathrm{id}} z} \boldsymbol{T}_{\mathrm{id},2}(s) - \boldsymbol{T}_{\mathrm{part,id}}(s), \tag{6.115}$$

$$\boldsymbol{T}_{\mathrm{part,id}}(s) = \tilde{\mathbf{a}}_{\mathrm{id}}^{-2} \mathbf{E}_{\mathbf{B},\mathrm{id}}^{-1} \hat{\boldsymbol{C}}_{\mathrm{id}}. \tag{6.116}$$

As the matrix $\tilde{\mathbf{a}}_{\mathrm{id}}^2$ is diagonal, its square root and inverse matrix can easily be calculated. Using the boundary conditions, the remaining factors are calculated:

$$\boldsymbol{T}_{\mathrm{id},i}(s) = (-1)^i \left(\mathrm{e}^{\tilde{\mathbf{a}}_{\mathrm{id}} \mathcal{L}} - \mathrm{e}^{-\tilde{\mathbf{a}}_{\mathrm{id}} \mathcal{L}} \right)^{-1} \left[-\boldsymbol{T}_{\mathrm{id,h},2} - \mathrm{e}^{(-1)^{i+1} \tilde{\mathbf{a}}_{\mathrm{id}} \mathcal{L}} \boldsymbol{T}_{\mathrm{id,h},1} \right], \quad i = 1,2, \tag{6.117}$$

$$\boldsymbol{T}_{\mathrm{id,h},j} = \frac{1}{s} \mathbf{E}_{\mathbf{B},\mathrm{id}}^{-1} \boldsymbol{T}_{j,\mathrm{id}} + \boldsymbol{T}_{\mathrm{part,id}}(s), \quad j = 1,2.$$

Now, the complete solution for the modal temperatures is known in the Laplace domain. Based on this, the real temperatures in the Laplace domain are calculated. The result needs to be transformed back into the time domain. Similar to section 6.1.2.a), some expressions cannot be directly transformed. So, the approximation from section 6.1.2.a) is extended for use here:

$$\mathrm{e}^{-\tilde{\mathbf{a}}_{\mathrm{id}} \mathcal{L}} \pm \mathbf{U}_N \approx \pm \mathbf{U}_N. \tag{6.118}$$

Then, the transformation back into the time domain is possible. The result is reshaped using that the matrix $\mathbf{D}_{\mathbf{B},\mathrm{id}}$ and functions of this matrix are diagonal and for two diagonal matrices, the product commutates. For a function $\mathbf{f}(\mathbf{B}_{\mathrm{id}})$, which can be expressed as a series, it is

$$\mathbf{E}_{\mathbf{B},\mathrm{id}} \mathbf{f}(\mathbf{D}_{\mathbf{B},\mathrm{id}}) \mathbf{E}_{\mathbf{B},\mathrm{id}}^{-1} = \mathbf{f}(\mathbf{B}_{\mathrm{id}}). \tag{6.119}$$

This formulation applies to the complementary error function of a matrix [147] and the matrix exponential function. It can be used to simplify the function evaluations for the implementation as those are easier to implement for diagonal matrices. All in all, the complete

temperature distribution in the time domain is equivalent to the solution for the single wire cable known from section 6.1.2.a):

$$\begin{aligned}\boldsymbol{T}_{\mathrm{id,La}}(z,t) = \boldsymbol{T}_{\mathrm{ic,id,La}}(z,t,\boldsymbol{T}_{0,\mathrm{id}}) + \boldsymbol{T}_{\mathrm{bc,id,La}}(z,t,\boldsymbol{T}_{1,\mathrm{id}}) \\ + \boldsymbol{T}_{\mathrm{bc,id,La}}(z_{\mathcal{L}},t,\boldsymbol{T}_{2,\mathrm{id}}) + \boldsymbol{T}_{\mathrm{inh,id,La}}(z,t,\boldsymbol{C}_{\mathrm{id}})\end{aligned} \tag{6.120}$$

with

$$\boldsymbol{T}_{\mathrm{ic,id,La}}(z,t,\boldsymbol{T}_{0,\mathrm{id}}) = -\Gamma(t)\boldsymbol{T}_{0,\mathrm{id}}\boldsymbol{\Lambda}_3(t)[1-\Lambda_1(z,t)-\Lambda_1(z_{\mathcal{L}},t)], \tag{6.121}$$

$$\boldsymbol{T}_{\mathrm{bc,id,La}}(z,t,T_{\mathrm{bc}}) = -\Gamma(t)\frac{\boldsymbol{T}_{\mathrm{bc}}}{2}\boldsymbol{\Lambda}_2(z,t), \tag{6.122}$$

$$\begin{aligned}\boldsymbol{T}_{\mathrm{inh,id,La}}(z,t,C_{\mathrm{id}}) = -\mathbf{B}_{\mathrm{id}}^{-1}\boldsymbol{C}_{\mathrm{id}}\Gamma(t) + \boldsymbol{T}_{\tilde{T}_0,\mathrm{su,La}}\left(z,t,\mathbf{B}_{\mathrm{id}}^{-1}\boldsymbol{C}_{\mathrm{id}}\right) \\ + \boldsymbol{T}_{\mathrm{bc,id,La}}\left(z,t,\mathbf{B}_{\mathrm{id}}^{-1}\boldsymbol{C}_{\mathrm{id}}\right) + \boldsymbol{T}_{\mathrm{bc,id,La}}\left(z_{\mathcal{L}},t,\mathbf{B}_{\mathrm{id}}^{-1}\boldsymbol{C}_{\mathrm{id}}\right),\end{aligned} \tag{6.123}$$

$$\Lambda_1(z,t) = \operatorname{erf}\left(\frac{z}{2}\sqrt{\frac{A_{\mathrm{id}}}{t}}\right), \boldsymbol{\Lambda}_2(z,t) = \boldsymbol{\theta}_1(z,t) + \boldsymbol{\theta}_2(z,t), \boldsymbol{\Lambda}_3(t) = \exp\left(-\frac{\mathbf{B}_{\mathrm{id}}}{A_{\mathrm{id}}}t\right),$$

$$\boldsymbol{\theta}_i(z,t) = \mathrm{e}^{(-1)^i z\sqrt{\mathbf{B}_{\mathrm{id}}}}\operatorname{erfc}\left(\frac{zA_{\mathrm{id}}\mathbf{U}_N + (-1)^i 2t\sqrt{\mathbf{B}_{\mathrm{id}}}}{2\sqrt{A_{\mathrm{id}}t}}\right), \quad i = 1,2.$$

For the implementation, however, the functions of the non-diagonal matrices are hard to calculate, e.g., for the error function, the series formulation has to be used. The convergence behavior is partly poor, so no sufficiently accurate values can be determined. Therefore, it is easier to apply the already known transformation matrices again to use the diagonal matrices as input for the functions. For the exponential function, a corresponding function is already provided by MATLAB.

c) Solution via Green's Functions in the Time Domain

Similar to Green's function for a single wire cable, an equivalent formulation for the arrangement of N identical cables is

$$\begin{aligned}\mathbf{G}_{\mathrm{id}}(z,t|\tilde{z},\tilde{t}) = \Gamma(t-\tilde{t})\sqrt{\frac{A_{\mathrm{id}}}{4\pi(t-\tilde{t})}}\exp\left(-\mathbf{B}_{\mathrm{id}}\frac{t-\tilde{t}}{A_{\mathrm{id}}}\right) \\ \cdot\sum_{n=-\infty}^{\infty}\left\{\exp\left(-A_{\mathrm{id}}\frac{(\tilde{n}+z-\tilde{z})^2}{4(t-\tilde{t})}\right) - \exp\left(-A_{\mathrm{id}}\frac{(\tilde{n}+z+\tilde{z})^2}{4(t-\tilde{t})}\right)\right\}.\end{aligned} \tag{6.124}$$

This approach works because $\mathbf{A}_{\mathrm{id}} = A_{\mathrm{id}}\mathbf{U}_N$ allows $\mathbf{A}_{\mathrm{id}}$ to commutate with each other matrix. Identically to the precede presented in section 6.1.2.b), the complete solution is a superposition of the solution parts that are caused by the different inhomogeneities:

$$\begin{aligned}
\boldsymbol{T}_{\mathrm{ic,id,G}}(z,t,\boldsymbol{T}_{0,\mathrm{id}}) &= \int_0^{\mathcal{L}} \mathbf{G}_{\mathrm{id}}(z,t|\tilde{z},0)\boldsymbol{T}_{0,\mathrm{id}}\,\mathrm{d}\tilde{z}, \\
&= -\Gamma(t)\boldsymbol{T}_{0,\mathrm{id}}\boldsymbol{\Lambda}_3(t)\left\{1-\Lambda_1(z,t)-\Lambda_1(z_{\mathcal{L}},t)+\sum_{n=1}^{\infty}\left[\Lambda_1(-z_{\mathcal{L}}+\tilde{n},t)\right.\right. \\
&\quad \left.\left.-\Lambda_1(z+\tilde{n},t)+\Lambda_1(-z_{\mathcal{L}}-\tilde{n},t)-\Lambda_1(z-\tilde{n},t)\right]\right\}, \qquad (6.125) \\
\boldsymbol{T}_{\mathrm{bc,id,G}}(z,t,\boldsymbol{T}_{\mathrm{bc}}) &= \int_0^t \sqrt{\frac{1}{A_{\mathrm{id}}\pi\tilde{t}}}\frac{\partial}{\partial z}\sum_{n=-\infty}^{\infty}\exp\left(-\frac{A_{\mathrm{id}}(\tilde{n}-z)^2}{4\tilde{t}}-\frac{\mathbf{B}_{\mathrm{id}}}{A_{\mathrm{id}}}\tilde{t}\right)\boldsymbol{T}_{\mathrm{bc}}\,\mathrm{d}\tilde{t} \\
&= -\Gamma(t)\frac{\boldsymbol{T}_{\mathrm{bc}}}{2}\left\{\boldsymbol{\Lambda}_2(z,t)+\sum_{n=1}^{\infty}[\boldsymbol{\Lambda}_2(z+\tilde{n},t)-\boldsymbol{\Lambda}_2(-z+\tilde{n},t)]\right\}, \qquad (6.126) \\
\boldsymbol{T}_{\mathrm{inh,id,G}}(z,t,\boldsymbol{C}_{\mathrm{id}}) &= \int_0^t\int_0^{\mathcal{L}} \mathbf{G}_{\mathrm{id}}(z,\hat{t}|\tilde{z},0)\boldsymbol{C}_{\mathrm{id}}\,\mathrm{d}\tilde{z}\,\mathrm{d}\hat{t} \\
&= -\mathbf{B}_{\mathrm{id}}^{-1}\boldsymbol{C}_{\mathrm{id}}\Gamma(t)+\boldsymbol{T}_{\tilde{T}_0,\mathrm{id,G}}\left(z,t,\mathbf{B}_{\mathrm{id}}^{-1}\boldsymbol{C}_{\mathrm{id}}\right)+\boldsymbol{T}_{\mathrm{bc,id,G}}\left(z,t,\mathbf{B}_{\mathrm{id}}^{-1}\boldsymbol{C}_{\mathrm{id}}\right) \\
&\quad +\boldsymbol{T}_{\mathrm{bc,id,G}}\left(z_{\mathcal{L}},t,\mathbf{B}_{\mathrm{id}}^{-1}\boldsymbol{C}_{\mathrm{id}}\right). \qquad (6.127)
\end{aligned}$$

The result is then, analog to the single wire cable:

$$\begin{aligned}
\boldsymbol{T}_{\mathrm{id,G}}(z,t) &= \boldsymbol{T}_{\mathrm{ic,id,G}}(z,t,\boldsymbol{T}_{0,\mathrm{id}})+\boldsymbol{T}_{\mathrm{inh,id,G}}(z,t,\boldsymbol{C}_{\mathrm{id}})+\boldsymbol{T}_{\mathrm{bc,id,G}}(z,t,\boldsymbol{T}_{1,\mathrm{id}}) \\
&\quad +\boldsymbol{T}_{\mathrm{bc,id,G}}(z_{\mathcal{L}},t,\boldsymbol{T}_{2,\mathrm{id}}). \qquad (6.128)
\end{aligned}$$

Again, for the implementation, the diagonalization of the matrix $\mathbf{B}_{\mathrm{id}}$ can be used for the matrix function evaluation. This way, series evaluations are avoided.

6.1.7 General Cable Arrangement Analog to the Electrical Problem

In this section, a thermal cable arrangement that can be regarded equivalently to the electrical domain as known from section 5.3.1 is analyzed for constant excitations neglecting the implicit parameter dependence. Via Green's functions in the Laplace domain, a solution for this rather general arrangement is derived.

In section 6.1.4.d), the general approach for the solution using Green's functions in the Laplace domain was presented. Based on these considerations, the functions $\boldsymbol{x}_1(t,n_{\mathrm{u}},\boldsymbol{T}_0,\boldsymbol{C})$ and $\boldsymbol{x}_2(t,n,\boldsymbol{T}_1-(-1)^n\boldsymbol{T}_2)$ have to be calculated. In the first step, only the homogeneous solution is analyzed. This has to be transformed back into the time domain. As only the part $\boldsymbol{X}_1(s,n_{\mathrm{u}},\boldsymbol{T}_0,\boldsymbol{C})$ depends on the Laplace variable s, only this expression needs to be transformed back into the time domain. Typically, a partial fraction decomposition is used for the transformation. In this case, the explicit formulation of the inverse matrix is necessary due to the dependence on the Laplace variable s but cannot directly be specified in the general case. That is why a different formulation is searched, which allows the transformation back

into the time domain. Equation (6.89) is rearranged to

$$\left[\mathbf{B} + n_{\mathrm{u},\mathcal{L}}^2 \mathbf{U}_N\right] \boldsymbol{X}_1(s, n_\mathrm{u}, \boldsymbol{T}_0, \boldsymbol{C}) + s\mathbf{A}\boldsymbol{X}_1(s, n_\mathrm{u}, \boldsymbol{T}_0, \boldsymbol{C}) = -\hat{\boldsymbol{C}}. \tag{6.129}$$

Using the initial value of $\boldsymbol{x}_1(t, n_\mathrm{u}, \boldsymbol{T}_0, \boldsymbol{C})$,

$$\boldsymbol{x}_1(0, n_\mathrm{u}, \boldsymbol{T}_0, \boldsymbol{C}) = \lim_{s\to\infty} s \cdot \boldsymbol{X}_1(s, n_\mathrm{u}, \boldsymbol{T}_0, \boldsymbol{C}) = \boldsymbol{T}_0, \tag{6.130}$$

and the correspondence

$$f'(t) \bullet\!\!-\!\!\circ\; sf(s) - f(0+), \tag{6.131}$$

equation (6.129) is transformed back into the time domain:

$$\left[\mathbf{B} + n_{\mathrm{u},\mathcal{L}}^2 \mathbf{U}_N\right] \boldsymbol{x}_1(t, n_\mathrm{u}, \boldsymbol{T}_0, \boldsymbol{C}) + \mathbf{A}\frac{\partial}{\partial t}\boldsymbol{x}_1(t, n_\mathrm{u}, \boldsymbol{T}_0, \boldsymbol{C}) = -\boldsymbol{C}, \tag{6.132}$$

which is a differential equation for the prefactors $\boldsymbol{x}_1(t, n_\mathrm{u}, \boldsymbol{T}_0, \boldsymbol{C})$. Rearranging leads to

$$\frac{\partial}{\partial t}\boldsymbol{x}_1(t, n_\mathrm{u}, \boldsymbol{T}_0, \boldsymbol{C}) = \boldsymbol{\Lambda}(n_\mathrm{u})\boldsymbol{x}_1(t, n_\mathrm{u}, \boldsymbol{T}_0, \boldsymbol{C}) - \mathbf{A}^{-1}\boldsymbol{C}, \tag{6.133}$$

$$\boldsymbol{\Lambda}(n) = -\mathbf{A}^{-1}\left[\mathbf{B} + n_{\mathcal{L}}^2 \mathbf{U}_N\right]. \tag{6.134}$$

Using the eigenvectors $\boldsymbol{v}_i(n)$ and eigenvalues $D_i(n)$ of the matrix $\boldsymbol{\Lambda}(n)$, which means

$$\boldsymbol{\Lambda}(n)\boldsymbol{v}_i(n) = D_i(n)\boldsymbol{v}_i(n), \tag{6.135}$$

gives the general homogeneous solution of the PDE (6.133) as a linear combination of the corresponding fundamental solutions:

$$\boldsymbol{x}_{1,\mathrm{hom}}(t, n_\mathrm{u}, \boldsymbol{T}_0, \boldsymbol{C}) = \sum_{i=1}^{N} b_{1,i}\boldsymbol{v}_i(n_\mathrm{u})\mathrm{e}^{D_i(n_\mathrm{u})t}. \tag{6.136}$$

A constant particulate solution can be directly found via rearranging:

$$\frac{\partial}{\partial t}\boldsymbol{x}_{1,\mathrm{part}}(t, n_\mathrm{u}, \boldsymbol{T}_0, \boldsymbol{C}) = 0 \Rightarrow \boldsymbol{x}_{1,\mathrm{part}}(t, n_\mathrm{u}, \boldsymbol{T}_0, \boldsymbol{C}) = -\left[\mathbf{B} + n_{\mathrm{u},\mathcal{L}}^2 \mathbf{U}_N\right]^{-1}\boldsymbol{C}. \tag{6.137}$$

The complete solution for $\boldsymbol{x}_1(t, n_\mathrm{u}, \boldsymbol{T}_0, \boldsymbol{C})$ then is

$$\boldsymbol{x}_1(t, n_\mathrm{u}, \boldsymbol{T}_0, \boldsymbol{C}) = \boldsymbol{x}_{1,\mathrm{part}}(t, n_\mathrm{u}, \boldsymbol{T}_0, \boldsymbol{C}) + \boldsymbol{x}_{1,\mathrm{hom}}(t, n_\mathrm{u}, \boldsymbol{T}_0, \boldsymbol{C}). \tag{6.138}$$

The prefactors $b_{1,i}$ of the linear combination are undetermined by now and have to be calcu-

lated via the evaluation of the initial condition

$$\boldsymbol{x}_1(0, n_\mathrm{u}, \boldsymbol{T}_0, \boldsymbol{C}) = \boldsymbol{T}_0. \tag{6.139}$$

This leads to

$$\boldsymbol{T}_0 + \left[\mathbf{B} + n_{\mathrm{u},\mathcal{L}}^2 \mathbf{U}_N\right]^{-1} \boldsymbol{C} = \sum_{i=1}^{N} b_{1,i} \boldsymbol{v}_i(n_\mathrm{u}), \tag{6.140}$$

where N is the number of conductors in the system. This system of linear equations has to be solved to find $b_{1,i}$, $i = 1, \ldots, N$. Then, the complete expression for $\boldsymbol{x}_1(t, n_\mathrm{u}, \boldsymbol{T}_0, \boldsymbol{C})$ is known. With $n_\mathrm{u} = 2n+1$ and $n_{\mathrm{u},\mathcal{L}} = (2n+1)\pi/\mathcal{L}$, the resulting solution parts for the initial condition and the inhomogeneity are then (by setting the other one to zero):

$$\boldsymbol{T}_{\tilde{\boldsymbol{T}}_0}(z, t, \boldsymbol{T}_0) = \boldsymbol{T}_{\mathrm{ic,GL}}(z, t, \boldsymbol{T}_0) = \frac{4}{\pi} \sum_{n=0}^{\infty} \sin\left(n_{\mathrm{u},\mathcal{L}} z\right) \frac{1}{n_\mathrm{u}} \boldsymbol{x}_1(t, n_\mathrm{u}, \boldsymbol{T}_0, \mathbf{0}), \tag{6.141}$$

$$\boldsymbol{T}_{\tilde{\boldsymbol{C}}}(z, t, \boldsymbol{C}) = \boldsymbol{T}_{\mathrm{inh,GL}}(z, t, \boldsymbol{C}) = \frac{4}{\pi} \sum_{n=0}^{\infty} \sin\left(n_{\mathrm{u},\mathcal{L}} z\right) \frac{1}{n_\mathrm{u}} \boldsymbol{x}_1(t, n_\mathrm{u}, \mathbf{0}, \boldsymbol{C}). \tag{6.142}$$

Analogously, the second solution part, which is used to consider inhomogeneous boundary conditions, is transformed back into the time domain. With the initial condition

$$\boldsymbol{x}_2(0, n, \boldsymbol{T}_\mathrm{bc}) = \mathbf{0}, \tag{6.143}$$

the solution in the time domain is

$$\boldsymbol{T}_{\tilde{\boldsymbol{T}}_1}(z, t, \boldsymbol{T}_1) = \boldsymbol{T}_{\mathrm{bc,GL}}(z, t, \boldsymbol{T}_1), \quad \boldsymbol{T}_{\tilde{\boldsymbol{T}}_2}(z, t, \boldsymbol{T}_2) = \boldsymbol{T}_{\mathrm{bc,GL}}(z_\mathcal{L}, t, \boldsymbol{T}_2), \tag{6.144}$$

$$\boldsymbol{T}_{\mathrm{bc,GL}}(z, t, \boldsymbol{T}_\mathrm{bc}) = \sum_{n=1}^{\infty} \frac{2n_\mathcal{L}}{\mathcal{L}} \sin\left(n_\mathcal{L} z\right) \boldsymbol{x}_2(t, n, \boldsymbol{T}_\mathrm{bc}) \tag{6.145}$$

with

$$\boldsymbol{x}_2(t, n, \boldsymbol{T}_\mathrm{bc}) = \left[\mathbf{B} + n_\mathcal{L}^2 \mathbf{U}_N\right]^{-1} \boldsymbol{T}_\mathrm{bc} + \sum_{i=1}^{N} b_{2,i} \boldsymbol{v}_i(n) \mathrm{e}^{D_i(n)t}, \tag{6.146}$$

$$\sum_{i=1}^{N} b_{2,i} \boldsymbol{v}_i(n) = -\left[\mathbf{B} + n_\mathcal{L}^2 \mathbf{U}_N\right]^{-1} \boldsymbol{T}_\mathrm{bc}. \tag{6.147}$$

Again, equation (6.147) represents a system of linear equations that has to be solved to find $b_{2,i}$, $i = 1, \ldots, N$. The complete solution in the time domain then is

$$\boldsymbol{T}_\mathrm{GL}(z, t) = \boldsymbol{T}_{\mathrm{ic,GL}}(z, t, \boldsymbol{T}_0) + \boldsymbol{T}_{\mathrm{inh,GL}}(z, t, \boldsymbol{C}) + \boldsymbol{T}_{\mathrm{bc,GL}}(z, t, \boldsymbol{T}_1) + \boldsymbol{T}_{\mathrm{bc,GL}}(z_\mathcal{L}, t, \boldsymbol{T}_2). \tag{6.148}$$

For each n, that should be considered, this calculation has to be repeated. Because of the iteration, for different times and positions, the matrices $\mathbf{B}$ and $\boldsymbol{C}$ are not constant, which means, that for each combination (z, t), the calculation has to be reperformed. All in all, this means a huge numerical effort. Nevertheless, via this approach, a general formulation for N arbitrary conductors (for formulations analog to the electrical domain) is found.

6.2 Consideration of Varying Initial and Boundary Conditions and Inhomogeneity

In this section, solution methods for spatial varying initial conditions, time varying boundary conditions, and for time and spatial varying inhomogeneities are discussed. The explicit time and spatial dependencies for the initial temperature $\tilde{\boldsymbol{T}}_0(z)$, the cable termination temperatures $\tilde{\boldsymbol{T}}_1(t)$ and $\tilde{\boldsymbol{T}}_2(t)$, and the excitation $\tilde{\boldsymbol{C}}(z, t)$ are considered. It is assumed that explicit functional relations describing these dependencies are known. The overall problem that has to be solved has the following form:

$$\tilde{\boldsymbol{C}}(z,t) = \frac{\partial^2 \boldsymbol{T}(z,t)}{\partial z^2} - \mathbf{A}\frac{\partial \boldsymbol{T}(z,t)}{\partial t} - \mathbf{B}\boldsymbol{T}(z,t), \tag{6.149}$$

$$\boldsymbol{T}(z,0) = \tilde{\boldsymbol{T}}_0(z), \quad \boldsymbol{T}(0,t) = \tilde{\boldsymbol{T}}_1(t), \quad \boldsymbol{T}(\mathcal{L},t) = \tilde{\boldsymbol{T}}_2(t). \tag{6.150}$$

This is a parabolic initial boundary value problem. The surface temperature can be calculated based on the known cable temperature in a second step:

$$\boldsymbol{T}_\mathrm{s}(z,t) = \boldsymbol{f}(\boldsymbol{T}(z,t), \boldsymbol{T}_\mathrm{s}(z,t)). \tag{6.151}$$

In principle, the procedures from the previous chapter can also be applied to this more general problem, but in most cases, the analytical solution can no longer be calculated. For the solution in the Laplace domain with approximation, the cable termination temperatures and the excitation must be transformed accordingly. The course $\tilde{\boldsymbol{T}}_0(z)$ is used instead of the constant $\boldsymbol{T}_0$. This makes the solution of the ODEs in the Laplace domain and the transformation back to the time domain complicated or impossible depending on the exact functional relation. When solving using Green's functions in the time domain, the corresponding dependencies in the integrals (see for example equations (6.48) to (6.50) for the single wire cable) are taken into account, so the integration becomes much more complicated and requires numerical methods. When using the solution via Green's functions in the Laplace domain, the these two difficulties occur in combination: On the one hand, (more challenging) transformations are necessary again, on the other hand, again integrals (see for example equations (6.53) to (6.55) for the single wire cable) appear. All in all, the direct mathematical consideration of varying initial and boundary conditions as well as excitations is therefore only possible in very rare special cases. Numerical approaches are often required.

The numerical **m**ethod **o**f **l**ines (MOL) [148] summarizes numerical solution techniques for parabolic PDEs and is divided into a vertical MOL and a horizontal MOL (Rothe method [149]). In the vertical MOL, the spatial discretization is performed in the first step and the direct solution or time discretization is performed in the second step. The reverse approach is used by the Rothe method, where the time discretization is done first.

For individual spatial and time discretizations, different methods can be used and combined in various ways. Altogether, the result is a large number of possible numerical approaches. The goal of this thesis is not to provide a complete essay on numerical methods. Rather, only the basics are outlined to indicate the diversity of the corresponding approaches. Therefore, using examples, the basic ideas of widely used methods are presented and discussed below. Specifically, the **f**inite **d**ifference **m**ethod (FDM), **f**inite **e**lement **m**ethod (FEM), **b**oundary **e**lement **m**ethod (BEM), and **f**inite **v**olume **m**ethod (FVM) are briefly introduced.

6.2.1 Finite Difference Method (FDM)

The basic idea of this approach is to approximate derivatives by difference quotients directly in the differential equations. For the first partial derivative of the function $\boldsymbol{f}$ with regard to the variable u, for example, the following approximations can be used:

$$\text{forward difference: } \frac{\partial \boldsymbol{f}(u)}{\partial u} \approx \frac{\boldsymbol{f}(u+\Delta u)-\boldsymbol{f}(u)}{\Delta u}, \tag{6.152}$$

$$\text{backward difference: } \frac{\partial \boldsymbol{f}(u)}{\partial u} \approx \frac{\boldsymbol{f}(u)-\boldsymbol{f}(u-\Delta u)}{\Delta u}, \tag{6.153}$$

$$\text{central difference: } \frac{\partial \boldsymbol{f}(u)}{\partial u} \approx \frac{\boldsymbol{f}(u+\Delta u)-\boldsymbol{f}(u-\Delta u)}{2\Delta u}. \tag{6.154}$$

With central differences, the result for the second derivative is

$$\frac{\partial^2 \boldsymbol{f}(u)}{\partial u^2} \approx \frac{\boldsymbol{f}(u-\Delta u)-2\boldsymbol{f}(u)+\boldsymbol{f}(u+\Delta u)}{(\Delta u)^2}. \tag{6.155}$$

This allows the formulation of the derivatives directly as a function of temperature values at discrete points. Thus, a system of equations is set up. This is used for the solution. To clarify this procedure, possible procedures for the solution of the PDE system (6.149) are exemplarily presented in the following. For illustration purposes, an equidistant grid in space and time (see figure 6.14) is used here. In addition, the following abbreviations are introduced:

$$\boldsymbol{T}(z-\Delta z,t)=\boldsymbol{T}_{i-1,j}, \quad \boldsymbol{T}(z,t)=\boldsymbol{T}_{i,j}, \tag{6.156}$$

$$\boldsymbol{T}(z+\Delta z,t)=\boldsymbol{T}_{i+1,j}, \quad \boldsymbol{T}(z,t+\Delta t)=\boldsymbol{T}_{i,j+1}, \ldots. \tag{6.157}$$

i is the spatial index and j is the temporal index. A similar notation is also used for $\boldsymbol{C}$.

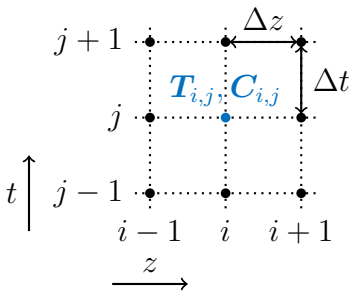

Figure 6.14: Grid in time and space for the numerical calculations.

a) Explicit Euler Method

Starting from PDE system (6.149), a vertical MOL is used in the explicit Euler method [150, pp. 80-85]. First, the spatial derivative is discretized via central differences:

$$\mathbf{A}\frac{\partial \boldsymbol{T}(z,t)}{\partial t} = \frac{\boldsymbol{T}(z-\Delta z,t) - 2\boldsymbol{T}(z,t) + \boldsymbol{T}(z+\Delta z,t)}{(\Delta z)^2} - \mathbf{B}\boldsymbol{T}(z,t) - \boldsymbol{C}(z,t). \quad (6.158)$$

In the next step, the time derivative is approximated by the forward difference:

$$\mathbf{A}\frac{\boldsymbol{T}_{i,j+1} - \boldsymbol{T}_{i,j}}{\Delta t} = \frac{\boldsymbol{T}_{i-1,j} - 2\boldsymbol{T}_{i,j} + \boldsymbol{T}_{i+1,j}}{(\Delta z)^2} - \mathbf{B}\boldsymbol{T}_{i,j} - \boldsymbol{C}_{i,j} \quad (6.159)$$

$$\Leftrightarrow \boldsymbol{T}_{i,j+1} = \Delta t \mathbf{A}^{-1}\left(\frac{\boldsymbol{T}_{i-1,j} - 2\boldsymbol{T}_{i,j} + \boldsymbol{T}_{i+1,j}}{(\Delta z)^2} - \mathbf{B}\boldsymbol{T}_{i,j} - \boldsymbol{C}_{i,j}\right) + \boldsymbol{T}_{i,j}. \quad (6.160)$$

Thus, an explicit calculation rule results for each time step. This method is easy to implement [150, p. 82] and quite fast since no matrix inversions are necessary (except for the inversion of $\mathbf{A}$, which needs to be computed only once). However, it can also diverge easily and is not always stable [150, p. 82].

b) Crank-Nicholson Method

As in the explicit Euler method, in the Crank-Nicholson method [150, pp. 87-88], the second spatial derivative is first discretized via central differences, see equation (6.158):

$$\mathbf{A}\frac{\partial \boldsymbol{T}(z,t)}{\partial t} = \boldsymbol{f}(z,t), \quad (6.161)$$

$$\boldsymbol{f}(z,t) = \frac{\boldsymbol{T}(z-\Delta z,t) - 2\boldsymbol{T}(z,t) + \boldsymbol{T}(z+\Delta z,t)}{(\Delta z)^2} - \mathbf{B}\boldsymbol{T}(z,t) - \boldsymbol{C}(z,t). \quad (6.162)$$

For time discretization,

$$\begin{aligned}\mathbf{A}\frac{\partial \boldsymbol{T}(z,t)}{\partial t} &\approx \mathbf{A}\frac{\boldsymbol{T}_{i,j+1} - \boldsymbol{T}_{i,j}}{\Delta t} \approx \frac{1}{2}\left(\boldsymbol{f}_{i,j+1} + \boldsymbol{f}_{i,j}\right) \\ &= \frac{1}{2}\left[\frac{\boldsymbol{T}_{i-1,j+1} - 2\boldsymbol{T}_{i,j+1} + \boldsymbol{T}_{i+1,j+1} + \boldsymbol{T}_{i-1,j} - 2\boldsymbol{T}_{i,j} + \boldsymbol{T}_{i+1,j}}{(\Delta z)^2}\right. \\ &\quad \left. - \mathbf{B}\left(\boldsymbol{T}_{i,j+1} + \boldsymbol{T}_{i,j}\right) - \left(\boldsymbol{C}_{i,j+1} + \boldsymbol{C}_{i,j}\right)\right]\end{aligned} \quad (6.163)$$

is used. Evaluating this equation for all spatial points i and rewriting yields the following system of linear equations, which has to be solved at each time step:

$$\begin{pmatrix} \mathbf{b} & \mathbf{a} & 0 & \dots & 0 \\ \mathbf{a} & \mathbf{b} & \mathbf{a} & \ddots & \vdots \\ 0 & \ddots & \ddots & \ddots & 0 \\ \vdots & \ddots & \mathbf{a} & \mathbf{b} & \mathbf{a} \\ 0 & \dots & 0 & \mathbf{a} & \mathbf{b} \end{pmatrix} \cdot \begin{pmatrix} \boldsymbol{T}_{2,j+1} \\ \vdots \\ \boldsymbol{T}_{i_{\max}-1,j+1} \end{pmatrix} = \begin{pmatrix} \boldsymbol{a}_2 - \mathbf{a}\boldsymbol{T}_{1,j+1} \\ \boldsymbol{a}_3 \\ \vdots \\ \boldsymbol{a}_{i_{\max}-2} \\ \boldsymbol{a}_{i_{\max}-1} - \mathbf{a}\boldsymbol{T}_{i_{\max},j+1} \end{pmatrix}, \tag{6.164}$$

$$\mathbf{a} = \frac{-1}{2(\Delta z)^2}\mathbf{U}_N, \quad \mathbf{b} = \frac{1}{(\Delta z)^2}\mathbf{U}_N + \frac{\mathbf{A}}{\Delta t} + \frac{\mathbf{B}}{2}, \quad i = 1, \dots, N,$$
$$\boldsymbol{a}_i = -\frac{1}{2}\left(\boldsymbol{C}_{i,j} + \boldsymbol{C}_{i,j+1}\right) + \left(\frac{\mathbf{A}}{\Delta t} - \frac{1}{(\Delta z)^2}\mathbf{U}_N - \frac{\mathbf{B}}{2}\right)\boldsymbol{T}_{i,j} - \mathbf{a}\left(\boldsymbol{T}_{i-1,j} + \boldsymbol{T}_{i+1,j}\right).$$

In contrast to the Euler method, the Crank-Nicholson method is implicit [151, pp. 182-183]. For each time step, a system of linear equations has to be solved. One advantage of this more laborious procedure is its stability [150, p. 88].

c) Spatial Discretization and Solution via Integration

In this approach, the first step is again the spatial discretization from above (see equation (6.158)). However, this equation is now evaluated directly at the different locations along the cable and the results are reformulated as a matrix-vector problem, where i again represents the spatial index:

$$\mathbf{A}^{-1}\begin{pmatrix} \mathbf{b} & \mathbf{a} & 0 & \dots & 0 \\ \mathbf{a} & \mathbf{b} & \mathbf{a} & \ddots & \vdots \\ 0 & \ddots & \ddots & \ddots & 0 \\ \vdots & \ddots & \mathbf{a} & \mathbf{b} & \mathbf{a} \\ 0 & \dots & 0 & \mathbf{a} & \mathbf{b} \end{pmatrix} \cdot \begin{pmatrix} \boldsymbol{T}_2 \\ \vdots \\ \boldsymbol{T}_{i_{\max}-1} \end{pmatrix} + \begin{pmatrix} -\boldsymbol{C}_2(t) - \mathbf{a}(t)\boldsymbol{T}_1 \\ -\boldsymbol{C}_3(t) \\ \vdots \\ -\boldsymbol{C}_{i_{\max}-2}(t) \\ -\boldsymbol{C}_{i_{\max}-1}(t) - \mathbf{a}\boldsymbol{T}_{i_{\max}} \end{pmatrix} = \begin{pmatrix} \dot{\boldsymbol{T}}_2 \\ \vdots \\ \dot{\boldsymbol{T}}_{i_{\max}-1} \end{pmatrix}$$
$$\Leftrightarrow \quad \hat{\mathbf{A}} \cdot \hat{\boldsymbol{T}}(t) + \hat{\boldsymbol{b}}(t) = \frac{\partial \hat{\boldsymbol{T}}(t)}{\partial t}, \tag{6.165}$$

$$\mathbf{a} = \frac{1}{(\Delta z)^2}\mathbf{U}_N, \quad \mathbf{b} = \frac{-2}{(\Delta z)^2}\mathbf{U}_N - \mathbf{B}.$$

The solution for this system of ODEs can be described analytically. For this purpose, the state-transition matrix or fundamental matrix [152, p. 9] is used, which is determined via diagonalization:

$$\boldsymbol{\Phi}(t) = \exp\left(\hat{\mathbf{A}}t\right). \tag{6.166}$$

Then, it follows [153]:

$$\hat{\boldsymbol{T}}(t) = \boldsymbol{\Phi}(t) \cdot \hat{\boldsymbol{T}}(0) + \int_0^t \boldsymbol{\Phi}(t-\hat{t})\hat{\boldsymbol{b}}(\hat{t})\,\mathrm{d}\hat{t}. \tag{6.167}$$

Depending on the exact form of the excitations $\boldsymbol{C}_i(t)$, sometimes this integral cannot be solved analytically. Then, numerical methods for integral determination are necessary. The basic idea of those methods is to divide the integration interval into shorter subintervals and then express the value for each subintegral by a finite sum of weighted function values. More information and concrete procedures can be found for example in [154, pp. 163-207] or [155, pp. 475-533].

6.2.2 Finite Element Method (FEM)

To apply the **f**inite **e**lement **m**ethod (FEM), a so-called weak formulation of the PDE is solved instead of the actual PDE. Using approach functions, the behavior in comparatively small elements is locally approximated, and those approximations are combined into a global solution. Based on the simplified scalar version of equation (6.158), the basic approach is presented. More detailed presentations of this widespread method can be found for example in [150, 156]. The beginning is a problem formulation in which the right side vanishes:

$$\frac{\partial^2 T(z,t)}{\partial z^2} - A\frac{\partial T(z,t)}{\partial t} - B\,T(z,t) - C(z,t) = 0. \tag{6.168}$$

If now instead of the exact solution $T(z,t)$ an approximate solution

$$T_{\mathrm{app}}(z,t) = \sum_{i=0}^{N+1} T_i(t)u_i(z) \tag{6.169}$$

built up from basic functions $u_i(z)$ and the searched temperature values $T_i(t)$ at discrete (spatial) locations i is used, the partial differential equation is no longer exactly satisfied and a residual res is obtained:

$$\frac{\partial^2 T_{\mathrm{app}}(z,t)}{\partial z^2} - A\frac{\partial T_{\mathrm{app}}(z,t)}{\partial t} - BT_{\mathrm{app}}(z,t) - C(z,t) = \mathrm{res}(z,t). \tag{6.170}$$

In the so-called method of weighted residuals, this residual is now multiplied individually with N weight or test functions $w_i(z), i = 1, ..., N$, and integrated over the entire space under consideration [157, pp. 57-60]. These integrals should vanish:

$$\int_0^{\mathcal{L}} \mathrm{res}(z,t)w_i(z)\,\mathrm{d}z = 0. \tag{6.171}$$

For the example, this gives the following integral, where $(\cdot)'$ abbreviates the spatial derivative and $\dot{(\cdot)}$ the temporal derivative:

$$\int_0^{\mathcal{L}} \left[T''(z,t)w_i(z) \; - \; A\dot{T}(z,t)w_i(z) \; - \; BT(z,t)w_i(z) \; - \; C(z,t)w_i(z) \right] \mathrm{d}z = 0. \tag{6.172}$$

This is a weak formulation of the problem. Depending on the choice of weight functions, different concrete methods can be derived from this rather general approach. In the Galerkin method, the basis functions of the (sought) approximate solution are also used as test functions: $w_i(z) = u_i(z)$. This approach is applied in the following. With partial integration as well as $w_i(z = 0) = 0$ and $w_i(z = \mathcal{L}) = 0$, the following relation is derived:

$$\int_0^{\mathcal{L}} T''(z,t)w_i(z)\,\mathrm{d}z = [T'(z)w_i(z)]_0^{\mathcal{L}} - \int_0^{\mathcal{L}} T'(z,t)w_i'(z)\,\mathrm{d}z = -\int_0^{\mathcal{L}} T'(z,t)w_i'(z)\,\mathrm{d}z. \tag{6.173}$$

This leads to

$$\int_0^{\mathcal{L}} \left[-T'(z,t)w_i'(z) \; - \; A\dot{T}(z,t)w_i(z) \; - \; BT(z,t)w_i(z) \; - \; C(z,t)w_i(z) \right] \mathrm{d}z = 0. \tag{6.174}$$

In the next step, the test functions $w_i(z)$, which are identical to the basis functions $u_i(z)$, are defined. Widely used choices are the so-called hat functions [156, p. 154], which are shown in figure 6.15. Effectively, a linear interpolation of the temperature development between the selected interpolation points is used here.

For the i-th test function, substituting the test functions and the approximate solution (see equation (6.169)) yields the following formulation:

$$\begin{aligned} 0 = &\sum_{j=0}^{N+1} T_j(t) \int_0^{\mathcal{L}} \left[-w_j'(z)w_i'(z) \; - \; Bw_j(z)w_i(z) \; - \; C(z,t)w_i(z) \right] \mathrm{d}z \\ &+ \sum_{j=0}^{N+1} \dot{T}_j(t) \int_0^{\mathcal{L}} \left[-Aw_j(z)w_i(z) \right] \mathrm{d}z. \end{aligned} \tag{6.175}$$

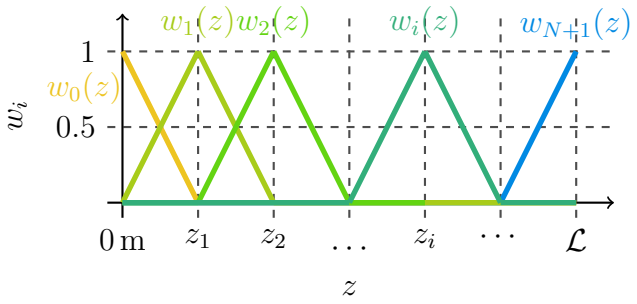

Figure 6.15: Spatial hat functions.

If this formulation is set up for all test functions $w_i(z), i = 1, ..., N$, and those equations are suitably rearranged, a matrix-vector problem of the following form is the result:

$$\hat{\mathbf{A}}_1 \boldsymbol{T} + \hat{\mathbf{A}}_2 \dot{\boldsymbol{T}} = \hat{\boldsymbol{b}} \tag{6.176}$$

with matrices $\hat{\mathbf{A}}_1$ and $\hat{\mathbf{A}}_2$. In the vector $\boldsymbol{T}$, the temperatures at the discrete evaluation points are summed up and the vector $\hat{\boldsymbol{b}}$ describes the (known) excitation. Overall, then, this spatial discretization provides a system of ODEs analog to section 6.2.1.c), which can be solved using appropriate methods.

6.2.3 Boundary Element Method (BEM)

This section gives a short overview of the **b**oundary **e**lement **m**ethod (BEM). For a more detailed discussion, see for example [158, 159].

The basis for the BEM is, as in the FEM, the weak formulation (6.172) of the problem [159, p. 37]. The basic idea now is to reformulate this by applying appropriate integral calculus rules to express the sought quantity depending only on the boundary elements [158, p. 43]. For this purpose, in the first step, the weak formulation of the differential equation is transformed in such a way that the use of Green's function as the test function significantly simplifies the expressions. An essential advantage of this method is that only the boundary of the considered volume has to be discretized [158, pp. 8-9] instead of the total volume, which is one dimension larger.

As for the FEM, the procedure is presented in simplified form using the already familiar scalar version of the general equation. In this example, the product rule is applied first:

$$\int_0^{\mathcal{L}} \left(T''(z,t)w(z) \, - \, T(z,t)w''(z)\right) \mathrm{d}z = \left[T'(z,t)w(z) \, - \, T(z,t)w'(z)\right]_0^{\mathcal{L}} . \tag{6.177}$$

Substituting together with $w(z = 0) = 0$ and $w(z = \mathcal{L}) = 0$ then yields

$$\begin{aligned} &\int_0^{\mathcal{L}} \left[T(z,t)w''(z) \, - \left(A\dot{T}(z,t) + BT(z,t)\right) w(z)\right] \mathrm{d}z \\ &= \int_0^{\mathcal{L}} C(z,t)w(z)\,\mathrm{d}z + \left[T(z,t)w'(z)\right]_0^{\mathcal{L}} . \end{aligned} \tag{6.178}$$

On the left side of this equation, in the integral, an expression of the form $(\mathrm{DGL\ for}\ w)\cdot T(z)$ is necessary. Then, the insertion of Green's function as test function w only leaves $T(z)$ on the left side. Therefore, equation (6.178) is transformed into the Laplace domain. For $C(z,t) = C(z)$, the transformation leads to

$$\int_0^{\mathcal{L}} \left[w''(\tilde{z},z,s) - (sA+B)\,w(\tilde{z},z,s)\right] T(\tilde{z})\,\mathrm{d}\tilde{z}$$
$$= \int_0^{\mathcal{L}} \left(\frac{C(\tilde{z})}{s} - AT_0(\tilde{z})\right) w(\tilde{z},z,s)\,\mathrm{d}\tilde{z} + \left[T(\tilde{z})w'(\tilde{z},z,t)\right]_{\tilde{z}=0}^{\mathcal{L}}. \tag{6.179}$$

For time-varying C, the appropriate transformation must be used. If now for $w(\tilde{z},z,s)$ the Green's function for the differential equation

$$w''(\tilde{z},z,s) - (sA+B)\,w(\tilde{z},z,s) = 0 \tag{6.180}$$

(see also equation (6.52)) is inserted, the integral on the left side of the equation vanishes:

$$T(z) = \int_0^{\mathcal{L}} \left(\frac{C(\tilde{z})}{s} - AT_0(\tilde{z})\right) w(\tilde{z},z,s)\,\mathrm{d}\tilde{z} + \left[T(\tilde{z})w'(\tilde{z},z,s)\right]_{\tilde{z}=0}^{\mathcal{L}}. \tag{6.181}$$

Thus, on the left side, the desired term arises. Due to the initial and boundary conditions, however, an integral over the entire volume still appears on the right side. Only for very simple special cases, this integral can be calculated analytically. In many cases, however, discretization is necessary again, so the main advantage of the BEM (no discretization in the complete volume) [158, pp. 8-10] no longer exists. The result is finally available in the Laplace domain and must still be transformed back into the time domain. This transformation cannot always be performed analytically. Then, numerical transformations are necessary. In principle, those can be traced back to the numerical approximation of the transformation integral [160, p. 100]. However, this can be challenging, so specific methods have been developed for the numerical evaluation of these integrals, see e.g. [160, pp. 327-355].

Due to the necessary discretization of the complete volume to take into account initial temperatures as well as excitations and due to the potential difficulties with the transformation back into the time domain, the use of BEM to solve the PDE causes considerable effort. Other methods are therefore more appropriate.

6.2.4 Finite Volume Method (FVM)

The last method to be shortly presented here is the **f**inite **v**olume **m**ethod (FVM). A more detailed discussion can for example be found in [161] or [162, chapter 31]. Once again, the basis is the weak formulation of the problem, see equation (6.172). As with the BEM, this is rewritten so that a boundary integral occurs for the flow. In the one-dimensional case, this boundary integral becomes an integral over a zero-**d**imensional (0 D) surface, i.e., the known evaluation at the two terminations. Because of $w(z) = 1$ and $w'(z) = 0$, the result is

$$\int_0^{\mathcal{L}} -\left(A\dot{T}(z,t) + BT(z,t)\right)\,\mathrm{d}z = \int_0^{\mathcal{L}} C(z,t)\,\mathrm{d}z + \left[T'(z,t)\right]_0^{\mathcal{L}}. \tag{6.182}$$

In contrast to the FEM, where compliance with this equation was required for (several) specific test functions, the test function $w(z) = 1$ is chosen now. Instead, the considered volume is discretized and it is required that the corresponding equation holds in each subvolume [161, p. 9]. For the 1 D case, the considered distance along the cable is divided into subvolumes as shown in figure 6.16. The corresponding formulation for the subvolume i is then:

$$\int_{z_{i-\frac{1}{2}}}^{z_{i+\frac{1}{2}}} -\left(A\dot{T}(z,t) + BT(z,t)\right)\,\mathrm{d}z = \int_{z_{i-\frac{1}{2}}}^{z_{i+\frac{1}{2}}} C(z,t)\,\mathrm{d}z + \left[T'(z,t)\right]_{z_{i-\frac{1}{2}}}^{z_{i+\frac{1}{2}}}. \tag{6.183}$$

For a subvolume i, the following reformulation allows the expression of the results in terms of mean values:

$$-A\int_{z_{i-\frac{1}{2}}}^{z_{i+\frac{1}{2}}} \dot{T}(z,t)\,\mathrm{d}z - B\int_{z_{i-\frac{1}{2}}}^{z_{i+\frac{1}{2}}} T(z,t)\,\mathrm{d}z = \Delta z\overline{C}_i + \left[T'(z,t)\right]_{z_{i-\frac{1}{2}}}^{z_{i+\frac{1}{2}}} \tag{6.184}$$

$$\Leftrightarrow -A\dot{\overline{T}}_i \;-\; B\overline{T}_i = \overline{C}_i + \frac{1}{\Delta z}\left[T'(z,t)\right]_{z_{i-\frac{1}{2}}}^{z_{i+\frac{1}{2}}}. \tag{6.185}$$

Here, $\overline{T}_i$ represents the mean temperature in the considered subvolume. Because of the interchangeability of the time derivative and averaging, $\dot{\overline{T}}_i$ is the associated mean of the time derivative. $\overline{C}_i$ is the mean of C in this volume. The temperature mean values are assigned to the position in the center of the cell:

$$\overline{T}_i = T(z_i). \tag{6.186}$$

Now, to find a representation for the temperature averages as new unknowns, the spatial derivative at the cell boundaries has to be approximated as a function of the averages $\overline{T}_i$. For this purpose, for example, an FDM approach can be used:

$$T'(z_{i-\frac{1}{2}}) \approx \frac{T(z_i) - T(z_{i-1})}{\Delta z} = \frac{\overline{T}_i - \overline{T}_{i-1}}{\Delta z}. \tag{6.187}$$

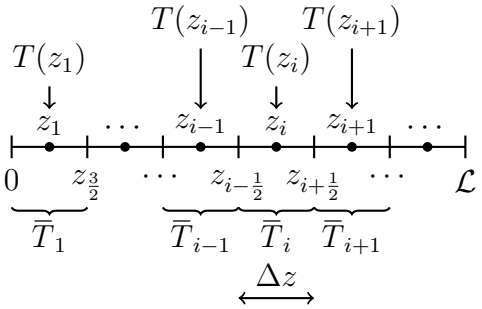

Figure 6.16: Spatial discretization with cells and coordinate positions for FVM.

For a single subvolume, this leads to a new ODE for the mean values of the temperatures in the subvolume, which are assigned to the values at the central points:

$$-A\dot{\overline{T}}_i - B\overline{T}_i = \overline{C}_i + \frac{\overline{T}_i - \overline{T}_{i-1}}{(\Delta z)^2}. \tag{6.188}$$

If the corresponding equations are now set up for all considered subvolumes and suitably transformed, a matrix-vector representation analog to equation (6.176) is again obtained, where now the temperature averages over the cells are the unknowns. Overall, this approach showed another possible spatial discretization. The time dependence has to be dealt with in a second step.

6.2.5 Approximation Based on Linear Solutions for Constant Excitations

In the previous sections, numerical solutions were presented, which in principle allow the consideration of variable initial and boundary conditions as well as excitations. Alternatively, a semi-analytical approximation based on the results of section 6.1 is presented here. First, it is assumed that the initial and boundary conditions as well as the excitation can be represented by a sequence of rectangular shapes depending on the time and the location, respectively. Real occurring courses must therefore be approximated in the first step of such a development. By superposition of the results from section 6.1 and by application of an analog procedure, suitable analytical solutions for these variable excitations are found. This procedure is an approximation, but compared to the consideration of only constant values, it allows an adaptation to changing conditions: For example, variable currents can be taken into account via a suitable worst case. Also, different ambient temperature ranges along the cable (spatially variable ambient temperature) as well as the consideration of temporal changes in the ambient temperatures (for example in form of an update after some time) can be considered. For the initial temperature distribution and the cable termination temperatures, the consideration of worst-case developments is also enabled.

a) Reformulation of the Solution for a Single Wire Cable

In the earlier examinations, the PDE from equation (6.23) with the constant initial and boundary conditions (see equations (6.24) and (6.25)) was solved. In this section, for the initial and boundary conditions and the inhomogeneity, rectangular shapes are assumed instead of the previously used constant values. To enable the isolated evaluation of the effects resulting from the ambient temperature T_e and the current I, the inhomogeneity $\tilde{C}_\mathrm{sw}$ in the PDE is split up into the two parts $\tilde{C}_{1,\mathrm{sw}}$ (depending on the ambient temperature) and $\tilde{C}_{2,\mathrm{sw}}$ (depending on the current):

$$\tilde{C}_\mathrm{sw}(z,t) = \tilde{C}_{1,\mathrm{sw}}(z,t) + \tilde{C}_{2,\mathrm{sw}}(z,t), \tag{6.189}$$

$$\tilde{C}_{1,\mathrm{sw}}(z,t) = C_{1,\mathrm{sw}}\Gamma(t) = -R'G'T_{\mathrm{e}}\Gamma(t), \tag{6.190}$$

$$\tilde{C}_{2,\mathrm{sw}}(z,t) = C_{2,\mathrm{sw}}\Gamma(t) = -R'P'_{\mathrm{el}}\Gamma(t). \tag{6.191}$$

Then, also in the solution approach (see equation (6.26)), two parts for the inhomogeneity appear,

$$T_{\tilde{C},\mathrm{sw}}(z,t,C_{\mathrm{sw}}) = T_{\tilde{C}_1,\mathrm{sw}}(z,t,C_{1,\mathrm{sw}}) + T_{\tilde{C}_2,\mathrm{sw}}(z,t,C_{2,\mathrm{sw}}). \tag{6.192}$$

In the earlier derived solutions for constant initial and boundary conditions as well as stimulation, the different solution parts were presented for three different approaches: Usage of the Laplace domain with approximation (see section 6.1.2.a)), usage of Green's functions in the time domain (see section 6.1.2.b)) and usage of Green's functions in the Laplace domain (see section 6.1.2.c)). In the following, for the individual contribution parts, approaches for the consideration of rectangularly shaped excitations instead of constant values are presented.

b) Rectangular Current

For the current, a single rectangular pulse as shown in figure 6.17 is assumed:

$$\tilde{I}(t) = I_i\left(\Gamma(t-t_{1,i,I}) - \Gamma(t-t_{2,i,I})\right). \tag{6.193}$$

Then, the corresponding heat flow is

$$\tilde{P}'_{\mathrm{el},i}(z,t) = I_i^2 R'_{\mathrm{ref}}\left(1+\eta_T(T_{\mathrm{sw}}(z,t)-T_{\mathrm{ref}})\right)\left(\Gamma(t-t_{1,i,I}) - \Gamma(t-t_{2,i,I})\right). \tag{6.194}$$

In the derivation of the earlier solutions, it was assumed that the heat flow is constant which is equivalent to the assumption of a constant cable temperature in combination with the constant current. Therefore, for each position (z,t), it is implicitly assumed that the used cable temperature holds for all times and spaces. This approximation decouples all positions and times because, for each combination (z,t), a different PDE is solved. The same approach is used here, which means the neglection of the z- and t-dependence of the cable temperature in the calculation of the heat flow and therefore, replacing $T_{\mathrm{sw}}(z,t)$ with the local, but constant

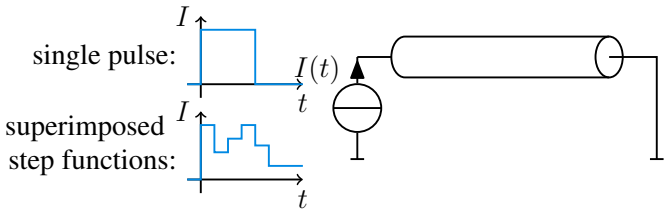

Figure 6.17: Rectangularly shaped current as excitation.

temperature $T_{\mathrm{sw,loc}}$. Then, the heat flow also follows a rectangular shape:

$$\tilde{P}'_{\mathrm{el},i}(z,t) = I_i^2 R'_{\mathrm{ref}} \left(1 + \eta_T (T_{\mathrm{sw,loc}} - T_{\mathrm{ref}})\right) \left(\Gamma(t - t_{1,i,I}) - \Gamma(t - t_{2,i,I})\right). \tag{6.195}$$

$\tilde{C}_{2,\mathrm{sw}}(t)$, therefore, becomes

$$\tilde{C}_{2,\mathrm{sw}}(t) = C_{2,\mathrm{sw},i} \left(\Gamma(t - t_{1,i,I}) - \Gamma(t - t_{2,i,I})\right), \tag{6.196}$$

$$C_{2,\mathrm{sw},i} = -R' I_i^2 R'_{\mathrm{ref}} \left(1 + \eta_T (T_{\mathrm{sw,loc}} - T_{\mathrm{ref}})\right). \tag{6.197}$$

Because of the assumed linearity in the solution, the new solution is found via relocation and superposition of the earlier derived solution:

$$T_{\tilde{C}_{2,\mathrm{sw}}}(z,t,C_{2,\mathrm{sw},i}) = T_{\mathrm{inh,sw}}\left(z, t - t_{1,i,I}, C_{2,\mathrm{sw},i}\right) - T_{\mathrm{inh,sw}}\left(z, t - t_{2,i,I}, C_{2,\mathrm{sw},i}\right). \tag{6.198}$$

For a superposition of several rectangular current shapes (see figure 6.17), the resulting profile becomes

$$\tilde{I}(t) = \sum_{i=1}^{i_{\max,C_{2,\mathrm{sw}}}} I_i \left(\Gamma(t - t_{1,i,I}) - \Gamma(t - t_{2,i,I})\right). \tag{6.199}$$

Then, using $\tilde{t}_1 = t - t_{1,i,I}$ and $\tilde{t}_2 = t - t_{2,i,I}$, the solution is

$$T_{\tilde{C}_{2,\mathrm{sw}}}(z,t,C_{2,\mathrm{sw},i}) = \sum_{i=1}^{i_{\max,C_{2,\mathrm{sw}}}} \left[T_{\mathrm{inh,sw}}\left(z, \tilde{t}_1, C_{2,\mathrm{sw},i}\right) - T_{\mathrm{inh,sw}}\left(z, \tilde{t}_2, C_{2,\mathrm{sw},i}\right)\right]. \tag{6.200}$$

c) Rectangular Cable Termination Temperatures

Rectangular cable termination temperatures as shown in figure 6.18 are taken into account similar to the approach used for the current. With $\tilde{t}_{1,j} = t - t_{1,i,T_j}$ and $\tilde{t}_{2,j} = t - t_{2,i,T_j}$, $j = 1, 2$, the corresponding solutions are derived:

$$T_{\mathrm{sw}}(0,t) = \tilde{T}_{1,\mathrm{sw}}(t) = \sum_{i=1}^{i_{\max,T_{1,\mathrm{sw}}}} T_{1,\mathrm{sw},i} \left(\Gamma(\tilde{t}_{1,1}) - \Gamma(\tilde{t}_{2,1})\right), \tag{6.201}$$

$$T_{\mathrm{sw}}(\mathcal{L},t) = \tilde{T}_{2,\mathrm{sw}}(t) = \sum_{i=1}^{i_{\max,T_{2,\mathrm{sw}}}} T_{2,\mathrm{sw},i} \left(\Gamma(\tilde{t}_{1,2}) - \Gamma(\tilde{t}_{2,2})\right) \tag{6.202}$$

$$\Rightarrow T_{\tilde{T}_{1,\mathrm{sw}}}(z,t) = \sum_{i=1}^{i_{\max,T_{1,\mathrm{sw}}}} \left[T_{\mathrm{bc,sw}}(z, \tilde{t}_{1,1}, T_{1,\mathrm{sw},i}) - T_{\mathrm{bc,sw}}(z, \tilde{t}_{2,1}, T_{1,\mathrm{sw},i})\right], \tag{6.203}$$

$$T_{\tilde{T}_{2,\mathrm{sw}}}(z,t) = \sum_{i=1}^{i_{\max,T_{2,\mathrm{sw}}}} \left[T_{\mathrm{bc,sw}}(z_{\mathcal{L}}, \tilde{t}_{1,2}, T_{2,\mathrm{sw},i}) - T_{\mathrm{bc,sw}}(z_{\mathcal{L}}, \tilde{t}_{2,2}, T_{2,\mathrm{sw},i})\right]. \tag{6.204}$$

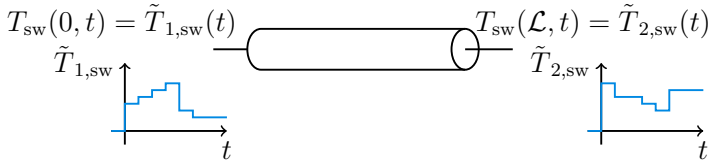

Figure 6.18: Rectangularly shaped cable termination temperatures.

d) Rectangular Initial Cable Temperature

A rectangular shape can also be assumed for the initial cable temperature as shown in figure 6.19 for several rectangles. Unlike the earlier solutions, now, the rectangular shape is given in the spatial coordinate z:

$$T_{\mathrm{sw}}(z,0) = \tilde{T}_{0,\mathrm{sw}}(z) = T_{0,\mathrm{sw},i}\left(\Gamma(z-z_1) - \Gamma(z-z_2)\right). \tag{6.205}$$

For this initial condition, the corresponding solution part of the PDE needs to be recalculated separately for all three solution approaches. For the solution via Green's functions in the time domain, the approach known from section 6.1.2.b) is applicable again, but the limits in the integration differ from the earlier presented solution. To ensure the invariance of each addend in the sum under the symmetry transformation

$$z \to \mathcal{L} - z, z_1 \to \mathcal{L} - z_2, z_2 \to \mathcal{L} - z_1, \tag{6.206}$$

indices are shifted. Then, the result for a rectangularly shaped initial temperature for the solution via Green's functions in the time domain is

$$\begin{aligned} T_{\mathrm{ic,sw,rect,G}}(z,t,T_{0,\mathrm{sw},i},z_1,z_2) = \frac{\Gamma(t)\Lambda_3(t)T_{0,\mathrm{sw},i}}{2} \Big[& \Lambda_1(z_2-z,t) - \Lambda_1(z_2+z-2\mathcal{L},t) \\ & - \Lambda_1(z_1-z,t) + \Lambda_1(z_1+z,t) - 2 + \sum_{n=1}^{\infty}\{\Lambda_1(z_2-z-\tilde{n},t) + \Lambda_1(z_2-z+\tilde{n},t) \\ & - \Lambda_1(z_2+z+2(n-1)\mathcal{L},t) - \Lambda_1(z_2+z-2(n+1)\mathcal{L},t) - \Lambda_1(z_1-z-\tilde{n},t) \\ & - \Lambda_1(z_1-z+\tilde{n},t) + \Lambda_1(z_1+z+\tilde{n},t) + \Lambda_1(z_1+z-\tilde{n},t)\}\Big]. \end{aligned} \tag{6.207}$$

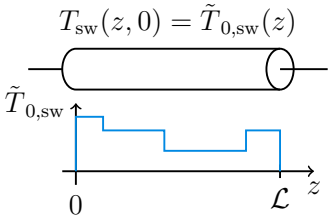

Figure 6.19: Rectangularly shaped initial cable temperature.

Neglecting the sum leads to the corresponding formulation for the solution from the Laplace domain with approximation:

$$T_{\mathrm{ic,sw,rect,La}}(z,t,T_{0,\mathrm{sw},i},z_1,z_2) = \frac{\Gamma(t)\Lambda_3(t)T_{0,\mathrm{sw},i}}{2}\left[\Lambda_1(z_2-z,t)-\Lambda_1(z_2+z-2\mathcal{L},t)\right.$$
$$\left.-\Lambda_1(z_1-z,t)+\Lambda_1(z_1+z,t)-2\right]. \tag{6.208}$$

Accordingly, for the solution via Green's functions in the Laplace domain, in the recalculation for the new initial condition, the limits of the integral change. The result in the time domain is

$$T_{\mathrm{ic,sw,rect,GL}}(z,t,T_{0,\mathrm{sw},i},z_1,z_2) \tag{6.209}$$
$$= \frac{2}{\pi}T_{0,\mathrm{sw},i}\sum_{n=1}^{\infty}\exp\left(-\frac{t}{A_{\mathrm{sw}}}\left(n_{\mathcal{L}}^2+B_{\mathrm{sw}}\right)\right)\sin\left(n_{\mathcal{L}}z\right)\left[\cos\left(n_{\mathcal{L}}z_1\right)-\cos\left(n_{\mathcal{L}}z_2\right)\right]\frac{1}{n}.$$

All in all, the corresponding solution part of the PDE is

$$T_{\tilde{T}_{0,\mathrm{sw}}}(z,t) = T_{\mathrm{ic,sw,rect}}(z,t,T_{0,\mathrm{sw},i},z_1,z_2). \tag{6.210}$$

For a linear combination of several rectangles (see figure 6.19), the initial temperature distribution is

$$\tilde{T}_{0,\mathrm{sw}}(z) = \sum_{i=1}^{i_{\max,T_{0,\mathrm{sw}}}} T_{0,\mathrm{sw},i}\left(\Gamma(z-z_{1,i,T_0})-\Gamma(z-z_{2,i,T_0})\right) \tag{6.211}$$

and the corresponding part of the solution becomes

$$T_{\tilde{T}_{0,\mathrm{sw}}}(z,t) = \sum_{i=1}^{i_{\max,T_{0,\mathrm{sw}}}} T_{\mathrm{ic,sw,rect}}(z,t,T_{0,\mathrm{sw},i},z_{1,i,T_{0,\mathrm{sw}}},z_{2,i,T_{0,\mathrm{sw}}}). \tag{6.212}$$

e) Rectangular Ambient Temperature

The ambient temperature does not only influence the inhomogeneous part $\tilde{C}_{1,\mathrm{sw}}(z,t)$ in the PDE but also appears in the parameter B_{sw} because there, the conductance G' describing the heat transfer from the cable to the ambient air appears. In this section, this dependence is not considered. For the calculation of the parameter B_{sw} for a specific position in space and time (z,t), only the value for the ambient temperature at exactly this position is considered. The influence of a rectangular ambient temperature in the inhomogeneous part $\tilde{C}_{1,\mathrm{sw}}(z,t)$ is evaluated in the following. Generally, considering a rectangularly shaped ambient temperature, spatial as well as time rectangles are possible. In practical applications, exactly rectangular ambient temperatures will not appear, but this approach can be used to approximate real ambient temperature developments. For a sum of rectangular shapes about the time, but a constant distribution about the spatial coordinate (see figure 6.20(a)), the ambient

temperature is

$$\tilde{T}_{\mathrm{e}}(z,t) = \sum_{i=1}^{i_{\max,C_{1,\mathrm{sw}}}} T_{\mathrm{e},i}\left(\Gamma(t-t_{1,i,T_{\mathrm{e}}}) - \Gamma(t-t_{2,i,T_{\mathrm{e}}})\right). \tag{6.213}$$

For the inhomogeneity, it follows

$$\tilde{C}_{1,\mathrm{sw}}(z,t) = \sum_{i=1}^{i_{\max,C_{1,\mathrm{sw}}}} C_{1,\mathrm{sw},i}\left(\Gamma(t-t_{1,i,T_{\mathrm{e}}}) - \Gamma(t-t_{2,i,T_{\mathrm{e}}})\right). \tag{6.214}$$

As mentioned before, the conductance G' depends on the ambient temperature. In addition, the ambient temperature appears explicitly in the calculation rule for $C_{1,\mathrm{sw},i}$:

$$C_{1,\mathrm{sw},i} = -R'G'(T_{\mathrm{e},i})T_{\mathrm{e},i}. \tag{6.215}$$

Analog to the consideration of rectangular current pulses, the corresponding solution is

$$T_{\tilde{C}_{1,\mathrm{sw}}}(z,t,C_{1,\mathrm{sw},i}) = \sum_{i=1}^{i_{\max,C_{1,\mathrm{sw}}}} \left[T_{\mathrm{inh}}(z,\tilde{t}_1,C_{1,\mathrm{sw},i}) - T_{\mathrm{inh}}(z,\tilde{t}_2,C_{1,\mathrm{sw},i})\right] \tag{6.216}$$

with $\tilde{t}_1 = t - t_{1,i,T_{\mathrm{e}}}$ and $\tilde{t}_2 = t - t_{2,i,T_{\mathrm{e}}}$. For spatial rectangular shapes without time dependence (see figure 6.20(b)), the ambient temperature and the inhomogeneity are as follows:

$$\tilde{T}_{\mathrm{e}}(z,t) = T_{\mathrm{e},i}(\Gamma(z-z_1) - \Gamma(z-z_2)), \tag{6.217}$$

$$\tilde{C}_{1,\mathrm{sw}}(z,t) = C_{1,\mathrm{sw},i}(\Gamma(z-z_1) - \Gamma(z-z_2)). \tag{6.218}$$

Then, similarly to the considerations for rectangular initial conditions, recalculations need to be performed. Again, only the limits in the necessary integrations have to be changed. For the solution with Green's functions in the time domain, the result is

$$\begin{aligned}
T_{\mathrm{inh,sw,rect,G}}(z,t,C_{1,\mathrm{sw},i},z_1,z_2) &= T_{\mathrm{ic,sw,rect,G}}\left(z,t,\frac{C_{1,\mathrm{sw},i}}{B_{\mathrm{sw}}},z_1,z_2\right) \\
&- \Gamma(t)\frac{C_{1,\mathrm{sw},i}}{2B_{\mathrm{sw}}}\Big\{-\mathrm{sgn}(z_1-z)+\mathrm{sgn}(z_2-z)+\frac{1}{2}\left[\mathrm{sgn}(z_2-z)\Lambda_2(|z_2-z|,t)\right. \\
&\left.+\Lambda_2(-z_2-z+2\mathcal{L},t)-\mathrm{sgn}(z_1-z)\Lambda_2(|z_1-z|,t)+\Lambda_2(z_1+z,t)\right]\Big\} \\
&- \Gamma(t)\frac{C_{1,\mathrm{sw},i}}{4B_{\mathrm{sw}}}\sum_{n=1}^{\infty}\left[-\Lambda_2(-z_2+z+\tilde{n},t)+\Lambda_2(z_2-z+\tilde{n},t)\right. \\
&- \Lambda_2(z_2+z+2(n-1)\mathcal{L},t)+\Lambda_2(-z_2-z+2(n+1)\mathcal{L},t)+\Lambda_2(-z_1+z+\tilde{n},t) \\
&\left.-\Lambda_2(z_1-z+\tilde{n},t)+\Lambda_2(z_1+z+\tilde{n},t)-\Lambda_2(-z_1-z+\tilde{n},t)\right].
\end{aligned} \tag{6.219}$$

For the Laplace approximation, the corresponding expression is

$$T_{\text{inh,sw,rect,La}}(z,t,C_{1,\text{sw},i},z_1,z_2) = T_{\text{ic,sw,rect,La}}\left(z,t,\frac{C_{1,\text{sw},i}}{B_{\text{sw}}},z_1,z_2\right) - \Gamma(t)\frac{C_{1,\text{sw},i}}{2B_{\text{sw}}}\left\{-\text{sgn}(z_1-z)+\text{sgn}(z_2-z)+\frac{1}{2}\left[\text{sgn}(z_2-z)\Lambda_2(|z_2-z|,t)\right.\right.$$
$$\left.\left.+\Lambda_2(-z_2-z+2\mathcal{L},t)-\text{sgn}(z_1-z)\Lambda_2(|z_1-z|,t)+\Lambda_2(z_1+z,t)\right]\right\}. \quad (6.220)$$

Using the solution via Green's functions in the Laplace domain, it follows

$$T_{\text{inh,sw,rect,GL}}(z,t,C_{1,\text{sw},i},z_1,z_2) = -\Gamma(t)\frac{2}{\pi}C_{1,\text{sw},i}\sum_{n=1}^{\infty}\frac{1-\exp\left(-\frac{t}{A_{\text{sw}}}\left(n_{\mathcal{L}}^2+B_{\text{sw}}\right)\right)}{B_{\text{sw}}+n_{\mathcal{L}}^2} \cdot\sin\left(n_{\mathcal{L}}z\right)\left[\cos\left(n_{\mathcal{L}}z_1\right)-\cos\left(n_{\mathcal{L}}z_2\right)\right]\frac{1}{n}. \quad (6.221)$$

For a single rectangle, the solution then is

$$T_{\tilde{C}_{1,\text{sw}}}(z,t) = T_{\text{inh,sw,rect}}(z,t,C_{1,\text{sw},i},z_1,z_2). \quad (6.222)$$

For a sum of several rectangles, again, the corresponding expressions for the single rectangles have to be superposed:

$$\tilde{C}_{1,\text{sw}}(z) = \sum_{i=1}^{i_{\max,T_\text{e}}} C_{1,\text{sw},i}\left(\Gamma(z-z_{1,i,T_\text{e}})-\Gamma(z-z_{2,i,T_\text{e}})\right) \quad (6.223)$$

$$\Rightarrow T_{\tilde{C}_{1,\text{sw}}}(z,t,C_{1,\text{sw},i}) = \sum_{i=1}^{i_{\max,C_{1,\text{sw}}}} T_{\text{inh,rect}}(z,t,C_{1,\text{sw},i},z_{1,i,T_\text{e}},z_{2,i,T_\text{e}}). \quad (6.224)$$

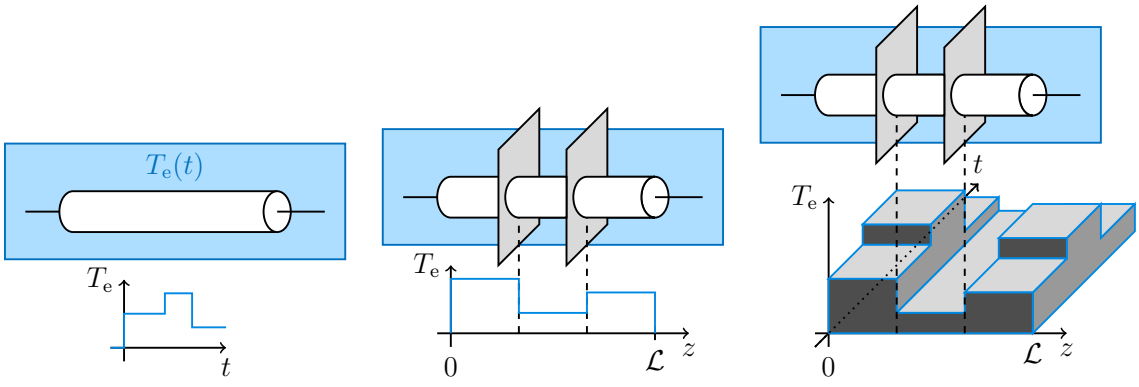

(a) (b) (c)

Figure 6.20: Rectangularly shaped environmental temperatures depending on (a) time, (b) space, or (c) both.

Rectangular shapes in the time and spatial coordinate (see figure 6.20(c)) are superposed for the general case:

$$\tilde{C}_1(z,t) = \sum_{i=1}^{i_{\max,C_{1,\mathrm{sw}}}} \sum_{j=1}^{j_{\max,C_{1,\mathrm{sw}}}} C_{1,\mathrm{sw},ij} \left(\Gamma(z - z_{1,i,T_\mathrm{e}}) - \Gamma(z - z_{2,i,T_\mathrm{e}})\right) \cdot \left(\Gamma(t - t_{1,j,T_\mathrm{e}}) - \Gamma(t - t_{2,j,T_\mathrm{e}})\right) \tag{6.225}$$

$$\Rightarrow T_{\tilde{C}_{1,\mathrm{sw}}}(z,t,C_{1,\mathrm{sw},ij}) = \sum_{i=1}^{i_{\max,C_{1,\mathrm{sw}}}} \sum_{j=1}^{j_{\max,C_{1,\mathrm{sw}}}} \left[T_{\mathrm{inh,rect}}(z, t - t_{1,j,T_\mathrm{e}}, C_{1,\mathrm{sw},ij}, z_{1,i,T_\mathrm{e}}, z_{2,i,T_\mathrm{e}}) - T_{\mathrm{inh,rect}}(z, t - t_{2,j,T_\mathrm{e}}, C_{1,\mathrm{sw},ij}, z_{1,i,T_\mathrm{e}}, z_{2,i,T_\mathrm{e}})\right]. \tag{6.226}$$

Here, the index i corresponds to the spatial dependence, the index j corresponds to the time dependence.

f) Application to Multiconductor Arrangement

For a multiconductor arrangement analog to the electrical domain, the rectangularly shaped conditions are considered equivalently to the single wire cable. The system of PDEs is formulated as given in equation (5.72) with

$$\boldsymbol{C} = \tilde{\boldsymbol{C}}_1(z,t) + \tilde{\boldsymbol{C}}_2(z,t). \tag{6.227}$$

$\tilde{\boldsymbol{C}}_1(z,t)$ considers the dependence on the environmental temperature T_e and $\tilde{\boldsymbol{C}}_2(t)$ depends on the current excitation. The solution is built up from the partial solutions for the different excitations and initial as well as boundary conditions:

$$\boldsymbol{T}(z,t) = \boldsymbol{T}_{\tilde{\boldsymbol{T}}_0}(z,t,\boldsymbol{T}_0) + \boldsymbol{T}_{\tilde{\boldsymbol{T}}_1}(z,t,\boldsymbol{T}_1) + \boldsymbol{T}_{\tilde{\boldsymbol{T}}_2}(z,t,\boldsymbol{T}_2) + \boldsymbol{T}_{\tilde{\boldsymbol{C}}_1}(z,t,\boldsymbol{C}_1) + \boldsymbol{T}_{\tilde{\boldsymbol{C}}_2}(z,t,\boldsymbol{C}_2). \tag{6.228}$$

In table 6.1, an overview of those solutions is given for constant and rectangular excitations. Implicitly, here, it is assumed that the rectangular excitations for all conductors change at the same positions in time and space.

The necessary functions for the solution based on the Laplace approximation for N identical conductors are given in equations (6.121) to (6.123) together with

$$\boldsymbol{T}_{\mathrm{ic,id,rect,La}}(z,t,\boldsymbol{T}_{0,\mathrm{id},i},z_1,z_2) = \frac{1}{2}\Gamma(t)[\Lambda_1(z_2 - z,t) - \Lambda_1(z_2 + z - 2\mathcal{L},t) - \Lambda_1(z_1 - z,t) + \Lambda_1(z_1 + z,t) - 2]\boldsymbol{\Lambda}_3(t)\boldsymbol{T}_{0,\mathrm{id},i}, \tag{6.229}$$

$$\boldsymbol{T}_{\mathrm{inh,id,rect,La}}(z,t,\boldsymbol{C}_{\mathrm{inh}},z_1,z_2) = \boldsymbol{T}_{\mathrm{ic,id,rect,La}}(z,t,\mathbf{B}_{\mathrm{id}}^{-1}\boldsymbol{C}_{\mathrm{inh}},z_1,z_2) \tag{6.230}$$

$$- \frac{1}{2}\Gamma(t)\left\{-\mathrm{sgn}(z_1 - z)\mathbf{U}_N + \mathrm{sgn}(z_2 - z)\mathbf{U}_N + \frac{1}{2}[\mathrm{sgn}(z_2 - z)\boldsymbol{\Lambda}_2(|z_2 - z|,t) + \boldsymbol{\Lambda}_2(-z_2 - z + 2\mathcal{L},t) - \mathrm{sgn}(z_1 - z)\boldsymbol{\Lambda}_2(|z_1 - z|,t) + \boldsymbol{\Lambda}_2(z_1 + z,t)]\right\}\mathbf{B}_{\mathrm{id}}^{-1}\boldsymbol{C}_{\mathrm{inh}}.$$

Table 6.1: Overview of solution parts for rectangular stimulations.

solution \ stimulus	constant	rectangular
$\boldsymbol{T}_{\tilde{\boldsymbol{T}}_0}(z,t,\boldsymbol{T}_0)$	$\boldsymbol{T}_{\mathrm{ic}}(z,t,\boldsymbol{T}_0)$	$\sum_{i=1}^{i_{\max,\boldsymbol{T}_0}} \boldsymbol{T}_{\mathrm{ic,rect}}(z,t,\boldsymbol{T}_{0,i},z_{1,i,\boldsymbol{T}_0},z_{2,i,\boldsymbol{T}_0})$
$\boldsymbol{T}_{\tilde{\boldsymbol{T}}_1}(z,t,\boldsymbol{T}_1)$	$\boldsymbol{T}_{\mathrm{bc}}(z,t,\boldsymbol{T}_1)$	$\sum_{i=1}^{i_{\max,\boldsymbol{T}_1}} [\boldsymbol{T}_{\mathrm{bc}}(z,t-t_{1,i,\boldsymbol{T}_1},\boldsymbol{T}_{1,i}) - \boldsymbol{T}_{\mathrm{bc}}(z,t-t_{2,i,\boldsymbol{T}_1},\boldsymbol{T}_{1,i})]$
$\boldsymbol{T}_{\tilde{\boldsymbol{T}}_2}(z,t,\boldsymbol{T}_2)$	$\boldsymbol{T}_{\mathrm{bc}}(z_{\mathcal{L}},t,\boldsymbol{T}_2)$	$\sum_{i=1}^{i_{\max,\boldsymbol{T}_2}} [\boldsymbol{T}_{\mathrm{bc}}(z_{\mathcal{L}},t-t_{1,i,\boldsymbol{T}_2},\boldsymbol{T}_{2,i}) - \boldsymbol{T}_{\mathrm{bc}}(z_{\mathcal{L}},t-t_{2,i,\boldsymbol{T}_2},\boldsymbol{T}_{2,i})]$
$\boldsymbol{T}_{\tilde{\boldsymbol{C}}_1}(z,t,\boldsymbol{C}_1)$	$\boldsymbol{T}_{\mathrm{inh}}(z,t,\boldsymbol{C}_1)$	$\sum_{i=1}^{i_{\max,\boldsymbol{C}_1}} \sum_{j=1}^{j_{\max,\boldsymbol{C}_1}} [\boldsymbol{T}_{\mathrm{inh,rect}}(z,t-t_{1,j,T_\mathrm{e}},\boldsymbol{C}_{1,ij},z_{1,i,T_\mathrm{e}},z_{2,i,T_\mathrm{e}}) - \boldsymbol{T}_{\mathrm{inh,rect}}(z,t-t_{2,j,T_\mathrm{e}},\boldsymbol{C}_{1,ij},z_{1,i,T_\mathrm{e}},z_{2,i,T_\mathrm{e}})]$
$\boldsymbol{T}_{\tilde{\boldsymbol{C}}_2}(z,t,\boldsymbol{C}_2)$	$\boldsymbol{T}_{\mathrm{inh}}(z,t,\boldsymbol{C}_2)$	$\sum_{i=1}^{i_{\max,\boldsymbol{C}_2}} [\boldsymbol{T}_{\mathrm{inh}}(z,t-t_{1,i,\boldsymbol{I}},\boldsymbol{C}_{2,i}) - \boldsymbol{T}_{\mathrm{inh}}(z,t-t_{2,i,\boldsymbol{I}},\boldsymbol{C}_{2,i})]$

The terms for the solution via Green's functions in the time domain for N identical conductors can be found in equations (6.125) to (6.127) together with

$$\begin{aligned}\boldsymbol{T}_{\mathrm{ic,id,rect,G}}(z,t,\boldsymbol{T}_{0,i},z_1,z_2) &= \boldsymbol{T}_{\mathrm{ic,id,rect,La}}(z,t,\boldsymbol{T}_{0,i},z_1,z_2) + \frac{1}{2}\Gamma(t)\sum_{n=1}^{\infty}[\Lambda_1(z_2-z-\tilde{n},t)\\ &+ \Lambda_1(z_2-z+\tilde{n},t) - \Lambda_1(z_2+z+2(n-1)\mathcal{L},t) - \Lambda_1(z_2+z-2(n+1)\mathcal{L},t)\\ &- \Lambda_1(z_1-z-\tilde{n},t) - \Lambda_1(z_1-z+\tilde{n},t) + \Lambda_1(z_1+z+\tilde{n},t)\\ &+ \Lambda_1(z_1+z-\tilde{n},t)]\boldsymbol{\Lambda}_3(t)\boldsymbol{T}_{0,i}, \end{aligned} \tag{6.231}$$

$$\begin{aligned}\boldsymbol{T}_{\mathrm{inh,id,rect,G}}(z,t,\boldsymbol{C}_{\mathrm{inh}},z_1,z_2) &= \boldsymbol{T}_{\mathrm{inh,id,rect,La}}(z,t,\boldsymbol{C}_{\mathrm{inh}},z_1,z_2)\\ &- \boldsymbol{T}_{\mathrm{ic,id,rect,La}}(z,t,\mathbf{B}_{\mathrm{id}}^{-1}\boldsymbol{C}_{\mathrm{inh}},z_1,z_2) + \boldsymbol{T}_{\mathrm{ic,id,rect,G}}(z,t,\mathbf{B}_{\mathrm{id}}^{-1}\boldsymbol{C}_{\mathrm{inh}},z_1,z_2)\\ &- \frac{1}{4}\Gamma(t)\sum_{n=1}^{\infty}[-\boldsymbol{\Lambda}_2(-z_2+z+\tilde{n},t) + \boldsymbol{\Lambda}_2(z_2-z+\tilde{n},t)\\ &- \boldsymbol{\Lambda}_2(z_2+z+2(n-1)\mathcal{L},t) + \boldsymbol{\Lambda}_2(-z_2-z+2(n+1)\mathcal{L},t) + \boldsymbol{\Lambda}_2(-z_1+z+\tilde{n},t)\\ &- \boldsymbol{\Lambda}_2(z_1-z+\tilde{n},t) + \boldsymbol{\Lambda}_2(z_1+z+\tilde{n},t) - \boldsymbol{\Lambda}_2(-z_1-z+\tilde{n},t)]\mathbf{B}_{\mathrm{id}}^{-1}\boldsymbol{C}_{\mathrm{inh}}. \end{aligned} \tag{6.232}$$

For the solution via Green's functions in the Laplace domain, the results are given in equations (6.141), (6.142), and (6.145) and are extended by

$$\boldsymbol{T}_{\mathrm{ic,rect,GL}}(z,t,\boldsymbol{T}_0,z_1,z_2) = \frac{2}{\pi}\sum_{n=1}^{\infty} T_{\mathrm{rect,GL}}(z,z_1,z_2,n)\boldsymbol{x}_1(t,n,\boldsymbol{T}_0,\mathbf{0}), \tag{6.233}$$

$$\boldsymbol{T}_{\mathrm{inh,rect,GL}}(z,t,\boldsymbol{C}_{\mathrm{inh}},z_1,z_2) = \frac{2}{\pi}\sum_{n=1}^{\infty} T_{\mathrm{rect,GL}}(z,z_1,z_2,n)\boldsymbol{x}_1(t,n,\mathbf{0},\boldsymbol{C}_{\mathrm{inh}}), \tag{6.234}$$

$$T_{\mathrm{rect,GL}}(z,z_1,z_2,n) = \frac{1}{n}\sin(n_{\mathcal{L}}z)\left[\cos(n_{\mathcal{L}}z_1) - \cos(n_{\mathcal{L}}z_2)\right]. \tag{6.235}$$

6.3 Consideration of Nonlinear Behavior

In this section, the implicit parameter dependence on the temperature is considered. The overall problem from equations (6.1) and (6.2) can then be classified as a system of coupled nonlinear implicit second order (parabolic) PDEs. This implicit system behavior, which cannot be represented explicitly, also is a challenge for numerical solution approaches, since such dependencies are not allowed in most basic methods. In this section, exemplary strategies are discussed, which nevertheless allow consideration of this nonlinear dependence. Once again, this presentation does not claim to be complete but is intended to provide exemplary options.

The determination of the surface temperature is non-trivial due to the implicit dependence even if the conductor temperature distribution is known. Then, according to equation (6.2), a self-consistent problem has to be solved. The solution can be found numerically directly via a fixed-point iteration or via root-finding algorithms.

6.3.1 Fixed-Point Iteration

In a fixed-point iteration (see, e.g., [155, pp. 199-204]), a solution for the following problem is searched:

$$u = f(u). \tag{6.236}$$

The start is an initial solution u_0. Evaluation of the function $f(u_0) = u_1$ then gives the next approximate solution for the (attracting) fixed-point. This new solution is inserted into f again and so on. Thus, the iteration rule for the determination of the i-th approximate solution is

$$u_i = f(u_{i-1}). \tag{6.237}$$

6.3.2 Root-Finding Algorithms

The self-consistent problem (6.236) can directly be transformed into a root-finding problem:

$$f(u) - u = \tilde{f}(u) = 0. \tag{6.238}$$

A wide variety of methods can be used for numerical root finding, of which only two are shortly mentioned here as examples.

a) Bisection Method

With the bisection method (see e.g. [163, p. 379]) a root with sign change is searched. A starting interval $[u_1, u_2]$ is necessary, in which the root must be located. Then the signs of $\tilde{f}(u_1)$, $\tilde{f}(u_2)$, and $\tilde{f}\left(\frac{u_1+u_2}{2}\right)$ (interval center) are compared. The estimation interval is then adjusted so that the edge point with the same sign as in the interval center is replaced by the interval center. The estimation interval has thus been halved. This procedure is continued iteratively until predefined termination criteria are met.

b) Newton's Method

In Newton's method (see e.g. [155, p. 272]) the iteration rule is

$$u_i = u_{i-1} - \frac{\tilde{f}(u_{i-1})}{\tilde{f}'(u_{i-1})}. \tag{6.239}$$

So, based on the previous approximate solution, the new solution is determined using the derivative (in the multidimensional case the Jacobian matrix). The (analytical or numerical) determination of this derivative can be challenging and sometimes causes considerable effort [155, pp. 274-275]. Then it may be worthwhile to approximate it. For this purpose, a generalization of the scalar secant method for the approximation of the derivative is used in the so-called Quasi-Newton method [155, pp. 274-279].

6.3.3 Application of the Earlier Described Numerical Approaches

In principle, the numerical methods presented in sections 6.2.1 to 6.2.4 can also be used here. If both temporal and spatial discretizations are available, the following procedure can be used: First, the system of equations or the direct solution formula is set up for a time step j. Then the temperature calculation for this time step is performed. The corresponding surface temperature is then determined via a fixed-point iteration or root-finding algorithm. This is used to determine the parameters $\tilde{\boldsymbol{C}}(\boldsymbol{T}(z,t), \boldsymbol{T}_\mathrm{s}(z,t), z, t)$ and $\mathbf{B}(\boldsymbol{T}_\mathrm{s}(z,t))$. These (spatially variable) parameters are the basis for the calculation of the next time step $j+1$. This approach can be used to take into account distributed implicit parameter dependencies along the cable only if there is a spatial discretization in that direction. The application of BEM is not possible here (setting up the appropriate Green's function for the overall problem is already problematic there). However, FEM, FDM, and FVM allow this procedure. Thus, an overall approach for temperature determination can be built up by superimposing several numerical methods.

6.3.4 Approximation Based on the Linear Approaches

Alternatively, an approach is presented in the following, which is based on the previous solutions for the linear case. Here, the solution is calculated individually for each combination of location and time (z,t) using the analytical relationships. A fixed-point iteration is then performed for each (z,t) individually to adjust the parameter values and the surface temperature, as shown in figure 6.21. All conductor temperature calculations are performed via the analytical solutions.

After a first initial temperature guess together with typical parameter values, the cable surface temperature is calculated. In the next step, the critical cable parameters (conductance for convection and radiation as well as the electrical losses) are recalculated followed by the conductor temperature calculation. After this first iteration, the second iteration starts again

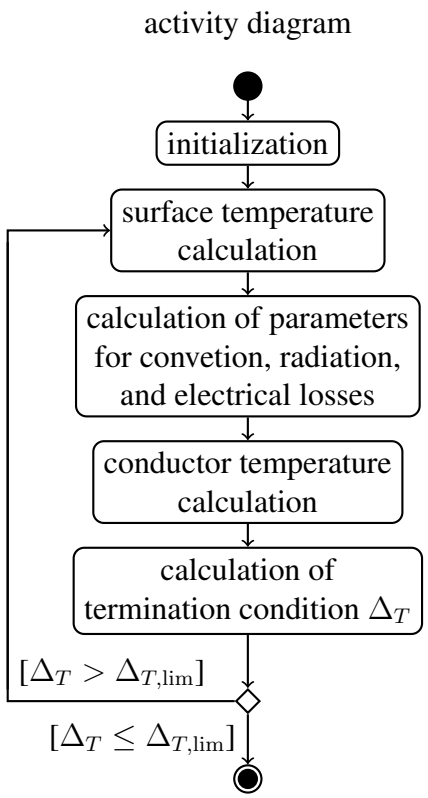

pseudocode	steps
initialize: $T_{i=0}$, $G'_{i=0}$;	step 0
$T_{\mathrm{s},i+1} = f(T_i, G'_i)$;	step 1
$G'_{i+1} = G'(T_{\mathrm{s},i+1})$; $P'_{\mathrm{el},i+1} = P'_{\mathrm{el}}(T_i)$; $B_{i+1} = R'G'_{i+1}$; $C_{i+1} = -R'\left(P'_{\mathrm{el},i+1} + G'_{i+1}T_{\mathrm{e}}\right)$;	step 2
$T_{i+1} = T(B_{i+1}, C_{i+1})$;	step 3
$\Delta_T = \lvert T_i - T_{i+1} \rvert$;	step 4
if $\Delta_T > \Delta_{T,\mathrm{lim}}$: go to step 1;	step 5

Figure 6.21: Iteration scheme to include nonlinear parameters, activity diagram, and pseudocode.

with the surface temperature calculation. As a stopping criterion, after each iteration $i + 1$, the difference Δ_T between the new and old conductor temperatures T is calculated:

$$\Delta_T = \left| T_i - T_{i+1} \right| . \tag{6.240}$$

This value is compared to a predefined value $\Delta_{T,\mathrm{lim}}$ to decide whether to stop the iteration or continue with a new round. In [A.3], $\Delta_{T,\mathrm{lim}} = 0.001\,\mathrm{K}$ is used to show the convergence behavior (six to seven iterations were necessary), although in real applications, normally such high precision is not required. Also, the necessary approximations in the models typically already cause higher temperature deviations.

By this procedure, a different PDE is gradually solved for each point (z, t) due to the different parameters. In particular, for the temperature calculation at each point, it is implicitly assumed that the used parameter values are valid for all times and places. To a certain extent, the direct coupling between the neighboring points is thus broken, and each combination (z, t) stands independently. In section 7.3.1.a), it is investigated how this approximation affects the temperature results. This approach provides a semi-analytical procedure that allows the analytical solutions to be used for temperature estimations with occurring nonlinearity. Due to the very fast convergence of the fixed-point iteration, other methods, such as Newton's

method, which is more complex but converges faster, are not considered further here.

In the further course of the thesis, the analytical solutions are always combined with the fixed-point iteration, if not mentioned differently. Exemplary MATLAB implementations of the complete solution approach for the single wire cable with constant excitations and the solution via Green's functions in the Laplace domain for a cable arrangement consisting of three not identical cables with constant excitations are given in appendix C.

7 Validation

In this section, the previously derived analytical solutions are validated. At first, the chosen numerical reference solutions are shortly resumed and the temperature measurement methods are presented. Then, the validations for the different cable arrangements follow.

7.1 Numerical Reference Solutions

7.1.1 Direct Solution of the Partial Differential Equations

As already discussed in sections 6.2 and 6.3, the PDEs can also be solved numerically. In the following, the methods that are used in the rest of this thesis are shortly presented.

a) Euler Method

The Euler method, see also section 6.2.1.a), is a very simple numerical approach. For the consideration of the implicit nonlinear temperature dependency, the approach from section 6.3.3 is used here, which means the iterative parameter adaption based on the known temperature as preparation for the next time step calculation. In the following, this basic approach is used for the complexity analysis of the single wire cable.

b) MATLAB “pdepe”

For the solution of the coupled PDEs, the function “pdepe” from MATLAB can directly be used, which solves systems of parabolic and elliptic PDEs by integrating the ODEs that are found from the PDEs via space discretization [164]. This basic approach was earlier discussed in section 6.2.1.c). Exemplarily, for the single wire cable, the corresponding formulation for the implementation in MATLAB is analog to equations (6.1) and (6.4):

$$A_{\mathrm{sw}} \frac{\partial T_{\mathrm{sw}}(z,t)}{\partial t} = \frac{\partial^2 T_{\mathrm{sw}}(z,t)}{\partial z^2} - B_{\mathrm{sw}} T_{\mathrm{sw}}(z,t) - C_{\mathrm{sw}}, \tag{7.1}$$

$$0 = T_{\mathrm{sw}} - T_{\mathrm{s}} - R'_{\mathrm{i}} G' (T_{\mathrm{sw}} - T_{\mathrm{e}}). \tag{7.2}$$

7.1.2 Equivalent Circuit Diagrams with Lumped Elements and Solution via Simscape

In [165], the thermal ECDs for the radial heat flow in cable segments of finite length are cascaded in the axial direction to find an axial transient thermal cable model. The complete ECD is implemented in MATLAB Simulink/Simscape and validated using measurements in [165]. This approach can be used for different cable arrangements based on the known ECDs for an infinitesimally short cable segment.

7.1.3 COMSOL Multiphysics

Using the FEM-based software COMSOL Multiphysics [166] (see also section 6.2.2), a numerical solution to the heat transfer problem in cables can be found that is completely independent of the ECD approach (and the necessary assumptions). For a single wire cable, rotational symmetry considerations allow for the analysis of only a 2 D cut of the complete 3 D model for a single wire cable, which drastically reduces the calculation effort.

7.2 Temperature Measurement in Transmission Lines

For temperature measurement, many different approaches can be used depending on the application (see for example [51, 167]). In this section, two approaches that are used for validation in the following are briefly presented. The same two approaches were also discussed in [A.7] and [A.9].

7.2.1 Indirect Temperature Measurement

The electrical cable resistance R_{cable} depends on the cable conductor temperature T. For small temperature rises, a linear dependence can be observed [142, p. 99] as already used for the calculation of the electrical losses (see equation (5.69)):

$$R_{\mathrm{cable}} = R_{\mathrm{ref}} \left(1 + \eta_T \left(T - T_{\mathrm{ref}}\right)\right). \tag{7.3}$$

The linear temperature dependence of the resistance is a good approximation over a large temperature range (nearly up to the melting temperature) for metals that are not magnetic [168, pp. 128-130]. Thus, this dependence is used in the following and its error is neglected. Based on a known reference resistance R_{ref} at a defined reference temperature T_{ref}, the cable resistance can be approximated for other temperatures. For copper, the linear temperature coefficient η_T at $T_{\mathrm{ref}} = 20\,^{\circ}\mathrm{C}$ is $3.93 \cdot 10^{-3}\,1/\mathrm{K}$ according to [169]. In this thesis, this temperature coefficient is also used for other reference temperatures of the same magnitude. This linear dependence is used to calculate the cable temperature from a cable resistance measurement as also proposed in [170]:

$$T = T_{\mathrm{ref}} + \frac{1}{\eta_T}\left(\frac{R_{\mathrm{cable}}}{R_{\mathrm{ref}}} - 1\right). \tag{7.4}$$

For the measurement of the cable resistance, a small measurement current I_{meas} is injected into the cable. This measurement current has to be chosen small enough to not relevantly change the cable temperature, but, on the other hand, to cause a measurable voltage drop along the cable. In this thesis, typically, the measurement current $I_{\mathrm{meas}} = 0.12\,\mathrm{A}$ is chosen. Then, the voltage drop between two positions along the cable (distance $\mathcal{L}_{\mathrm{meas}}$) is measured, which allows the calculation of the resistance along this section. To avoid additional voltage drops across the voltage measurement contacts, the measurement current is not directly in-

jected via the voltage contacts but at the cable ends (four-terminal sensing). So, the distance between those current injection points is the complete cable length, $\mathcal{L}$. Both, impressing the measurement current and measuring the corresponding (typically very low) voltage can be performed by appropriate **s**ource **m**easurement **u**nits (SMUs). An overview of the general measurement setup is given in figure 7.1.

From the measured cable resistance R_{cable}, the cable temperature T is calculated via equation (7.4). The result is the mean temperature across the section for the voltage measurement. That is why this method is especially applicable for the measurement of the cable temperature across a section along which a constant temperature is expected, for example in the middle of a long cable under homogeneous environmental conditions. The measurement of axial temperature profiles using this method leads to problems. Very low voltage drops result when using short sections for the voltage measurement. In addition, the connections for the voltage measurement distort the cable temperature: As the insulation has to be removed there and additional thermal bridges are added to the system, the cable temperature will be slightly lower locally around the connections. If many connections are close to each other, this effect gains importance and cannot be neglected. To sum up, this method is more feasible for the measurement across a (longer) cable section with a constant temperature.

For the temperature calculation, in addition to the continuously recorded quantities and the linear temperature coefficient of the conductor material, the reference resistance of the cable at a known reference temperature is required. Therefore, a reference measurement is always performed before the actual temperature measurement in this thesis. There, the cable resistance is measured without a load current. The ambient temperature is recorded separately. It is assumed that the cable temperature during the reference measurement equals this ambient temperature. Accordingly, the cable must be stored for a sufficiently long time without a load in the corresponding environment, so its temperature equals the ambient temperature.

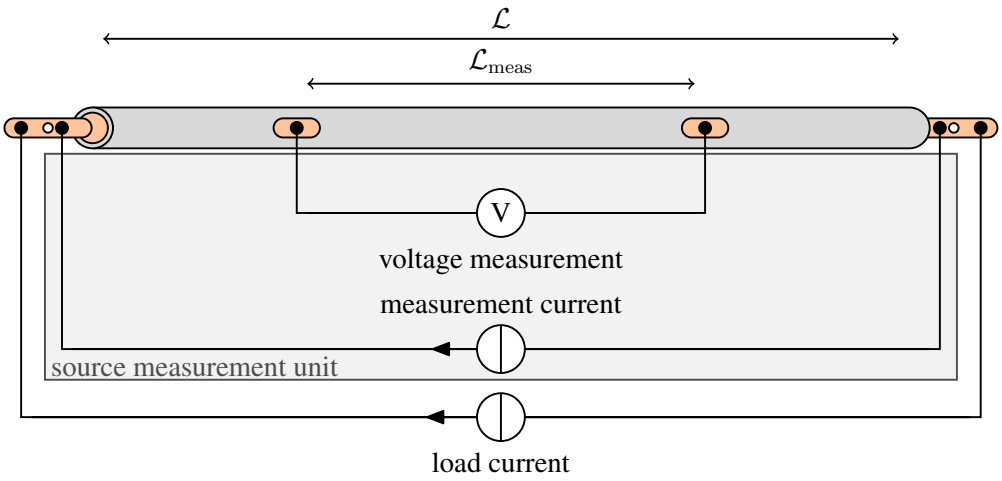

Figure 7.1: Scheme for the measurement setup.

a) Single Measurement

If a load current I heats the cable, the additional (small) measurement current I_{meas} is not necessary. On the other hand, this measuring current hardly changes the occurring temperatures and is also required for the voltage measurement without a load current. Therefore, in this thesis, indirect temperature measurements are always performed with an additional measurement current that is injected via the SMU. If, for example, the load current is switched off during the measurement, the measured voltage drops abruptly but does not drop to zero. If the measurement and load currents are known, the associated temperature curve can be calculated. An example of this procedure is shown in figure 7.2.

To analyze the uncertainties of the measurement results, an exemplary twisted pair cable is used[9]. The parameters of the individual cables are given in table D.1, cable (1). The twisted pair cable is loaded with $10\,\mathrm{A}$ on one of the two cables.

In principle, the uncertainty limit Δ_f for a quantity f calculated from quantities u_1 and u_2 with known maximal uncertainties Δ_{u_1} and Δ_{u_2} can be expressed as

$$\Delta_f = \left|\frac{\partial f}{\partial u_1}\right| \Delta_{u_1} + \left|\frac{\partial f}{\partial u_2}\right| \Delta_{u_2} \tag{7.5}$$

in accordance with the uncertainty estimations for resistance measurement in [171] and inspired by [167, p. 60] as well as appendix D of [172]. Based on this, the uncertainty limits of the temperature are calculated. The individual quantities that are used in the temperature calculation with the respective ranges of the uncertainty limits are also shown in figure 7.2. The cable is loaded with the load current $I + \Delta_I$ with

$$\Delta_I = 0.2\,\% \cdot 120\,\mathrm{A} = 0.24\,\mathrm{A} \tag{7.6}$$

according to [173]. For the case without load current, it is assumed here that no current flows, so $I \pm \Delta_I = 0\,\mathrm{A}$. In addition, the measurement current $I_{\mathrm{meas}} \pm \Delta_{I_{\mathrm{meas}}} = 0.12\,\mathrm{A} \pm \Delta_{I_{\mathrm{meas}}}$ with

$$\Delta_{I_{\mathrm{meas}}} = 0.03\,\% \cdot I_{\mathrm{meas}} + 1.5\,\mathrm{mA} \tag{7.7}$$

according to [171] flows in the cable. The corresponding total current is $I_{\mathrm{t}} = I + I_{\mathrm{meas}}$ with the uncertainty limit

$$\Delta_{I_{\mathrm{t}}} = \Delta_I + \Delta_{I_{\mathrm{meas}}}. \tag{7.8}$$

The voltage drop that is measured between the two voltage connections is $U \pm \Delta_U$ with

$$\Delta_U = 0.02\,\% \cdot U + 350\,\mu\mathrm{V} \tag{7.9}$$

according to [171]. From the total current and the measured voltage drop, the electrical re-

[9] The measurements were performed by student assistant Julian Hohmann.

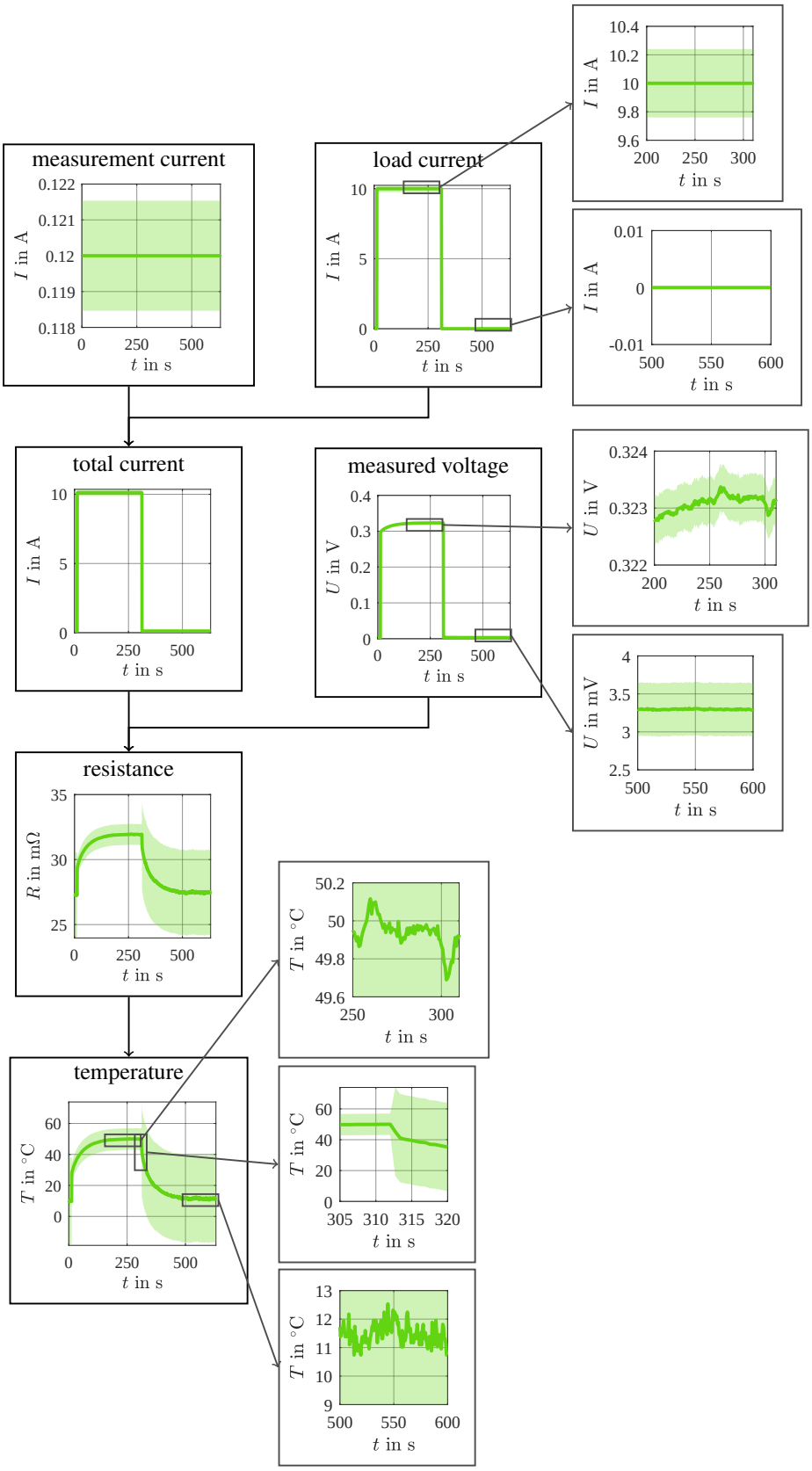

Figure 7.2: Cable temperature determination from the measured quantities using a single voltage measurement for each temperature calculation. The uncertainty limits are indicated transparently.

sistance between the voltage connections is calculated according to

$$R_{\mathrm{cable}} = \frac{U}{I_{\mathrm{t}}}. \tag{7.10}$$

The associated uncertainty limit is

$$\Delta_{R_{\mathrm{cable}}} = \left|\frac{1}{I_{\mathrm{t}}}\right| \Delta_U + \left|\frac{U}{I_{\mathrm{t}}^2}\right| \Delta_{I_{\mathrm{t}}}. \tag{7.11}$$

In the last step, the cable temperature is calculated according to equation (7.4) with the uncertainty limit

$$\Delta_T = \frac{1}{\eta_T R_{\mathrm{ref}}} \Delta_{R_{\mathrm{cable}}} + \frac{R_{\mathrm{cable}}}{\eta_T R_{\mathrm{ref}}^2} \Delta_{R_{\mathrm{ref}}} + \Delta_{T_{\mathrm{ref}}}. \tag{7.12}$$

Here, it is assumed that the linear temperature coefficient of the conductor material is exact: $\Delta_{\eta_T} = 0$. The reference temperature T_{ref} and the reference resistance R_{ref} are determined via a reference measurement before the actual temperature measurement as already mentioned above. Both quantities are recorded several times (in this example 15 times) and the mean value is used as the measured value. The associated uncertainty limits are calculated from the individually measured values $R_{\mathrm{ref},i}$ and $T_{\mathrm{ref},i}$, respectively, according to section 5.4.2 of [172] with the coverage factor 2:

$$\Delta_{R_{\mathrm{ref}}} = 2 \cdot \sqrt{\frac{1}{15 \cdot (15-1)} \sum_{i=1}^{15} \left(R_{\mathrm{ref},i} - R_{\mathrm{ref}}\right)^2} = 1.7 \, \frac{\mu\Omega}{\mathrm{m}}, \tag{7.13}$$

$$\Delta_{T_{\mathrm{ref}}} = 2 \cdot \sqrt{\frac{1}{15 \cdot (15-1)} \sum_{i=1}^{15} \left(T_{\mathrm{ref},i} - T_{\mathrm{ref}}\right)^2} = 1.2 \cdot 10^{-3} \, \mathrm{K}. \tag{7.14}$$

Overall, very large uncertainty limits are shown for the temperature. The observed measurement noise is much smaller. The large limits are primarily caused by the offset error of the voltage measurement, which depends on variables such as ambient temperature and humidity but is almost constant during measurement. In the case of a load current, the voltage that has to be measured is comparatively large, so this offset error plays almost no role here. In the case without load current, on the other hand, only the small measurement current flows, so the voltage drop is also very small. Here, the offset error plays a much greater role. This can also be seen from the fact that the specific temperature curve shows unphysical jumps at the times when the load current is switched on and off. The noise influence also becomes greater when the load current is switched off. This is because although the load current is associated with a comparatively high error margin, this offset hardly varies during a measurement. An additional source of error can occur here if the load current has to be measured. Then, on the one hand, the synchronization accuracy between current and voltage

measurement and, on the other hand, the accuracy of the current measurement itself plays a role. Overall, it can be stated that this simple measurement approach is not suitable for temperature detection at small or vanishing load currents, in particular, due to the offset error of the voltage measurement. To reduce this error, a suitable calibration has to be performed in advance.

b) Differential Measurement Approach

An alternative to calibration for the elimination of the voltage measurement offset error is the use of a differential measurement approach, which was originally proposed in [174]. In this approach, only the voltage drop that directly follows from the measurement current is evaluated. That is why the corresponding voltages for negative and positive measurement currents are compared. As it is not possible to measure both of those voltages at the same time and due to the changing cable temperature, three voltage measurements are performed as shown in figure 7.3: From the first and third measurements, which use the negative measurement current, an estimation for the voltage drop in the middle between those measurements is calculated using linear interpolation. At this central time, the voltage drop is measured using the positive measurement current. By evaluating the difference between the voltages for positive and negative measurement current and referring it to the measurement currents, the cable resistance is calculated independently from the load current:

$$R_{\text{cable}} = \frac{2U_2 - U_1 - U_3}{2I_2 - I_1 - I_3} = \frac{2U_2 - U_1 - U_3}{4I_{\text{meas}}}. \tag{7.15}$$

The temperature determination via this procedure is shown together with the associated uncertainty limits in figure 7.4. For the individual measurement currents and measured voltages, the offset error plays a role as in the previous section. This offset can be easily recognized by the differences in the absolutes of the measured voltages with positive and negative measurement current ($3.8\,\text{mV}$ vs. $3.3\,\text{mV}$). However, since this offset is almost constant during

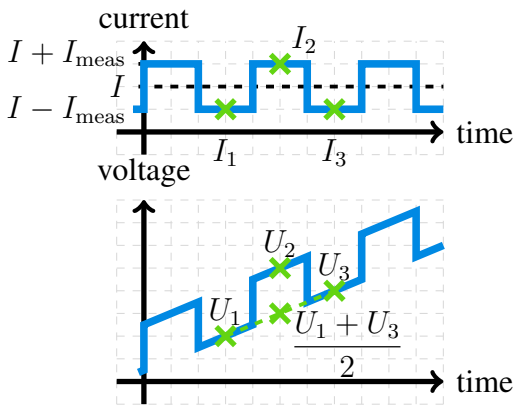

Figure 7.3: Three-point measurement to eliminate load current dependence.

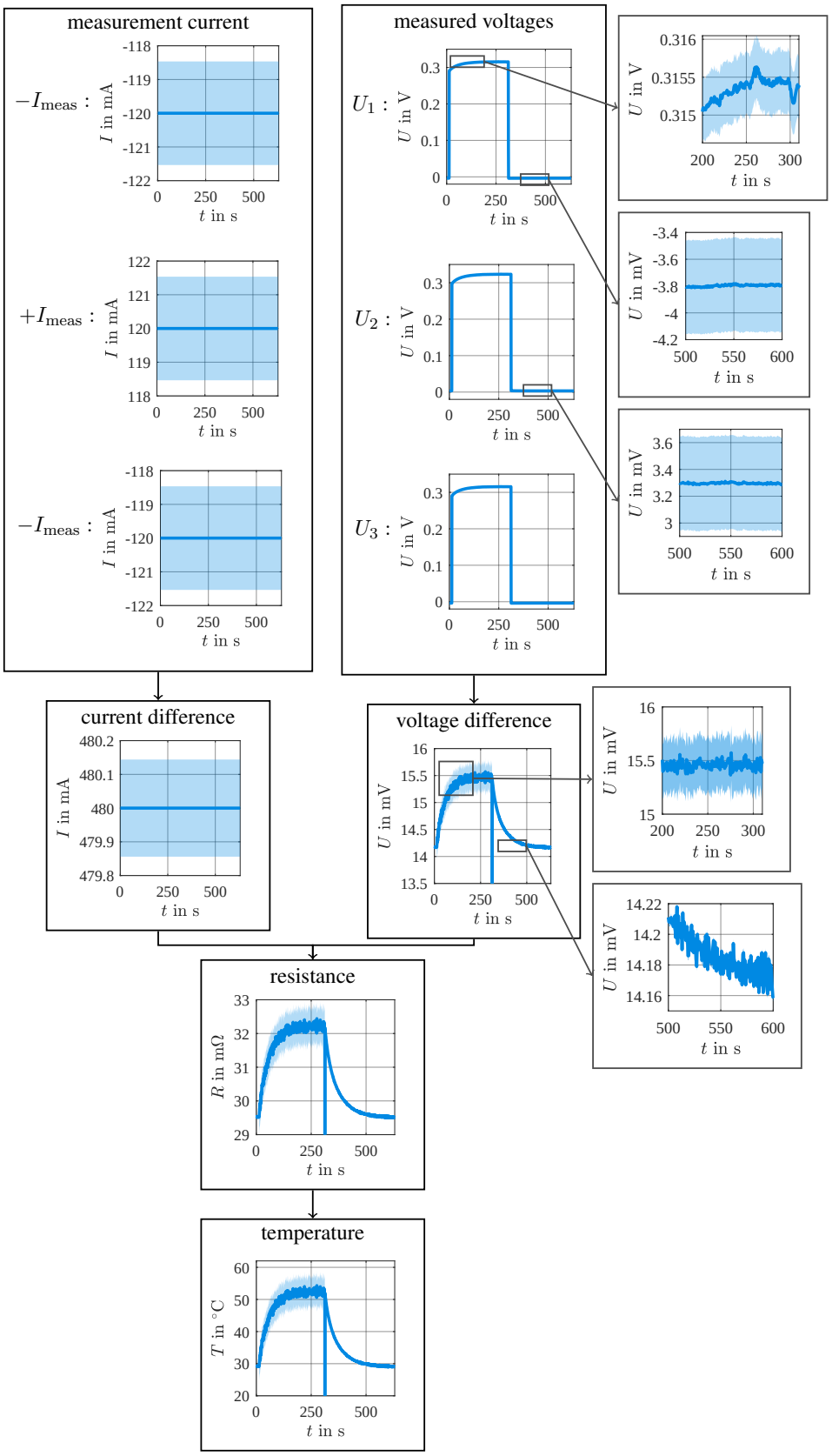

Figure 7.4: Cable temperature determination from the measured quantities using three voltage measurements for each temperature calculation. The uncertainty limits are indicated transparently.

measurement, it is eliminated by the difference calculation. For the case with load current, however, the voltage difference is now in a different order of magnitude than the originally measured voltage ($15.5\,\mathrm{mV}$ vs. $0.3\,\mathrm{V}$). The relative error is thus amplified, resulting in more noisy data. Overall, with the load current turned on, the determined temperature is much noisier than before. In the case of cooling, the error is considerably smaller and the unphysical jumps no longer occur. Only at the moment of load current switching off, a single outlier appears: If the load current is switched off between the three related measurements, the voltage curve can no longer be described by the assumed linear approximation and the current values do not satisfy the assumptions. Accordingly, this one measured value is incorrect and cannot be used.

The direct comparison between the results of both measurement variants is shown in figure 7.5. Overall, the differential measurement shows noisier data with somewhat lower uncertainty limits for the case with load current, but the case without load current is recorded much better. Therefore, this approach will always be used in the further course of this thesis.

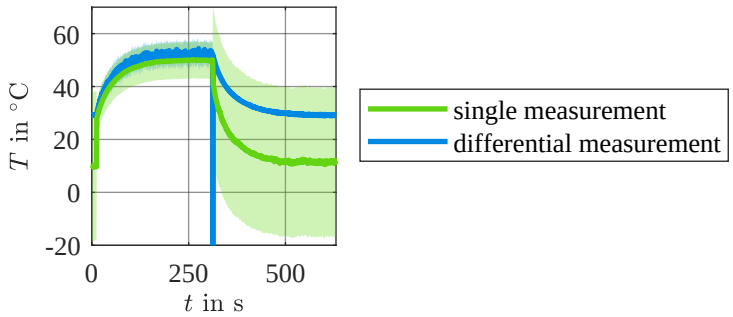

Figure 7.5: Temperatures and uncertainty limits for both measurement approaches.

c) Post-Processing

The temperature data originally collected from the measurement are post-processed in three steps. These are presented in the following. In the first step, the time axis is adjusted so that at the time $t = 0\,\mathrm{s}$ the current is switched on. In the second step, the outliers are corrected, which were already mentioned above and resulted from changes in the load current during the three related measurements. For this purpose, those points i are searched where $|T_i - T_{i+1}| > 5\,\mathrm{K}$. The temperature value at location $i + 1$ is then replaced by the average of the two surrounding values T_i and T_{i+2}. Because of the very noisy measured values due to the different magnitudes of the measured voltages and the differential voltages with load current, filtering is necessary. In principle, different approaches such as low-pass filtering or moving average filters [175] can be used here. In this thesis, moving average filters over 41 points (symmetrically less towards the edges) are always used. In order not to falsify the kink in the temperature when the load current is switched off, an edge is also set here for the filtering. An overview of the individual steps with exemplary curves is shown in figure 7.6.

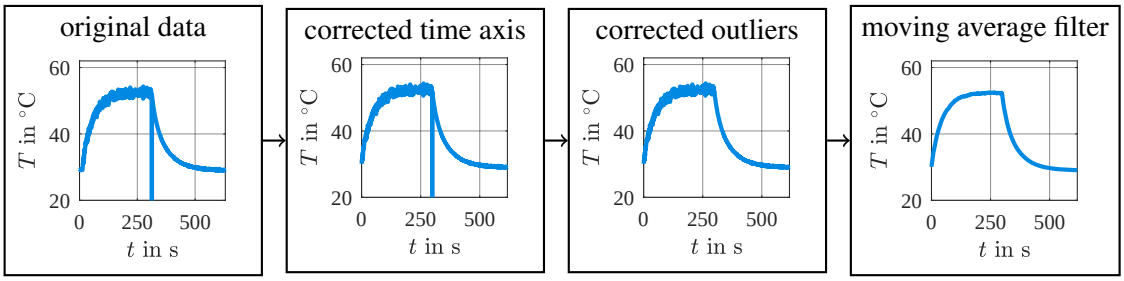

Figure 7.6: Post-processing of the measured temperature data.

d) Other Errors

Up to now, mainly the direct influence of the measurement technology on the measured cable temperatures has been investigated. This caused a deviation between the measured temperatures and the temperatures that actually occur. In addition, other errors can arise due to the non-ideal use of the measurement technology: For example, suboptimal contacts can cause highly noisy measurement data or systematically too high measured voltages, or cable breaks in the connections can make measurement impossible. These deviations caused by incorrect handling must therefore be avoided.

In addition, the inner conductor temperatures can differ from the temperatures occurring in the ideally laid cable without measurement equipment due to different influences. For the contacts for the voltage measurements, the cable is locally damaged as the insulation is removed and thermal bridges are introduced. Thus, the cable temperature locally drops. However, the influence of this decrease on the measured temperature is negligible, because in this thesis always sufficiently long cable sections are provided between the voltage connections, so the average cable temperature is only minimally influenced by the local changes. In principle, there are also influences at the current insertion points, where additional heat sources are generated in case of poor contact. However, since the voltage measurement is performed comparatively far away from this, these errors are also not relevant. The real setup differs from an installation purely in the air. On the one hand, additional elements appear near the cable due to the measurement equipment, and on the other hand, the cable is set up at a height of about $15\,\mathrm{cm}$ to $30\,\mathrm{cm}$ above a tabletop. Both effects restrict free convection, but this effect is so small that it hardly causes any distortion of the measured data. The occurrence of additional airflow in the laboratory that has not been recorded or taken into account is more critical. Then, in addition to the considered free convection, forced convection occurs, which cannot be reproduced. The influence caused by this additional heat dissipation cannot be directly measured and thus quantified, but it is estimated to be a few Kelvin. As an alternative to laying the cables freely in the laboratory with the associated possible forced convection, the measuring box from [174] is available for the measurements, in which the cables can be placed. The measurement equipment is then connected through small openings. This significantly reduces the forced convection, but the free convection is even more

restricted than before and the ambient air in the measurement box heats up more due to the hot cable than in the overall laboratory without a box. Overall, similar temperature changes are expected as in the case without a measurement box, but these cannot be quantified here either. In this thesis, both approaches, i.e. placing the cable freely in the air and placing the cable in the measurement box, are used. Overall, the expected temperature deviations due to the additional mentioned effects are below the uncertainty limits caused by the measurement equipment.

e) Exemplary Study on Reproducibility

To analyze the reproducibility of the measurement results between repeated measurements, several measurements are performed using the exemplary twisted pair cable from section 7.2.1.a) again. This time, the twisted pair cable is loaded with $5\,\mathrm{A}$, $7.5\,\mathrm{A}$, and $10\,\mathrm{A}$, on one or both cables. The different measurements[10] are summed up in table D.2. The steady-state temperature is calculated via averaging over a period of $60\,\mathrm{s}$ in the flat temperature range. To exclude slightly different ambient conditions, the difference between the measured temperatures and the mean value of the steady-state ambient temperature is evaluated. As an example, in figure 7.7 the curves for (a) the loaded (case 1) and (b) the unloaded (case 4) cable at a current of $10\,\mathrm{A}$ in one conductor are shown. It can be observed from this figure that the measured temperatures can vary even after correction with the ambient temperature. In the next step, the deviation of the steady-state temperatures obtained for the different load cases (corrected with the mean value of the ambient temperature for the steady state) from the mean value of this quantity is shown first as an absolute value (in Kelvin)

$$\Delta T_{\mathrm{abs}} = T_{\mathrm{stst}} - T_{\mathrm{e}} - \mathrm{mean}(T_{\mathrm{stst}} - T_{\mathrm{e}}) \tag{7.16}$$

and then also relative to the mean value

$$\Delta T_{\mathrm{rel}} = \left| \frac{T_{\mathrm{stst}} - T_{\mathrm{e}} - \mathrm{mean}(T_{\mathrm{stst}} - T_{\mathrm{e}})}{\mathrm{mean}(T_{\mathrm{stst}} - T_{\mathrm{e}})} \right| . \tag{7.17}$$

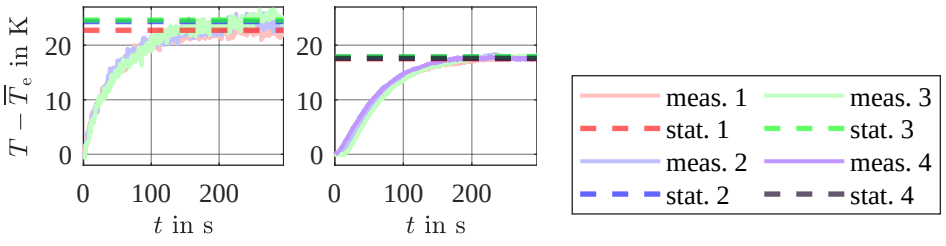

(a) (b)

Figure 7.7: Comparison between several measurements with current $10\,\mathrm{A}$. Measurement of (a) loaded cable (case 1) and (b) unloaded cable (case 4).

[10]The measurements were performed by student assistant Julian Hohmann.

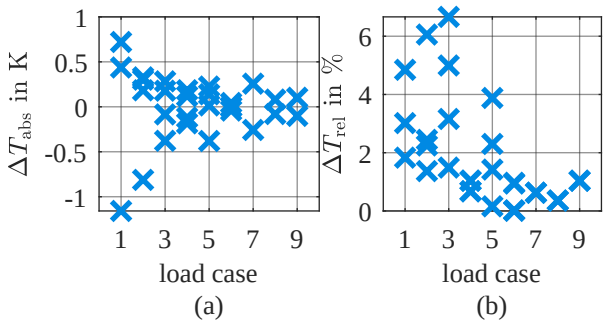

Figure 7.8: Comparison between several measurements for different load cases. (a) Absolute and (b) relative deviation from the mean value.

The results are presented in figure 7.8. In nearly all investigated cases the temperature differences are within $\pm 1\,\mathrm{K}$, only in a single loading case do higher deviations occur. In relative terms, this is equivalent to a maximum of $7\,\%$. These deviations must be kept in mind, especially if statements about the general behavior and the required parameters are determined from individual measurements: The measurement results presented in the further course of this thesis are therefore not exact, but can show deviations of up to a few Kelvin.

7.2.2 Thermocouple Temperature Measurement

For the measurement of the axial cable temperature distribution, often thermocouples can be used. Those consist of two metallic wires of different materials that are connected at one side (hot junction) [142, p. 631]. Then, at the other wire ends (cold junction), a voltage drop between those two wires appears that depends on the temperature difference between the connected and the unconnected wire ends due to the Seebeck effect [176, 177]. Different metal combinations can be used for this purpose. In this thesis, type K thermocouples are chosen, which consist of Chromel and Alumel [178]. They are widely spread due to the nearly linear temperature dependence of the thermocouple voltage (about $40\,\mu\mathrm{V/K}$) and the wide application range ($-200\,^{\circ}\mathrm{C}$ to $1260\,^{\circ}\mathrm{C}$) [176, pp. 92-96] in combination with low costs.

For the evaluation of the thermocouple voltage and the conversion to a temperature, different boards and instruments are available. Typically, an amplification of the relatively low thermocouple voltages is used in combination with a compensation of the cold junction temperature. To protect the sensitive electronics from damage and ensure the designed behavior, the thermocouples themselves have to be installed electrically insulated from the cable potential and the potentially high currents. This can for example be achieved by using Kapton tape, which is electrically insulating but thermally comparatively conductive.

To measure the local cable temperature, the thermocouple has to be connected thermally to the conductor. The temperature at the hot junction has to be as close as possible to the searched conductor temperature, so the measured temperature directly depends on the quality of the thermal connection between the cable and the thermocouple, which has by far the most important influence on the accuracy of the measured temperature in most cases. In ad-

dition, the thermocouple itself influences the measured temperature: As a thermal connection between the conductor and the thermocouple is necessary, the thermocouple leads away heat from the conductor itself and therefore influences the measurement, especially for very thin cables. This effect is studied in section 7.3.2. Other uncertainties coming from the measurement equipment as the amplifier or the voltage reading are not further evaluated here, as their influence on the overall measured temperature is negligible compared to the earlier described effects. Nevertheless, overall, the accuracy of the thermocouple temperature measurement is assumed to be worse than for the indirect temperature due to the retroactive effect and the highly sensible dependence on the thermal contact quality.

7.3 Validation of the Analytical Solutions

In this section, the analytical solutions for selected different cable arrangements are validated and analyzed using copper cables with **p**oly**v**inyl **c**hloride (PVC) insulation. For the copper conductors, the specific heat capacity per volume $c_\mathrm{c} = 3.4 \cdot 10^6\,\mathrm{J/(Km^3)}$, the thermal conductivity $\lambda_\mathrm{c} = 386\,\mathrm{W/(Km)}$, and the linear temperature coefficient $\eta_T = 3.93 \cdot 10^{-3}\,1/\mathrm{K}$ are used. For the PVC insulation layer, the specific heat capacity per volume $c_\mathrm{i} = 2.245 \cdot 10^6\,\mathrm{J/(Km^3)}$ and the thermal conductivity $\lambda_\mathrm{i} = 0.21\,\mathrm{W/(Km)}$ are assumed.

7.3.1 Single Wire Cable

At first, the solutions for a single wire cable are analyzed. After a comparison of the analytical solution with the numerical solution and measurement results, the convergence behavior of the Green's functions solutions and the influence of the cable length are analyzed followed by a complexity analysis of the presented solutions.

a) Analytical Solutions vs. Numerical Reference Solutions

In this section, the analytical methods are validated via comparison with numerical reference solutions for a $6\,\mathrm{mm^2}$ single wire copper cable (conductor radius $r_\mathrm{c} \approx 1.4\,\mathrm{mm}$, resistivity $\rho = 1.86 \cdot 10^{-8}\,\Omega\mathrm{m}$ at $20\,^\circ\mathrm{C}$, length $\mathcal{L} = 1\,\mathrm{m}$). The insulation (outer radius $r_\mathrm{i} = 2\,\mathrm{mm}$) consists of PVC. At $t = 0\,\mathrm{s}$, a constant current of $70\,\mathrm{A}$ is switched on at $t = 0\,\mathrm{s}$. The ambient air temperature T_e and the initial cable temperature T_0 are $15\,^\circ\mathrm{C}$. One cable termination is fixed at the temperature $T_1 = 10\,^\circ\mathrm{C}$, the other termination has the temperature $T_2 = 50\,^\circ\mathrm{C}$.

For this cable, the transient axial temperature distribution is calculated using three numerical solutions (MATLAB function "pdepe", see section 7.1.1.b); Simscape, see section 7.1.2 and COMSOL, see section 7.1.3) and the presented analytical solutions (see sections 6.1.1.c) and 6.1.2). For the solution via Green's functions in the time domain, $n_\mathrm{max} = 1$ is used as the upper limit of the sum, for the solution via Green's functions in the Laplace domain, $n_\mathrm{max,ic,inh} = 10$ is used as the upper limit for the parts resulting from the initial conditions and the inhomogeneity, $n_\mathrm{max,bc} = 2000$ is used for the part from the boundary conditions. In section 7.3.1.c), the convergence behavior of those two solutions is analyzed.

In figure 7.9, the results for the calculated temperature along the cable at $t = 1000\,\mathrm{s}$ and the time-dependent conductor temperature in the central cable section are shown. All results fit well together. That is why in the next step, the absolute differences between the calculated temperatures and the solution via COMSOL are evaluated as presented in figure 7.10. For all solutions, maximum deviations of about $2.5\,\mathrm{K}$ are the result. Only for the semi-infinite solution, as expected, on the second half of the cable, much higher deviations appear because there, the corresponding second boundary condition is not considered.

In the derivation of the solutions for the implicitly nonlinear PDE (5.51), a two-step procedure was used: First, the linearized form of the differential equation was solved (see section 6.1.2). In the second step, the temperature dependence of the parameters P'_{el} and G' (in the

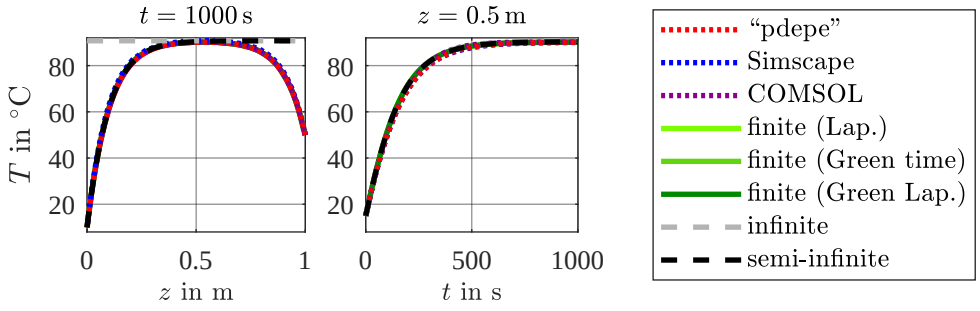

(a) (b)

Figure 7.9: (a) Axial cable temperature distribution in the steady state and (b) transient temperature development in the central cable section. Most of the data in this plot were already published in [A.3].

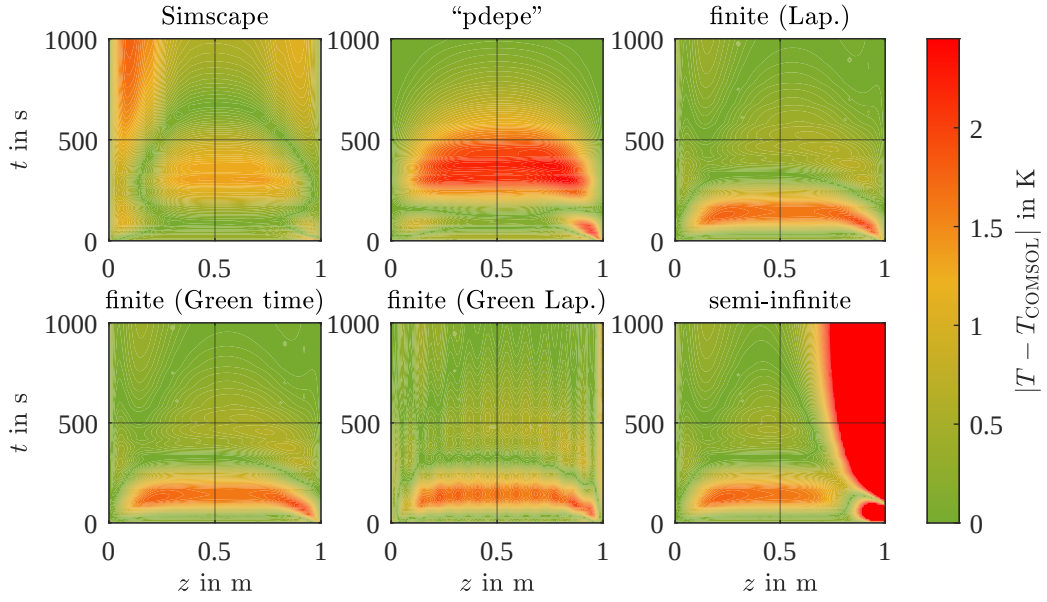

Figure 7.10: Absolute differences between temperatures calculated with COMSOL and the other numerical and analytical solutions, respectively. Most of the data in this plot were already published in [A.3].

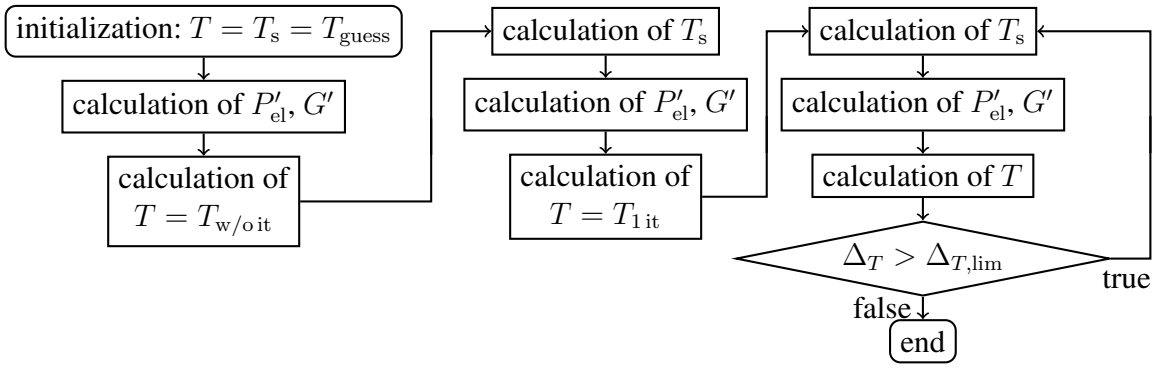

Figure 7.11: Procedure for the analysis of the influence of the iterations.

elements B_sw and C_sw of the PDE) was taken into account by applying a superimposed fixed point iteration (see section 6.3.4). This adds a numerical part to the purely analytical solution, which increases the computational effort. Therefore, the influence of this iteration is now analyzed. For this purpose, the procedure shown in figure 7.11 is used: The cable and surface temperatures T and T_s are first initialized with an estimated temperature T_guess. This is used to calculate the parameters P'_el and G' and then the conductor temperature T. Thus, this temperature $T_\mathrm{w/o\,it}$ represents the result without iteration. Then the first iteration follows: The surface temperature is calculated. Based on this, the recalculation of the parameters and the conductor temperature after one iteration, $T_\mathrm{1\,it}$, follows. Besides the calculated temperature without iteration and after one iteration, the temperature after convergence of the fixed-point iteration with $\Delta_{T,\mathrm{lim}} = 0.001\,\mathrm{K}$ is determined. For comparison, the solution of the PDE is also calculated using the MATLAB function “pdepe”.

In the following, the $6\,\mathrm{mm}^2$ copper cable from above is again analyzed. For the ambient, initial, and termination temperatures, $T_\mathrm{e} = T_0 = T_1 = T_2 = 60\,^\circ\mathrm{C}$ is assumed. For the currents $I = 15\,\mathrm{A}$ and $I = 70\,\mathrm{A}$, the corresponding temperature curves at the cable center ($z = 0.5\,\mathrm{m}$) without iteration, after the first iteration, after convergence, and from the numerical solution for the estimated initialization temperatures, $T_\mathrm{guess} = 60\,^\circ\mathrm{C}$ and $T_\mathrm{guess} = 105\,^\circ\mathrm{C}$ are compared in figure 7.12. It is shown that the analytical solution after convergence fits well with the numerical solution, but especially the solution without iteration can deviate significantly from the actual temperatures. Already the first iteration leads to massively improved temperatures. The calculated temperatures without iteration can be both higher and lower than the actual cable temperature. It is also possible that already without iteration a good agreement between analytical and numerical solution results. To investigate the occurring effects more precisely, the absolute (ΔT_abs) and relative (ΔT_rel) differences between the analytical and the numerical solution are determined:

$$\Delta T_\mathrm{abs} = \left| T - T_\mathrm{num} \right|, \quad \Delta T_\mathrm{rel} = \left| \frac{T - T_\mathrm{num}}{T_\mathrm{stst,num,mid} - T_\mathrm{e}} \right|. \tag{7.18}$$

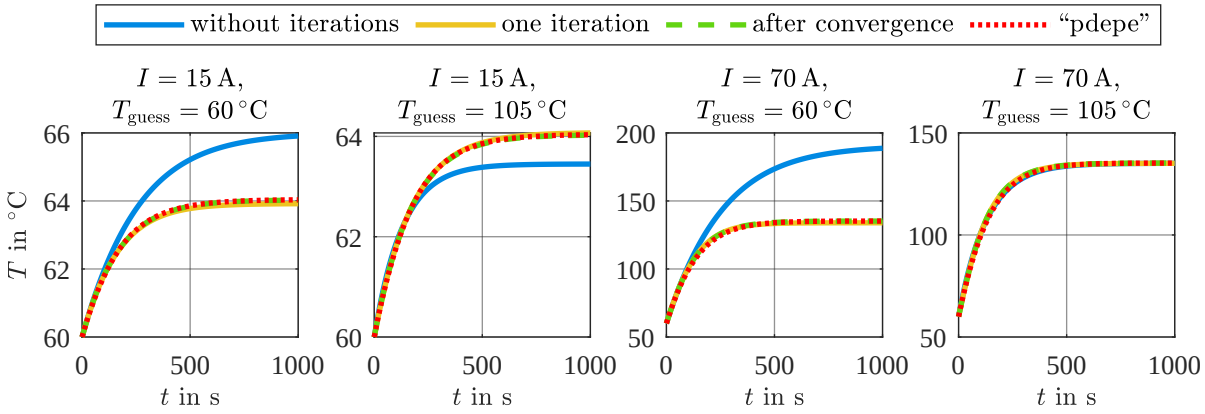

Figure 7.12: Comparison between analytically calculated temperatures with and without iterations and numerically calculated temperatures for different currents and initialization temperatures.

For the determination of the relative temperature difference, the temperature difference is related to the temperature deviation from the ambient temperature for the steady state in the center of the conductor, $T_{\mathrm{stst,num,mid}}$. 101 equally distributed time points between $0\,\mathrm{s}$ and $1000\,\mathrm{s}$ as well as 101 equally distributed positions along the cable between $0\,\mathrm{m}$ and $1\,\mathrm{m}$ are considered. After the absolute and relative differences are calculated point by point, the results are further processed: On the one hand, the average (mean) is taken over the entire (z, t) range, and on the other hand, the maximum (max) is determined.

Using this approach, the accuracy of the estimated temperature as a function of the load current is investigated first. The results are shown in figure 7.13 for $T_{\mathrm{guess}} = 105\,^{\circ}\mathrm{C}$. It can be seen that the absolute error increases, but the relative error decreases as the current increases. The absolute error is on average below $1\,\mathrm{K}$, so a good overall agreement is found even without iteration. For small currents (and thus also small temperature increase compared to the environmental temperature), the relative deviation can nevertheless exceed $25\,\%$ at the maximum, but after only one iteration this is already significantly reduced.

The dependence on the estimated temperature T_{guess} is investigated for $I = 70\,\mathrm{A}$ in figure 7.14. Here, a peak at the position of the ambient temperature appears: If the ambient temperature is assumed for the conductor and surface temperature, the heat transfer between the cable surface and the environment is significantly limited, so the cable reaches higher temperatures and the occurring mean absolute differences are higher than before. Therefore, the choice of the assumed initialization temperature plays an important role in the quality of the temperature estimation without iteration.

Overall, even the first iteration can cause a massive improvement in the accuracy of the temperature estimation. This also shows the very fast convergence behavior of the iteration. Therefore, in the further course of this thesis, always the solution with iteration is used. In principle, however, the direct analytical solution without iteration can also be used for a

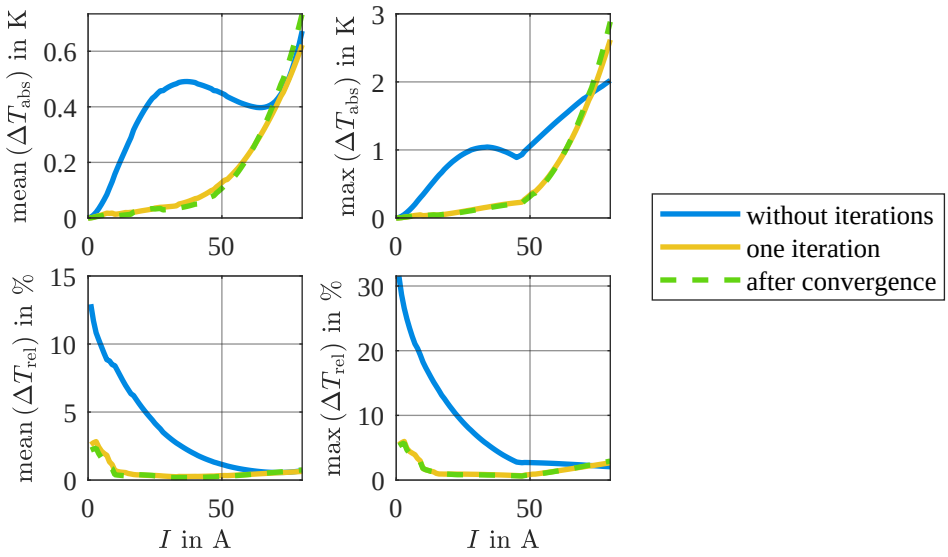

Figure 7.13: Mean and maximum values of the absolute and relative temperature differences dependent on the load current.

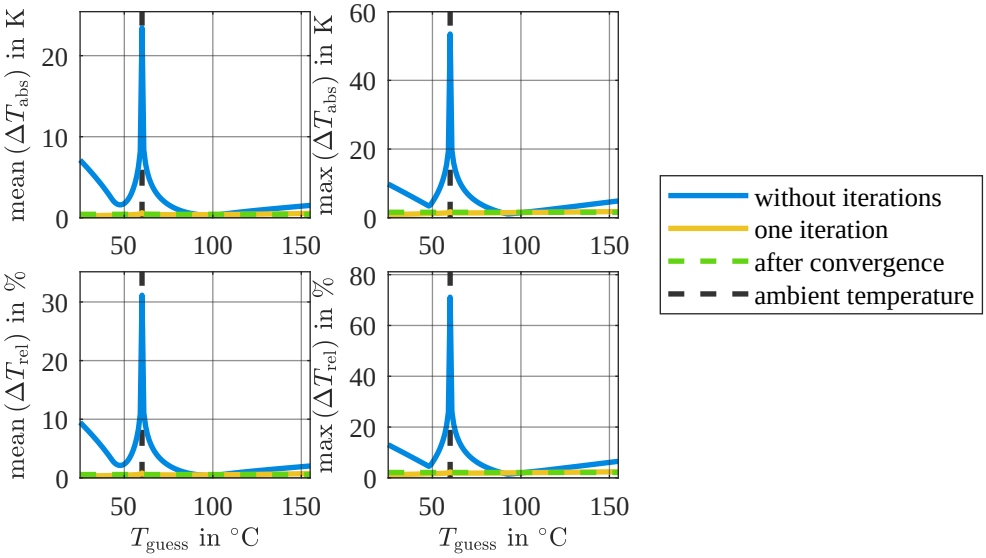

Figure 7.14: Mean and maximum values of the absolute and relative temperature differences dependent on the estimated initialization temperature.

first temperature estimation if the initialization temperature is suitable and/or only a small temperature rise compared to the environmental temperature appears which corresponds to small currents.

b) Analytical Solutions vs. Measurement Results

In this section, the previously derived calculation formulas are compared to measurement results. This section is based on [A.9]. A $1.5\,\mathrm{mm}^2$ single wire copper cable (cable data see table D.1, cable (3)) with PVC insulation and the length $\mathcal{L} = 1.5\,\mathrm{m}$ is analyzed. This ca-

ble is connected to large copper plates to fix the cable termination temperatures at constant values during the short measurements. The probe connections for the indirect temperature measurement are at the positions $z = 0.35\,\mathrm{m}$ and $z = 1.15\,\mathrm{m}$, and at the positons $z = 5\,\mathrm{cm}$, $z = 10\,\mathrm{cm}$, and $z = 75\,\mathrm{cm}$ thermocouples are connected to the conductor. At the time $t = 0\,\mathrm{s}$, a current $I = 30\,\mathrm{A}$ is switched on.

In the cable modeling, by now, a solid conductor was assumed. Unlike, the analyzed flexible cable consists of several strands with small air gaps in between. That is why an effective copper cross-section and a geometrical cross-section are introduced. The analyzed cable consists of 30 strands (diameter $d_{\mathrm{strand}} = 0.25\,\mathrm{mm}$). Thus, the copper-filled area $\mathcal{A}_{\mathrm{co}}$ and the effective copper radius $r_{\mathrm{c,eff}}$ are

$$\mathcal{A}_{\mathrm{co}} = 30 \cdot \pi \cdot \left(\frac{d_{\mathrm{strand}}}{2}\right)^2 \approx 1.47\,\mathrm{mm}^2 \Rightarrow r_{\mathrm{c,eff}} \quad = \sqrt{\frac{\mathcal{A}_{\mathrm{co}}}{\pi}} \approx 0.68\,\mathrm{mm}. \tag{7.19}$$

This effective radius is used for the parameters that characterize the conductor, namely the thermal per unit length capacitance for the conductor $\mathcal{C}'_{\mathrm{c}}$ and the axial thermal per unit length resistance R'. For the parameters that describe the insulation, the geometrical inner insulation radius is relevant. From the outer cable radius $r_{\mathrm{i}} = 1.7\,\mathrm{mm}$ and the insulation layer thickness $d_{\mathrm{i}} = 0.7\,\mathrm{mm}$, the inner insulation radius

$$r_{\mathrm{c,geom}} = r_{\mathrm{i}} - d_{\mathrm{i}} = 1\,\mathrm{mm} \tag{7.20}$$

is calculated. This value is used for the parameters for the insulation, namely the thermal per unit length capacitance for the insulation $\mathcal{C}'_{\mathrm{i}}$ and the thermal per unit length resistance R'_{i} that is used to model the heat flow through the insulation.

In the calculation of the per unit length resistance R'_{i} (see section 5.2.2) the modeled insulation was a perfect hollow cylinder. In the real cable, the insulation is defined by the strands and therefore significantly differs from this assumption (see figure 7.15, cross-section of the insulation). The green circle represents the outer insulation circumference, the black circle shows the assumed inner insulation circumference and the yellow curve shows the real inner insulation surface. As the yellow curve is much longer than the black one, the coupling area between the conductor and the insulation is much higher than considered before. Assuming that the heat flow depends on the coupling area, thus, the correction factor k_{i} for the per unit length resistance R'_{i} is introduced as the relation between the lengths of the black and the yellow curves:

$$k_{\mathrm{i}} \approx 0.7 \Rightarrow R'_{\mathrm{i,corr}} = k_{\mathrm{i}} \cdot R'_{\mathrm{i}}. \tag{7.21}$$

This value is used throughout this thesis for all stranded conductors if not stated differently.

During the measurement, the cable heats the environment (see figure 7.16(b)). Due to the low variations, in the calculations, the constant temperature $25\,^{\circ}\mathrm{C}$ is assumed, which is as

well the temperature at the cable terminations and the initial cable temperature. In figure 7.16, the axial (a) and transient (b) results are shown. For the transient case, in addition, the absolute difference between the calculated temperatures and the temperatures measured with

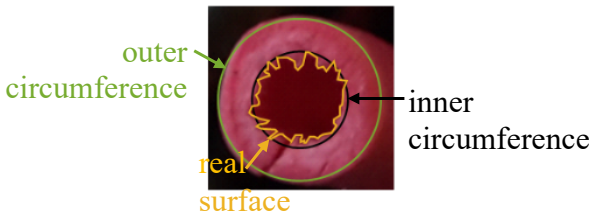

Figure 7.15: Cross-section of the insulation with the assumed outer circumference (green), inner circumference (black), and the real inner surface (yellow). A similar figure was earlier published in [A.9].

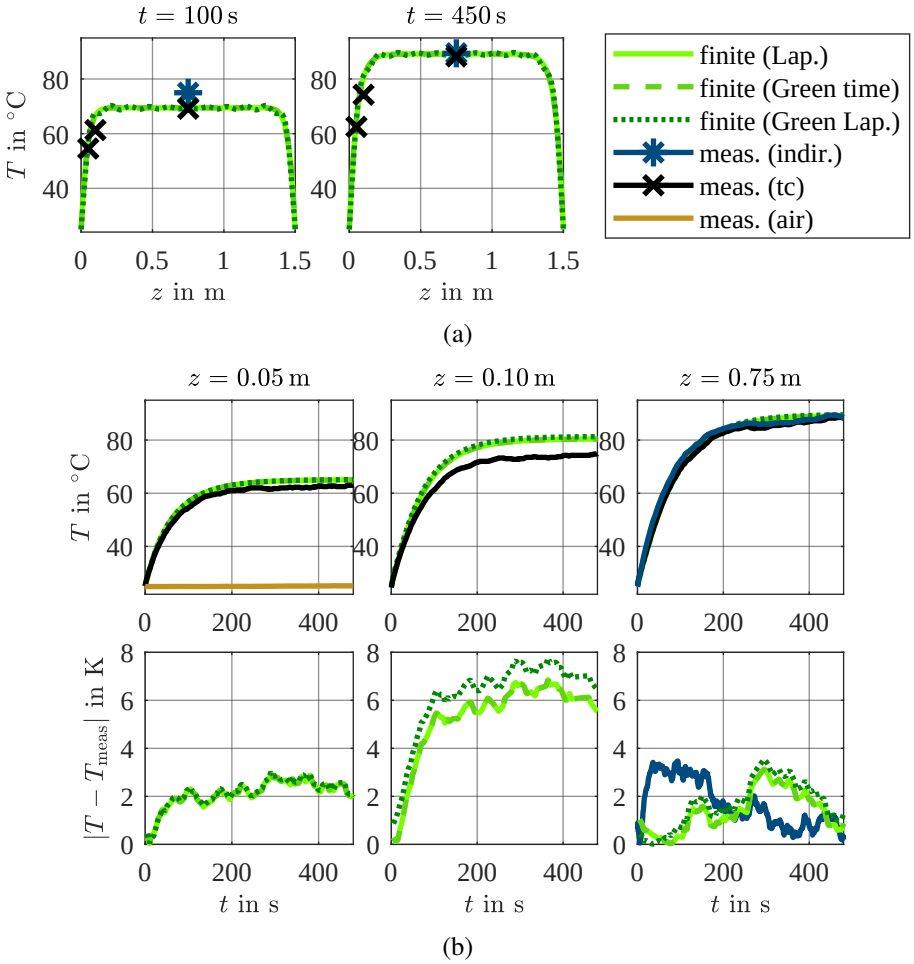

Figure 7.16: (a) Axial cable temperature distribution for the two different times $t = 100\,\mathrm{s}$ and $t = 450\,\mathrm{s}$. (b) Calculated and measured transient temperature development at the fixed positions $z = 5\,\mathrm{cm}$, $z = 10\,\mathrm{cm}$, and $z = 75\,\mathrm{cm}$ (cable center). Absolute values and deviation from the thermocouple measurement results. Most of the data in this figure were already published in [A.9].

the thermocouples is presented. The differences are lower than $8\,\mathrm{K}$ for all cases. As expected, the temperatures that are measured with the thermocouples are lower than the calculated temperatures because the thermocouple itself leads away heat from the conductor. As the difference between both performed measurement approaches lies in the same magnitude as the differences compared to the calculations, all in all, good accordance between calculation and measurement is found.

c) Convergence Behavior of Green's Functions Solutions

In this section, the convergence behavior of the Green's functions solutions is evaluated using the $6\,\mathrm{mm}^2$ single wire copper cable already known from section 7.3.1.a) with the reduced length $\mathcal{L} = 0.1\,\mathrm{m}$ because especially for short cables, the approximation from the Laplace solution is not valid and additional addends lead to better accuracy. The environmental air temperature T_e and the initial cable temperature T_0 are both $25\,^\circ\mathrm{C}$ and the cable termination temperatures are $T_1 = T_2 = 50\,^\circ\mathrm{C}$. As a numerical reference, the corresponding calculated temperature using the MATLAB function "pdepe" (see section 7.1.1.b)) is used. This section is based on [A.4].

In figure 7.17, for the analysis of the convergence behavior of the Green's functions series solutions (T_G for time-domain **G**reen's functions, T_GL for **L**aplace domain **G**reen's functions), the deviations between the calculated temperatures and the reference are presented for the beginning and the center of the cable depending on the number of considered addends. In addition, the corresponding deviation for the **L**aplace domain solution with **a**pproximation (T_La, see section 6.1.2.a)) is given, which shows a much larger deviation than most of the

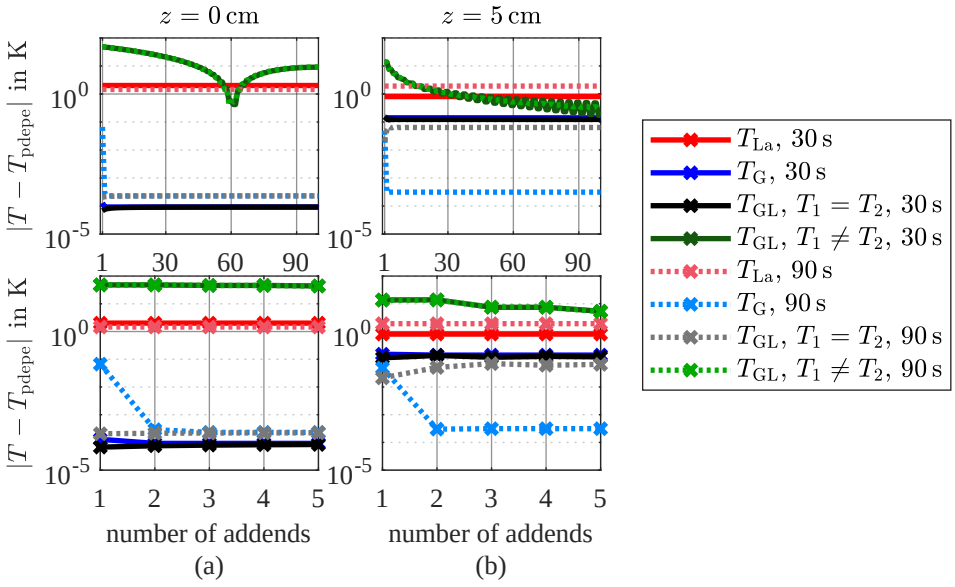

Figure 7.17: Deviation between analytically and numerically calculated temperatures depending on the number of addends at (a) the beginning and (b) the center of the cable. The data in this plot were already published in [A.4].

Green's functions-based solutions. In the second line, a zoom to the first few addends is given. Only the Green's functions solution from the Laplace domain with consideration of different cable termination temperatures shows higher deviations and very slow convergence behavior. Due to the unsteady behavior of this solution near the cable terminations, the slightly higher value $z = 1\,\mathrm{mm}$ was used for the calculation at the cable beginning. The bad convergence behavior limits the practical applicability of this solution, as many addends have to be taken into account for a precise result, which also massively increases the calculation effort.

d) Influence of Cable Length

In section 6.1.2.a), an approximation was used to enable an analytical transformation of the Laplace domain solution to the time domain. This approximation is analyzed in this section. At first, the approximated and analytically transformed solution is compared to a numerical inversion (Gaver-Stehfest-algorithm [115], parameter $M = 3$) of the Laplace domain expression from equations (6.32) and (6.34) without approximation for a $6\,\mathrm{mm}^2$ cable. This analysis is based on [A.3]. For the ambient, initial, and boundary temperatures, $T_\mathrm{e} = T_0 = T_1 = T_2 = 25\,^\circ\mathrm{C}$ is used. For the three cable lengths $\mathcal{L} = 0.3\,\mathrm{m}$, $\mathcal{L} = 0.5\,\mathrm{m}$, and $\mathcal{L} = 1\,\mathrm{m}$, figure 7.18(a) shows the analytically and numerically calculated temperatures and their differences along the normalized axial coordinate $z/\mathcal{L}$ for the time $t = 1000\,\mathrm{s}$. In figure 7.18(b), the corresponding time-dependent temperature development for the central cable section is shown. For the longest cable with length $\mathcal{L} = 1\,\mathrm{m}$, analytical and numerical

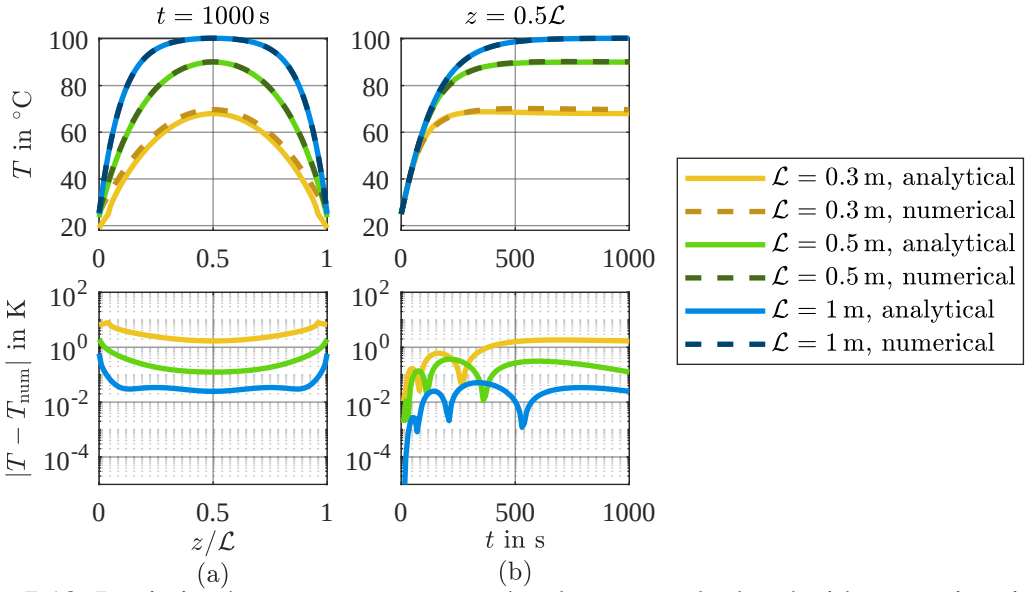

Figure 7.18: Deviation between temperature development calculated with approximation and analytical solution vs. numerical transformation back into time domain for different cable lengths. (a) Axial temperature distribution at $t = 1000\,\mathrm{s}$. (b) Transient temperature development in the central section of the cable. Most of the data in this plot were already published in [A.3].

solutions match well (difference much lower than $1\,\mathrm{K}$). For the shorter cables, higher deviations appear, which shows that then, the approximation of the Laplace domain solution can lead to errors.

The following considerations concerning this effect are based on [A.4]. At the cable's beginning and in the central section of the cable, the deviation between analytically and numerically calculated cable temperatures at the time $t = 1000\,\mathrm{s}$ is shown depending on the cable length in figure 7.19. An exponential growth of the deviations of the approximation for short cables is observed, which also appears (for lower cable lengths) when using only one additional addend from the Green's functions solution in the time domain. Using five addends from this solution or ten addends from the Laplace domain solution for identical cable end temperatures leads to good accordance over the complete analyzed area down to cable lengths of $0.1\,\mathrm{m}$. In the central cable section, the consideration of additional addends also improves the accuracy for short cables. For longer cables, the Laplace domain Green's functions solution shows a worse behavior than the time domain Green's functions solution.

To analyze the influence of the cable cross-section area on the accuracy of the Laplace domain solution with approximation, a critical cable length $\mathcal{L}_{\mathrm{crit}}$ is introduced in [A.4]. For this critical cable length, the steady-state temperature in the central cable section is compared to the reference and the maximum length is chosen under which the deviation exceeds $3\,\mathrm{K}$. For the cables whose parameters are given in table D.3 those critical cable lengths are calculated using the bisection method (see also section 6.3.2.a)) with an allowed uncertainty of $1\,\mathrm{mm}$ loading each cable with a current that leads to a steady-state central cable temperature of $(100 \pm 0.2)\,^{\circ}\mathrm{C}$. The results are shown in figure 7.20. The observed relation between conductor radius and critical cable length is linear, which means that especially for comparatively short cables with high cross-sections, the approximation from section 6.1.2.a) leads to errors. Then, the use of Green's functions-based series formulations can improve the accuracy.

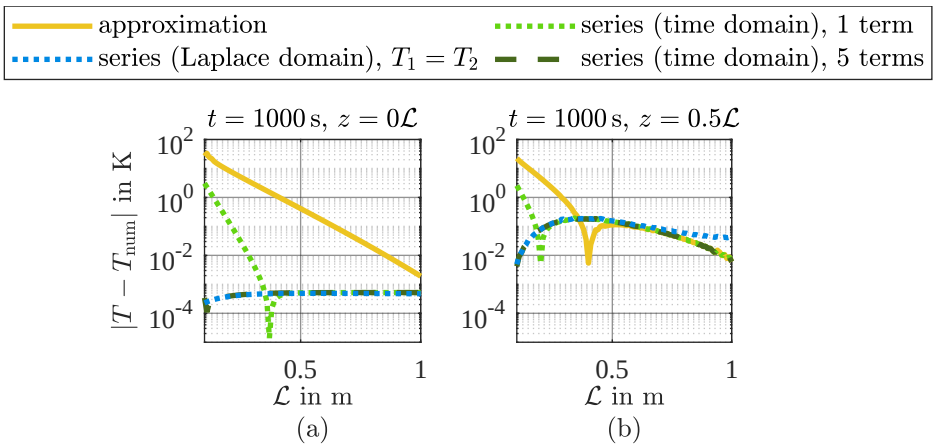

Figure 7.19: Deviation between the analytically and numerically calculated temperatures depending on the cable length (a) at the beginning and (b) in the central section of the cable after $t = 1000\,\mathrm{s}$. The data in this plot were already published in [A.4].

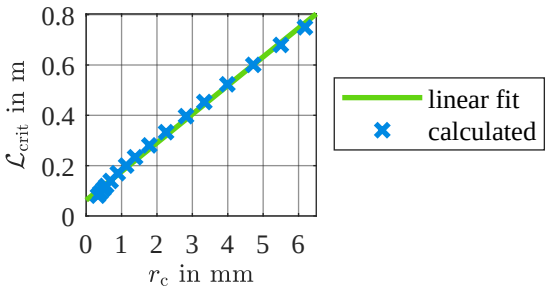

Figure 7.20: Critical cable length depending on the conductor radius. Comparable data were already published in [A.4].

e) Complexity Analysis

The comparison of the calculation efforts of the different solutions, which is presented in this section, is based on [A.3]. The total calculation effort for the analytical solution

$$e_{\mathrm{total}} = e_{\mathrm{pre}} + (e_{\mathrm{sol}} + e_{\mathrm{it}}) \cdot \sum_{j=1}^{J} i_{\mathrm{max},j} \tag{7.22}$$

depends on the effort for the precalculations e_{pre} (identical for each combination (z,t)), the effort for the necessary calculations in each iteration to update B_{sw} and C_{sw} (e_{it}), the effort of the temperature calculation itself (e_{sol}) and the number of necessary iteration steps $i_{\mathrm{max},j}$ for each combination j of z and t. $e_{\mathrm{sol,La}}$ describes the solution via approximation in the Laplace domain (see section 6.1.2.a)), $e_{\mathrm{sol,G},n}$ is the additional effort for solution calculation with Green's functions in the time domain for each addend n (see section 6.1.2.b)) and $e_{\mathrm{sol,GL},n}$ the effort for solution calculation with Green's functions in the Laplace domain for each addend n (see section 6.1.2.c)). In table 7.1, the numbers of mathematical operations for the different solution parts are given. Those numbers are meant to give a rough approach to the complexities of the different solutions but are highly dependent on the exact form of the used expression for the solutions. Optimizations could be performed to reduce those numbers. In contrast to the analytical solutions, the simplest numerical method is the first order or Euler method ([150], see also section 7.1.1.a), $e_{\mathrm{sol,Euler}}$). The usage of different methods may on the one hand increase the accuracy of the calculated temperatures, but on the other hand, also leads to greater calculation effort. So, the usage of the Euler method allows finding a minimum for the numerical calculation effort. The iteration for the consideration of the nonlinear parameter dependence is different here as no recalculation of temperature is necessary: The last parameter values are used for the calculation of the next time step. The overall effort, therefore, is

$$e_{\mathrm{total,Euler}} = e_{\mathrm{pre}} + e_{\mathrm{sol}} \cdot J + e_{\mathrm{it}} \cdot \sum_{j=1}^{J} i_{\mathrm{max},j}. \tag{7.23}$$

Again, in table 7.1 the necessary operations for the temperature calculation of a single time-spatial point are counted.

To find an overall effort estimation, the operations are weighted due to their individual calculation effort. This highly depends on the used implementations. As the first approach, here, the analysis from [179] is used. There, factors for multiplication, addition, division, square root, and exponential functions are given. Based on these data, the effort for the other operations is estimated (red entries in table 7.1). This estimation is meant to give a rough approach. If, for example, for multiplication, a higher effort is necessary than for addition, the individual numbers would change, but the basic statements that are found in the following would still hold. For the different solutions, the weighted sums of the elemental operations are calculated (see table 7.1) via the following dependencies:

$$e_{\mathrm{pre}} = 11w_{\mathrm{m}} + 2w_{\mathrm{a}} + 3w_{\mathrm{d}} + 5w_{\mathrm{z}} + w_{\mathrm{l}}, \tag{7.24}$$

$$e_{\mathrm{it}} = 40w_{\mathrm{m}} + 27w_{\mathrm{a}} + 6w_{\mathrm{d}} + w_{\mathrm{b}} + 21w_{\mathrm{z}} + 3w_{\mathrm{p}}, \tag{7.25}$$

$$e_{\mathrm{sol,La}} = 30w_{\mathrm{m}} + 14w_{\mathrm{a}} + 8w_{\mathrm{d}} + 11w_{\mathrm{r}} + 5w_{\mathrm{x}} + 7w_{\mathrm{z}} + 6w_{\mathrm{e}}, \tag{7.26}$$

$$e_{\mathrm{sol,G}} = n_{\max} \cdot (58w_{\mathrm{m}} + 20w_{\mathrm{a}} + 12w_{\mathrm{d}} + 28w_{\mathrm{r}} + 8w_{\mathrm{x}} + 5w_{\mathrm{z}} + 12w_{\mathrm{e}}) + e_{\mathrm{sol,La}}, \tag{7.27}$$

$$\begin{aligned} e_{\mathrm{sol,GL}} = {} & n_{\max,\mathrm{i}} \cdot (7w_{\mathrm{m}} + 6w_{\mathrm{a}} + 4w_{\mathrm{d}} + w_{\mathrm{x}} + 4w_{\mathrm{z}} + w_{\mathrm{s}}) \\ & + n_{\max,\mathrm{bc}} \cdot (9w_{\mathrm{m}} + 3w_{\mathrm{a}} + 3w_{\mathrm{d}} + w_{\mathrm{x}} + 3w_{\mathrm{z}} + 2w_{\mathrm{s}}) + 2w_{\mathrm{m}} + 2w_{\mathrm{d}}, \end{aligned} \tag{7.28}$$

$$e_{\mathrm{sol,Euler}} = 5w_{\mathrm{m}} + 6w_{\mathrm{a}} + 2w_{\mathrm{d}} + w_{\mathrm{z}}. \tag{7.29}$$

Here, $e_{\mathrm{sol,G}}$ is the effort for solution calculation with Green's functions in the time domain (see section 6.1.2.b)) and $e_{\mathrm{sol,GL}}$ is the effort for solution calculation with Green's functions

Table 7.1: Complexity analysis for different solutions. Most of the data in this table were already published in [A.3].

	e_{pre}	e_{it}	$e_{\mathrm{sol,La}}$	$e_{\mathrm{sol,G},n}$	$e_{\mathrm{sol,GL},n}$		$e_{\mathrm{sol,Euler}}$	weight [179]
					ic+inh	bc		
multiplication	11	40	30	58	7	9	4	$w_{\mathrm{m}} = 1$
addition	2	27	14	20	6	3	5	$w_{\mathrm{a}} = 1$
division	3	6	8	12	4	3	2	$w_{\mathrm{d}} = 4$
square root	0	0	11	28	0	0	0	$w_{\mathrm{r}} = 4$
exponential function	0	0	5	8	1	1	0	$w_{\mathrm{x}} = 8$
absolute value	0	1	0	0	0	0	0	$w_{\mathrm{b}} = 1$
allocation	5	21	7	5	4	3	0	$w_{\mathrm{z}} = 1$
error function	0	0	6	12	0	0	0	$w_{\mathrm{e}} = 8$
sine	0	0	0	0	1	2	0	$w_{\mathrm{s}} = 8$
power (non-integer)	0	3	0	0	0	0	0	$w_{\mathrm{p}} = 8$
natural logarithm	1	0	0	0	0	0	0	$w_{\mathrm{l}} = 8$
weighted sum (example)	38	137	215	403	49	51	17	

in the Laplace domain (see section 6.1.2.c)). As expected, the effort for the Euler method is lower than for the analytical approaches. But those approaches also go ahead with an advantage: As all combinations (z, t) are calculated independently from each other, precasting the temperature far in the future (for constant conditions) is no more expensive concerning calculation effort than the calculation of a very close time step, as no discretization is needed. Thus, the necessary calculation effort can be reduced compared to the numerical solution, although the effort for a single combination is higher than in the simplest numerical case.

7.3.2 System of Single Wire Cables

In this section, the model for a system of single wire cables from section 6.1.3 is validated with measurement results. This section is based on [A.7]. For this purpose, a $0.14\,\mathrm{mm}^2$ PVC-insulated copper cable with the length $\mathcal{L} = 1.61\,\mathrm{m}$ is loaded with the current $I = 6.5\,\mathrm{A}$. Along the cable, between $z = 18\,\mathrm{cm}$ and $z = 143\,\mathrm{cm}$, the indirect temperature measurement is performed. In between those two connections, thermocouples are connected to the cable with a distance of $25\,\mathrm{cm}$. In this way, the temperature is measured directly at the connection. This setup is shown in figure 7.21.

In addition, the environmental temperature is measured and only the differences concerning this temperature are compared for different measurements. The results are shown in figure 7.22. As expected, the temperatures measured with the indirect temperature measurement are higher than the temperatures measured with thermocouples. For comparison, the indirect temperature measurement is additionally performed without any connected thermocouples,

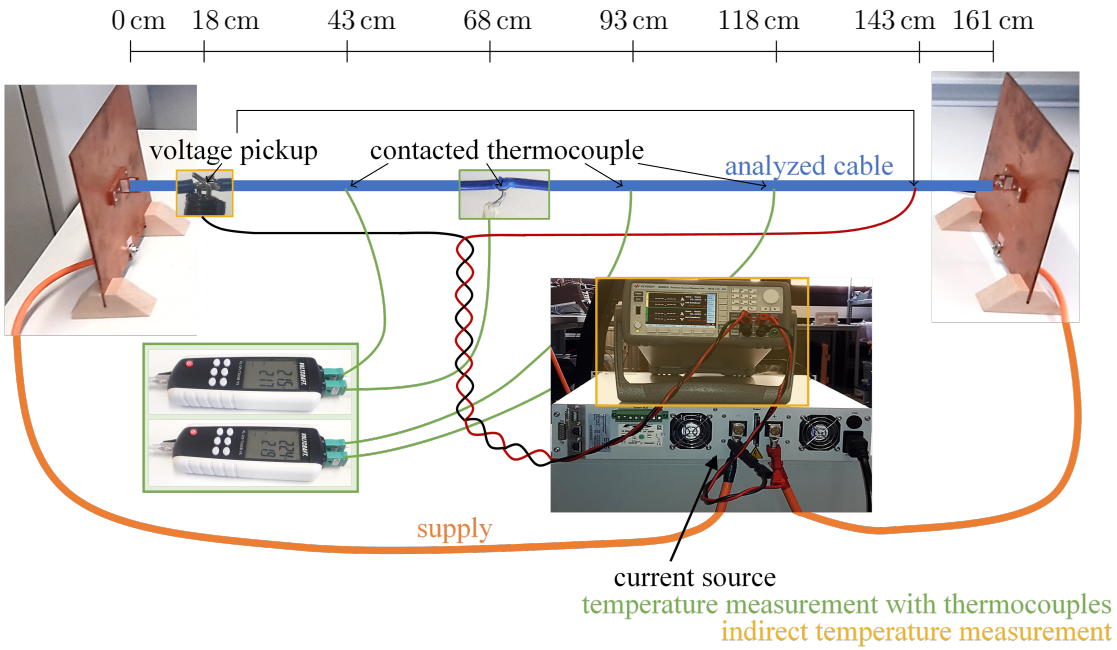

Figure 7.21: Measurement setup for combined indirect temperature measurement (yellow) and thermocouple measurement (green).

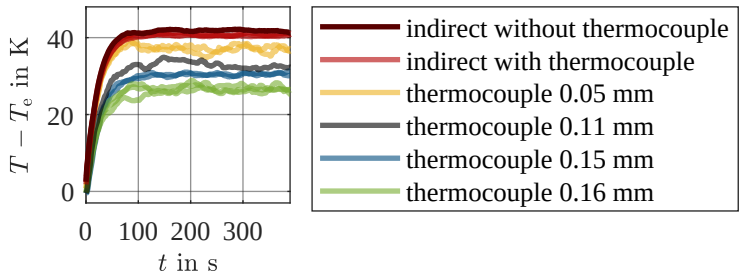

Figure 7.22: Measurement results for different thermocouples and indirect temperature measurement. For the thermocouples, the wire radius r_{tc} is given.

which leads to the highest values. For the different thermocouples (especially different wire radii) it can be systematically observed, that the measured temperatures are higher for smaller thermocouple wire radii r_{tc}.

The predictions from the presented model and the real measurement results are compared in the following. In the model, a continuous cable is assumed. Both wires of the thermocouple are combined into one effective conductor with the same overall conductor area, which leads to the radius

$$r_{\mathrm{tc,eff}} = \sqrt{2} r_{\mathrm{tc}}, \tag{7.30}$$

where r_{tc} is the real thermocouple wire radius. In the middle of the first cable, a second cable is thermally connected assuming an ideal thermal coupling and electrical insulation from the conductor potential as shown in figure 7.23.

The current I flows through the complete first cable and no current is assumed to flow in the second cable. Both cables are modeled with the inner conductor material copper and the insulation material PVC. As the real thermocouple does not consist of these materials, this is a first approximation: In the real thermocouple as well, metal inner conductors and insulating surroundings are used, but the chosen materials vary. It is expected that the error due to the not perfectly fitting parameters is low, especially in comparison with other assumptions (one effective inner conductor instead of two separated conductors, neglection of the fact that the thermocouple insulation typically does end a few millimeters before the hot junction, neglection of the added Kapton tape and the openings for the contacts).

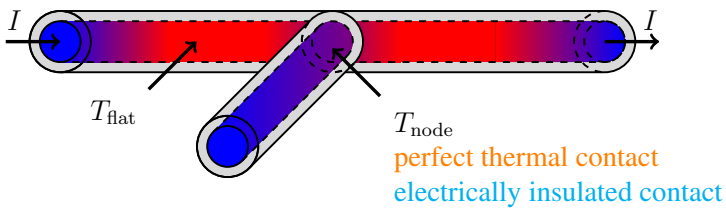

Figure 7.23: Modeled cable arrangement for the evaluation of the influence of thermocouples on the cable temperature.

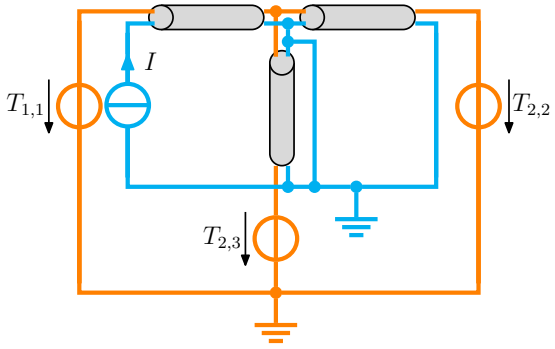

Figure 7.24: Thermal (orange) and electrical (blue) connections between the involved cables.

The setup is modeled using the presented analytical solution as well as the Simscape implementation of cascaded ECDs (see section 7.1.2). The necessary ECD combining the electrical and thermal model for the Simscape solution is given in figure 7.24. The choice of the given cable end temperatures $T_{1,1}$, $T_{2,2}$, and $T_{2,3}$ is not relevant for this analysis, so they can exemplarily be set to the environmental temperature.

In the following, several combinations of different cables for the loaded cable and the cable that leads away the heat are analyzed. The cable data from table D.3 are used. Using the analytical solution, all combinations of loaded and connected cables are analyzed for the two environmental temperatures $20\,^{\circ}\mathrm{C}$ and $85\,^{\circ}\mathrm{C}$. To achieve a flat area in the center of the cable for all cross-sections, all three modeled cable parts have a length of $\mathcal{L} = 5\,\mathrm{m}$. The steady state is analyzed. That is why the time $t = 8000\,\mathrm{s}$ is chosen. Different load currents are chosen for the loaded cables to achieve a temperature at the cable center of $50\,^{\circ}\mathrm{C}$, $85\,^{\circ}\mathrm{C}$, $105\,^{\circ}\mathrm{C}$, and $155\,^{\circ}\mathrm{C}$ for the lower environmental temperature and $105\,^{\circ}\mathrm{C}$ and $155\,^{\circ}\mathrm{C}$ for the higher one. Then, the relative deviation

$$\Delta T_{\mathrm{rel}} = \frac{T_{\mathrm{flat}} - T_{\mathrm{node}}}{T_{\mathrm{flat}} - T_{\mathrm{e}}} \tag{7.31}$$

between the temperature at the cable center T_{flat} and the temperature at the node T_{node} (see figure 7.23) is evaluated depending on the relation

$$\hat{r} = \frac{r_{\mathrm{tc,eff}}}{r_{\mathrm{c,load}}} \tag{7.32}$$

between the radius $r_{\mathrm{c,load}}$ of the loaded conductor and the radius $r_{\mathrm{tc,eff}}$ of the unloaded conductor. For the case that the unloaded cable has a conductor radius that is less or equal to the conductor radius of the loaded cable, a linear behavior is found and fitted using the function

$$f(\hat{r}) = a_1 \hat{r} + a_0. \tag{7.33}$$

The found parameters for the Simscape model results are

$$a_{1,\mathrm{S}} \approx 0.32, \quad a_{0,\mathrm{S}} \approx -0.0033 \tag{7.34}$$

and for the analytical approach

$$a_{1,\mathrm{a}} \approx 0.35, \quad a_{0,\mathrm{a}} \approx -0.011. \tag{7.35}$$

The results are presented in figure 7.25(a), where the measurement results are also marked. Overall, good accordance between both calculations and the measurement results can be observed. For $\hat{r} = 1$, which means that the cable with the current has the same radius as the effective thermocouple, a deviation value of about a third appears, which fits well with the intuition for this case. In figure 7.25(b), a wider parameter range is evaluated with the analytical approach. The complete curve is fitted exponentially using the function

$$\begin{aligned} f(\hat{r}) &= b_1 - b_2 \mathrm{e}^{-b_3 \hat{r}}, \\ b_1 &\approx 0.89, \quad b_2 \approx 0.91, \quad b_3 \approx 0.50. \end{aligned} \tag{7.36}$$

The curve flattens with higher $\hat{r}$ and slowly converges to 1, which means that all the heat is led away via the connected thermocouple.

Based on this analysis, a condition for the choice of appropriate thermocouples for temperature measurement in thin wire cables can be defined. To achieve a deviation ΔT_{rel} lower than $10\,\%$, the effective thermocouple conductor radius $r_{\mathrm{tc,eff}}$ has to be lower than a third of the conductor radius of the measured cable $r_{\mathrm{c,meas}}$:

$$r_{\mathrm{tc,eff}} < \frac{1}{3} r_{\mathrm{c,meas}}. \tag{7.37}$$

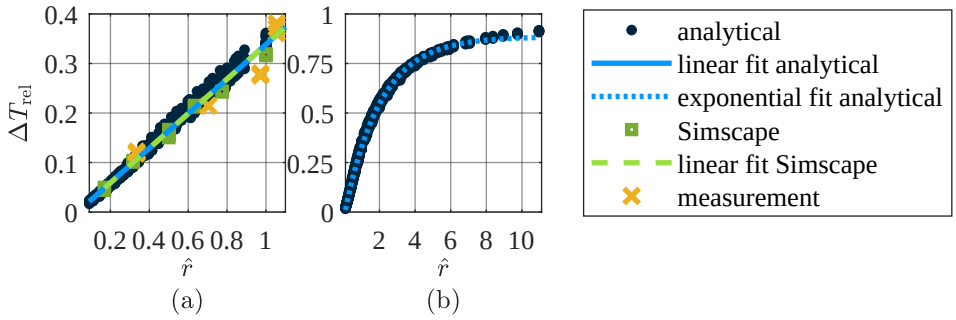

Figure 7.25: Temperature deviation depending on the relation between the conductor radii. (a) Comparison between Simscape and analytical calculation and measurement. (b) Analytical calculation for a wider parameter range.

With equation (7.30), for the wire conductor radius of the thermocouple r_{tc}, it follows

$$r_{\mathrm{tc}} < \frac{1}{3\sqrt{2}} r_{\mathrm{c,meas}} \approx \frac{1}{4} r_{\mathrm{c,meas}}. \tag{7.38}$$

This approximation can be used to enable the choice of appropriate thermocouples for temperature measurement, especially in cables with small cross-section areas. Exemplary, for a $25\,\mathrm{mm}^2$ cable, a thermocouple with a conductor radius below $0.71\,\mathrm{mm}$ is sufficient, which is fulfilled for most thermocouples (exemplary radii see for example figure 7.22). For a $1.5\,\mathrm{mm}^2$ cable, still all analyzed thermocouples can be used (conductor radius below $0.17\,\mathrm{mm}$), but for a $0.14\,\mathrm{mm}^2$ cable, a thermocouple with a maximum conductor radius of $0.05\,\mathrm{mm}$ is necessary to achieve a deviation ΔT_{rel} lower than $10\,\%$.

7.3.3 Two Single Wire Cables

In practical applications, not only single wire cables consisting of an inner conductor and insulation are used, but arrangements with several conductive structures appear. In addition to shielded single cables, these can also be multicore cables or arrangements of several single cables. The temperatures of the individual conductive structures then depend on each other. In the modeling, this is represented by a coupling conductance, which is introduced directly between the two conductive structures. However, the determination of this conductance is challenging in many cases.

For the special case of a symmetrical cable arrangement surrounded by a common filling, analytical estimations can still be found [145]. For other cases, different approaches are necessary. In the following, an approach for a twisted pair cable is shown, i.e. two twisted identical single wire cables.

a) Identical Cables

Some considerations in this section are based on [A.8]. In principle, the contact resistance between two adjacent surfaces could analytically be described if the exact surface structure was known. In practice, however, this procedure cannot be applied to the presented problem as those parameters massively depend on variables like the contact pressure between the cables, which cannot easily be measured directly. In addition to the direct heat conduction path across the contact area, heat radiation between the cable surfaces appears. The coupling conductance should directly model the thermal coupling between the two inner conductors, so heat conduction through the insulation layers has to be taken into account. All in all, different effects contribute to the coupling between the conductor temperatures. In the modeling, all these effects can be approximately summed up in a single, constant coupling conductance G'_{12}. Furthermore, the second cable reduces radiation and convection at the cable surface and only a part of the heat conduction through the insulation leads heat to the environment. Therefore, a correction factor k is needed. This correction factor is assumed to be constant

for a given cable. For the conductors $i = 1, 2$, therefore, the corrected conductance

$$G'_{ii}(T_i, T_\mathrm{e}) = \frac{1}{k}\tilde{G}'_{ii}(T_{i,\mathrm{m}}, T_\mathrm{e}) \tag{7.39}$$

is used to describe the coupling between conductor and environment. $\tilde{G}'_{ii}$ is the corresponding resistance for a single wire cable laid freely in the air, which depends (indirectly) on the inner conductor temperature $T_{i,\mathrm{m}}$ and (directly) on the ambient temperature T_e.

In the following, two methods[11] are presented to find k and G'_{12} based on the measured steady-state values of the conductor temperatures for a sufficiently long cable. The simplified ECD for the radial steady state is shown in figure 7.26. Exemplary, those methods are applied to the cable and measurement result from section 7.2.1.e).

In the first step, a current is applied to only one cable ($I_1 = I$, $I_2 = 0\,\mathrm{A}$). The radial steady-state temperatures of both cables are measured ($T_{1,\mathrm{m}}$ for the loaded cable and $T_{2,\mathrm{m}}$ for the unloaded cable). Then, the cable parameters can be calculated as outlined in figure 7.27(a). Applying this approach (method 1) shows high variations in the reconstructed parameters using different measurements, even from the same current loads (see figure 7.28(a)). Between different load cases, this effect is even more dominant. In some cases, even unphysical values are found ($k < 1$). The parameters seem to react very sensitively to small changes in the measured temperatures.

In the second step, the first approach is therefore extended by another measurement ($\mathrm{m1}$). Here, both conductors are loaded with identical currents ($I_1 = I_2 = I$). Thus, $T_{1,\mathrm{m1}} = T_{2,\mathrm{m1}}$ follows for the radial steady-state temperatures, since two identical cables are used. Then no heat flows across G'_{12} and only k appears. From this measurement, k is calculated:

$$k = \frac{\tilde{G}'_{11}(T_{1,\mathrm{m1}}, T_{\mathrm{e,m1}})}{P'_{\mathrm{el},1,\mathrm{m1}}} \left(T_{1,\mathrm{m1}} - T_{\mathrm{e,m1}}\right). \tag{7.40}$$

The second measurement ($\mathrm{m2}$, only one cable loaded) is then used to determine the coupling conductance. Figure 7.27(b) shows the entire procedure of this method 2.

Both methods are compared for an exemplary twisted pair cable. The required measure-

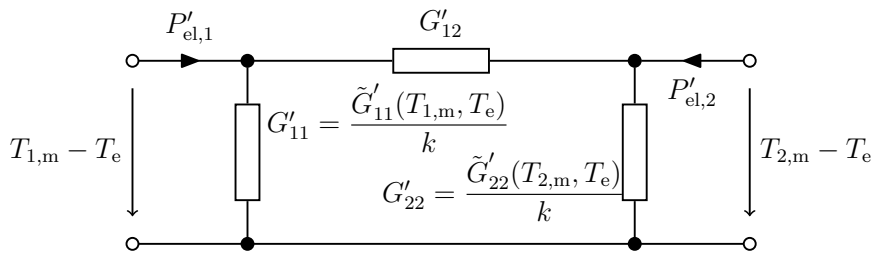

Figure 7.26: Simplified ECD for the radial steady state for two coupled identical cables.

[11] The original versions of methods 1 and 2 were proposed by student assistant Julian Hohmann.

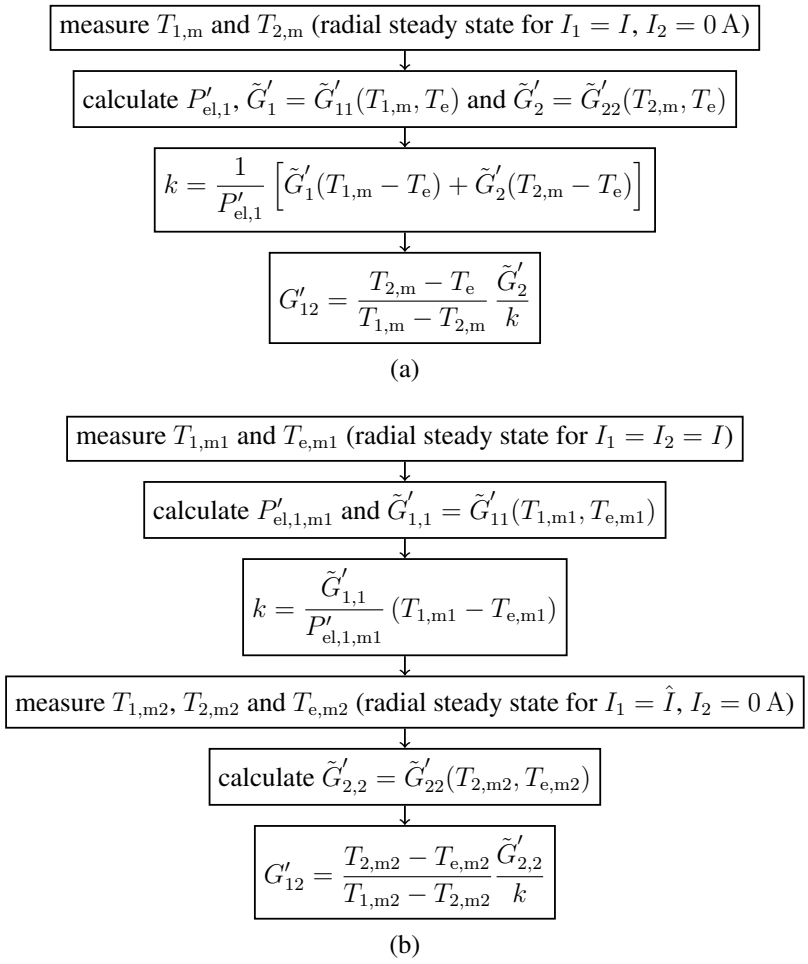

Figure 7.27: Calculation of k and G'_{12} via (a) method 1 and (b) method 2.

ments are performed with currents of $5\,\mathrm{A}$, $7.5\,\mathrm{A}$, and $10\,\mathrm{A}$ (measurements from reproducibility analysis in section 7.2.1.e)). The calculated parameters are given in figure 7.28(a). With the second method, the fluctuations of the correction factor k for the same current load are significantly smaller than with the first method. Systematically, it is observed that the correction factor increases for higher current loads. In both cases, the determined coupling conductances fluctuate more significantly.

In figure 7.28(b), a short overview of notations is given: Little illustrations of the cable cross-section are used to indicate the load case (cable with and without current) and the cable for which the temperature is shown in the corresponding figure.

In the next step, the analytically calculated radial transient temperature developments using the different sets of parameters are compared (see figure 7.28(c)). The temperatures calculated with the parameters of high current loads tend to be higher than the corresponding temperatures with the parameters of lower current loads. Therefore, the usage of high current measurements for the parameter calculation is proposed as worst case.

Based on the already known measurement data, this procedure is now applied: For the

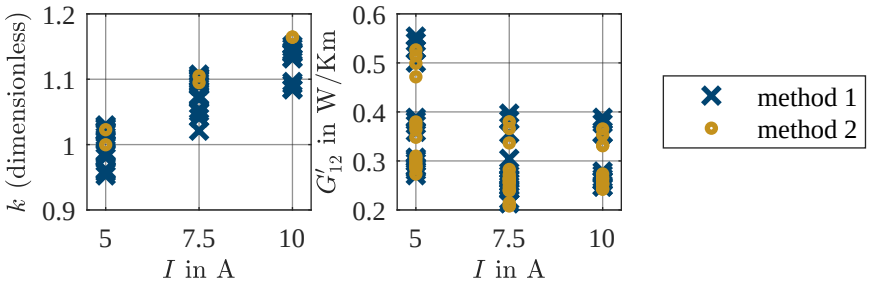

(a)

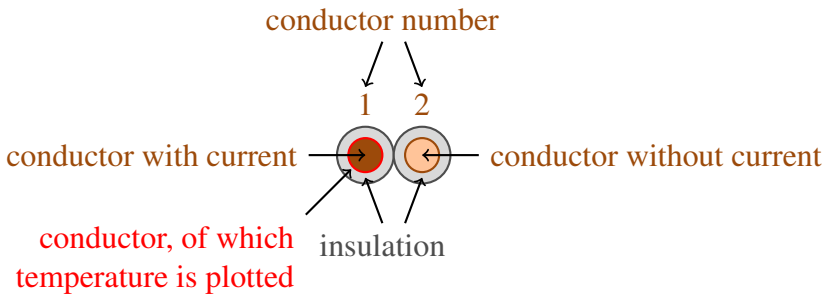

(b)

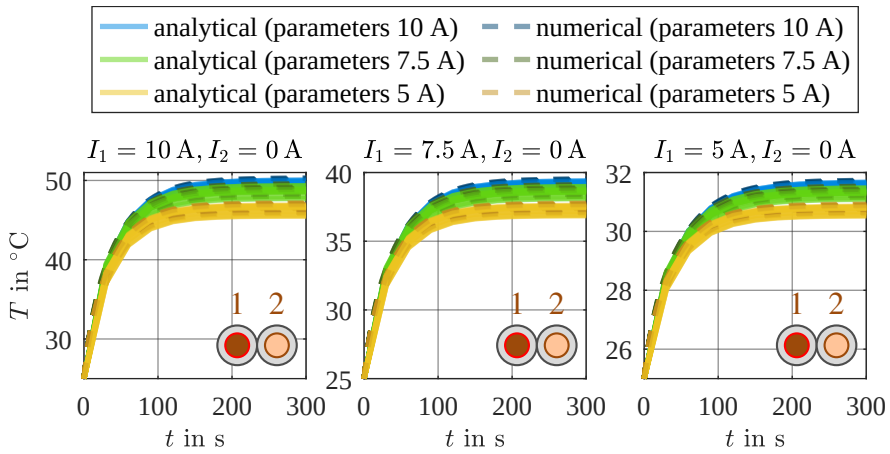

(c)

Figure 7.28: (a) Determined parameters k and G'_{12} for a cable arrangement of two identical single wire cables from repeated measurements. (b) Example of the illustrations used in the following to visualize cables with and without current and the cable that is chosen for the plot. (c) Numerically ("pdepe") and analytically calculated temperature development for cable 1 using the parameters from the different measurements (10 A, 7.5 A, and 5 A).

parameter determination, 10 A measurements are used as a worst-case estimation. The determined pairs of k and G'_{12} are shown in figure 7.29(a).

The temperature curves calculated with these different parameter sets are compared with the measured temperature curves (see figure 7.29(b)). All temperature curves are displayed transparently, so a higher color intensity indicates a more common appearance of the corre-

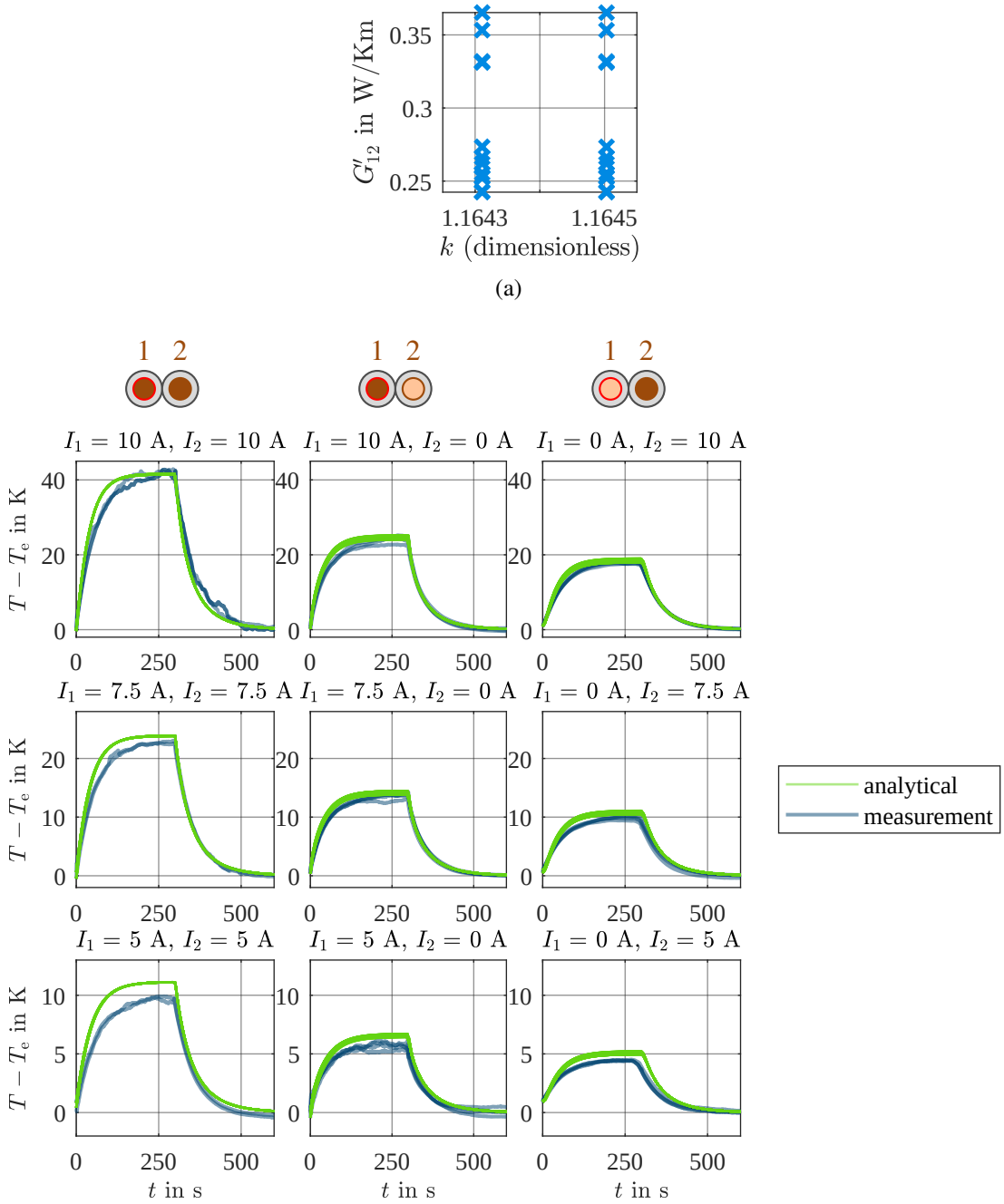

(a)

(b)

Figure 7.29: (a) Parameter pairs for two coupled single wire cables reconstructed from repeated measurements with a load current of 10 A. (b) Measured and calculated temperature developments for cable 1 for different load scenarios. All curves are plotted transparently.

sponding values. For high current loads, the measured and calculated temperatures fit well, for lower current loads the calculated values are slightly higher and can be understood as the worst case.

For the same cable arrangement (length $\mathcal{L} = 0.6\,\mathrm{m}$) and the currents $I_1 = 15\,\mathrm{A}$ and $I_2 = 0\,\mathrm{A}$, the different axial analytical solutions are compared to the solution that is derived via the function "pdepe" from MATLAB. For k and G'_{12}, the mean values from the previous analysis are used:

$$k = 1.16, \quad G'_{12} = 0.29\,\frac{\mathrm{W}}{\mathrm{Km}}. \tag{7.41}$$

The cable terminations are at the temperatures $T_{1,\mathrm{id},i} = 10\,^\circ\mathrm{C}$ and $T_{2,\mathrm{id},i} = 50\,^\circ\mathrm{C}$, $i = 1, 2$. The initial temperature for both cables and the environmental temperature are both $25\,^\circ\mathrm{C}$. For the solution via Green's functions in the time domain, one term is used in addition to the solution with approximation. The axial temperature distribution at $t = 300\,\mathrm{s}$ and the transient temperature development in the center of the cable are shown in figure 7.30 for the comparison between analytical and numerical ("pdepe") solutions. The following abbreviations are used: c1: cable 1, c2: cable 2, simp.: simplified, Lap.: Laplace, id.: identical, Gr.: Green, and iter.: iterative. In figure 7.31, the absolute deviations between the analytical and numerical solutions are shown depending on the time t and the axial coordinate z for both cables. Overall, a good agreement is observed for the first three solutions (Laplace domain solution with an approximation for two (possibly different) cables, Laplace domain solution with an approximation for identical cables, and time domain Green's functions solution for identical cables) with deviations below $1\,\mathrm{K}$ from the numerical solution. For the iterative approach based on the single wire solutions, deviations of up to nearly $15\,\mathrm{K}$ appear especially in the transient case. This is because in this solution, the temperature of one conductor is fixed for the calculation of the other conductor's temperature and thus, implicitly, the calculated temperature is assumed from the beginning. If now, for example, the conductors heat up and the temperature at $t = 50\,\mathrm{s}$ is calculated, the first guess for the first conductor temperature is used to calculate the second conductor temperature. The result will be too high because the high value for the first temperature is assumed from the start of the calculation of the second temperature. In the iterative approach, this (too high) second temperature is then used to correct the first temperature - finding a too high first temperature as well. So overall, this assumption

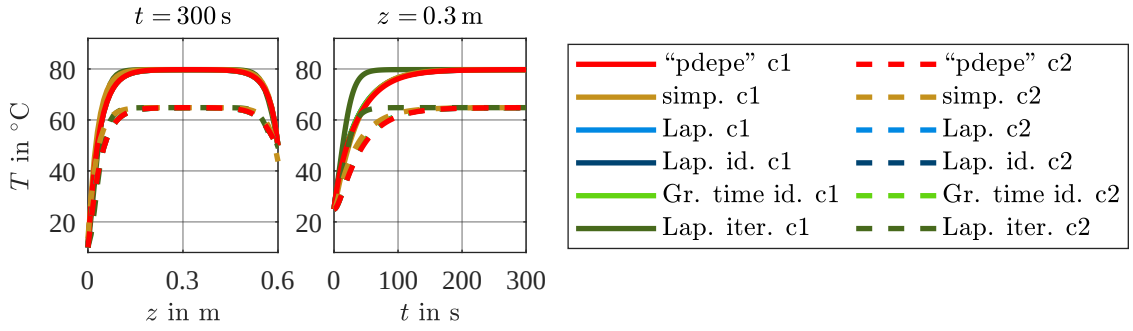

Figure 7.30: Numerically ("pdepe") and analytically calculated axial (left) and transient (right) temperatures for an arrangement of two identical single wire cables.

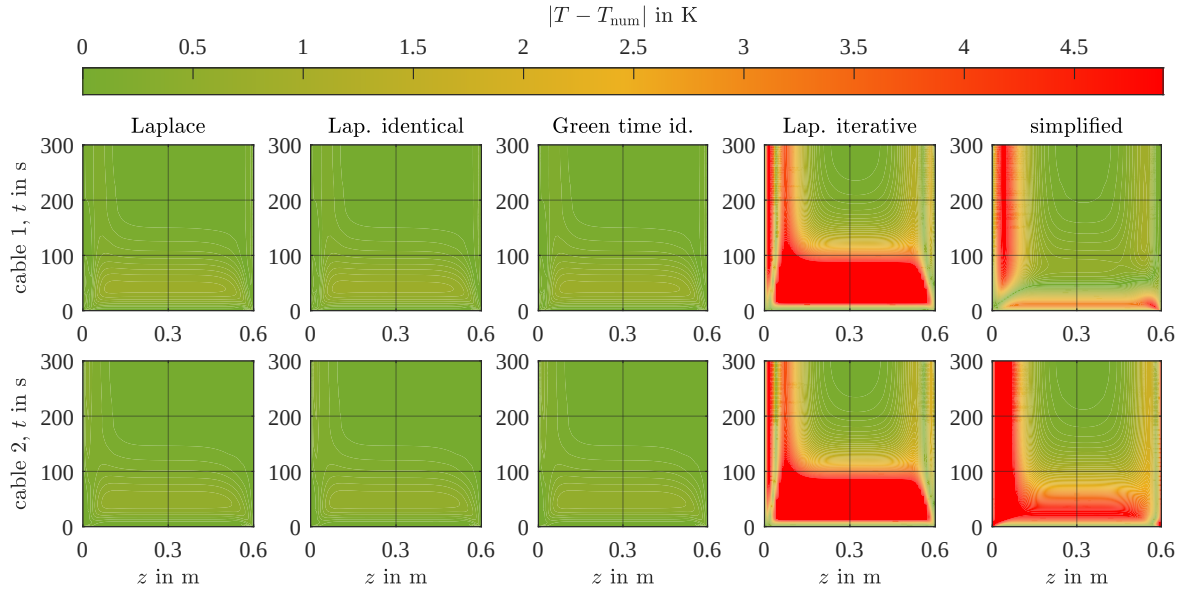

Figure 7.31: Difference between numerically ("pdepe") and analytically calculated temperatures for an arrangement of two identical single wire cables.

of a constant temperature of the second conductor causes too fast transient responses, both at heating up and cooling down. At the very beginning of the calculation, this effect reduces as then, the assumption is more reasonable. Similar effects appear for the axial coordinate z. The simplified solution leads to deviations below $5.5\,\mathrm{K}$ for the first conductor and up to $21.7\,\mathrm{K}$ for the second conductor and can only be used for the rough estimation of the first conductor temperature.

b) Different Cables

In this section, the solutions for two different coupled single wire cables are analyzed. In this case, for each cable $i = 1, 2$ a specific correction factor k_i is necessary, so

$$G'_{11} = \frac{\tilde{G}'_{11}(T_1, T_\mathrm{e})}{k_1}, \quad G'_{22} = \frac{\tilde{G}'_{22}(T_2, T_\mathrm{e})}{k_2}. \tag{7.42}$$

Again, radial steady-state temperatures are measured. Two measurements $\mathrm{m1}$ and $\mathrm{m2}$ are performed: In the first measurement, only the first cable is loaded with a current, and in the second measurement, only the second cable is loaded. By evaluating the ECD (analog to the one presented in figure 7.26), the necessary dependencies for the calculation of the parameters are derived. The complete approach is shown in figure 7.32.

This approach is used to calculate the cable parameters for an arrangement of two different twisted single wire cables. An overview of the cable parameters of the individual cables is given in table D.1, cables (5) (cable 1 in the following) and (2) (cable 2 in the following). The measured temperature developments on both cables for the two chosen load cases are

measure $T_{1,\mathrm{m1}}$, $T_{2,\mathrm{m1}}$ and $T_{\mathrm{e,m1}}$ (radial steady state for $I_1 = I$ and $I_2 = 0\,\mathrm{A}$)

↓

measure $T_{1,\mathrm{m2}}$, $T_{2,\mathrm{m2}}$ and $T_{\mathrm{e,m2}}$ (radial steady state for $I_1 = 0\,\mathrm{A}$ and $I_2 = \hat{I}$)

↓

calculate $P'_{\mathrm{el},1,\mathrm{m1}}$, $\tilde{G}'_{1,1} = \tilde{G}'_{11}(T_{1,\mathrm{m1}}, T_{\mathrm{e,m1}})$, $\tilde{G}'_{2,1} = \tilde{G}'_{22}(T_{2,\mathrm{m1}}, T_{\mathrm{e,m1}})$,
$P'_{\mathrm{el},2,\mathrm{m2}}$, $\tilde{G}'_{1,2} = \tilde{G}'_{11}(T_{1,\mathrm{m2}}, T_{\mathrm{e,m2}})$, $\tilde{G}'_{2,2} = \tilde{G}'_{22}(T_{2,\mathrm{m2}}, T_{\mathrm{e,m2}})$

↓

$$G'_{12} = \frac{1}{2}\left[\frac{P'_{\mathrm{el},1,\mathrm{m1}}(T_{1,\mathrm{m2}} - T_{\mathrm{e,m2}})\tilde{G}'_{1,2}}{\tilde{G}'_{1,1}(T_{2,\mathrm{m2}} - T_{1,\mathrm{m2}})(T_{1,\mathrm{m1}} - T_{\mathrm{e,m1}}) + \tilde{G}'_{1,2}(T_{1,\mathrm{m1}} - T_{2,\mathrm{m1}})(T_{1,\mathrm{m2}} - T_{\mathrm{e,m2}})} + \frac{P'_{\mathrm{el},2,\mathrm{m2}}(T_{2,\mathrm{m1}} - T_{\mathrm{e,m1}})\tilde{G}'_{2,1}}{\tilde{G}'_{2,2}(T_{1,\mathrm{m1}} - T_{2,\mathrm{m1}})(T_{2,\mathrm{m2}} - T_{\mathrm{e,m2}}) + \tilde{G}'_{2,1}(T_{2,\mathrm{m2}} - T_{1,\mathrm{m2}})(T_{2,\mathrm{m1}} - T_{\mathrm{e,m1}})}\right]$$

↓

$$k_1 = \frac{T_{1,\mathrm{m2}} - T_{\mathrm{e,m2}}}{T_{2,\mathrm{m2}} - T_{1,\mathrm{m2}}}\frac{\tilde{G}'_{1,2}}{G'_{12}}, \quad k_2 = \frac{T_{2,\mathrm{m1}} - T_{\mathrm{e,m1}}}{T_{1,\mathrm{m1}} - T_{2,\mathrm{m1}}}\frac{\tilde{G}'_{2,1}}{G'_{12}}$$

Figure 7.32: Calculation of G'_{12}, k_1, and k_2 for two different coupled single wire cables.

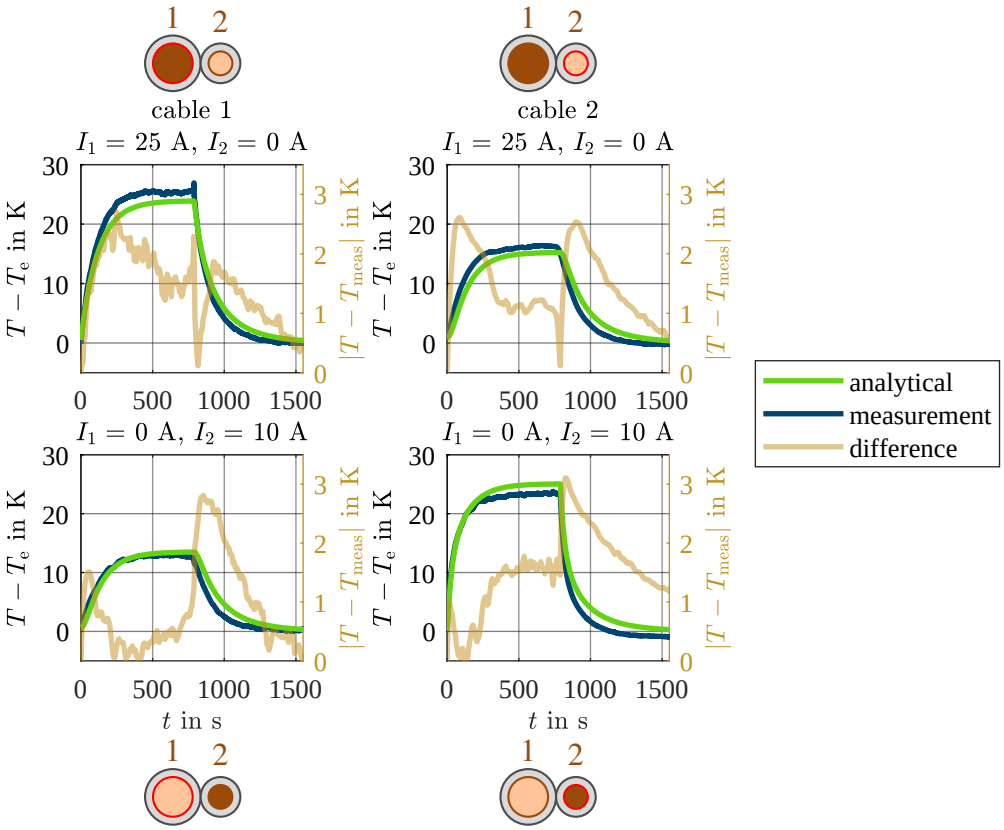

Figure 7.33: Measured (blue) and analytically calculated (green) temperature developments and differences (ochre) for different load scenarios of two different coupled single wire cables.

shown in figure 7.33 (blue curves)[12]. The steady-state temperatures are again calculated via averaging. The reconstructed parameters are

$$G'_{12} = 0.16\,\frac{\mathrm{W}}{\mathrm{Km}}, \quad k_1 = 1.27, \quad k_2 = 1.46. \tag{7.43}$$

As expected, for the smaller cable, a higher reduction factor appears as the bigger cable covers a bigger angle range than vice versa. Using these parameters, the expected temperature development is calculated analytically via the solution for an infinitely long cable. The results (difference to environmental temperature, green) and the difference between the measured and calculated temperatures (ochre) are shown in figure 7.33 in the first column for the first cable and the second column for the second cable. The difference is lower than $3.5\,\mathrm{K}$.

For the same cable arrangement, numerically and analytically calculated axial and transient temperature developments are compared for the load currents $I_1 = 40\,\mathrm{A}$ and $I_2 = 10\,\mathrm{A}$ with $T_\mathrm{e} = T_{0,\mathrm{tsw},i} = 25\,^\circ\mathrm{C}$, $T_{1,\mathrm{tsw},i} = 10\,^\circ\mathrm{C}$, $T_{2,\mathrm{tsw},i} = 50\,^\circ\mathrm{C}$, $i = 1, 2$. For the solution via Green's functions in the Laplace domain, 10 terms are considered for the sum that deals with the initial condition and the inhomogeneity and 500 terms are used in the sum that describes the boundary conditions. In figure 7.34, the axial temperature distributions and the transient temperature development in the cable center are shown for the different analytical solutions. The following abbreviations are used: $\mathrm{c1}$: cable 1, $\mathrm{c2}$: cable 2, $\mathrm{simp.}$: simplified, $\mathrm{Lap.}$: Laplace, $\mathrm{Gr.}$: Green, and $\mathrm{iter.}$: iterative. In figure 7.35, the absolute differences between analytically and numerically calculated temperatures are shown for both cables depending on the axial coordinate z and the time t. For the solution in the Laplace domain and the solution via Green's functions in the Laplace domain, the maximum deviation reaches about $2\,\mathrm{K}$. In the iterative approach based on the single wire cable, the maximum deviation is higher than $11\,\mathrm{K}$. In the simplified solution, the temperature of the first cable deviates by a maximum of about $3\,\mathrm{K}$ from the numerical result, the second cable temperature deviates up to more than $20\,\mathrm{K}$. Overall, the observed effects are quite similar to the arrangement of two identical cables from the previous section.

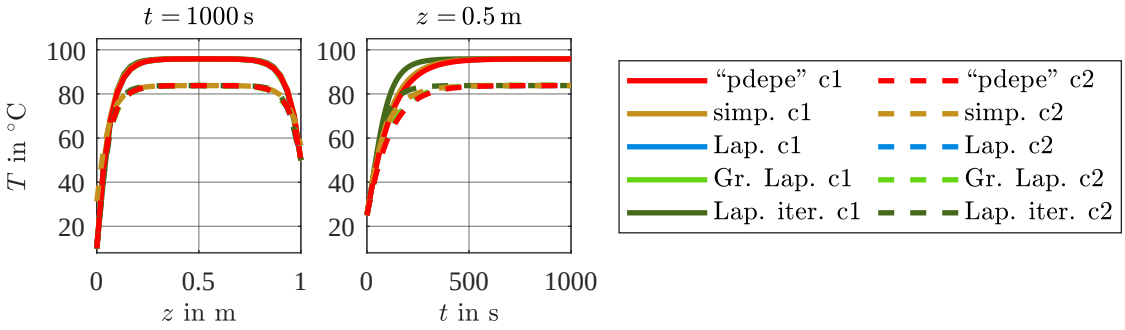

Figure 7.34: Numerically ("pdepe") and analytically calculated axial (left) and transient (right) temperatures for an arrangement of two different single wire cables.

[12]The measurements were performed by student assistant Murat Sahan.

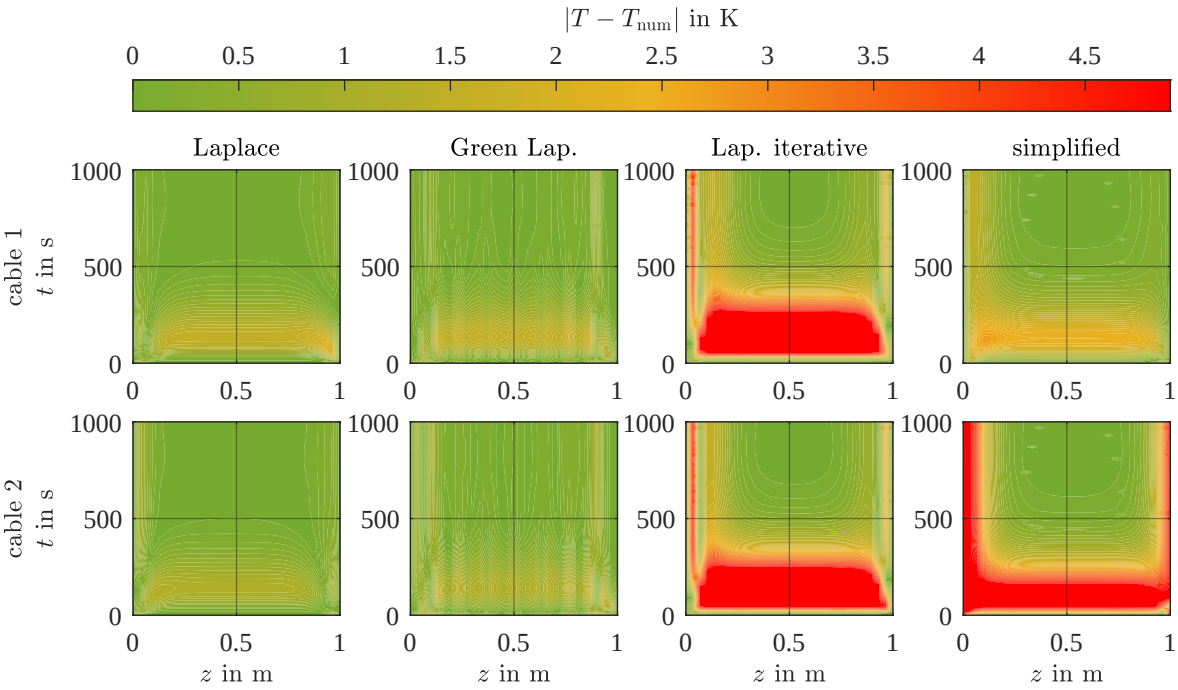

Figure 7.35: Difference between numerically ("pdepe") and analytically calculated temperatures for an arrangement of two different single wire cables.

7.3.4 Coaxial Cable

In this section, the derived analytical solutions for a coaxial cable are validated. At first, a comparison between the measured[13] and calculated radial temperature development is performed. The parameters of the analyzed cable are given in table D.4. The difference to environmental temperature for the measured (blue) and calculated (green) temperatures and the difference between those temperatures (ochre) are shown in figure 7.36. The difference is lower than $6\,\mathrm{K}$.

For the same cable, numerically and analytically calculated temperature developments are compared for the load currents $I_{\mathrm{c}} = I_{\mathrm{sh}} = 15\,\mathrm{A}$ with environmental and initial temperatures $T_{\mathrm{e}} = T_{0,\mathrm{c}} = T_{0,\mathrm{sh}} = 25\,^{\circ}\mathrm{C}$ and cable termination temperatures $T_{1,\mathrm{c}} = T_{1,\mathrm{sh}} = T_{2,\mathrm{c}} = T_{2,\mathrm{sh}} = 50\,^{\circ}\mathrm{C}$. For the solution via Green's functions in the Laplace domain, 100 terms are considered for the sum that deals with the initial condition and the inhomogeneity. The other expression is not needed due to the identical cable termination temperatures. In figure 7.37, the axial temperature distributions and the transient temperature development in the center of the cable are shown. The following abbreviations are used: $\mathrm{c.}$: conductor, $\mathrm{sh.}$: shield, $\mathrm{simp.}$: simplified, $\mathrm{Lap.}$: Laplace, $\mathrm{Gr.}$: Green, and $\mathrm{iter.}$: iterative. In figure 7.38, the absolute differences between analytically and numerically calculated temperatures are shown for the inner conductor and the shield. For the solution in the Laplace domain and the solution via Green's functions in the Laplace domain, the maximum deviation is about $1.5\,\mathrm{K}$. In the

[13] The measurements were performed by student assistant Murat Sahan.

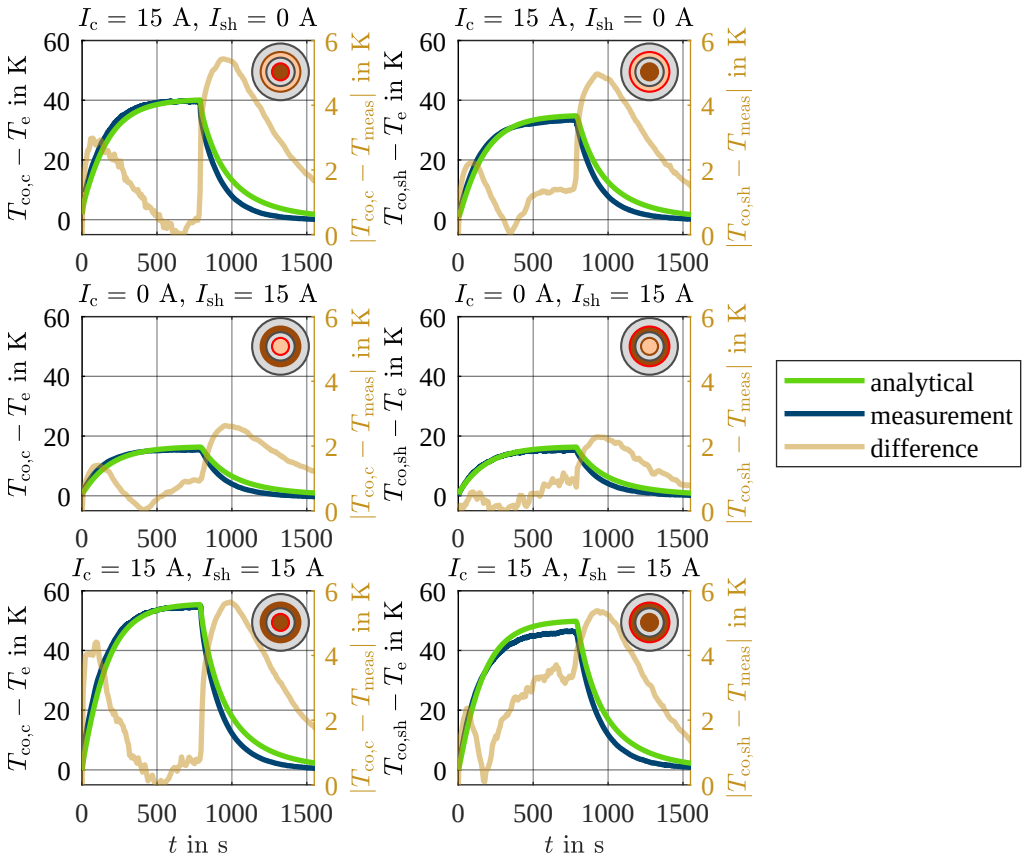

Figure 7.36: Measured (blue) and analytically calculated (green) temperature developments and differences (ochre) for different load scenarios (inner conductor and/or shield loaded with 15 A).

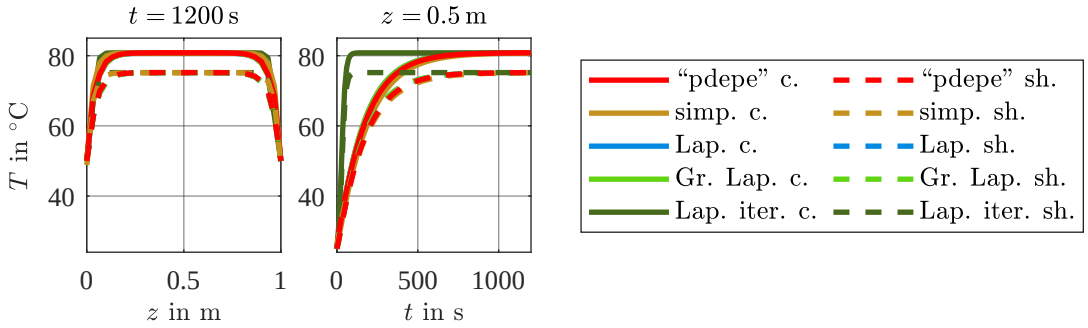

Figure 7.37: Numerically ("pdepe") and analytically calculated axial (left) and transient (right) temperatures for a coaxial cable.

iterative approach based on the single wire cable, the deviations reach values higher than 35 K. That is due to the assumptions made here: As implicitly, for the conductor temperature calculation, a constant shield temperature (and vice versa) is assumed, again, way too fast transient responses are the result. Compared to the two conductor arrangement this effect is even stronger here because the coupling between the inner conductor and shield is dominant for the inner conductor. In contrast, using the simplified solution, the temperature of the inner conductor and shield deviates by a maximum between 5 K and 7 K from the numerical

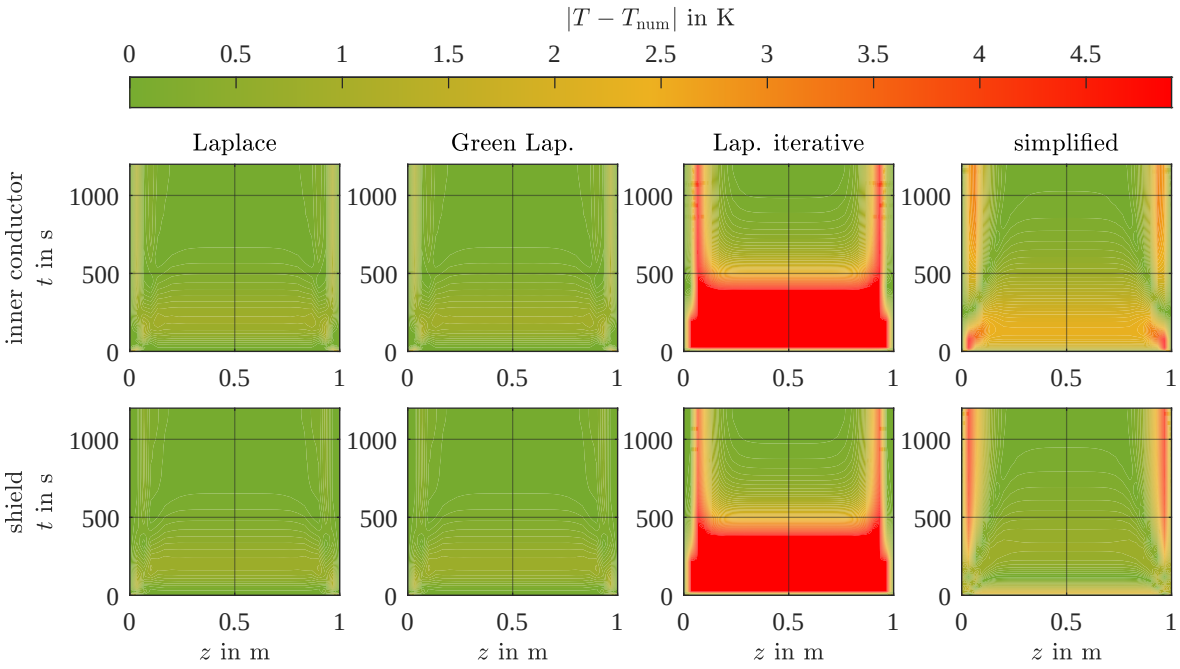

Figure 7.38: Difference between numerically ("pdepe") and analytically calculated temperatures for a coaxial cable.

result. In contrast to the case of two single wire cables, here, this approach can be used to approximate the cable temperatures.

7.3.5 Identical Single Wire Cables

In this section, the derived solutions for N identical single wire cables are validated with measurement results and a numerical solution. A twisted cable built up from three identical single wire cables is evaluated for this purpose. In the first step, again, the coupling conductances $G'_{12} = G'_{13} = G'_{23}$ have to be determined as well as the correction factor k analog to section 7.3.3.a). Due to symmetry considerations, the same procedure can be applied as before (see figure 7.27(b)). The first measurement is now performed with the same load current for all three cables (thus, $I_1 = I_2 = I_3 = I$, $P'_{\mathrm{el},1} = P'_{\mathrm{el},2} = P'_{\mathrm{el},3}$, $G'_{11} = G'_{22} = G'_{33}$, $T_{1,\mathrm{m1}} = T_{2,\mathrm{m1}} = T_{3,\mathrm{m1}}$). For the second measurement, only one cable is loaded with current ($I_1 = I, I_2 = I_3 = 0\,\mathrm{A}$, $G'_{22} = G'_{33}$, $T_{2,\mathrm{m2}} = T_{3,\mathrm{m2}}$). Then, the same equations as in figure 7.27(b) are used to find the necessary values.

The evaluated cable consists of three $2.5\,\mathrm{mm}^2$ copper cables (parameters of the individual cables see table D.1, cable (4)). Using measurements with $I = 30\,\mathrm{A}$ as described above, $k = 1.46$ and $G'_{12} = 0.15\,\mathrm{W/Km}$ are determined.

Using those parameters, in figure 7.39 the analytically calculated and measured[14] temperatures are compared for different load scenarios (first line: all cables with current $I = 30\,\mathrm{A}$, second line: two cables with current $I = 30\,\mathrm{A}$, third line: one cable with current $I = 30\,\mathrm{A}$).

[14]The measurements were performed by student assistant Murat Sahan.

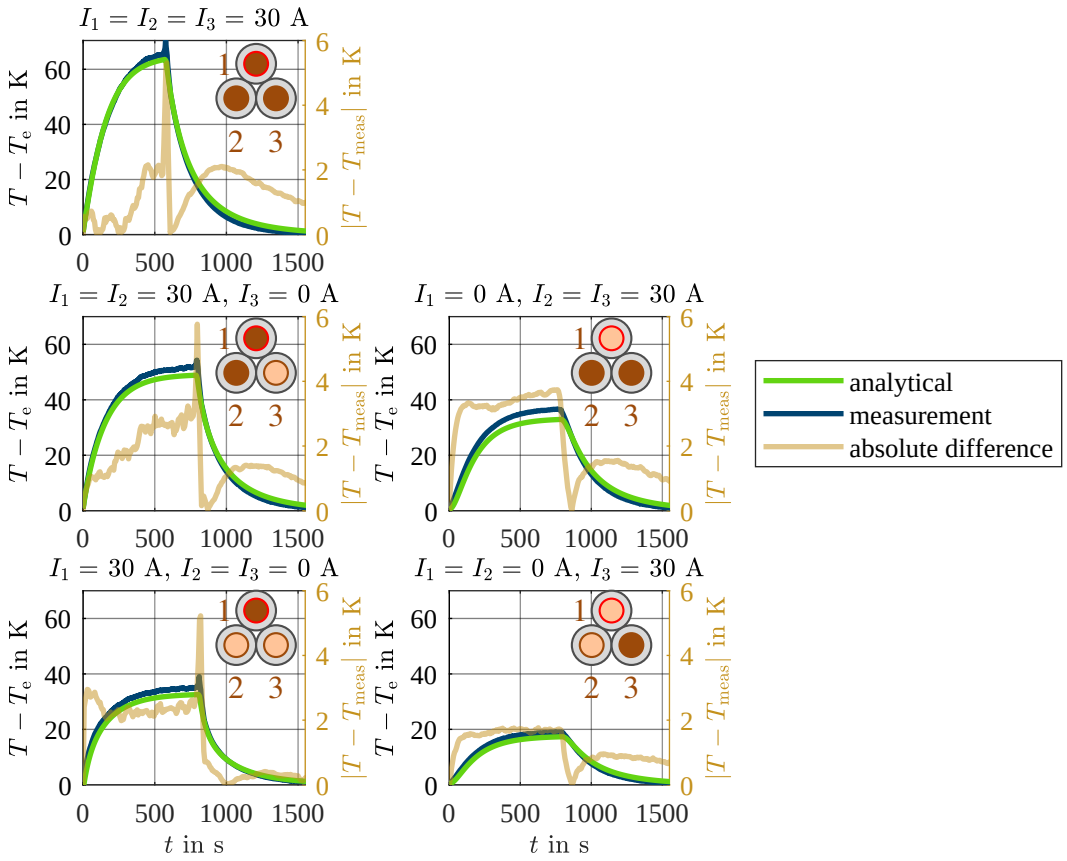

Figure 7.39: Measured and analytically calculated temperatures for cable 1 of an arrangement of three identical single wire cables under different load scenarios.

The temperature development (difference to environmental temperature, green and blue) and the absolute difference between the calculated and measured temperatures (ochre) are shown. For the cable heating up, in most cases, the differences are below $4\,\mathrm{K}$.

For the same cable arrangement and the currents $I_1 = 40\,\mathrm{A}$, $I_2 = 25\,\mathrm{A}$ and $I_3 = 0\,\mathrm{A}$, the axial analytical solutions are compared to the numerical solution (MATLAB function "pdepe"). The cable terminations are at the temperatures $T_{1,\mathrm{id},i} = T_{2,\mathrm{id},i} = 50\,^\circ\mathrm{C}$ with $i = 1, 2, 3$. The initial temperature for all three cables and the environmental temperature are both $22\,^\circ\mathrm{C}$. For the solution via Green's functions in the Laplace domain, ten terms of the sum are considered, for the solution via Green's functions in the time domain, one term is used in addition to the solution with approximation. The axial temperature developments at $t = 1000\,\mathrm{s}$ and the transient temperature developments in the cable centers are shown in figure 7.40. The following abbreviations are used: $\mathrm{c1}$: cable 1, $\mathrm{c2}$: cable 2, $\mathrm{c3}$: cable 3, $\mathrm{Lap.}$: Laplace, $\mathrm{id.}$: identical, and $\mathrm{Gr.}$: Green. In figure 7.41, the absolute deviations between the analytical and numerical solutions are given depending on the time t and the axial coordinate z. Overall, good accordance is observed. In the solution via Green's functions from the Laplace domain, an oscillation is observed that results from the sine in the solution. Using more terms of the solution reduces this effect.

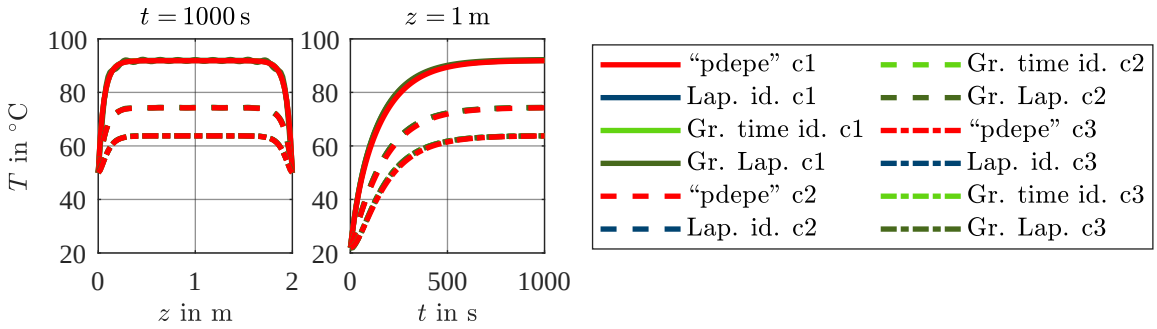

Figure 7.40: Numerically ("pdepe") and analytically calculated axial (left) and transient (right) temperatures for an arrangement of three identical single wire cables.

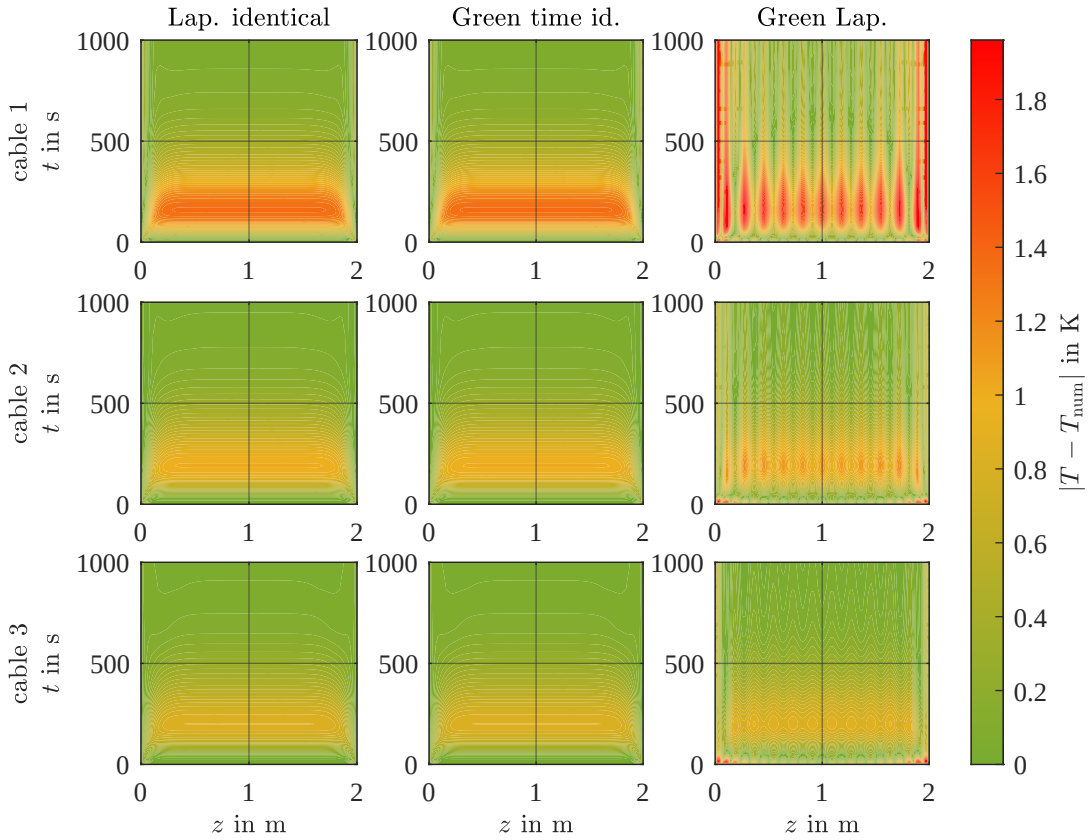

Figure 7.41: Difference between numerically ("pdepe") and analytically calculated temperatures for an arrangement of three identical single wire cables.

7.3.6 General Cable Arrangement Analog to Electrical Problem

a) Three Wire Cable

In this section, the analytical solution for the calculation of a general cable arrangement analog to the electrical problem is validated. Exemplary, an arrangement consisting of two identical single wire cables (cable 2 and 3) and a third, different cable (cable 1) is analyzed.

The unknown parameters that have to be determined by measurement are $G'_{12} = G'_{13}$, G'_{23}, k_1, and $k_2 = k_3$ due to symmetry considerations. To find those parameters, three measurements are necessary. In the first measurement, only cable 1 is loaded with a current. In the

second measurement, cables 2 and 3 are loaded with an identical current. In both cases, cables 2 and 3 have identical temperatures, which means that G'_{23} does not play any role and the corresponding temperature nodes can be summarized. Then, a formulation analog to the one for two different cables (see figure 7.32) results. Finally, a third measurement is necessary for the determination of G'_{23}. In this measurement, only cable 3 is loaded with a current. An overview of the complete procedure including the necessary calculation formulas is given in figure 7.42.

This procedure is tested with a twisted cable consisting of one $2.5\,\mathrm{mm}^2$ copper cable (cable 1, cable (5) in table D.1) and two $0.5\,\mathrm{mm}^2$ copper cables (cables 2 and 3, cable (2) in table D.1). The complete cable has a length of $2.45\,\mathrm{m}$ before the twisting and $2.24\,\mathrm{m}$ in the twisted state. The distance between the connections for the voltage measurement for the indirect temperature measurement in the cable center is $1.29\,\mathrm{m}$ ($1.23\,\mathrm{m}$) for cable one before (after) twisting, $1.25\,\mathrm{m}$ ($1.15\,\mathrm{m}$) for cable two, and $1.21\,\mathrm{m}$ ($1.10\,\mathrm{m}$) for cable three.

The measured[15] temperature developments for the different necessary load cases are shown

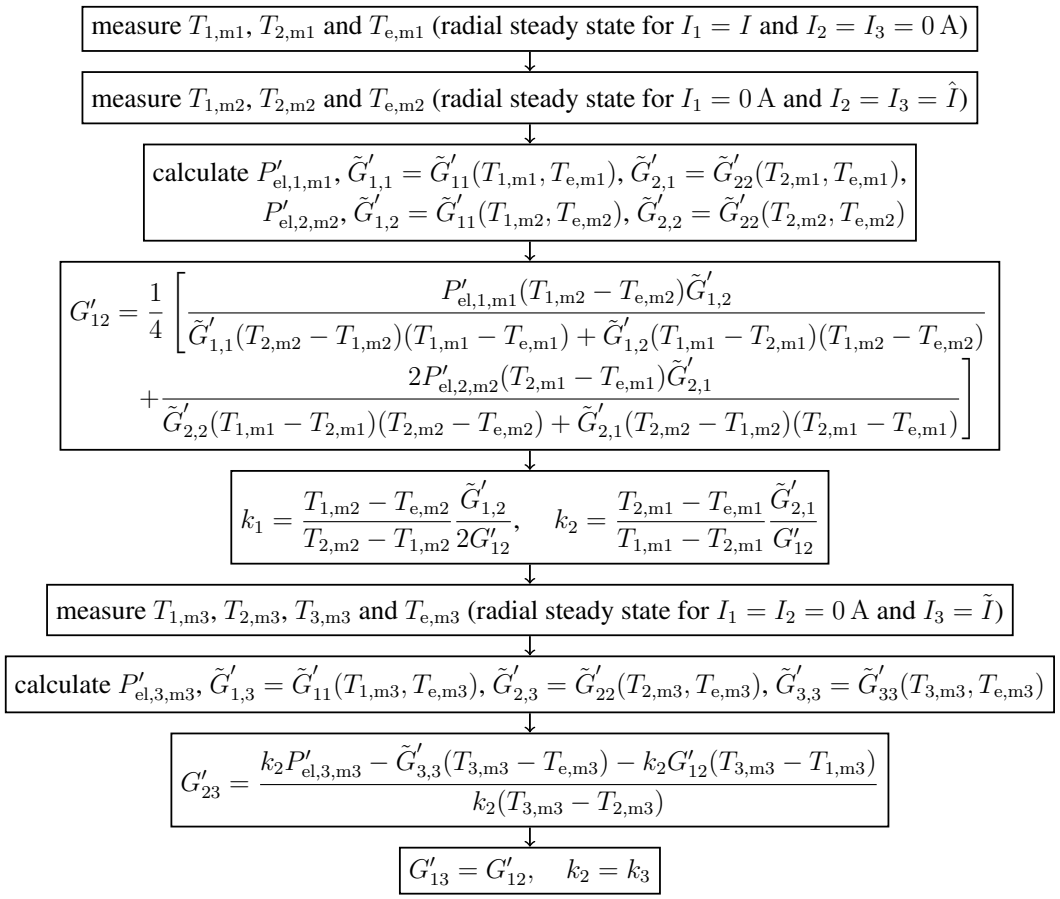

Figure 7.42: Calculation of G'_{12}, G'_{23}, k_1, and k_2 for an arrangement of two identical single wire cables and a third different single wire cable.

[15]The measurements were performed by student assistant Murat Sahan.

in figure 7.43 (blue curves). The reconstructed parameters are

$$G'_{12} = 0.13\,\frac{\mathrm{W}}{\mathrm{Km}},\ G'_{23} = 0.17\,\frac{\mathrm{W}}{\mathrm{Km}},\ k_1 = 1.55,\ k_2 = k_3 = 2.01. \tag{7.44}$$

Again, $k_2 = k_3$ is higher than k_1 because the bigger cable 1 stronger suppresses convection and radiation of the smaller cables in comparison with the other way round. G'_{23} is higher than $G'_{12} = G'_{13}$. As the insulations have thicknesses of $0.8\,\mathrm{mm}$ and $0.65\,\mathrm{mm}$, the coupling path between the two identical (smaller) cables is shorter than the one between the smaller and the thicker conductor, which is why $G'_{12} < G'_{23}$ is reasonable.

With these parameters, the transient temperature development in the central region of a long cable is calculated. The differences to the environmental temperature and the difference between the measured and calculated temperatures (ochre) are shown in figure 7.43. The difference is lower than $4\,\mathrm{K}$ in nearly all cases.

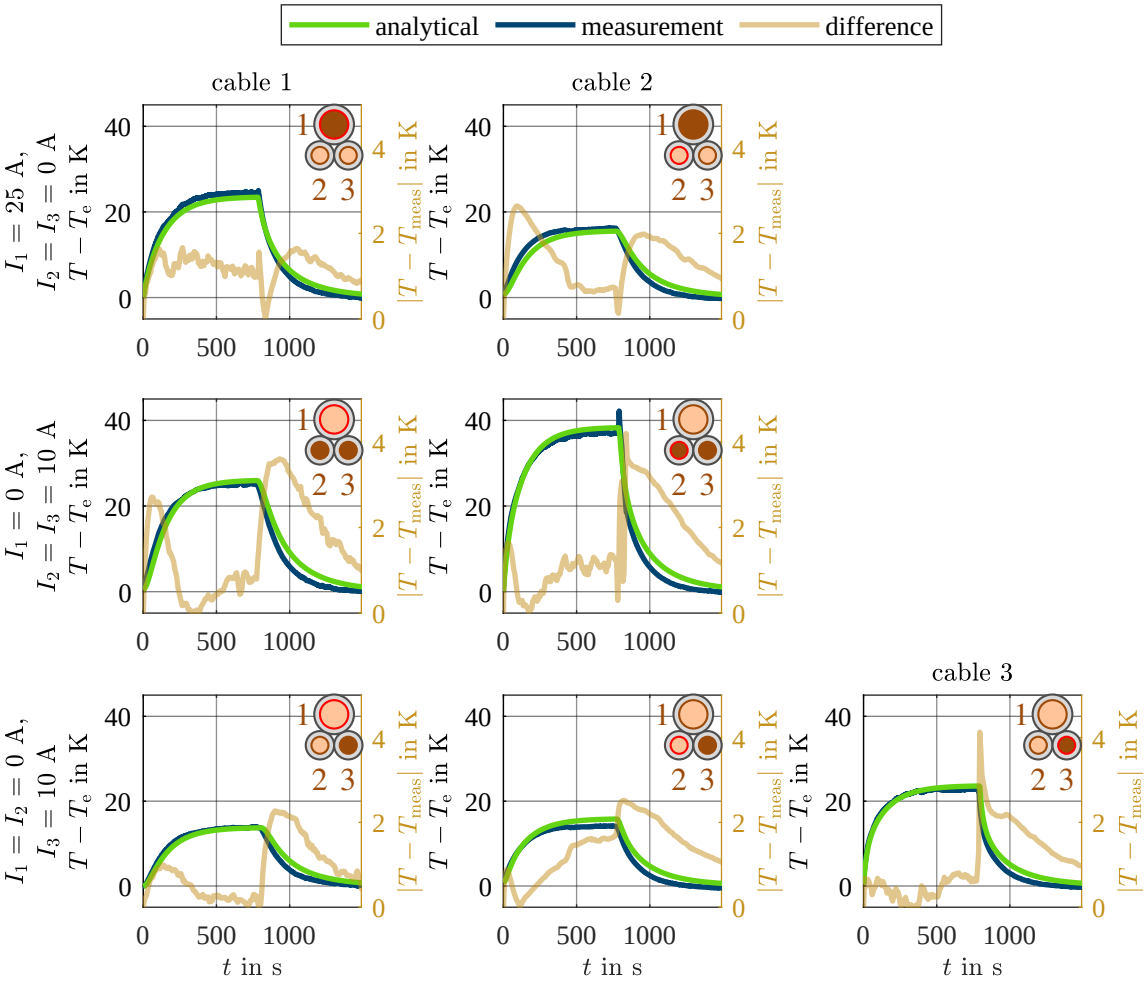

Figure 7.43: Measured (blue) and analytically calculated (green) temperature developments for different load scenarios. The absolute difference between the results is plotted transparently in ochre.

For this cable arrangement, numerically and analytically calculated axial and transient temperature developments are compared for the load currents $I_1 = 30\,\mathrm{A}$ and $I_2 = I_3 = 10\,\mathrm{A}$. The environmental temperature, as well as the initial cable temperature, is $T_\mathrm{e} = 25\,^\circ\mathrm{C}$ and the cable terminations are at the temperatures $T_{1,i} = 10\,^\circ\mathrm{C}$ and $T_{2,i} = 50\,^\circ\mathrm{C}$, $i = 1, 2, 3$. 10 terms are considered for the first sum in the solution (initial condition and inhomogeneity) and 500 terms are used for the second sum (boundary conditions). In figure 7.44, the calculated axial temperature distributions and the transient temperature development in the center of the cable are shown. The following abbreviations are used: c1: cable 1, c2: cable 2, c3: cable 3, Lap.: Laplace, Gr.: Green, st. st.: steady state, and inf.: infinitely long cable (radial). In figure 7.45, the absolute differences between analytically and numerically calculated temperatures are shown for all three cables depending on the axial coordinate z and the time t. The deviation reaches a maximum of about 7 K. As can be seen, again, an oscillating behavior is observed. This can be reduced by using more terms of the sum, which, on the other hand, leads to a higher computational effort.

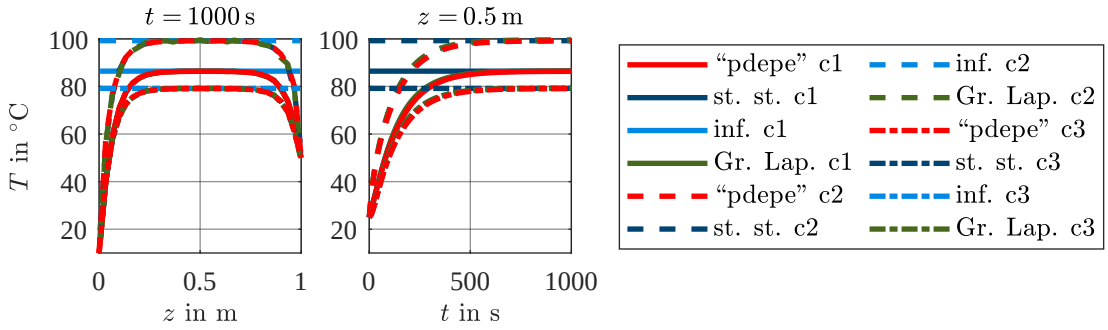

Figure 7.44: Numerically ("pdepe") and analytically calculated axial (left) and transient (right) temperatures for an arrangement of three single wire cables that are not all identical.

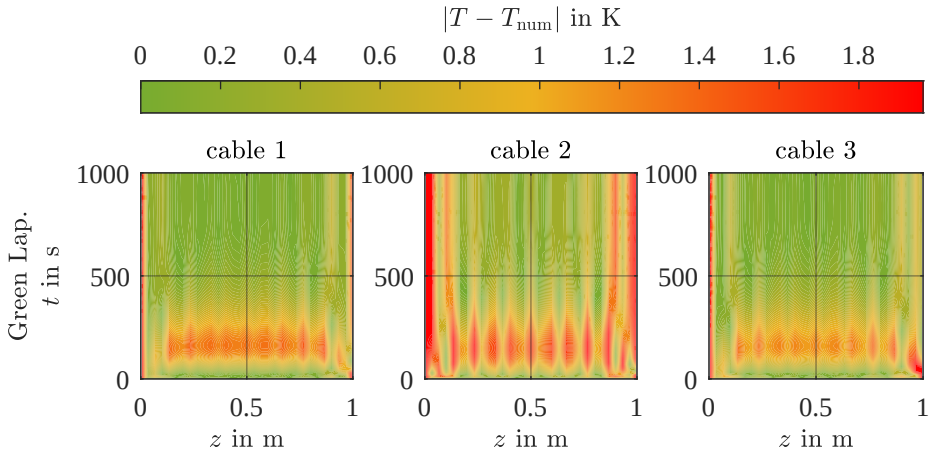

Figure 7.45: Difference between numerically ("pdepe") and analytically calculated temperatures for an arrangement of three single wire cables that are not all identical.

b) Complex Application Example

In this section, the limitations of the above-presented approaches concerning practically relevant conductor arrangements are discussed. For this purpose, the wiring harness of a VW Golf V is studied which was analyzed in [2] and [58]. This cable harness consists of 33 individual cables with common outer insulation. In [2], measured data and numerically calculated radial steady-state temperature distributions (FEM approach) are compared. The exact positioning of the cables in the bundle is relevant for the maximum occurring temperatures but is not known for the measured bundle [2]. Instead, only a template is known into which the cables are placed in the production process and then compressed. However, [2] proposes an algorithm that allows the estimation of the cable distribution in the final bundle based on this template. This results in the conductor arrangement shown in figure D.1 [2].

For this estimated conductor arrangement, a radial ECD is now constructed. For each conductor, a heat source and a capacitance are used. For the sheath, a single capacitance and a radial thermal resistance are assumed. Convection and radiation at the bundle surface are represented by a conductance, and the ambient temperature is modeled by a temperature (voltage) source. The heat flow between the individual conductors and between the conductors and the outer insulation is modeled using conductances. As a simple approximation, three constant conductances are assumed: Between two adjacent cables, the conductance G'_1 is assumed. Between the conductor and the outer insulation, the conductance G'_2 is assumed for direct contact and the conductance G'_3 for indirect contact (cable close to insulation, but not touching). Table D.7 gives an overview of the positions for these three conductance values.

The associated differential equation is determined and its radial steady-state solution is implemented. The still unknown coupling coefficients G'_1, G'_2, and G'_3 are varied with a step size of $0.05\,\mathrm{W/Km}$ between $0\,\mathrm{W/Km}$ and $1.5\,\mathrm{W/Km}$ and the differences to the measurement results from [2] are rated via the root mean square (RMS) evaluation. The best agreement is obtained for $G'_1 = 0.3\,\mathrm{W/Km}$, $G'_2 = 1.05\,\mathrm{W/Km}$, and $G'_3 = 0.5\,\mathrm{W/Km}$ with $\mathrm{RMS} \approx 2\,\mathrm{K}$. The radial steady-state temperatures calculated with this method are compared to the measured and calculated temperatures from [2] in figure 7.46(a). The differences from the measured values are shown in figure 7.46(b). Overall, there is good agreement with deviations between calculated and measured temperatures, which tend to be even lower than the deviations of the numerical solution from [2]. In contrast, the temperature differences between the different conductors are not always correctly reproduced, but a slightly smoothed temperature distribution is calculated.

The next step is to investigate whether also an axial model can be found for this problem. In the previous ECD, axial thermal resistances for the inner conductors have to be added. At this point, the sheath consideration is problematic: On its inner side, where no conductor is in direct contact, there is a capacitance. This initially results in a formulation in the

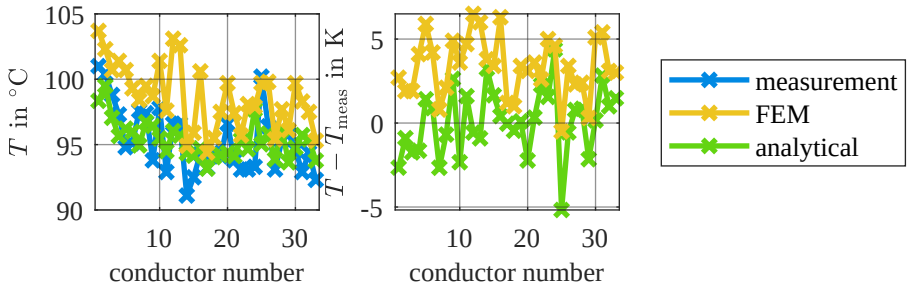

Figure 7.46: Measured and calculated steady-state temperatures for the radial transient model. Measured and numerically calculated temperatures are taken from [2]. Temperatures and differences between calculated and measured temperatures.

form according to section 5.3.2, which does not behave equivalently to the formulation from the electrical domain and accordingly cannot be treated with the methods proposed above. Therefore, it is necessary to revise the ECD so that capacitances appear only at conductors. Therefore, the capacitance of the sheath is divided among the conductors directly coupled to the insulation (n) in the ratio of the coupling strengths:

$$\hat{C}'_n = C'_n + k_n C'_{\mathrm{she}}, \qquad k_n = \frac{G'_{\mathrm{coup},n}}{\sum_{j=1}^{33} G'_{\mathrm{coup},j}}. \tag{7.45}$$

Here, $G'_{\mathrm{coup},n}$ describes the coupling between conductor n and the sheath (i.e. $G'_{\mathrm{coup},n} = 0$ or $G'_{\mathrm{coup},n} = G'_2$ or $G'_{\mathrm{coup},n} = G'_3$). In addition, the conductance for the transition between the cable surface and the environment is connected directly in series with the conductance for the coupling individually for each conductor coupled to the sheath, resulting in the overall ECD and thus the differential equation for 33 coupled single wire cables. The three unknown conductances have to be readjusted. The best agreement with the measurement results is obtained for the combination $G'_1 = 0.9\,\mathrm{W/Km}$, $G'_2 = 0.2\,\mathrm{W/Km}$, and $G'_3 = 0\,\mathrm{W/Km}$ with $\mathrm{RMS} \approx 4\,\mathrm{K}$. For this new model, the calculated radial steady-state temperatures are

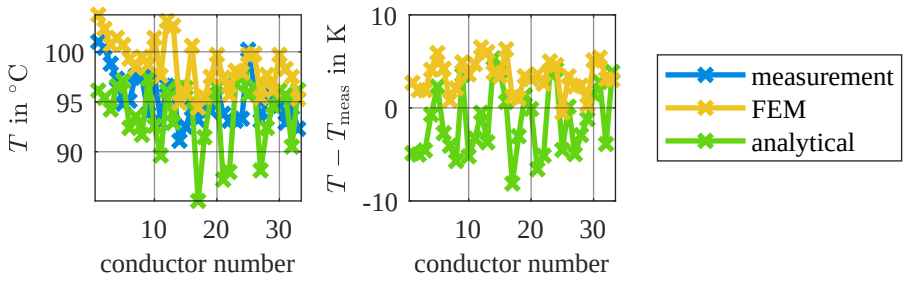

Figure 7.47: Measured and calculated steady-state temperatures for the axial transient model. Measured and numerically calculated temperatures are taken from [2]. Temperatures and differences between calculated and measured temperatures.

again compared with the measured and calculated temperatures from [2] (see figure 7.47). Compared to the previous model, larger deviations of up to $8.1\,\mathrm{K}$ show up. Nevertheless, this model can be used for a first estimation of the transient and axial behavior.

Overall, this complex practical example shows that despite only limited parameter availability, especially for the couplings, and thus, drastic assumptions (reduction to three simple adjusted parameters), an acceptable accuracy of the temperature calculations is achieved. Thus, first estimations of transient and axial processes are also possible.

7.3.7 Rectangular Pulse Excitations

In this section, the presented solutions for rectangular pulse excitations from section 6.2.5 are validated. As an example, a PVC-insulated $1.5\,\mathrm{mm}^2$ copper cable (length $\mathcal{L} = 1\,\mathrm{m}$, measured parameters $r_\mathrm{c} = 0.7\,\mathrm{mm}$, $r_\mathrm{i} = 1.5\,\mathrm{mm}$, $R'_\mathrm{ref} = 12\,\mathrm{m\Omega/m}$ at $T_\mathrm{ref} = 23.2\,^\circ\mathrm{C}$) is analyzed. If not mentioned differently, in the following, the current $I = 25\,\mathrm{A}$ is assumed to be switched on at $t = 0\,\mathrm{s}$. The environmental temperature is $T_\mathrm{e} = 22\,^\circ\mathrm{C}$, which is as well the temperature of the cable at $t = 0\,\mathrm{s}$. In addition, the cable termination temperatures are fixed to $T_1 = 10\,^\circ\mathrm{C}$ and $T_2 = 50\,^\circ\mathrm{C}$, respectively. For this cable, in the following, the different approaches for the consideration of rectangular pulse excitations are compared to the numerical solution using the MATLAB function “pdepe”. For the analytical solution, the finite solution from the Laplace domain with approximation and analytical transformation back into the time domain is used.

a) Current Step Function Profile

For the validation of the solution for a current step function profile based on [A.10], exemplarily, the current development presented in figure 7.48(a) is used ($15\,\mathrm{A}$ for $400\,\mathrm{s}$, $10\,\mathrm{A}$ for $350\,\mathrm{s}$, and $25\,\mathrm{A}$ for $250\,\mathrm{s}$). The measured and analytically and numerically calculated temperature developments and the absolute differences to the measurement results are given in figure 7.48(a), respectively. Generally speaking, the calculated values are a bit higher than the measured ones, but the maximum deviation is lower than $3\,\mathrm{K}$. Especially for the first load current, measured and calculated temperatures fit very well (deviation lower than $1\,\mathrm{K}$). Overall, the deviation between both calculated temperatures is much lower than the deviation from the measured temperatures.

In the next step, the analytically and numerically calculated axial and transient temperatures are compared. In figure 7.48(b), the analytically calculated temperatures are shown depending on the time t and the spatial coordinate z together with the absolute difference between analytically and numerically calculated temperatures in figure 7.48(c). The deviation is below $0.4\,\mathrm{K}$ for all points (z, t).

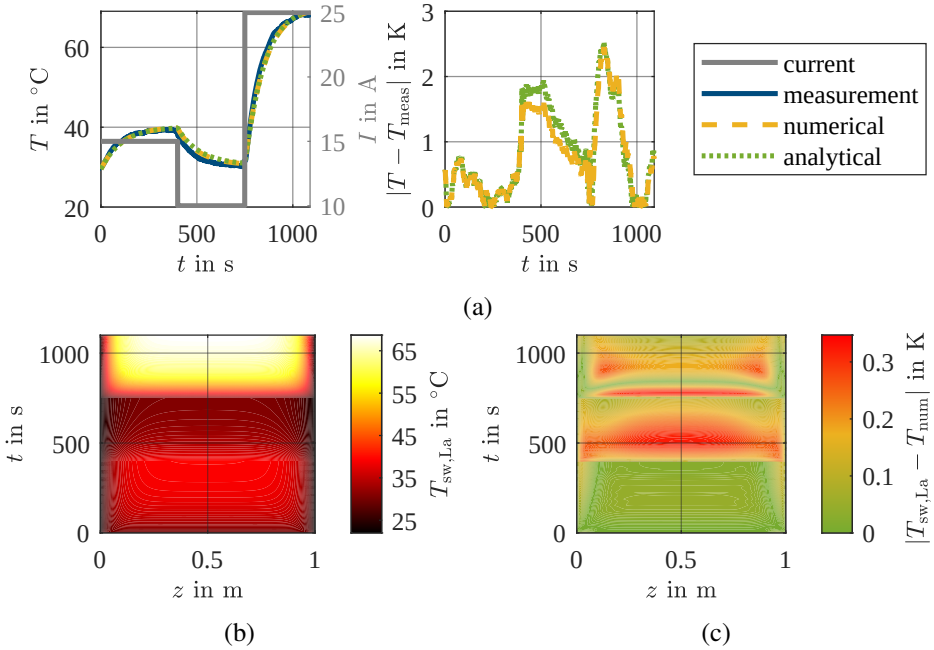

Figure 7.48: (a) Comparison between numerically and analytically calculated temperatures and measurement results (left axis) for rectangular current profile (right axis) and deviation between calculated and measured temperatures. (b) Analytically calculated cable temperature and (c) deviation between numerically and analytically calculated temperatures. The data in this figure were already published in [A.10].

b) Rectangular Cable Termination Temperature Profile

For the validation of the calculation formulas considering rectangularly shaped cable termination temperature profiles, the temperature developments shown in figure 7.49(a) are used, which were also used in [A.10]. In figures 7.49(b) and (c), the analytically calculated temperatures and the deviation between analytical and numerical solutions are presented. Close to the cable terminations and the changing points of the cable termination temperatures, in very few cases deviations over $0.5\,\mathrm{K}$ appear, but for the vast majority of points (z, t) the deviation is lower.

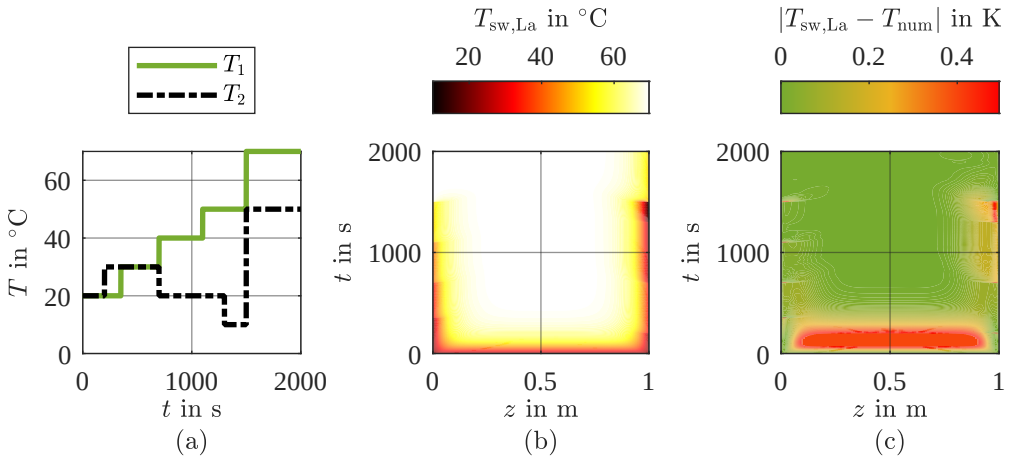

Figure 7.49: (a) Rectangular cable termination temperature profiles. (b) Analytically calculated cable temperature. (c) Deviation between numerically and analytically calculated temperatures. The data in this figure were already published in [A.10].

c) Rectangular Initial Cable Temperature Profile

In the next step, the solution for initial cable temperature profiles is validated using the profile shown in figure 7.50(a). The deviation between the analytically (see figure 7.50(b)) and numerically calculated temperature development is shown in figure 7.50(c). Overall, good accordance between both solutions is observed.

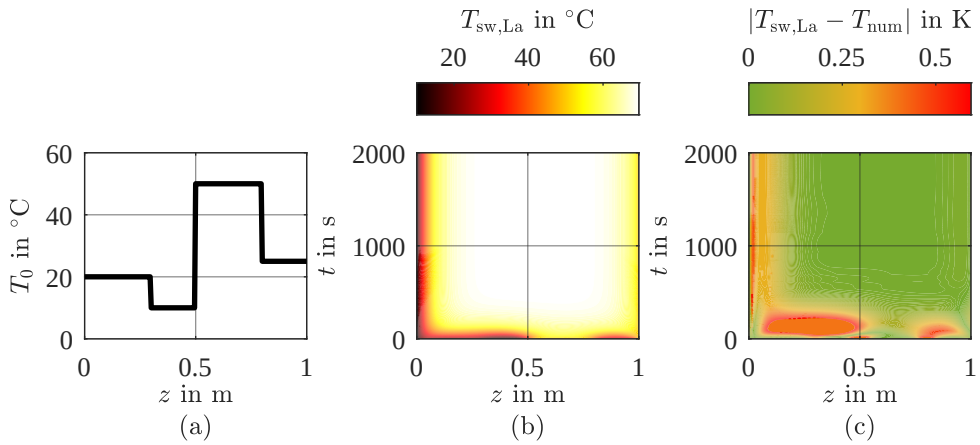

Figure 7.50: (a) Initial cable temperature profile. (b) Analytically calculated cable temperature. (c) Deviation between numerically and analytically calculated temperatures.

d) Environmental Temperature Profiles

Rectangularly Shaped Environmental Temperature Time Dependence: Using the time-varying environmental temperature shown in figure 7.51(a), the analytically calculated temperature development and the deviation between analytical and numerical solutions is shown in figure 7.51 (b) and (c), respectively, as earlier published in [A.10]. As before, very good accordance is observed for most combinations (z, t) (lower than $0.6\,\mathrm{K}$). Higher deviations appear only for some points close to the changing of the environmental temperature.

Environmental Temperature Zones: For axially varying, but temporal constant environmental temperatures, the used profile together with the analytically calculated temperature development and the absolute difference between analytically and numerically calculated cable temperatures are shown in figure 7.52. Again, only low deviations appear and all in all, good accordance is observed.

Combination of Time and Spatial Rectangular Environmental Temperature Profile: In the last step, both time and spatial varying rectangularly shaped environmental temperatures are assumed as shown in figure 7.53(a). As in the previous calculations, the difference (see figure 7.53(c)) between numerically and analytically (see figure 7.53(b)) calculated temperatures is below $1\,\mathrm{K}$ for nearly all combinations of time t and spatial coordinate z.

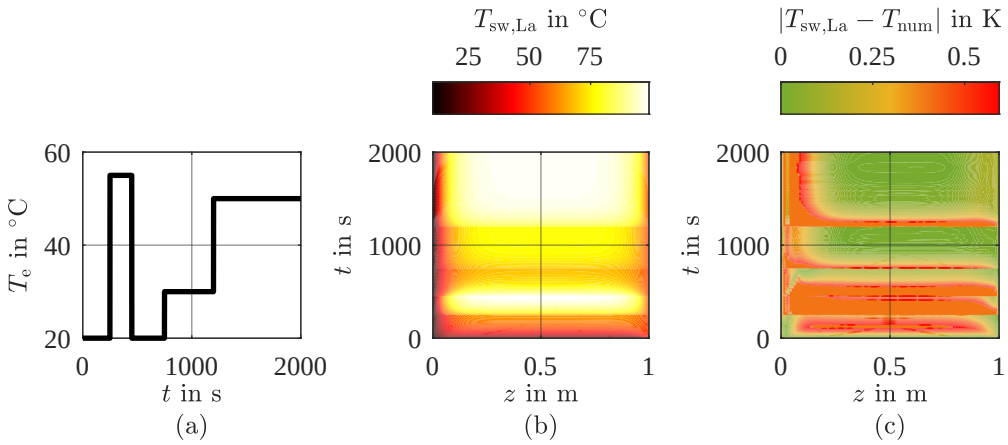

Figure 7.51: (a) Time-dependent environmental temperature profile. (b) Analytically calculated cable temperature. (c) Deviation between numerically and analytically calculated temperatures. The data in this figure were already published in [A.10].

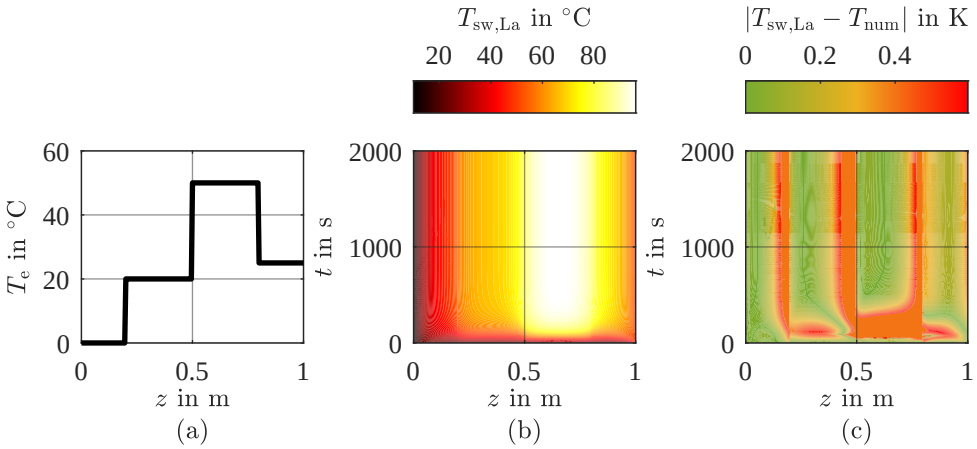

Figure 7.52: (a) Spatial environmental temperature profile. (b) Analytically calculated cable temperature. (c) Deviation between numerically and analytically calculated temperatures.

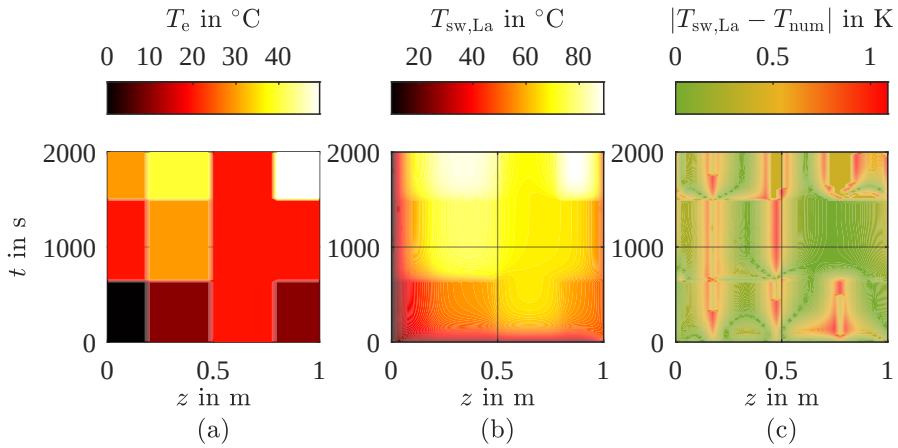

Figure 7.53: (a) Environmental temperature profile for a combination of time and spatial dependence. (b) Analytically calculated cable temperature. (c) Deviation between numerically and analytically calculated temperatures.

8 Discussion and Application Examples

In this chapter, the proposed and validated models are discussed. The model accuracies for the individual cable arrangements from the validation are compared followed by a discussion of the accuracies of the analytical solutions. In addition, a comparison is made between the new models and earlier temperature calculation methods, and an exemplary protection strategy is presented as an application example.

8.1 Model Accuracy

To analyze the basic accuracy of the modeling approach, the deviations ΔT between the analytical calculations for an infinitely long cable and the measurement results obtained via the indirect temperature measurement are first summarized for the investigations from the last chapter. The results are shown in figure 8.1. Both the temporal mean and maximum values are shown. Overall, there is a good agreement with a maximum average difference of about $3\,\mathrm{K}$ between measurement and calculation. With one exception, mean deviations of more than $2\,\mathrm{K}$ only occur for the coaxial cable. Thus, here, the selected modeling approach seems to be less accurate than for the other cable arrangements. Improvements could be made by refining the modeling, for example by taking into account that the shield is not solid. Since the temperature measurement is also not exact but can even lead to larger deviations than the observed ones according to section 7.2.1, the overall agreement between calculation and measurement is very good. The fact that the deviations are even below the expected measurement accuracy is also favored by the fact that the same measurements were simulated which were also used for parameter determination if coupled cables were involved. Taking into account the model assumptions (see section 5.2) and the measurement inaccuracies, the agreements are good overall, so the selected models are suitable for reproducing the observed effects.

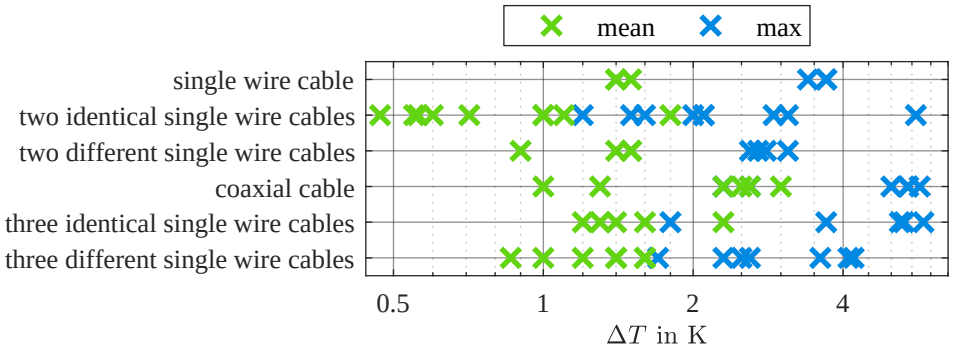

Figure 8.1: Mean and maximum values of temperature differences between analytical calculations and measurement results.

8.2 Analytical Solution Approach Accuracy

In addition to the accuracy of the modeling approaches, the selected solution methods go ahead with additional assumptions and therefore add a further uncertainty factor. To estimate the overall accuracy of the proposed calculation rules, an overview of the deviations ΔT between the numerical ("pdepe") and analytical calculation results with regard to the different solution approaches is therefore presented in figure 8.2. Again, the mean and maximum values are given. In the considered cases, using the Laplace approximation, the temperature profile can be similarly well reproduced as when using the solutions based on Green's functions. The mean deviations are below 1 K. However, as shown in section 7.3.1.d), the Green's functions-based solutions have an advantage for very short cables. Overall, the iterative solution approach, in which in each step one quantity is set constant, leads to results that are significantly worse than the results that are determined using the other solutions. In addition, the exact runtime is difficult to predict due to the additional iterations. This approach is therefore less suitable. On average, the solution via simplified ECD can predict the temperatures well for some cases. For other cases, there can also be larger deviations, so the use of this solution must be critically weighed in each individual case.

Table 8.1 gives an overview of the presented methods for the individual cable arrangements with central notes on their applicability. From the user's point of view, the assumptions made for constant initial and boundary conditions are critical for all methods, since these will rarely occur in reality and therefore, worst-case assumptions are often necessary for the calculations. A further challenge is the parameter availability for the cables as well as the initial and boundary conditions.

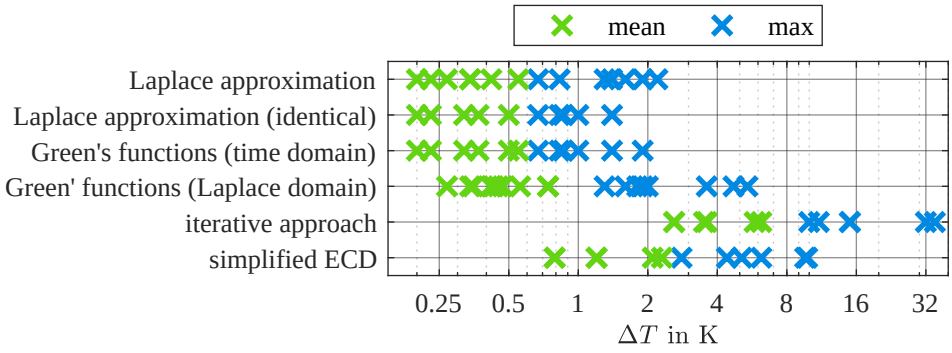

solution approach:	**sections**
Laplace approximation:	6.1.2.a), 6.1.4.c), 6.1.5.b)
Laplace approximation (identical):	6.1.6.b)
Green's functions (time domain):	6.1.2.b), 6.1.6.c)
Green's functions (Laplace domain):	6.1.2.c), 6.1.4.d), 6.1.5.c), 6.1.7
iterative approach:	6.1.4.e), 6.1.5.d)
simplified ECD:	6.1.4.f), 6.1.5.e)

Figure 8.2: Mean and maximum values of temperature differences between analytical and numerical calculations.

Table 8.1: Overview of calculation methods with hints regarding applicability.

	solution approach							
	radial steady state	**axial steady state**	**radial transient**	**Laplace domain with approximation**	**Green's functions time domain**	**Green's functions Laplace domain**	**Laplace domain-based iterative approach**	**simplified solution approach**
cable arrangement	/	boundary conditions necessary	initial condition necessary	initial and boundary conditions necessary				
single wire cable	suitable as a first approach, very fast, very simple, sufficient only for special cases or as worst case	fast, simple, spatial boundary conditions necessary, that are often difficult to determine, often worst-case assumptions, in many practically relevant cases, the additional effort is not justified by the additional information	fast, simple, practically more relevant than axial steady state, allows consideration of transient effects	approximation not very precise for short cables	flexibly extendable for short cables	flexibly extendable for short cables, convergence problems for boundary conditions		
two single wire cables / coaxial cable				complicated, practically often not applicable due to complexity			very unprecise, practically not relevant, especially in the transient area	can be used as a first approach (only for the temperature of the first cable in the case of two single wire cables)
identical single wire cables				matrix-vector formulation, manageable complexity	flexibly extendable for short cables	(not explicitly shown, but the solution from the general cable arrangement is applicable)		
general analog to the electrical problem						very general applicability, flexibly extendable for short cables, convergence problems for boundary conditions		

Overall, the proposed methods can therefore currently only be used for special applications. A large-scale application is possible in principle, but due to the necessary worst-case assumptions, some potential advantages of a direct temperature calculation (for example higher accuracy) cannot be fully exploited.

8.3 Comparison of New Models with Literature Approaches for the Single Wire Cable

In this section, the new temperature calculation rules are compared with the approaches that are given in the literature. The methods of this thesis do not result in fundamentally new model accuracies or modeling possibilities. Thus, the overall calculation results are not better than the results of previous models, e.g. in terms of accuracy. Nevertheless, this thesis focuses on new aspects that have not yet been widely used.

This includes on the one hand the joint consideration of axial and transient effects in a single model. Previous models that consider these two effects together are mostly based on numerical approaches [30, 54, 57, 59, 180–185]. Not all of these sources specifically describe cable temperatures. For example, single-walled carbon nanotubes are described in [180] and interconnects in [181]. An analytical consideration of the axial and transient heat propagation processes can be found, for example, in [186], although no cables are modeled here either. In this respect, analytical or semi-analytical calculation rules for the axial transient temperature development in cables are new in this thesis.

On the other hand, this thesis provides a discussion of similarities between electrical and thermal domains. Thus, the understanding of thermal propagation processes analogous to the electrical domain in terms of similarities and differences has been discussed in more detail than in the literature (see, for example, [133, 181, 187, 188]). The focus is on other aspects of the still complicated relations describing thermal effects on cables. In addition to the well-known specifically thermal methods, new methods can thus be applied to the thermal domain.

In earlier research, mostly numerical models were used to accurately describe temperature distributions. In contrast, this thesis focuses on analytical models. This simplifies parameter studies and accelerates computations. An implementation using simple hardware for the monitoring of critical systems is also enabled. In principle, some simplifying assumptions were necessary for this thesis, not all of which are required in numerical approaches. In this respect, a suitable analytical approach cannot be provided for all practically relevant applications. However, the proposed approaches can be used for many relevant cases, in which some quantities may not be known exactly. An example of such parameter studies is presented in appendix E. There, systematic effects are studied using many temperature calculations for different cables. Based on this, local and temporal characteristic cable quantities are defined,

which enable the normalization of temperature curves. Thus, a comparison between different temperature developments is possible independent of the cable size. To derive these relationships, the corresponding temperature curves are calculated for a wide variety of cables. Using numerical methods the effort of these calculations would be enormous. The use of analytical approaches allows the corresponding variations in a much lower time.

In summary, no methods have been proposed for the single wire cable that can provide different results than already known methods. However, the semi-analytical calculation formulas are new, which leads to less computational effort and is thus more flexible to use.

8.4 Comparison of New Models with Literature Approaches for Multiconductor Arrangements

In this section, the new methods for multiconductor arrangements are compared with the earlier approaches. Thermal models for bundles were already developed in the past, see e.g. [23, 58–61, 81, 85, 102–107]. Often, these models are based on simplifying assumptions or result in complicated relationships. Motivated by the analogy between the electrical and thermal domains, this thesis focuses on a formulation in matrix-vector form, which describes the corresponding relationships clearly and elegantly. The matrix-vector formulation of the problem that was found via the presented generalized approach for the description of the thermal problem for multiconductor arrangements allows the application of simple numerical methods for the solution, see e.g. Euler's method, for the linearized case. A superimposed iteration as also for the analytical solutions can be used to consider the nonlinearities. In contrast to 3 D discretized models, much simpler solutions become available that cause less implementation effort. Such a solution is exemplarily applied at the end of this chapter for the protection of a **p**ower **o**ver **d**ata **l**ine (PoDL) cable.

In the past, often massively simplifying assumptions regarding the geometry of the described conductor arrangement were made when creating thermal models. Very often, it is assumed that the cable is laid freely in the air. This assumption is also used throughout this thesis. Since the modeling of coupled multiconductor arrangements is often very complicated, so far mainly single conductors were considered, and bundle models only rarely occurred. In addition, it is often neglected that the modeled conductor is not solid but is composed of many individual strands. These two approximations will be investigated in detail in the following by applying the presented methods. First, the error of the estimated temperature is analyzed if only a single wire cable in the air is modeled instead of an arrangement consisting of two single wire cables. In the next section, the influence of the strands on the cable temperatures is evaluated.

8.4.1 Comparison Between Single Wire Cable and Two Single Wire Cables

In this section, the influence of the second cable on the conductor temperatures is systematically analyzed. Since this is expected to depend on the coupling strength between the two cables, it is first investigated within which bandwidth this coupling strength ranges by using an example. Based on this, systematic comparisons between the expected single wire cable and twisted pair cable temperatures follow.

a) Parameter Range

As shown in section 7.3.3.a), the parameters k and G'_{12} can be determined from measurements. To estimate their variation, two twisted pair cables are constructed from $0.14\,\mathrm{mm}^2$ cables (identical to the one that was also used in section 7.3.2, parameters see table D.5). One of the wires is only loosely twisted, and the other one is tightly twisted. A photo of a short section of these two cables can be found in figure 8.3. Before twisting, the individual cables each have a length of $1.6\,\mathrm{m}$. The associated geometrical parameters after twisting are listed in table D.6. These two cables are loaded for $300\,\mathrm{s}$ with a current of $I = 6\,\mathrm{A}$ through one or both cables. The measured differences to the environmental temperature are presented in figure 8.4.

Based on these results, the second method from section 7.3.3.a) (see figure 7.27(b)) is used to estimate the associated parameters. For the loosely twisted cable, $k = 1.31$ and $G'_{12} = 0.19\,\mathrm{W/Km}$ are obtained, and for the tightly twisted cable, $k = 1.29$ and $G'_{12} = 0.31\,\mathrm{W/Km}$ are found. A comparison with the parameters determined in section 7.3.3.a) (see figure 7.28) shows that values of k can also occur closer to 1 and that G'_{12} can vary

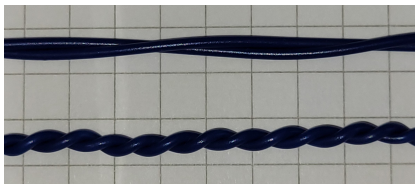

Figure 8.3: Photo of a section of the two twisted pair cables.

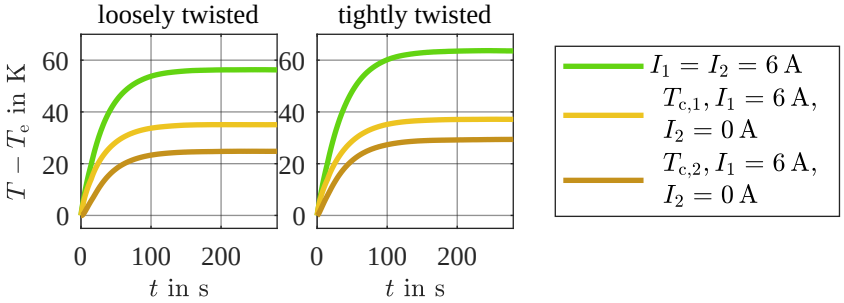

Figure 8.4: Measurement results for the two twisted pair cables.

over a larger parameter range. Therefore, values of k between 1 and 1.4 and G'_{12} between $0.05\,\mathrm{W/Km}$ and $1\,\mathrm{W/Km}$ are considered in the following.

b) Comparison

The influence of a second single wire cable twisted with the first one is analyzed in this section. For this purpose, the expected temperature curve for a single wire cable is compared with the temperatures of two twisted single wire cables using an identical current load (in one or both conductors). As an example, such curves are shown in figure 8.5 for a twisted pair cable (parameters of individual cables as above) with the mean values of the metrologically determined coupling parameters, i.e. $k = 1.3$ and $G'_{12} = 0.25\,\mathrm{W/Km}$. For a current of $6\,\mathrm{A}$, it can be seen that in the case of the twisted pair cable, the reached temperatures are higher than for the single wire cable if the current flows through both conductors. If only one conductor is loaded, lower temperatures result compared to the single wire cable. This effect is systematically investigated in the next step.

For this purpose, for conductor cross-sections between $1\,\mathrm{mm}^2$ and $120\,\mathrm{mm}^2$ (parameters see table D.3), currents are selected in each case so the radial steady-state single conductor temperatures $50\,^\circ\mathrm{C}$, $85\,^\circ\mathrm{C}$, $105\,^\circ\mathrm{C}$, or $140\,^\circ\mathrm{C}$ are achieved at ambient temperatures $20\,^\circ\mathrm{C}$ and $85\,^\circ\mathrm{C}$, respectively, using only the two higher temperatures for $T_\mathrm{e} = 85\,^\circ\mathrm{C}$. The relative deviations of the radial steady-state temperatures resulting from the different loading cases for the twisted pair cable from the radial steady-state single wire temperature are analyzed:

$$\Delta T_\mathrm{rel} = \frac{T_\mathrm{tsw} - T_\mathrm{sw}}{T_\mathrm{sw} - T_\mathrm{e}}. \tag{8.1}$$

In figure 8.6, the mean values of the calculated results are shown in bold. The range of results (minimum and maximum values) is indicated by the transparent tube. In figure 8.6(a), the dependence on G'_{12} is investigated for the constant value $k = 1.3$. For equal current load in both conductors (green), no dependence on G'_{12} is shown as expected, since no heat flow occurs between the two conductors due to the same temperature in both conductors. Larger couplings in the case of only one loaded conductor cause the temperatures of the two

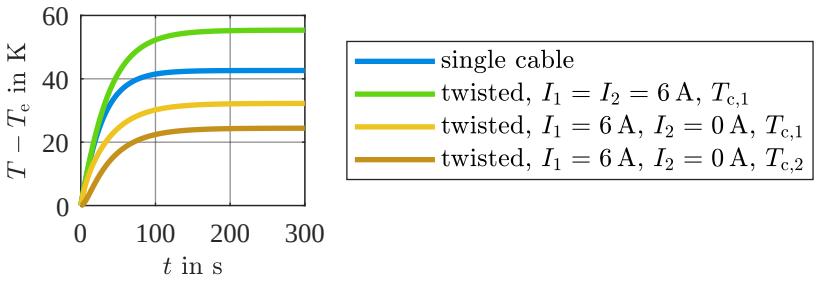

Figure 8.5: Exemplary calculated radial transient temperature developments for a single wire cable in contrast to two single wire cables.

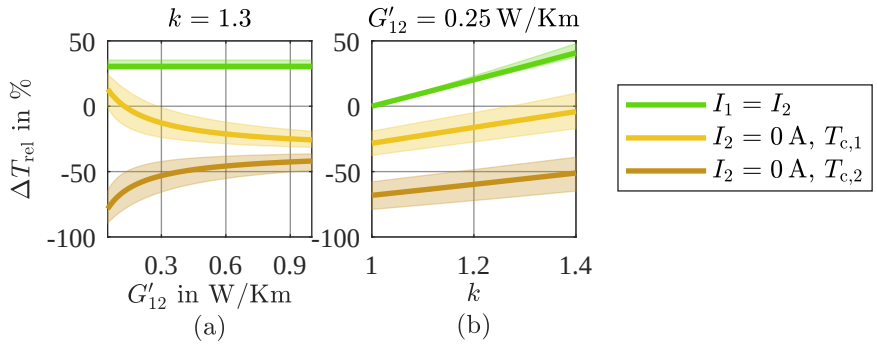

Figure 8.6: Relative temperature deviation depending on (a) G'_{12} and (b) k.

conductors of the twisted pair cable (yellow and ochre) to get closer together. The second (unloaded) conductor cools the loaded conductor on the one hand. On the other hand, the heat dissipation to the environment is reduced (mediated by k). In the case of very poor coupling between the two conductors, the reduction of the heat dissipation to the environment dominates, resulting in a higher conductor temperature overall than in the single conductor case. For larger couplings, the improved heat dissipation via heat conduction through the second conductor dominates. In figure 8.6(b), for the fixed value $G'_{12} = 0.25\,\mathrm{W/Km}$ an analog investigation is performed to determine the dependence on k. Overall, it can be seen here that increasing values of k lead to increased conductor temperatures in all cases, as expected, because this means a deterioration of the heat dissipation to the environment.

In conclusion, it is noted that the appearing temperatures of a single wire cable and a twisted pair cable can significantly differ, so only the consideration of a single wire cable freely in the air is not sufficient for a twisted pair cable. For the correct modeling of the influence of the second single wire cable, the cable parameters have to be known, especially the parameters describing the coupling. As the arrangement of two single wire cables is the simplest case of a multiconductor arrangement, also the smallest deviations from the simple single wire cable appear. Nevertheless, it was shown, that these deviations can be relevant. So, for the general case of a multiconductor arrangement, even higher deviations can appear if only the single wire cable is considered, and thus, for accurate temperature estimations, always the bundle has to be taken into account.

8.4.2 Comparison Between Solid Conductor and Stranded Conductor

In the literature, solid conductors are often assumed and the influence of the individual strands on the temperatures is not considered. In this thesis, this influence has so far only been considered by a rough parameter adjustment (see section 7.3.1.b)) but has not yet been systematically analyzed. This will be done in this section. The measurement of the temperature curves for the individual strands is extremely complicated. Therefore, a computational model based on the models for identical conductors is used instead, which allows estimations and parameter studies.

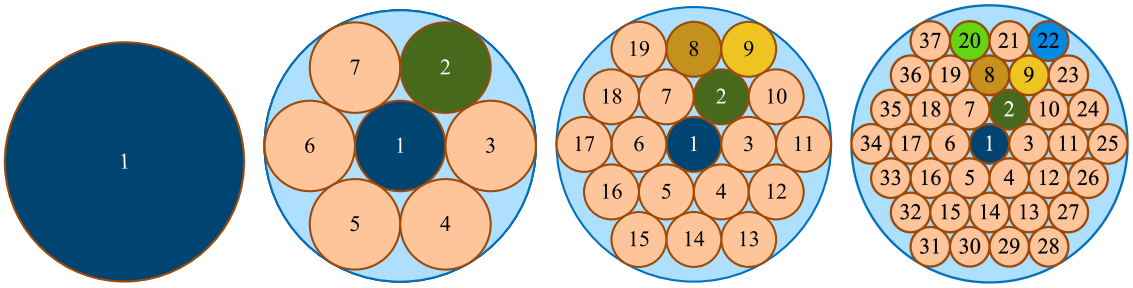

Figure 8.7: Cross-sections of the four analyzed cables with different strand numbers, from left to right cable one to cable four. Colored strands are analyzed in the following (others behave in the same way due to symmetry considerations).

In this section, common insulation around all strands is not considered. Instead, only the metal strands themselves are modeled. As an example, the four configurations shown in figure 8.7 are considered: In addition to one solid conductor, arrangements of 7, 19, and 37 strands with the same total copper cross-section as the one solid conductor are considered. Those strands are arranged in an idealized manner, in the form of the tightest packing. This ideal arrangement is thus closest to a solid conductor. For real systems with non-ideal arrangements, larger effects are to be expected than described in the following.

a) Parameter Range

To set up a suitable model for these conductor arrangements, a length-related conductance is required that describes the direct coupling strength between two adjacent strands. This cannot directly be measured, since the individual strand temperatures cannot easily be measured. Therefore, a rough estimate of the possible magnitudes is given here. For the arrangement of two (insulated) single wire cables, the value $G'_{12} = 0.6\,\mathrm{W/Km}$ was determined in section 7.3.3.a) as the maximum coupling conductor value. Here, the coupling was mediated via an insulation layer. In the case of directly adjacent individual strands, a much stronger coupling is therefore expected, even if these are coated. In the further course, the value $G'_{12} = 1\,\mathrm{W/Km}$ is therefore used as a minimum limit value for the parameter space. To determine a maximum value, the procedure for coupling resistance calculation from [106] is applied. Setting the outer cable radii to r_c leads to

$$G'_{12} = \lambda_\mathrm{c}\sqrt{\frac{\varepsilon}{r_\mathrm{c}}}, \quad \varepsilon = 2r_\mathrm{c} - 2\sqrt{r_\mathrm{c}^2 - h^2}. \tag{8.2}$$

Unlike in the rest of this thesis and the overview of mathematical symbols, ε is defined as in [106]. If an overlap is assumed in the entire "viewing angle" of two identical strands (i.e. over an angle of $\pi/6$), it is:

$$\tan\left(\frac{\pi}{6}\right) = \frac{h}{r_\mathrm{c}} \quad \Rightarrow h = \frac{r_\mathrm{c}\sqrt{3}}{3} \tag{8.3}$$

$$\Rightarrow \varepsilon = 2r_\mathrm{c}\left(1-\sqrt{\frac{2}{3}}\right) \quad \Rightarrow G'_{12} = \lambda_\mathrm{c}\sqrt{2\left(1-\sqrt{\frac{2}{3}}\right)}. \tag{8.4}$$

With $\lambda_\mathrm{c} = 386\,\mathrm{W/Km}$ it follows $G'_{12} = 234\,\mathrm{W/Km}$. Therefore, in the following, $G'_{12} = 250\,\mathrm{W/Km}$ is used as the maximum value.

b) Parameter Studies

Using an exemplary copper cross-section of $1.5\,\mathrm{mm}^2$ and a total current of $33\,\mathrm{A}$, the temperature development is investigated for environmental, initial, and termination temperatures of $25\,^\circ\mathrm{C}$. In the case of several strands, the total current is divided equally among all strands without taking into account displacement effects. A transition conductance between the strand and the environment is only determined for the outer strands. In total, for this coupling, a circle is used which encloses the outer strands (see the blue circle in figure 8.7). For this circle, R'_α, i.e. the influence of radiation and convection, is determined as shown in section 5.2.2. This total conductance is then distributed among the surface strands in a way that takes into account that for some strands four of the six potential neighboring places are occupied but for others only three. The result are factors of $1/6$ (7 strands), $2/30$ or $3/30$ (19 strands), and $2/42$ or $3/42$ (37 strands). For $G'_{12} = 3\,\mathrm{W/Km}$, the transient temperature profiles of the individual strands are calculated. The results can be found in figure 8.8 for all four cables. Zooms close to the steady state are shown in the second line. For symmetry reasons, only the marked strands are analyzed (see figure 8.7). In particular, a comparison of the solid conductor with the other cables shows a significant reduction in the occurring temperatures of about $10\,\mathrm{K}$. The temperature differences within the bundle itself are comparatively small ($< 1\,\mathrm{K}$).

In the next step, only those temperatures are considered which appear in the long term in the middle of a long cable. For this purpose, the radial steady-state solution (see section 6.1.1.a)) is used. First, the occurring strand temperatures are plotted as a function of G'_{12}. The results are given in figure 8.9: The strand temperatures depend on the number of strands. The size of G'_{12} determines how far apart the different strand temperatures are, whereby the conductor temperatures in one cable differ by less than $1\,\mathrm{K}$ in the investigated cases.

The maximum occurring strand temperatures together with the mean value over all strand temperatures in one cable and the difference ΔT between maximum and minimum strand temperature are shown in figure 8.10 for the four cables as a function of G'_{12}. Deviations of about $10\,\mathrm{K}$ occur in both the maximum and average temperature values comparing the solid conductor to the stranded conductor. The difference between the minimum and maximum strand temperature in the bundle, on the other hand, is much smaller. Overall, the influence of the exact coupling strength is comparatively small. For the total temperatures that are formed, rather the total dissipated heat and thus the modeling of the coupling of the outer

strands to the environment plays the decisive role.

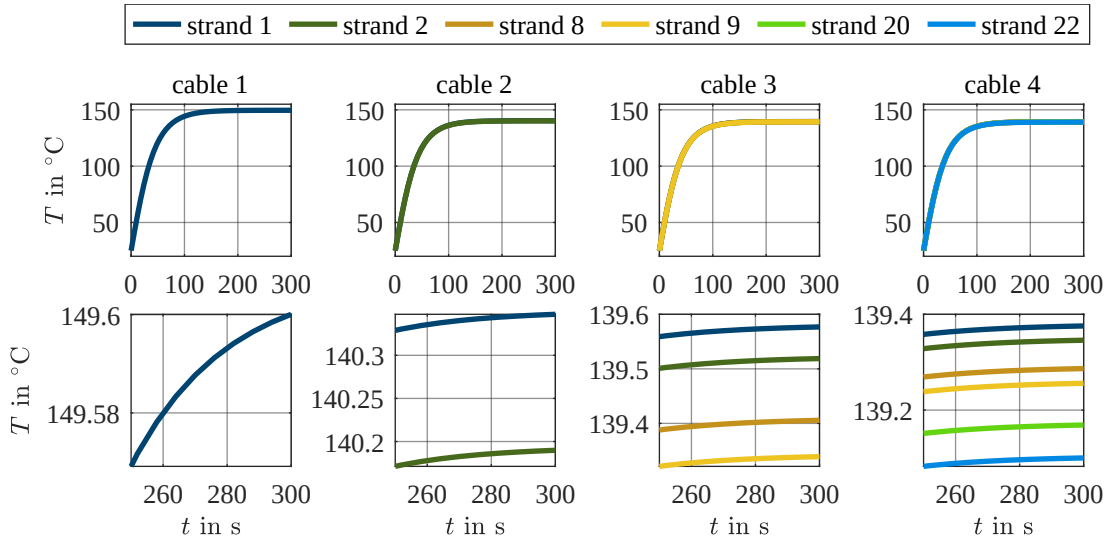

Figure 8.8: Temperature developments for the four stranded conductors with zoom to the steady state (second line).

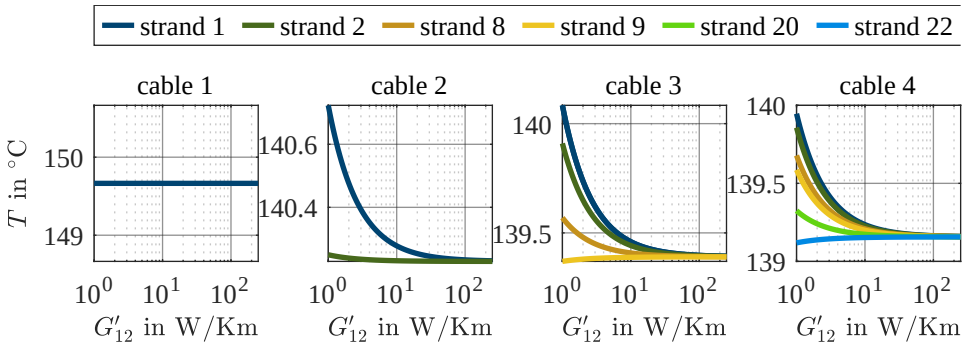

Figure 8.9: Steady-state strand temperatures of a long cable for the four different cables depending on G'_{12}.

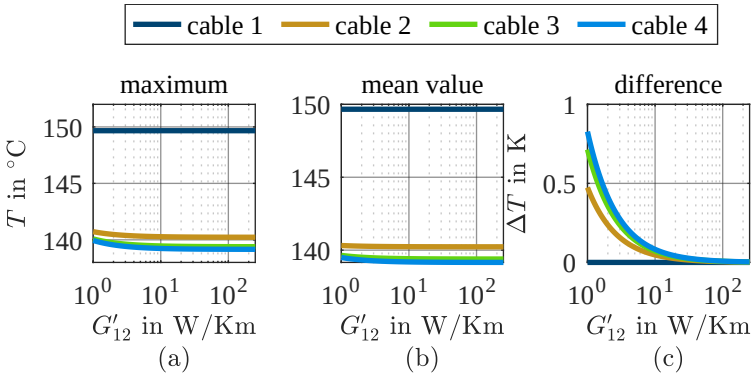

Figure 8.10: (a) Maximum and (b) mean values of the steady-state strand temperatures of a long cable for the four different cables depending on G'_{12}. (c) Difference between maximal and minimal temperatures.

c) Comparison to Earlier Modeling

Finally, the new results are compared with the previously used modeling approaches. So far, the correction factor $k_\mathrm{i} = 0.7$ was used for the radial thermal resistance due to the insulation R_i, which resulted from the larger surface area compared to the ideal circular shape. Here, too, an increased surface area of the stranded conductor is observed in comparison to the solid conductor with the same copper cross-section, whereby the actual coupling area is again approximated by a circle (with a larger radius). Compared to the solid cable, the factors are $\sqrt{7}/3 \approx 0.88$, $\sqrt{19}/5 \approx 0.87$, and $\sqrt{37}/7 \approx 0.87$. These are thus noticeably larger than the factor 0.7 from before. This can be explained on the one hand by the fact that in the presented modeling the actual course of the strand surfaces on the outside of the cable was not taken into account, but instead, only a circle was assumed for simplification. Strictly speaking, the relevant surface area is larger than the one that was taken into account, so real heat dissipation is better than assumed. However, the exact quantification is complicated here due to different effects that influence each other, so the proposed worst case is used. In addition, for the arrangement of the conductors themselves, an idealized arrangement in densest 2 D packing was adopted, so as much copper as possible is accommodated in the intended radius. In real arrangements, the actual conductor arrangement may deviate significantly from this ideal case, so the cable surface area can be increased even with the same copper cross-section. In real arrangements, it can therefore be assumed that the heat dissipation is more efficient than assumed above, so the presented investigation represents a worst case. All in all, therefore, even greater deviations can appear in reality.

To sum up, a stranded conductor is associated with larger space requirements than an analog solid conductor, and therefore a stronger heat dissipation can be observed. The maximum temperatures that occur are therefore noticeably reduced. In contrast, the temperature differences between the individual strands are small and negligible in many practically relevant cases. In principle, the largest temperature jump occurs at the transition from a solid conductor to a conductor made of 7 strands. An increase in the number of strands then only leads to minor changes in the maximum temperatures.

8.5 Application Example

In this section, an exemplary protection strategy for a twisted pair cable is presented. Such cables are used, for example, for **p**ower **o**ver **d**ata **l**ine (PoDL) applications [4]. In this approach, communication cables are also used for the power supply of low- to medium-power consumers. Thin twisted pair cables are therefore typical. As an example, a vehicular application is considered. For example, due to a fault at the device, unexpected high currents and associated fast cable heating can occur, so a suitable protection strategy is required. In this section, the previously developed methods are used for such a protection strategy for two coupled single wire cables, which is implemented and tested.

8.5.1 Algorithm

Overall, this section is not meant to give an accurate practical example for a concrete application, but it should demonstrate the basic applicability of the presented models for the protection and monitoring of real systems. On a microcontroller, a fuse protection strategy can freely be implemented. This allows many functions. The algorithm that is proposed in the following intends to give an example of possible strategies.

The basis for all temperature calculations in this thesis is the known current through the cables. Thus, also in this section, it is assumed, that this current is measured. Based on the current, an overcurrent shutdown can be directly implemented: As soon as the measured current exceeds a predefined value, it can be switched off without further calculations. For the temperature-dependent switching, a simple time step procedure is used to continuously calculate the coupled conductor temperatures based on the model for two single wire cables, because it was shown in section 8.4.1 that only the consideration of one single wire cable can lead to high deviations from the real temperatures. With the time step j, it follows

$$\boldsymbol{T}_{j+1} = -\frac{\Delta t}{A}\left(\boldsymbol{C} + \mathbf{B}\boldsymbol{T}_j\right) + \boldsymbol{T}_j. \tag{8.5}$$

Based on these temperatures, the tripping decision is made. Specifically, in this example, the fuse trips as soon as one of the two conductor temperatures reaches or exceeds the temperature T_{lim} and switches on again as soon as both calculated conductor temperatures are below the temperature $T_{\mathrm{hys}} < T_{\mathrm{lim}}$. A distinction is made between a "**no**rmal case" (index no) and an "**em**ergency case" (index em): For the "emergency case" it is assumed that it is a particularly critical case and therefore the supply should be maintained as long as possible. Accordingly, the thresholds are set higher for this case ($T_{\mathrm{lim,em}} = 75\,^{\circ}\mathrm{C}$, $T_{\mathrm{hys,em}} = 65\,^{\circ}\mathrm{C}$) than for the normal case ($T_{\mathrm{lim,no}} = 60\,^{\circ}\mathrm{C}$, $T_{\mathrm{hys,no}} = 45\,^{\circ}\mathrm{C}$). At the end of the active load case (e.g., the shutdown of a vehicle), the status switches from the case "vehicle on" to "vehicle off" and the temperature continues to be monitored until it is only $0.1\,\mathrm{K}$ above the ambient temperature. This little offset makes sure that the temperature calculation finally shuts down and does not run for a very long time as the cable temperature only asymptotically gets to the environmental temperature. After that, continuous monitoring is terminated. This ensures in particular that the information about the previous load and thus the starting temperature of the cable is not lost, especially if a second load is applied before the cable has mostly cooled down. Figure 8.11 shows this protection strategy in the form of an activity diagram.

An additional feature is added to the strategy via the previously presented analytical calculation methods: Forecasts of possible overloads are generated and corresponding warnings are returned if, for example, in the next minute an overload is expected (assuming a constant current). This enables more advanced strategies to be implemented at a higher level for dealing with possible cable overheating even before it occurs. Specifically, based on the radial

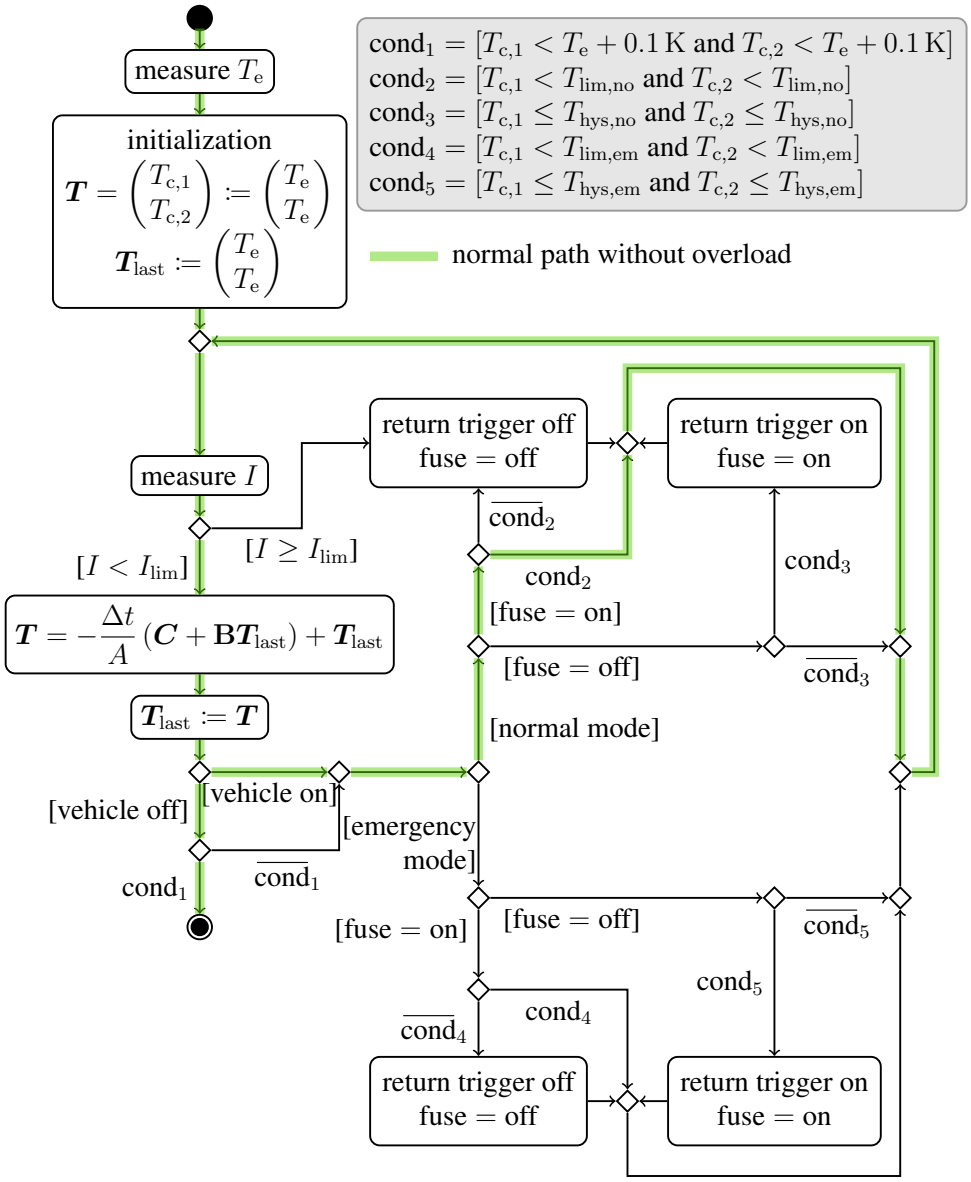

Figure 8.11: Activity diagram for the protection strategy.

model for the cable arrangement of two single wire cables (see section 6.1.1), the expected temperatures after $60\,\text{s}$ of load are calculated with the last measured current value. Then, if either temperature is above the allowable limit temperature, the temperature is also calculated for an interval half as long ($30\,\text{s}$). Up to a minimum interval of $3.75\,\text{s}$, this continues until a time is found when the maximum allowable temperature is not exceeded. The calculated lower and upper time limits for the expected overheating are then returned.

8.5.2 Implementation

This protection strategy is now implemented and tested. Figure 8.12(a) shows a simplified version of a small part of an automotive board net: A battery supplies different loads via a **p**ower **d**istribution **u**nit (PDU), that sums up distribution, protection, and switches. The

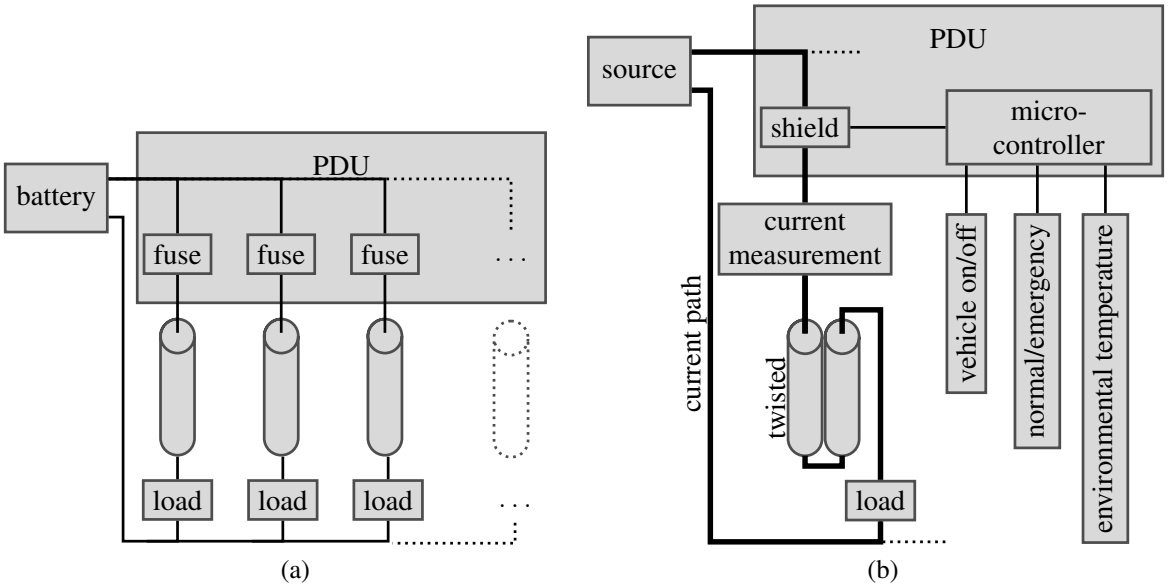

Figure 8.12: (a) Simplified partial automotive board net. (b) Test setup for the application of the presented protection strategy.

circuit for one such load is now chosen and the earlier described protection is implemented (see figure 8.12(b)).

The tightly twisted pair cable from section 8.4.1.a) is chosen as the device under test. An Arduino Due is used as the microcontroller for the calculations. The high-side switch shield with BTS50010-1TAD from Infineon is connected as a switch. A source is used to supply the shield with a voltage of $12\,\mathrm{V}$ and to provide the current to load the cables. A Hall effect-based integrated circuit (Pololu ACS715) is used to measure the current, which is connected directly to the current path and read out via the Arduino. Both cables are loaded with the same current in the following, and thus, they are connected in series and a single load is sufficient, at which the desired current is specified via control from MATLAB. The ambient temperature is measured by the digital 1-wire temperature sensor DS18B20: Every $10\,\mathrm{s}$ the value for the ambient temperature is read out and updated in the calculation. In addition, two pushbuttons are provided, which enable the switching between “normal case” and “emergency case” and between “vehicle on” and “vehicle off”. An overview of this arrangement is given in figure 8.12(b). Via the indirect temperature measurement (see section 7.2.1), the conductor temperature of one of the two cables is measured in parallel.

8.5.3 Exemplary Measurement

The implemented protection strategy is tested using an example. Figure 8.13 shows the results: Both cables are loaded with a preset current of $I_{\mathrm{preset}} = 7\,\mathrm{A}$. However, the measured current deviates up to about $0.2\,\mathrm{A}$. The measured and calculated cable temperatures

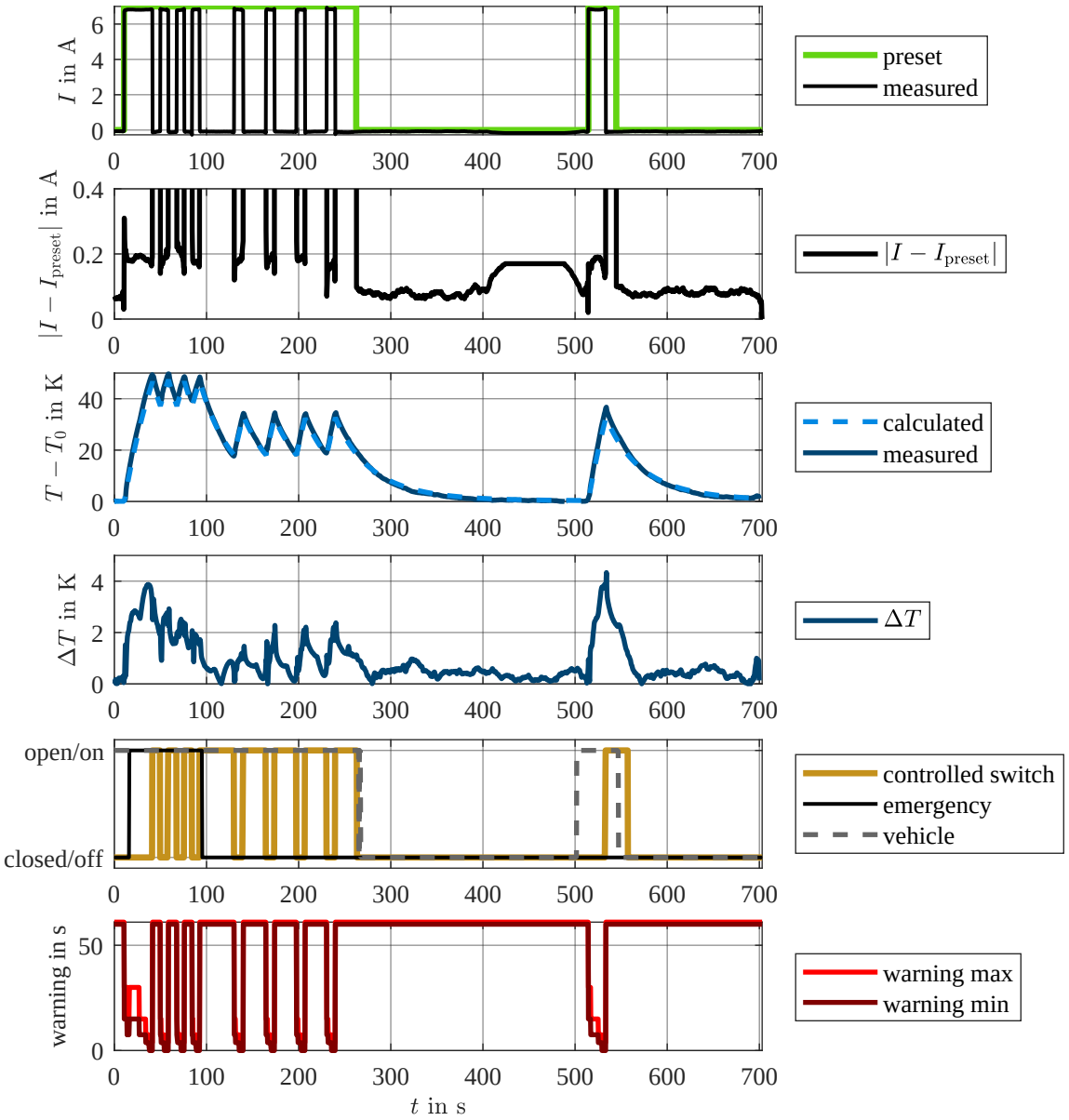

Figure 8.13: Exemplary measurement results for the application of the protection strategy.

are corrected with the initial cable temperature. Their difference

$$\Delta T = |T - T_0 - (T_{\mathrm{meas}} - T_{\mathrm{meas},0})| \tag{8.6}$$

is almost everywhere below $4\,\mathrm{K}$, mostly even below $2\,\mathrm{K}$. During rapid temperature rises, larger deviations occur than for slow temperature changes. This is because short-time transients are only partially considered via the selected model because radial heat conduction and heat storing have to be separated from each other and are each modeled only via a single element. In accordance with [143], an improvement of the simulation of highly transient effects is possible, for example, by splitting the cable capacitances, so not all of the capacitance

is already effective on the inside of the insulation. However, this also changes the differential equation, so the presented solution methods for two identical cables cannot directly be applied. A significant increase in the occurring deviations during the measurement cannot be observed. Parallel to continuous temperature monitoring, the prediction of the expected overload cases is carried out, which provides reliable predictions of the tripping times. Based on the first warning, the system is switched to the emergency case at the beginning of the measurement. Accordingly, at a cable temperature of $75\,^{\circ}\mathrm{C}$ the circuit is interrupted and switched on again after both conductor temperatures fall below $65\,^{\circ}\mathrm{C}$. After the circuit is interrupted for the fourth time with these limits, it is switched to the normal case, where four more shutdowns are observed. After that, the current is switched off and the fuse is set to the "vehicle off" state. Approximately $70\,\mathrm{s}$ after the current is switched off, the continuous temperature monitoring ends, and a constant value is assumed. Only shortly before the current is switched on again, the fuse is again set to the "vehicle on" state. This is followed by another current pulse which causes the fuse to switch off the current once again. This case is similarly well reproduced as the first load.

In the exemplary measurement of the previous section, it was assumed that the current path on which the overcurrent heats up the cable is switched on again after a certain cooling phase, which, in contrast to the simple fuse, can be implemented easily due to the free programmability. Nevertheless, the question arises whether it makes sense at all to reconnect a path with an overcurrent.

In principle, e.g. switching operations in the vehicle electrical system can generate propagating short-term pulses that may exceed defined maximum overcurrent limits, but only last for such a short time that even a fuse does not heat up sufficiently to operate. However, if this overcurrent is detected by the current measurement, the electronic fuse may still trip. In this case, it makes sense to switch on the current again, since there is no fault on the corresponding load. If tripping was caused by a calculated overtemperature, then a fault in the consumer that is supplied via the cable is more likely. However, it is also conceivable that several consumers are supplied via a common cable and protected with a common fuse. Then a fault in one of the consumers is sufficient to cause an overcurrent. Another consumer may still be functioning properly. In this case, it can make sense to supply this consumer again from time to time: For example, a camera could record at least some images in this way, which can be better than a complete failure. Another possible case is the joint supply of several consumers via a comparatively thin cable, so a maximum load of all consumers at the same time very rarely occurs, but permanently leads to the exceeding of the permissible conductor temperatures. Even then, it may make sense to switch on again, ideally coupled with a higher decision level at which a further overload case is avoided by regulating individual consumers. All in all, it can therefore make sense to switch a current on, even if these are primarily special cases.

8.5.4 Comparison to Melting Fuse

The designed protection strategy is now compared with an exemplary fuse. For this purpose, it is first assumed that a nominal current of $1\,\mathrm{A}$ flows through the two cables and the fuse is designed for a maximum continuous current of $3\,\mathrm{A}$. At an overcurrent of $7\,\mathrm{A}$, such a fuse would accordingly operate in less than one second. In figure 8.14, the associated current and temperature developments of such a fuse are compared with those resulting from the protection strategy shown above. In the beginning, the cables are loaded with the nominal current $1\,\mathrm{A}$ for $60\,\mathrm{s}$. Then the current is increased to the fault value of $7\,\mathrm{A}$. The fuse operates almost immediately ($< 1\,\mathrm{s}$), even though the cable has not yet experienced a significant temperature rise. In contrast, the overcurrent load is tolerated by the controlled switch for about $18.7\,\mathrm{s}$, so valuable time can be gained in an emergency. This means that the system can still be transferred to a safe state before failure. Switching individual loads on or off via the higher-level load management system can also help to deal with the fault. Overall, the controlled switch offers significantly more flexibility during operation.

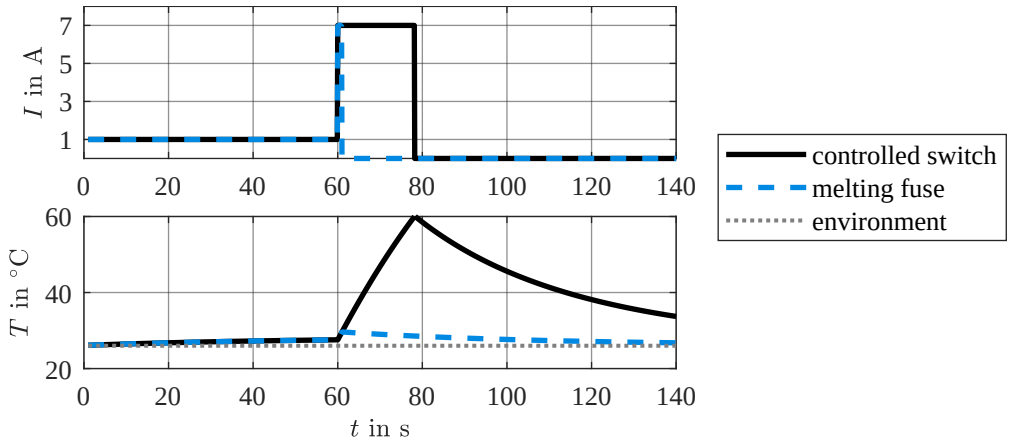

Figure 8.14: Comparison between the proposed protection strategy and a melting fuse.

Overall, the presented examples show that the derived methods can be used for protection and monitoring purposes. Links with higher levels and advanced smart fuse protection strategies are conceivable due to the high flexibility of the approach, even for much more complex systems.

9 Summary and Outlook

In this thesis, analytical thermal cable models based on the well-known electrical TL theory were developed, validated, and analyzed.

The necessity for those models was shown by a discussion of the drawbacks of melting fuses and controlled switches with a current-based decision: As both of them are not based on knowledge of the real cable temperature, high safety margins have to be taken into account. To avoid those, fast and sufficiently precise thermal cable models are necessary.

After shortly resuming the state of the art regarding thermal and electrical effects on TLs, the analogy between the electrical and thermal domain was discussed in detail to motivate the application of approaches from the electrical to the thermal domain. Both domains were compared concerning the basic physical equations, typical modeling goals, and basic assumptions for the modeling: In the electrical domain, the TEM assumption plays a major role, which is closely related to the reference conductor concept. Since a thermal analog to the magnetic field does not exist and the electric field concept cannot be directly transferred to the thermal domain, there is no physical thermal reference conductor. Also, the understanding of capacitances in both domains varies. Nevertheless, systematic similarities were found that allowed the application of methods known from the electrical domain to thermal problems.

Based on the heat equation, for a single wire cable, a simplified PDE was derived, in which only one spatial variable (axial direction, along the cable) remains using symmetry considerations and integration. A necessary approximation was to split up heat conduction and heat capacity. The result was a PDE analog to the form known from the electrical domain. Thus, also a corresponding ECD was used for the description. For the application to a multiconductor arrangement, a general approach was presented that allows the derivation of the system of coupled PDEs and the ECDs directly from the physical arrangement without complex integration of the heat equation. The assumptions in both the electrical and thermal domains were compared and the models were characterized.

The nonlinear system of coupled PDEs was linearized in the first step to allow analytical solutions for constant excitations. Using these assumptions, several analytical calculation formulas were derived for the direct temperature calculation based on Laplace domain solutions, Green's functions, simplification of the ECDs and PDEs, or iterations. Explicit formulas were given for special important cable arrangements such as a single wire cable, a system of several axially combined single wire cables, two single wire cables, a coaxial cable, and an arrangement of N identical single wire cables. In the next step, numerical and analytical approaches for time and spatial varying initial and boundary conditions and excitations were presented. For the consideration of the nonlinear parameter dependence and the solution of the resulting self-consistent problem, different approaches were presented and a fast con-

verging fixed-point iteration was chosen for the remainder of the thesis. The solutions were validated with measured and numerically calculated reference temperatures. In this context, a procedure was proposed for the determination of some of the cable parameters, that describe the interference between different conductors. This interference highly depends for example on surface effects and pressure, and thus is very challenging to be directly measured. In the presented approach, measured steady-state temperatures were evaluated to find the parameters based on very few and easy measurements.

The derived and validated solution approaches were discussed in the next step. It was shown that the accuracy of the basic model is within only a few Kelvin and thus, high enough for many practically relevant applications. Many of the presented solution approaches allow temperature determination in good agreement with numerical solutions. The models considering both the axial and radial heat flow along the cable together with the analytical solution approaches enable faster temperature calculations than the mostly numerical established methods. Compared to previous models, the understanding analogous to the electrical domain provides a new perspective and new options for temperature determination. The (semi-)analytical models allow calculations also for non-trivial conductor arrangements with nevertheless manageable effort. It was shown that the exact conductor arrangement is very relevant for the developing temperatures. Bundle arrangements must be taken into account because neglecting them can result in too low estimated temperatures. If a stranded conductor is approximated by a solid conductor, the predicted temperatures are too high due to the lower coupling to the (cooling) environment, so this approximation can be made as a worst-case scenario to reduce the calculation effort. Finally, a complete protection strategy for a twisted pair cable was developed, implemented, and tested in a laboratory environment. This included current-based online monitoring of the cable temperature considering also the cooling behavior, different temperature trigger levels depending on the safety relevance, and an estimation of the future temperature development in combination with a warning function. This example shows that the developed approaches can be used for temperature-based cable protection and allow for flexible new switching strategies.

In future work, more complex cable systems with several loads with different safety requirements should be protected by a network of combined controlled switches. Together with PDUs, early fault detection and extremely flexible strategies for the reaction to faults can be implemented to reach high overall reliability and safety.

In this thesis, only air installation was considered. The proposed models can be extended for other installation types in further work. Firstly, this covers external air flows and thus, forced convection. In addition, there may be other elements in the vicinity of the modeled cables that can limit free convection. Preliminary investigations indicate that free air installation does not necessarily describe the worst case for cable temperatures, even if other elements near the described cable are not actively dissipating heat. For example, a plate above

the cable can relevantly limit the free convection and therefore the heat dissipation of the cable. Quantification of these effects and appropriate consideration in modeling approaches should follow in future work. In addition, (heated or unheated) objects in direct contact with the cables can also significantly change the conductor temperatures. Similar to the consideration of the coupling between different conductors in a bundle, an adjustment of the model via additional resistances and a coupling with the thermal models for the corresponding components will then be necessary. Overall, the proposed models should be extended and reshaped in such a way that coupling to other thermal models such as contact models is enabled and the approaches can be used, for example, as part of larger simulation models.

References

[1] L. Brabetz et al. “Evaluation of future topologies and architectures for high-reliability electrical distribution systems”. In: *SAE Int. J. Adv. & Curr. Prac. in Mobility* 4.2 (Apr. 2020), pp. 2347–2355. DOI: 10.4271/2020-01-1296.

[2] F. P. Loos. “Joule heating in connecting structures of automotive electric devices – modelling, simulation and optimization”. PhD thesis. Universität der Bundeswehr München, June 2014.

[3] G. Yilmaz and S. E. Karlik. “A distributed optical fiber sensor for temperature detection in power cables”. In: *Sens. Actuator A Phys.* 125.2 (Jan. 2006), pp. 148–155. DOI: 10.1016/j.sna.2005.06.024.

[4] “IEEE Standard for Ethernet”. In: *IEEE Std 802.3-2018 (Revision of IEEE Std 802.3-2015)* (2018), pp. 1–5600. DOI: 10.1109/IEEESTD.2018.8457469.

[5] A. Wright and G. Newbery. *Electric fuses*. 3. ed. Vol. 49. London, UK: Inst. Electrical Engineers, 2004. ISBN: 978-0-86341-399-5.

[6] J. Asta, T. Humphrey, and G. Parkhurst. “Comparison of circuit protection devices”. In: *Int. Congr. Exposition* (Detroit, MI, USA, Feb. 27–Mar. 2, 1995). SAE International. DOI: 10.4271/950300.

[7] F. Doljack. “PolySwitch PTC devices - a new low-resistance conductive polymer-based PTC device for overcurrent protection”. In: *IEEE Trans. Compon., Hybrids, Manuf. Technol.* 4.4 (Dec. 1981), pp. 372–378. DOI: 10.1109/TCHMT.1981.1135838.

[8] S. Cheng, K. Tom, and M. Pecht. “Failure precursors for polymer resettable fuses”. In: *IEEE Trans. Device Mater. Rel.* 10.3 (Sept. 2010), pp. 374–380. DOI: 10.1109/TDMR.2010.2053371.

[9] T. Itoh et al. “Design considerations on the P. P. F. for a control center”. In: *IEEE Trans. Power App. Syst.* PAS-92.4 (July 1973), pp. 1292–1297. DOI: 10.1109/TPAS.1973.293814.

[10] Y. Wada et al. “Usefulness of permanent power fuse in control centers with molded case circuit breakers”. In: *IEEE Trans. Ind Appl.* IA-16.1 (Jan. 1980), pp. 30–39. DOI: 10.1109/TIA.1980.4503744.

[11] J.-L. Gelet. “To the origins of fuses”. In: *2007 8th Int. Conf. El. Fuses Appl.* (Ceyrat, France, Sept. 10–12, 2007). IEEE, pp. 1–8. DOI: 10.1109/ICEFA..4419958.

[12] M. S. Agarwal, A. D. Stokes, and P. Kovitya. “Pre-arcing behaviour of open fuse wire”. In: *J. Phys. D: Appl. Phys.* 20.10 (Oct. 1987), pp. 1237–1242. DOI: 10.1088/0022-3727/20/10/005.

[13] S. Ito, T. Miyatake, and Y. Kawase. “Heat analysis of a fuse for semiconductor devices protection using 3-D finite element method”. In: *IEEE Trans. Magn.* 36.4 (July 2000), pp. 1377–1380. DOI: 10.1109/20.877695.

[14] E. Torres et al. “Thermal analysis of medium voltage fuses using the finite element method”. In: *2005 IEEE Russia Power Tech* (St. Petersburg, Russia, June 27–30, 2005). IEEE, pp. 1–5. DOI: 10.1109/PTC.2005.4524671.

[15] E. Torres et al. “New FEM Model for thermal analysis of medium voltage fuses”. In: *19th Int. Conf. Electricity Distrib.* (Vienna, Austria, May 21–24, 2007), pp. 1–4.

[16] H. Feshki Farahani, M. Asadi, and A. Kazemi. “Analysis of thermal behavior of power system fuse using finite element method”. In: *2010 4th Int. PEOCO* (Shah Alam, Malaysia, June 23–24, 2010). IEEE, pp. 189–195. DOI: 10.1109/PEOCO.2010.5559169.

[17] R. Vilums and A. Buikis. “Conservative averaging and finite difference methods for transient heat conduction in 3D fuse”. In: *WSEAS Trans. Heat Mass Tranf.* 3.1 (Jan. 2008), pp. 111–124.

[18] R. Vilums et al. “Cylindrical model of transient heat conduction in automotive fuse using conservative averaging method”. In: *Proc. 13th WSEAS Int. Conf. Appl. Math.* (Puerto de la Cruz, Spain, Dec. 15–17, 2008). WSEAS, pp. 355–360.

[19] J. G. Kassakian. “Automotive electrical systems - the power electronics market of the future”. In: *15th Annual IEEE APEC 2000* (New Orleans, LA, USA, Feb. 6–10, 2000). IEEE, pp. 3–9. DOI: 10.1109/APEC.2000.826075.

[20] Littlefuse Europe GmbH. *Blade Fuses*. URL: www.littelfuse.com/media?resourcetype=datasheets&itemid=4942dc86-661a-470b-a3bb-3499eab7f138&filename=littelfuse-atof-datasheet (visited on 09/11/2022).

[21] S. Önal and S. Frei. “Elektrothermische Modellierung von Kfz-Schmelzsicherungen für dynamische Belastungen”. In: *AmE 2016* (Dortmund, Germany, Mar. 1–2, 2016). VDE Verlag.

[22] “Application guide for low-voltage fuses”. In: *IEC TR 61818-2003* (2003).

[23] L. Gysen, M. Ayeb, and L. Brabetz. “Cable bundle protection and cross-section reduction by using a centralized smart fusing strategy”. In: *2018 IEEE Inf. Conf. ESARS-ITEC* (Nottingham, UK, Nov. 7–9, 2018). IEEE, pp. 1–5. DOI: 10.1109/ESARS-ITEC.2018.8607448.

[24] M Wortberg. “Intelligente Absicherung und bedarfsgerechte Energieversorgung im Bordnetz für dynamische Lasten”. In: *Fachkongress Bordnetze im Automobil* (Ludwigsburg, Germany, Apr. 12–13, 2013).

[25] “Guidance concerning the permissible temperature rise for parts of electrical equipment, in particular for terminals”. In: *IEC 60943:2009* (2009).

[26] “Military Handbook Reliability prediction of electronic equipment”. In: *MIL HDBK-217F* (1991).

[27] A. K. Sang et al. “One centimeter spatial resolution temperature measurements in a nuclear reactor using Rayleigh scatter in optical fiber”. In: *IEEE Sensors J.* 8.7 (July 2008), pp. 1375–1380. DOI: 10.1109/JSEN.2008.927247.

[28] S. D. Dyer et al. “Analysis of a distributed fiber-optic temperature sensor using single-photon detectors”. In: *Opt. express* 20.4 (Jan. 2012), pp. 3456–3466. DOI: 10.1364/OE.20.003456.

[29] T. Schulz. “Grundsatzuntersuchung zum Temperaturverhalten elektrischer Leitungen und deren Schutzelemente auf Schmelzleiterbasis in Kfz-Bordnetzen”. PhD thesis. Universität der Bundeswehr München, Jan. 2003.

[30] A. Ilgevicius. “Analytical and numerical analysis and simulation of heat transfer in electrical conductors and fuses”. PhD thesis. Universität der Bundeswehr München, Nov. 2004.

[31] R. J. Millar. “A comprehensive approach to real time power cable temperature prediction and rating in thermally unstable environments”. PhD thesis. Helsinki University of Technology, Nov. 2006.

[32] D. Zhang. “Optimierung zwangsgekühlter Energiekabel durch dreidimensionale FEM-Simulationen”. PhD thesis. Universität Duisburg-Essen, Oct. 2009.

[33] K. Dvorsky. “Analysis of an nonlinear bondary value problem with application to heat transfer in electric cables”. PhD thesis. Universität der Bundeswehr München, Jan. 2013.

[34] H. C. Nguyen. “Modelisation electrothermique de systeme electrique electronique automobile et pilotage de mosfet intelligents pour proteger les faisceaux, eviter les courts circuits aggraves et diminuer masse de cablage”. PhD thesis. Université de Bordeaux, Mar. 2013.

[35] R. S. Olsen. “Dynamic loadability of cable based transmission grids”. PhD thesis. Technical University of Denmark, Aug. 2013.

[36] M. Diebig. “Entwicklung einer Methodik zur simulationsbasierten Dimensionierung von Kfz-Bordnetzen”. PhD thesis. Technische Universität Dortmund, June 2016.

[37] H. Neumeier. “Entwicklung einer neuen Messmethodik zur thermischen Untersuchung von Leitungsbündeln in Fahrzeugbordnetzen”. PhD thesis. Universität Kassel, Oct. 2017.

[38] F. Mahiddini. “Modélisation couplée CEM-thermique d’architectures de câblages électriques embarquées”. PhD thesis. Université de Toulouse, Dec. 2018.

[39] C. Balzer. “Calculation of ampacity ratings of power cable systems by the use of thermal quadrupoles under consideration of soil properties”. PhD thesis. Technische Universität Darmstadt, Nov. 2020.

[40] D. Enescu et al. “Dynamic thermal rating of electric cables: A conceptual overview”. In: *2020 55th Int. UPEC* (Turin, Italy, Sept. 1–4, 2020). IEEE, pp. 1–6. DOI: 10.1109/UPEC49904.2020.9209809.

[41] G. J. Anders. *Rating of electric power cables: Ampacity computations for transmission, distribution, and industrial applications*. New York, NY, USA: McGraw-Hill, 1997. ISBN: 978-0-7803-1177-0.

[42] G. J. Anders. *Rating of electric power cables in unfavorable thermal environment*. Piscataway, NJ, USA: Wiley, 2005. ISBN: 978-0-471-67909-7.

[43] N. Mohd Zainuddin et al. “Review of thermal stress and condition monitoring technologies for overhead transmission lines: Issues and challenges”. In: *IEEE Access* 8 (Jan. 2020), pp. 120053–120081. DOI: 10.1109/ACCESS.2020.3004578.

[44] S. H. Hasan Kazmi et al. “Thermoelectric modelling and optimization of offshore windfarm export systems - state of the art”. In: *2019 1st GPECOM* (Nevsehir, Turkey, June 12–15, 2019). IEEE, pp. 331–336. DOI: 10.1109/GPECOM.2019.8778513.

[45] E. Fernandez et al. “Review of dynamic line rating systems for wind power integration”. In: *Renew. Sust. Energ. Rev.* 53 (Jan. 2016), pp. 80–92. DOI: 10.1016/j.rser.2015.07.149.

[46] “Electric cables - Calculation of the current rating - Part 1-1: Current rating equations (100 % load factor) and calculation of losses - General”. In: *IEC 60287-1-1:2006* (2006).

[47] “Electric cables - Calculation of the current rating - Part 2-1: Thermal resistance - Calculation of the thermal resistance”. In: *IEC 60287-2-1:2015* (2015).

[48] “Calculation of the cyclic and emergency current rating of cables. Part 1: Cyclic rating factor for cables up to and including 18/30(36) kV”. In: *IEC 60853-1:1985* (1985).

[49] “Calculation of the cyclic and emergency current rating of cables. Part 2: Cyclic rating of cables greater than 18/30 (36) kV and emergency ratings for cables of all voltages”. In: *IEC 60853-2:1989* (1989).

[50] “Road vehicles — 60 V and 600 V single-core cables — Part 1: Dimensions, test methods and requirements for copper conductor cables”. In: *ISO 6722-1:2011* (2006).

[51] “IEEE Guide for Temperature Monitoring of Cable Systems”. In: *IEEE Std 1718-2012* (June 2012), pp. 1–35. DOI: 10.1109/IEEESTD.2012.6214562.

[52] “Thermosimulationsmodelle”. In: *ZVEI Technischer Leitfaden 0101* (2020).

[53] C. Holyk and G. J. Anders. “Power cable rating calculations - a historical perspective [history]”. In: *IEEE Ind. Appl. Mag.* 21.4 (July 2015), pp. 6–64. DOI: 10.1109/MIAS.2015.2417094.

[54] J. He et al. “Thermal analysis of HTS power cable using 3-D FEM model”. In: *IEEE Trans. Appl. Supercond.* 23.3 (Feb. 2013), pp. 5402404–5402404. DOI: 10.1109/TASC.2013.2247651.

[55] R. Benato et al. “Finite element model of a 3 m long three-core armoured submarine cable”. In: *2016 AEIT Int. Annual Conf.* (Capri, Italy, Oct. 5–7, 2016). IEEE, pp. 1–6. DOI: 10.23919/AEIT.2016.7892758.

[56] B. Zhou et al. “Temperature field simulation and ampacity optimisation of 500 kV HVDC cable”. In: *J. Eng.* 2019.16 (Jan. 2019), pp. 2448–2453. DOI: 10.1049/joe.2018.8586.

[57] L. Brabetz, M. Ayeb, and H. Neumeier. “A new approach to the thermal analysis of electrical distribution systems”. In: *SAE 2011 World Congr. Exhibition* (Detroit, MI, USA, Apr. 12–14, 2011). SAE International. DOI: 10.4271/2011-01-1437.

[58] F. Loos, K. Dvorsky, and H.-D. Liess. “Two approaches for heat transfer simulation of current carrying multicables”. In: *Math. Comput. Simul.* 101 (Jan. 2014), pp. 13–30. DOI: 10.1016/j.matcom.2014.01.008.

[59] Q. Zhan et al. “Real-time calculation of three core cable conductor temperature based on thermal circuit model with thermal resistance correction”. In: *J. Eng.* 2019.16 (Jan. 2019), pp. 2036–2041. DOI: 10.1049/joe.2018.8739.

[60] C. Holyk et al. “Simulation and measurement of the steady-state temperature in multi-core cables”. In: *Electr. Power Syst. Res.* 116 (Nov. 2014), pp. 54–66. DOI: 10.1016/j.epsr.2014.05.001.

[61] S. L. Rickman and C. J. Iannello. “Heat transfer analysis in wire bundles for aerospace vehicles”. In: *Proc. 14th Int. Conf. HT* (Ancona, Italy, Sept. 7–9, 2016). Ed. by B. Sundén and C. A. Brebbia. WIT Press, pp. 53–63. DOI: 10.2495/HT160061.

[62] C. Fu, W. Si, and Y. Liang. “On-line computation of the underground power cable core’s temperature and ampacity based on FEM and environment detection”. In: *2018 CMD* (Perth, Australia, Sept. 23–26, 2018). IEEE, pp. 1–5. DOI: 10.1109/CMD.2018.8535720.

[63] D. Dai, M. Hu, and L. Luo. “Calculation of thermal distribution and ampacity for underground power cable system by using electromagnetic-thermal coupled model”. In: *2014 IEEE EIC* (Philadelphia, PA, USA, June 8–11, 2014). IEEE, pp. 303–306. DOI: 10.1109/EIC.2014.6869397.

[64] A. Sedaghat et al. “Enhanced thermal model of power cables installed in ducts for ampacity calculations”. In: *IEEE Trans. Power Del.* 33.5 (Jan. 2018), pp. 2404–2411. DOI: 10.1109/TPWRD.2018.2841054.

[65] H. Brakelmann, P. Lauter, and G. J. Anders. “Current rating of multicore cables”. In: *IEEE Trans. Ind Appl.* 41.6 (Nov. 2005), pp. 1566–1573. DOI: 10.1109/TIA.2005.857471.

[66] A. Sedaghat and F. Leon. “Thermal analysis of power cables in free air: Evaluation and improvement of the IEC standard ampacity calculations”. In: *IEEE Trans. Power Del.* 29.5 (Jan. 2014), pp. 2306–2314. DOI: 10.1109/TPWRD.2013.2296912.

[67] M. Bau et al. “Steady state modelling of three-core wire armoured submarine cables: Power losses and ampacity estimation based on FEM and IEC”. In: *2016 51st Int. UPEC* (Coimbra, Portugal, Sept. 6–9, 2016). IEEE, pp. 1–6. DOI: 10.1109/UPEC.2016.8114078.

[68] J. Orsagova and P. Toman. “Application of thermal models of digital protective relays in cable protection”. In: *IET 9th Int. Conf. DPSP* (Glasgow, UK, Mar. 17–20, 2008). IET, pp. 513–515. DOI: 10.1049/cp:20080090.

[69] J. Grandvuillemin et al. “Thermal modelling of enclosed cables in automotive applications”. In: *2007 IEEE Veh. Power Propulsion Conf.* (Arlington, TX, USA, Sept. 9–12, 2007). IEEE, pp. 730–735. DOI: 10.1109/VPPC.2007.4544220.

[70] D. Lauria, M. Pagano, and C. Petrarca. “Transient thermal modelling of HV XLPE power cables: Matrix approach and experimental validation”. In: *2018 IEEE PESGM* (Portland, OR, USA, Aug. 5–10, 2018). IEEE, pp. 1–6. DOI: 10.1109/PESGM.2018.8586514.

[71] R. Olsen et al. “Modelling of dynamic transmission cable temperature considering soil-specific heat, thermal resistivity, and precipitation”. In: *IEEE Trans. Power Del.* 28.3 (June 2013), pp. 1909–1917. DOI: 10.1109/TPWRD.2013.2263300.

[72] R. S. Olsen and U. S. Gudmundsdottir. “Dynamic temperature estimation and real time emergency rating of transmission cables”. In: *2012 IEEE PESGM* (San Diego, CA, USA, July 22–26, 2012). IEEE, pp. 1–8. DOI: 10.1109/PESGM.2012.6345324.

[73] P.-Y. Wang et al. “Dynamic thermal analysis of high-voltage powe cable insulation for cable dynamic thermal rating”. In: *IEEE Access* 7 (Jan. 2019), pp. 56095–56106. DOI: 10.1109/ACCESS.2019.2913704.

[74] M. Lei et al. “Study on thermal model of dynamic temperature calculation of single-core cable based on Laplace calculation method”. In: *2010 IEEE ISEI* (San Diego, CA, USA, June 6–9, 2010). IEEE, pp. 1–7. DOI: 10.1109/ELINSL.2010.5549825.

[75] M. J. O. Strutt. “The distribution of temperature in alternating current conductors”. In: *London, Edinburgh Dublin Philos. Mag. J. Sci.* 5.31 (May 1928), pp. 904–914. DOI: 10.1080/14786440508564533.

[76] J. B. Prime and J. G. Valdes. “System to monitor the conductor temperature of underground cables”. In: *IEEE Trans. Power App. Syst.* PAS-100.1 (Jan. 1981), pp. 143–153. DOI: 10.1109/TPAS.1981.316896.

[77] H. Kalis and A. Lasis. “Simple algorithms for calculation of the axial – symmetric heat transport problem in a cylinder”. In: *Math. Model. Anal.* 6.2 (Dec. 2001), pp. 262–269. DOI: 10.3846/13926292.2001.9637165.

[78] A. Buikis and H. Kalis. “Calculation of electromagnetic fields, forces and temperature in a finite cylinder”. In: *Math. Model. Anal.* 7.1 (Sept. 2002), pp. 21–32. DOI: 10.1080/13926292.2002.9637174.

[79] L. Brabetz et al. “Impact of the vehicle environment on the thermal behavior of the electrical wiring”. In: *SAE Int. J. Adv. & Curr. Prac. in Mobility* 4.4 (Mar. 2022), pp. 1335–1343. DOI: 10.4271/2022-01-0133.

[80] Michael Blauth. “Analytical and experimental investigation of the electrical-thermal behaviour of electrical contact systems”. In: *Br. J. Appl. Sci. Technol.* 4.1 (Jan. 2014), pp. 18–39. DOI: 10.9734/BJAST/2014/5536.

[81] H. D. Liess and A. Ilgevicius. “Analytical versus numerical calculations of physical problems. The benefits of its combinations”. In: *Math. Model. Anal.* 8.4 (Dec. 2003), pp. 291–302. DOI: 10.3846/13926292.2003.9637231.

[82] G. J. Anders et al. “Advanced modeling techniques for dynamic feeder rating systems”. In: *IEEE Trans. Ind. Appl.* 39.3 (May 2003), pp. 619–626. DOI: 10.1109/TIA.2003.810648.

[83] R. Huang et al. “Dynamic cable ratings for smarter grids”. In: *IEEE PES ISGT Europe 2013* (Lyngby, Denmark, Oct. 6–9, 2013). IEEE, pp. 1–5. DOI: 10.1109/ISGTEurope.2013.6695230.

[84] R. Olsen, J. Holboell, and U. S. Gudmundsdottir. “Electrothermal coordination in cable based transmission grids”. In: *IEEE Trans. Power Syst.* 28.4 (Nov. 2013), pp. 4867–4874. DOI: 10.1109/TPWRS.2013.2278040.

[85] H. Brakelmann and G. J. Anders. “Transient thermal response of multiple power cables with temperature dependent losses”. In: *IEEE Trans. Power Del.* 36.6 (Dec. 2021), pp. 3937–3944. DOI: 10.1109/TPWRD.2021.3051316.

[86] H. Brakelmann and G. J. Anders. “Transient thermal response of power cables with temperature dependent losses”. In: *IEEE Trans. Power Del.* 36.5 (Oct. 2021), pp. 2777–2784. DOI: 10.1109/TPWRD.2020.3026779.

[87] J. Taler and P. Duda. *Solving direct and inverse heat conduction problems*. Berlin, Germany: Springer, 2006. ISBN: 978-3-540-33470-5.

[88] D. A. Douglass. “Weather-dependent versus static thermal line ratings (power overhead lines)”. In: *IEEE Trans. Power Del.* 3.2 (Apr. 1988), pp. 742–753. DOI: 10.1109/61.4313.

[89] S. D. Foss and R. A. Maraio. “Dynamic line rating in the operating environment”. In: *IEEE Trans. Power Del.* 5.2 (Apr. 1990), pp. 1095–1105. DOI: 10.1109/61.53127.

[90] T. O. Seppa. “Accurate ampacity determination: Temperature-sag model for operational real time ratings”. In: *IEEE Trans. Power Del.* 10.3 (July 1995), pp. 1460–1470. DOI: 10.1109/61.400930.

[91] D. A. Douglass and A.-A. Edris. “Real-time monitoring and dynamic thermal rating of power transmission circuits”. In: *IEEE Trans. Power Del.* 11.3 (July 1996), pp. 1407–1418. DOI: 10.1109/61.517499.

[92] D. A. Douglass, A. A. Edris, and G. A. Pritchard. “Field application of a dynamic thermal circuit rating method”. In: *IEEE Trans. Power Del.* 12.2 (Apr. 1997), pp. 823–831. DOI: 10.1109/61.584390.

[93] M. Matus et al. “Identification of critical spans for monitoring systems in dynamic thermal rating”. In: *IEEE Trans. Power Del.* 27.2 (Apr. 2012), pp. 1002–1009. DOI: 10.1109/TPWRD.2012.2185254.

[94] A. Safdarian et al. “Benefits of real-time monitoring to distribution systems: Dynamic thermal rating”. In: *IEEE Trans. Smart Grid* 6.4 (July 2015), pp. 2023–2031. DOI: 10.1109/TSG.2015.2393366.

[95] D. A. Douglass et al. “A review of dynamic thermal line rating methods with forecasting”. In: *IEEE Trans. Power Del.* 34.6 (Dec. 2019), pp. 2100–2109. DOI: 10.1109/TPWRD.2019.2932054.

[96] H. J. Li, K. C. Tan, and Q. Su. “Assessment of underground cable ratings based on distributed temperature sensing”. In: *IEEE Trans. Power Del.* 21.4 (Oct. 2006), pp. 1763–1769. DOI: 10.1109/TPWRD.2006.874668.

[97] L. Zhang et al. “Temperature analysis based on multi-coupling field and ampacity optimization calculation of shore power cable considering tide effect”. In: *IEEE Access* 8 (Jan. 2020), pp. 119785–119794. DOI: 10.1109/ACCESS.2020.3005305.

[98] H. Brakelmann and G. Anders. “Ampacity reduction factors for cables crossing thermally unfavorable regions”. In: *IEEE Trans. Power Del.* 16.4 (Oct. 2001), pp. 444–448. DOI: 10.1109/61.956718.

[99] Y.-H. Zhang et al. “Ampacity and temperature field calculation of 10 kV XLPE cables laid in pipes”. In: *Proc. 2011 ICEEI* (Bandung, Indonesia, July 17–19, 2011). IEEE, pp. 1–4. DOI: 10.1109/ICEEI.2011.6021810.

[100] Y.-L. Zheng et al. “Optimization design for rating calculations of power cables in pipes”. In: *Proc. 2011 ISEIM* (Kyoto, Japan, Sept. 6–10, 2011). IEEE, pp. 417–420. DOI: 10.1109/ISEIM.2011.6826358.

[101] Y. Shen et al. “Promoting cable ampacity by filling low thermal resistivity medium in ducts”. In: *2013 IEEE PES APPEEC* (Hong Kong, China, Dec. 8–11, 2013). IEEE, pp. 1–4. DOI: 10.1109/APPEEC.2013.6837287.

[102] Y. Liu et al. “A coupled conduction convection and radiation problem for three insulated cables suspended in air”. In: *Comput. Mech.* 22.4 (Oct. 1998), pp. 326–336. DOI: 10.1007/s004660050364.

[103] G. Anders, A. Napieralski, and W. Zamojski. “Calculation of the internal thermal resistance and ampacity of 3-core screened cables with fillers”. In: *IEEE Trans. Power Del.* 14.3 (July 1999), pp. 729–734. DOI: 10.1109/61.772307.

[104] R. Ciegis et al. “Numerical simulation of the heat conduction in electrical cables”. In: *Math. Model. Anal.* 12.4 (Dec. 2007), pp. 425–439. DOI: 10.3846/1392-6292.2007.12.425-439.

[105] Y. Du and X. H. Wang. “Electrical and thermal analysis of parallel single-conductor cable installations”. In: *2009 IEEE IAS Annu. Meet.* (Houston, TX, USA, Oct. 4–8, 2009). IEEE, pp. 1–6. DOI: 10.1109/IAS.2009.5324885.

[106] L. Brabetz and M. Ayeb. “A statistical analysis of the thermal behavior of electrical distribution systems”. In: *SAE Int. J. Passenger Cars – Electron. Electr. Syst.* 7.1 (Jan. 2014), pp. 119–124. DOI: 10.4271/2014-01-0223.

[107] H. Harbrecht and F. Loos. “Optimization of current carrying multicables”. In: *Comput. Optim. Appl.* 63.1 (Jan. 2016), pp. 237–271. DOI: 10.1007/s10589-015-9764-2.

[108] Y. C. Liang and Y. M. Li. “On-line dynamic cable rating for underground cables based on DTS and FEM”. In: *WSEAS Trans. Circuits Syst.* 7.4 (Apr. 2008), pp. 229–238. DOI: 10.5555/1482050.1482059.

[109] J. H. Neher and M. H. McGrath. “The calculation of the temperature rise and load capability of cable systems”. In: *Trans. American Inst. Electr. Eng. III: Power App. Syst.* 76.3 (Jan. 1957), pp. 752–764. DOI: 10.1109/AIEEPAS.1957.4499653.

[110] C. R. Paul. *Analysis of multiconductor transmission lines*. 2. ed. Hoboken, NJ, USA: Wiley, 2008. ISBN: 978-0-470-13154-1.

[111] R. Achar and M. S. Nakhla. “Simulation of high-speed interconnects”. In: *Proc. IEEE* 89.5 (May 2001), pp. 693–728. DOI: 10.1109/5.929650.

[112] G. Antonini, A. Orlandi, and S. A. Pignari. “Review of Clayton R. Paul studies on multiconductor transmission lines”. In: *IEEE Trans. Electromagn. Compat.* 55.4 (June 2013), pp. 639–647. DOI: 10.1109/TEMC.2013.2265038.

[113] R. Nuricumbo-Guillen et al. “Computation of transient profiles along non-uniform transmission lines using the numerical Laplace transform”. In: *2018 IEEE ICHVE* (Athens, Greece, Sept. 10–13, 2018). IEEE, pp. 1–4. DOI: 10.1109/ICHVE.2018.8642169.

[114] N. A.-Z. R-Smith and L. Brancik. “On two-dimensional numerical inverse laplace transforms with transmission line applications”. In: *2016 PIERS* (Shanghai, China, Aug. 8–11, 2016). IEEE, pp. 227–231. DOI: 10.1109/PIERS.2016.7734298.

[115] J. Abate and W. Whitt. “A unified framework for numerically inverting Laplace transforms”. In: *INFORMS J. Comput.* 18.4 (Jan. 2006), pp. 408–421. DOI: 10.1287/ijoc.1050.0137.

[116] D. Spina et al. “Efficient variability analysis of electromagnetic systems via polynomial chaos and model order reduction”. In: *IEEE Trans. Compon. Packag. Manuf. Technol.* 4.6 (Jan. 2014), pp. 1038–1051. DOI: 10.1109/TCPMT.2014.2312455.

[117] G. Antonini. “A Green’s function-based method for the transient analysis of transmission lines”. In: *2007 ICEAA* (Turin, Italy, Sept. 17–21, 2007). IEEE, pp. 375–378. DOI: 10.1109/ICEAA.2007.4387316.

[118] G. Antonini. “A dyadic Green’s function based method for the transient analysis of lossy and dispersive multiconductor transmission lines”. In: *IEEE Trans. Microw. Theory Techn.* 56.4 (Apr. 2008), pp. 880–895. DOI: 10.1109/TMTT.2008.919651.

[119] G. Antonini and L. Camillis. “Time-domain Green’s function-based sensitivity analysis of multiconductor transmission lines with nonlinear terminations”. In: *IEEE Microw. Wireless Compon. Lett.* 19.7 (Jan. 2009), pp. 428–430. DOI: 10.1109/LMWC.2009.2022120.

[120] D. Spina et al. “Time-domain Green’s function-based parametric sensitivity analysis of multiconductor transmission lines”. In: *IEEE Trans. Compon. Packag. Manuf. Technol.* 2.9 (Jan. 2012), pp. 1510–1517. DOI: 10.1109/TCPMT.2012.2186570.

[121] M. Lauretis et al. “Enhanced delay-rational Green’s method for cable time domain analysis”. In: *2015 ICEAA* (Turin, Italy, Sept. 7–11, 2015). IEEE, pp. 1228–1231. DOI: 10.1109/ICEAA.2015.7297314.

[122] M. Lauretis, G. Antonini, and J. Ekman. “A SPICE realization of the delay-rational Green’s-function-based method for multiconductor transmission lines”. In: *IEEE Trans. Electromagn. Compat.* 58.4 (Jan. 2016), pp. 1158–1168. DOI: 10.1109/TEMC.2016.2546552.

[123] T. Dhaene and D. de Zutter. “Selection of lumped element models for coupled lossy transmission lines”. In: *IEEE Trans. Comput.-Aided Design Integr. Circuits Syst.* 11.7 (July 1992), pp. 805–815. DOI: 10.1109/43.144845.

[124] X. Zeng and T. Wong. “Simulation of intermodulation generation in nonlinear transmission line”. In: *Proc. 39th Midwest Symp. Circuits Syst.* (Ames, IA, USA, Aug. 21, 1996). IEEE, pp. 1185–1188. DOI: 10.1109/MWSCAS.1996.593082.

[125] A. S. Mootaab, S. H. Fathi, and B. Vahidi. “State-space transient analysis of corona for AC and impulse voltage”. In: *2009 Int. Conf. EPECS* (Sharjah, United Arab Emirates, Nov. 10–12, 2009). IEEE, pp. 1–5.

[126] W. Jia and W. Xiaohui. “A numerical method for calculating lightning transient of transmission line with corona”. In: *2010 Int. Conf. ISDEA* (Changsha, China, Oct. 13–14, 2010). IEEE, pp. 129–132. DOI: 10.1109/ISDEA.2010.242.

[127] C. Collado, J. Mateu, and J. M. O’Callaghan. “Nonlinear simulation and characterization of devices with HTS transmission lines using harmonic balance algorithms”. In: *IEEE Trans. Appl. Supercond.* 11.1 (Mar. 2001), pp. 1396–1399. DOI: 10.1109/77.919612.

[128] A. R. Sridhar et al. “Fast EMI analysis via transverse partitioning and waveform relaxation”. In: *IEEE Trans. Electromagn. Compat.* 51.2 (May 2009), pp. 358–371. DOI: 10.1109/TEMC.2008.2005827.

[129] J. E. Schutt-Aine and R. Mittra. “Nonlinear transient analysis of coupled transmission lines”. In: *IEEE Trans. Circuits Syst* 36.7 (Jan. 1989), pp. 959–967. DOI: 10.1109/31.31331.

[130] A. Orlandi and C. R. Paul. “FDTD analysis of lossy, multiconductor transmission lines terminated in arbitrary loads”. In: *IEEE Trans. Electromagn. Compat.* 38.3 (Aug. 1996), pp. 388–399. DOI: 10.1109/15.536069.

[131] J. Kasper and R. Vick. “The effect of a bend on the stochastic-field coupling to a single wire transmission line over a conductive ground plane”. In: *2019 Int. Symp. EMC Europe* (Barcelona, Spain, Sept. 2–6, 2019). IEEE, pp. 476–480. DOI: 10.1109/EMCEurope.2019.8871831.

[132] T. Sekine, S. Usuki, and K. T. Miura. “Variability analysis of a non-uniform transmission line using stochastic Galerkin method”. In: *2020 Int. Symp. EMC Europe* (Rome, Italy, Sept. 23–25, 2020). IEEE, pp. 1–6. DOI: 10.1109/EMCEUROPE48519.2020.9245845.

[133] P. Hui and H. S. Tan. “A transmission-line theory for heat conduction in multilayer thin films”. In: *IEEE Trans. Compon., Packag. Manuf. Technol. B* 17.3 (Aug. 1994), pp. 426–434. DOI: 10.1109/96.311793.

[134] M. März and P. Nance. “Thermal modeling of power electronic system”. In: *Infineon Application Note* (Feb. 2000).

[135] W. Mathis and A. Reibiger. *Küpfmüller Theoretische Elektrotechnik: Elektromagnetische Felder, Schaltungen und elektronische Bauelemente*. 20., aktualisierte Auflage. Berlin, Germany: Springer, 2017. ISBN: 978-3-662-54837-0.

[136] T. L. Bergman, ed. *Introduction to heat transfer*. 6th ed. Hoboken, NJ, USA: Wiley, 2011. ISBN: 978-0-470-50196-2.

[137] H. D. Baehr and K. Stephan. *Wärme- und Stoffübertragung*. Berlin, Germany: Springer, 2019. ISBN: 978-3-662-58440-8.

[138] VDI-Gesellschaft Verfahrenstechnik und Chemieingenieurwesen. *VDI-Wärmeatlas*. Berlin, Germany: Springer, 2013. ISBN: 978-3-642-19981-3.

[139] B. Kipp. "Analytische Berechnung thermischer Vorgänge in permanentmagneterregten Synchronmaschinen". PhD thesis. Helmut-Schmidt-Universität der Bundeswehr Hamburg, Jan. 2008.

[140] S. W. Churchill and H. H. Chu Hui. "Correlating equations for laminar and turbulent free convection from a horizontal cylinder". In: *Int. J. Heat Mass Transf.* 18.9 (Sept. 1975), pp. 1049–1053. DOI: 10.1016/0017-9310(75)90222-7.

[141] X. Zeng and T. Wong. "A model-based automotive smart fuse approach considering environmental conditions and insulation aging for higher current load limits and short-term overload operations". In: *IEEE Int. Conf. ESARS-ITEC* (Nottingham, UK, Nov. 7–9, 2018), pp. 1–6. DOI: 10.1109/ESARS-ITEC.2018.8607390.

[142] J. Fraden. *Handbook of modern sensors*. Fifth Edition. Cham, Germany: Springer, 2016. ISBN: 978-3-319-19302-1.

[143] F. C. Van Wormer. "An improved approximate technique for calculating cable temperature transients [includes discussion]". In: *Trans. AIEE. III: Power App. Syst.* 74.3 (Jan. 1955), pp. 277–281. DOI: 10.1109/AIEEPAS.1955.4499079.

[144] F. Aras and Y. Biçen. "Thermal modelling and analysis of high-voltage insulated power cables under transient loads". In: *Comput. Appl. Eng. Educ.* 21.3 (Oct. 2010), pp. 516–529. DOI: 10.1002/cae.20497.

[145] N. Vierheilig. "Erwärmungsberechnung mehradriger Kabel und Leitungen im symmetrischen und unsymmetrischen Dauerbetrieb". In: *Archiv f. Elektrotechnik* 76.6 (Nov. 1993), pp. 443–450. DOI: 10.1007/BF01576024.

[146] H. Triebel. *Höhere Analysis*. Berlin, Germany: VEB Deutscher Verl. d. Wiss., 1972. ISBN: 978-387-1-44583-5.

[147] J. C. Cortes et al. "The complementary error matrix function and its role solving coupled diffusion mathematical models". In: *Math. Comput. Model.* 42.9 (Nov. 2005), pp. 1023–1034. DOI: 10.1016/j.mcm.2004.11.004.

[148] S. Hamdi, W. E. Schiesser, and G. W. Griffiths. "Method of lines". In: *Scholarpedia* 2.7 (2007), pp. 2859–2859. DOI: 10.4249/scholarpedia.2859.

[149] R. Chapko and R. Kress. “Rothe’s Method for the Heat Equation and Boundary Integral Equations”. In: *J. Integral Equ. Appl.* 9.1 (Mar. 1997), pp. 47–69. DOI: 10.1216/jiea/1181075987.

[150] Z. Li, Z. Qiao, and T. Tang. *Numerical solution of differential equations, Introduction to finite difference and finite element methods*. Cambridge, UK: Cambridge University Press, 2017. ISBN: 978-1-31667-872-5.

[151] R. J. LeVeque. *Finite difference methods for ordinary and partial differential equations: Steady-state and time-dependent problems*. Philadelphia, PA, USA: SIAM, 2007. ISBN: 978-0-89871-629-0.

[152] C. K. Chui and G. Chen. *Linear Systems and Optimal Control*. Berlin, Germany: Springer, 1989. ISBN: 978-3-642-61312-8.

[153] M. Baake and U. Schlägel. “The Peano–Baker Series”. In: *Proc. Steklov Inst. Math.* 275.1 (Dec. 2011), pp. 155–159. DOI: 10.1134/S0081543811080098.

[154] R. W. Freund and R. H. W. Hoppe. *Stoer/Bulirsch: Numerische Mathematik*. Berlin, Germany: Springer, 2007. ISBN: 978-3-540-45389-5.

[155] M. Hermann. *Numerische Mathematik*. München, Germany: Oldenbourg Wissenschaftsverlag, 2011. ISBN: 978-3-486-70820-2.

[156] Gregoire Allaire. *Numerical analysis and optimization: An introduction to mathematical modelling and numerical simulation*. New York, NY, USA: Oxford University Press, 2007. ISBN: 978-0-19-920521-9.

[157] O. C. Zienkiewicz, R. L. Taylor, and J. Z. Zhu. *The finite element method: Its basis and fundamentals*. Burlington, MA, USA: Elsevier, 2005. ISBN: 978-0-7506-6320-5.

[158] A. A. Becker. *The boundary element method in engineering: A complete course*. Cambridge, UK: McGraw-Hill, 1992. ISBN: 0-07-707439-4.

[159] A. Sutradhar, L. J. Gray, and G. H. Paulino. *Symmetric Galerkin boundary element method*. Berlin, Germany: Springer, 2008. ISBN: 978-3-540-68772-6.

[160] B. Davies. *Integral Transforms and Their Applications*. Berlin, Germany: Springer, 2002. ISBN: 978-1-4684-9283-5.

[161] Robert E., Thierry G., and Raphaèle H. “Finite volume methods”. In: *Solution of Equation in Rn (Part 3), Techniques of Scientific Computing (Part 3)*. Vol. 7. Handbook of Numerical Analysis. Amsterdam, Netherlands: Elsevier, 2000, pp. 713–1018. DOI: 10.1016/S1570-8659(00)07005-8.

[162] B. E. Rapp. *Microfluidics: Modeling, mechanics, and mathematics*. Amsterdam, Netherlands: Elsevier, 2017. ISBN: 978-1-4557-3141-1.

[163] D. Lau. *Algebra und diskrete Mathematik. 1: Grundbegriffe der Mathematik, algebraische Strukturen 1, lineare Algebra und analytische Geometrie, numerische Algebra*. Berlin, Germany: Springer, 2007. ISBN: 978-3-540-72364-6.

[164] MathWorks. *pdepe*. URL: [(visited on 09/11/2022).

[165] S. Önal, M. Kiffmeier, and S. Frei. "Modellbasierte intelligente Sicherungen mit umgebungsadaptiver Anpassung der Auslöseparameter". In: *EEHE* (Würzburg, Germany, June 12–13, 2018).

[166] Comsol Multiphysics GmbH. *COMSOL Multiphysics*. URL: %C2%B6 (visited on 09/11/2022).

[167] P. R. N. Childs. *Practical temperature measurement*. Amsterdam, Netherlands: Elsevier, 1972. ISBN: 978-0-7506-5080-9.

[168] S. O. Kasap. *Principles of electronic materials and devices*. 3. ed. New York, NY, USA: McGraw-Hill, 2006. ISBN: 0-07-295791-3.

[169] J. H. Dellinger. "The temperature coefficient of resistance of copper". In: *J. Franklin Inst.* 170.3 (Sept. 1910), pp. 213–216. DOI: 10.1016/S0016-0032(10)90872-7.

[170] V. Quintard et al. "Temperature measurements of metal lines under current stress by high-resolution laser probing". In: *IEEE Trans. Instrum. Meas.* 48.1 (Feb. 1999), pp. 69–74. DOI: 10.1109/19.755063.

[171] Keysight Technologies. *B2900A Series Precision Source/Measurement Unit*. URL: www.keysight.com/us/en/assets/7018-02794/data-sheets/5990-7009.pdf (visited on 09/11/2022).

[172] "Grundlagen der Meßtechnik, Teil 3: Auswertung von Messungen einer einzelnen Meßgröße, Meßunsicherheit". In: *DIN 1319-3:1996-05* (1996).

[173] Elektro-Automatik GmbH & Co. KG. *Instruction Manual PS 8000 2U Laboratory Power Supply*. URL: www.elektroautomatik.com/shop/media/pdf/8d/f9/ec/09230130.pdf (visited on 09/11/2022).

[174] D. Strehl. "Entwicklung eines Messaufbaus zur Bestimmung von elektrisch-thermischen Parametern für die Modellierung von Fahrzeugleitungen und -sicherungen". Bachelor's thesis. Technische Universität Dortmund, June 2012.

[175] H. Magsi et al. "Analysis of signal noise reduction by using filters". In: *2018 iCoMET* (Sukkur, Pakistan, Mar. 3–4, 2018). IEEE, pp. 1–6. DOI: 10.1109/ICOMET.2018.8346412.

[176] T. W. Kerlin and M. Johnson. *Practical thermocouple thermometry*. Second Edition. Research Triangle Park, NC, USA: ISA, 2012. ISBN: 978-1-937560-27-0.

[177] C. J. Yeager and S. S. Courts. “A review of cryogenic thermometry and common temperature sensors”. In: *IEEE Sensors J.* 1.4 (Dec. 2001), pp. 352–360. DOI: 10.1109/7361.983476.

[178] K. T. Nabila et al. “Multi-probe Thermocouple Transducer For Simultaneous Temperature Measurement”. In: *2019 IEEE 5th I2CT* (Bombay, India, Mar. 29–31, 2019). IEEE, pp. 1–4. DOI: 10.1109/I2CT45611.2019.9033632.

[179] C. Addison et al. “The genesis distributed-memory benchmarks. Part 1: Methodology and general relativity benchmark with results for the SUPRENUM computer”. In: *Concurr. Comput. Pract. Exper.* 5.1 (Feb. 1993), pp. 1–22. DOI: 10.1002/cpe.4330050102.

[180] L. Yu, M. Tang, and J. Mao. “Transient electro-thermal analysis of single-walled carbon nanotube (SWCNT) with transmission line model”. In: *2009 APMC* (Singapore, Dec. 7–10, 2009). IEEE, pp. 563–566. DOI: 10.1109/APMC.2009.5384166.

[181] Q. Shang, X. Li, and J. Mao. “Transient thermal analysis of global interconnects based on transmission lines”. In: *2012 APEMC* (Singapore, May 21–24, 2012). IEEE, pp. 245–248. DOI: 10.1109/APEMC.2012.6237947.

[182] R. Assaf, R. A. Z. Daou, and X. Moreau. “Time domain response for the fractional order transfer function characterizing the thermal diffusive interface”. In: *2015 3rd Int. Conf. TAEECE* (Beirut, Lebanon, Apr. 29–May 1, 2015). IEEE, pp. 190–194. DOI: 10.1109/TAEECE.2015.7113625.

[183] X. Meng, Z. Wang, and G. Li. “Dynamic analysis of core temperature of low-voltage power cable based on thermal conductivity”. In: *Can. J. Electr. Comput. Eng.* 39.1 (2016), pp. 59–65. DOI: 10.1109/CJECE.2015.2496205.

[184] D. Yan J. ad Jiao. “Matrix-free time-domain method for thermal analysis in unstructured meshes”. In: *2017 IEEE AP-S/URSI* (San Diego, CA, USA, July 9–14, 2017). IEEE, pp. 1793–1794. DOI: 10.1109/APUSNCURSINRSM.2017.8072939.

[185] Q. Min et al. “Electrical–thermal cosimulation of coaxial TSVs with temperature-dependent MOS effect using equivalent circuit models”. In: *IEEE Trans. Electromagn. Compat.* 62.5 (Oct. 2020), pp. 2247–2256. DOI: 10.1109/TEMC.2020.2973811.

[186] M. W. Abdulrahman. “Exact analytical solution for two-dimensional heat transfer equation through a packed bed reactor”. In: *Proc. 6th World Congr. MCM* (Virtual, Aug. 16–18, 2020). Avestia, pp. 167-1–167-10. DOI: 10.11159/htff20.167.

[187] V. M. Fatic and D. A. Castleberry. “Application of Lagrangian with reverse time scales to transients in RC-transmission lines. I. Propagation”. In: *38th MWSCAS* (Rio de Janeiro, Brazil, Aug. 13–16, 1995). IEEE, pp. 937–940. DOI: 10.1109/MWSCAS.1995.510244.

[188] V. M. Fatic and D. A. Castleberry. “Application of Lagrangian with reverse time scales to transients in RC-transmission lines. II. Diffusion”. In: *38th MWSCAS* (Rio de Janeiro, Brazil, Aug. 13–16, 1995). IEEE, pp. 1313–1316. DOI: 10.1109/MWSCAS.1995.510339.

Publications of the Author

[A.1] S. Önal, A. Henke, and S. Frei. “Switching strategies for smart fuses based on thermal models of different complexity”. In: *15th Int. Conf. EVER* (Virtual, Sept. 10–12, 2020). ©2020 IEEE (www.ieee.org). IEEE, pp. 1–10. DOI: 10.1109/EVER48776.2020.9243932.

[A.2] A. Henke and S. Frei. “Potentials of the application of the electrical transmission line theory for thermal investigations on cables”. In: *Adv. Radio Sci.* 19 (Dec. 2021). ©2021 Authors (www.creativecommons.org/licenses/by/4.0), pp. 1–10. DOI: 10.5194/ars-19-1-2021.

[A.3] A. Henke and S. Frei. “Fast analytical approaches for the transient axial temperature distribution in single wire cables”. In: *IEEE Trans. Ind. Electron.* 69.4 (Apr. 2022). ©2021 IEEE (www.ieee.org), pp. 4158–4166. DOI: 10.1109/TIE.2021.3071699.

[A.4] A. Henke and S. Frei. “Analytical approaches for fast computing of the thermal load of vehicle cables of arbitrary length for the application in intelligent fuses”. In: *Proc. 7th Int. Conf. VEHITS* (Virtual, Apr. 28–30, 2021). ©2021 Scitepress (www.vehits.scitevents.org/?y=2021). SciTePress, pp. 396–404. DOI: 10.5220/0010433003960404.

[A.5] A. Henke and S. Frei. “Analytic approaches for the transient temperature distribution in a single cable for smart fuses and ampacity derating calculation”. In: *Proc. 6th World Congr. MCM* (Virtual, Aug. 16–18, 2020). ©2020 International ASET Inc. (www.international-aset.com). Avestia, pp. 138-1–138-9. DOI: 10.11159/htff20.138.

[A.6] A. Henke and S. Frei. “Transient temperature calculation in a single cable using an analytic approach”. In: *JFFHMT* 7 (Nov. 2020). ©2020 Authors (www.creativecommons.org/licenses/by/3.0), pp. 58–65. DOI: 10.11159/jffhmt.2020.006.

[A.7] A. Henke and S. Frei. “Local temperature reduction in thin wire cables due to contacted thermocouples”. In: *IEEE Trans. Dielectr. Electr. Insul.* accepted to be published (2023). ©2023 IEEE (www.ieee.org). DOI: 10.1109/TDEI.2023.3247981.

[A.8] A. Henke and S. Frei. “Analytical thermal cable model for bundles of identical single wire cables”. In: *IEEE Trans. Power Electron.* manuscript submitted for publication (2023). ©2023 IEEE (www.ieee.org).

[A.9] A. Henke and S. Frei. “Analytical thermal cable models for ampacity derating calculation in smart fuses”. In: *EEHE Conf.* (Virtual, Nov. 8–9, 2021).

[A.10] A. Henke and S. Frei. “Temperature calculation for single wire cables with time varying step function excitations”. In: *J. Enhanc. Heat Transf.* 29.3 (May 2022). ©2022 Begell House Inc. (www.begellhouse.com), pp. 103–116. DOI: 10.1615/JEnhHeatTransf.2022040442.

List of Bachelor and Master Theses Supervised by the Author

1. J. Böllhoff, “Erweiterung und messtechnische Validierung von analytischen elektrothermischen Modellen für Kfz- Rundleitungen”, B.Sc. thesis, TU Dortmund University, On-board Systems Lab, Dortmund, Germany, Apr. 2020.

2. X. Zhou, “Development and implementation of an intelligent fusing strategy for PoDL-networks based on analytical thermal cable models”, M.Sc. thesis, TU Dortmund University, On-board Systems Lab, Dortmund, Germany, Oct. 2021.

3. N. Ebel, “Entwicklung und Realisierung einer intelligenten Absicherungsstrategie zum Leitungsschutz unter Verwendung von strombasierten Temperaturberechnungen”, B.Sc. thesis, TU Dortmund University, On-board Systems Lab, Dortmund, Germany, Oct. 2021.

4. H. Kilic, “Optimierung und Validierung einer intelligenten Absicherungsstrategie auf einer elektronischen Sicherung unter Verwendung von strombasierten Temperaturberechnungen”, B.Sc. thesis, TU Dortmund University, On-board Systems Lab, Dortmund, Germany, Mar. 2022.

5. H. Gong, “Untersuchung des Einflusses von Komponenten in der Nähe eines bestromten Leiters auf dessen Temperatur”, B.Sc. thesis, TU Dortmund University, On-board Systems Lab, Dortmund, Germany, Jun. 2022.

6. M. Schwierz, “Simulationsbasiertes Training eines neuronalen Netzes zur Diagnose von Leitungsfehlern in Kfz-Energieversorgungssystemen”, B.Sc. thesis, TU Dortmund University, On-board Systems Lab, Dortmund, Germany, Jan. 2023.

Appendices

A Modeling of a Multiconductor Arrangement

define radial nodes:
  for each conductive layer i: define one node $m_{\mathrm{c},i}$;
  for each insulation layer i:
    if (inner neighbor $\neq$ conductor): define nodes $m_{\mathrm{i,in},i}$ at inner limits;
    if (outer neighbor $\neq$ conductor): define node $m_{\mathrm{i,out},i}$ at outer limit;
    if (concentric layer & short term transients): define node $m_{\mathrm{i,mid},i}$ in insulation;
find general form of PDE:
  for each defined node i:
    add nodal temperature to temperature vector $\boldsymbol{T}$;
    add a new line and column to matrices $\mathbf{A}$ to $\mathbf{D}$;
equivalent circuits and matrix entries for individual elements:
  for each conductive layer i:
    draw equivalent circuit with nodes $m_{\mathrm{c},z,i}$, $m_{\mathrm{c},z+\mathrm{d}z,i}$ and ref;
    define or expand matrix entries for node $m_{\mathrm{c},i}$;
    for each conductive layer $j > i$:
      if (consider coupling between conductor i and j):
        draw equivalent circuit with nodes $m_{\mathrm{c},i}$ and $m_{\mathrm{c},j}$;
        expand matrix entries for node $m_{\mathrm{c},i}$;
        define matrix entries for node $m_{\mathrm{c},j}$;
  for each filling layer i:
    draw equivalent circuit, nodes $m_{\mathrm{f,in},1,i}$, ..., $m_{\mathrm{f,in},N,i}$, $m_{\mathrm{f,out},i}$, ref;
    define or expand matrix entries for nodes $m_{\mathrm{f,in},1,i}$, ..., $m_{\mathrm{f,in},N,i}$, $m_{\mathrm{f,out},i}$;
  for each concentric insulation layer i:
    draw equivalent circuit, nodes $m_{\mathrm{i,in},i}$, $m_{\mathrm{i,out},i}$, $m_{\mathrm{i,mid},i}$ (short-term transients), ref;
    define or expand matrix entries for nodes $m_{\mathrm{i,in},i}$, $m_{\mathrm{i,out},i}$, $m_{\mathrm{i,mid},i}$ (short-term transients);
  for each cable surface i:
    draw equivalent circuit with nodes $m_{\mathrm{s},i}$ and ref;
    expand matrix entries for node $m_{\mathrm{s},i}$;
parameter calculation:
  for each conductive layer i:
    calculate heat capacitance with equation (5.77);
    calculate heat flow with equation (5.78);
    calculate resistance with equation (5.79);
  for each concentric insulation layer i:
    calculate conductance with equation (5.82);
    if (simple RC-structure or long-term transients):
      calculate heat capacitance with equation (5.81);
      if (long-term transients): calculate $p_{\mathrm{i},i}$ with equation (5.86);
    if (short-term transients):
      calculate first heat capacitance with equation (5.89);
      calculate second heat capacitance with equation (5.90);
      calculate $p_{\mathrm{i},i}$ with equation (5.91);
  for each filling layer i:
    calculate capacitance with equation (5.95);
    for each inner structure j:
      calculate conductances (analytically, numerically or via measurement);
  for each cable surface i:
    calculate conductance with equation (5.99);
  for all considered couplings between conductors i and j:
    calculate conductance G'_{ij} (analytically, numerically or via measurement);

Figure A.1: Steps for the determination of the PDE from the physical setup (pseudocode).

Table A.1: Matrix entries for the different elements.

	$\tilde{\mathbf{A}}$	$\tilde{\mathbf{B}}$	$\tilde{\boldsymbol{C}}$	$\tilde{\mathbf{D}}$
conductor	$\begin{matrix} & m_\mathrm{c} \\ m_\mathrm{c} & (\mathcal{C}'_\mathrm{c}) \end{matrix}$	/	$m_\mathrm{c}\left(P'_\mathrm{el,c}\right)$	$\begin{matrix} & m_\mathrm{c} \\ m_\mathrm{c} & \left(\frac{1}{R'_\mathrm{c}}\right) \end{matrix}$
insul. RC	$\begin{matrix} & m_\mathrm{i,in} \\ m_\mathrm{i,in} & (\mathcal{C}'_\mathrm{i}) \end{matrix}$	$\begin{matrix} & m_\mathrm{i,in} & m_\mathrm{i,out} \\ m_\mathrm{i,in} & G'_\mathrm{i} & -G'_\mathrm{i} \\ m_\mathrm{i,out} & -G'_\mathrm{i} & G'_\mathrm{i} \end{matrix}$	/	/
insul. V.-W. (long)	$\begin{matrix} & m_\mathrm{i,in} & m_\mathrm{i,out} \\ m_\mathrm{i,in} & p_\mathrm{i,lo}\mathcal{C}'_\mathrm{i} & \\ m_\mathrm{i,out} & & (1-p_\mathrm{i,lo})\mathcal{C}'_\mathrm{i} \end{matrix}$	$\begin{matrix} & m_\mathrm{i,in} & m_\mathrm{i,out} \\ m_\mathrm{i,in} & G'_\mathrm{i} & -G'_\mathrm{i} \\ m_\mathrm{i,out} & -G'_\mathrm{i} & G'_\mathrm{i} \end{matrix}$	/	/
insul. V.-W. (short)	$\begin{matrix} & m_\mathrm{i,in} & m_\mathrm{i,mid} & m_\mathrm{i,out} \\ m_\mathrm{i,in} & p_\mathrm{i}\mathcal{C}'_{\mathrm{i},1} & & \\ m_\mathrm{i,mid} & & (1-p_\mathrm{i})\mathcal{C}'_{\mathrm{i},1}+p_\mathrm{i}\mathcal{C}'_{\mathrm{i},2} & \\ m_\mathrm{i,out} & & & (1-p_\mathrm{i})\mathcal{C}'_{\mathrm{i},2} \end{matrix}$	$\begin{matrix} & m_\mathrm{i,in} & m_\mathrm{i,mid} & m_\mathrm{i,out} \\ m_\mathrm{i,in} & 2G'_\mathrm{i} & -2G'_\mathrm{i} & \\ m_\mathrm{i,mid} & -2G'_\mathrm{i} & 4G'_\mathrm{i} & -2G'_\mathrm{i} \\ m_\mathrm{i,out} & & -2G'_\mathrm{i} & 2G'_\mathrm{i} \end{matrix}$	/	/
filling	$\begin{matrix} & m_\mathrm{f,out} \\ m_\mathrm{f,out} & (\mathcal{C}'_\mathrm{f}) \end{matrix}$	$\begin{matrix} & m_{\mathrm{f,in},1} & m_{\mathrm{f,in},2} & \dots & m_{\mathrm{f,in},N} & m_\mathrm{f,out} \\ m_{\mathrm{f,in},1} & G'_{\mathrm{f},1} & & & & -G'_{\mathrm{f},1} \\ m_{\mathrm{f,in},2} & & G'_{\mathrm{f},2} & & & -G'_{\mathrm{f},2} \\ \vdots & & & \ddots & & \vdots \\ m_{\mathrm{f,in},N} & & & & G'_{\mathrm{f},N} & -G'_{\mathrm{f},N} \\ m_\mathrm{f,out} & -G'_{\mathrm{f},1} & -G'_{\mathrm{f},2} & \dots & -G'_{\mathrm{f},N} & \sum_{i=1}^{N} G'_{\mathrm{f},i} \end{matrix}$	/	/
surface	/	$\begin{matrix} & m_\mathrm{s} \\ m_\mathrm{s} & (G'_\mathrm{s}) \end{matrix}$	$m_\mathrm{s}\left(-G'_\mathrm{s}T_\mathrm{e}\right)$	/
coupling	/	$\begin{matrix} & m_{\mathrm{c},1} & m_{\mathrm{c},2} \\ m_{\mathrm{c},1} & G'_{12} & -G'_{12} \\ m_{\mathrm{c},2} & -G'_{12} & G'_{12} \end{matrix}$	/	/

B Solution for Arrangement of Two Conductors

For the direct solution in the Laplace domain with approximation, the solution for case 1 is given in the following. For both subcases, the following parameters are used:

$$
\begin{aligned}
\lambda_2 &= \frac{A_{22}B_{11} + A_{11}B_{22}}{A_{11}A_{22}}, \quad \lambda_3 = \frac{B_{11}B_{22} - B_{12}B_{21}}{A_{11}A_{22}},\\
\lambda_{22} &= \frac{1}{2}(A_{11} - A_{22}), \quad \lambda_{23} = \frac{1}{2}(B_{11} - B_{22}),\\
\mathbf{A}^{-1}\mathbf{B} &= \mathbf{V}\mathbf{D}\mathbf{V}^{-1},\\
\begin{pmatrix} T_{\infty,1} \\ T_{\infty,2} \end{pmatrix} &= \mathbf{V}\exp(-\gamma t)\cdot\mathbf{V}^{-1}(\boldsymbol{T}_{0,\mathrm{tu}} + \mathbf{B}^{-1}\boldsymbol{C}) - \mathbf{B}^{-1}\boldsymbol{C},\\
\mathrm{PBZ}(k, a_9, a_6) &= -\frac{\exp(-a_9 t)}{2}\\
&\quad\cdot\left[\exp(-a_6\sqrt{a_{2,k} - a_{1,k}a_9}\left\{\mathrm{erf}\left(\frac{|a_6|a_{1,k} - 2\sqrt{a_{2,k} - a_{1,k}a_9}t}{2\sqrt{a_{1,k}t}}\right) - 1\right\}\right.\\
&\quad\left.+\exp(a_6\sqrt{a_{2,k} - a_{1,k}a_9}\left\{\mathrm{erf}\left(\frac{|a_6|a_{1,k} + 2\sqrt{a_{2,k} - a_{1,k}a_9}t}{2\sqrt{a_{1,k}t}}\right) - 1\right\}\right],\\
a_{9,\pm} &= - = \frac{1}{2}(\lambda_2 \pm Q),\\
f_1(y,l) &= A_{11}A_{22}\left(T_{yl} - T_{0l}\right),\\
f_2(y,l) &= A_{3-l,3-l}C_l + (A_{22}B_{11} + A_{11}B_{22})T_{yl} - (3-2l)A_{11}B_{2,3-l}T_{0,\mathrm{tu},1}\\
&\quad + (3-2l)A_{22}B_{1,2-l}T_{0,\mathrm{tu},2},\\
f_3(y,l) &= (3-2l)B_{2,3-l}C_{\mathrm{tu},1} - (3-2l)B_{1,3-l}C_{\mathrm{tu},2}\\
&\quad + (B_{11}B_{22} - B_{12}B_{21})T_{yl},\\
P_1(n) &= \mathrm{PBZ}(+, a_{9,+}, z + nL) - \mathrm{PBZ}(+, a_{9,+}, -z + (2-n)\mathcal{L}),\\
P_2(n) &= \mathrm{PBZ}(-, a_{9,+}, z + nL) - \mathrm{PBZ}(-, a_{9,+}, -z + (2-n)\mathcal{L}),\\
P_3(n) &= \mathrm{PBZ}(+, a_{9,-}, z + nL) - \mathrm{PBZ}(+, a_{9,-}, -z + (2-n)\mathcal{L}),\\
P_4(n) &= \mathrm{PBZ}(-, a_{9,-}, z + nL) - \mathrm{PBZ}(-, a_{9,-}, -z + (2-n)\mathcal{L}),\\
P_5(n) &= \mathrm{PBZ}(+, 0, z + nL) - \mathrm{PBZ}(+, 0, -z + (2-n)\mathcal{L}),\\
P_6(n) &= \mathrm{PBZ}(-, 0, z + nL) - \mathrm{PBZ}(-, 0, -z + (2-n)\mathcal{L}).
\end{aligned}
$$

The solution for the subcase $\hat{A} \neq 0 \wedge \hat{B} \neq 0$ is

$$
\begin{aligned}
T(z,t) = T_{\infty,l} &+ F_1(1,l)P_1(0) - F_2(1,l)P_2(0) + F_5(1,l)P_3(0) - F_4(1,l)P_4(0)\\
&+ F_6(1,l)P_5(0) - F_7(1,l)P_6(0) - F_1(2,l)P_1(1) + F_2(2,l)P_2(1)\\
&- F_5(2,l)P_3(1) + F_4(2,l)P_4(1) - F_6(2,l)P_5(1) + F_7(2,l)P_6(1)\\
&+ F_3(1,l)[-\mathrm{PBZ}(-, W, z) + \mathrm{PBZ}(+, W, z) + \mathrm{PBZ}(-, W, -z + 2\mathcal{L})
\end{aligned}
$$

$$- \mathrm{PBZ}(+, W, -z + 2\mathcal{L})] + F_3(2, l)[-\mathrm{PBZ}(-, W, z + \mathcal{L})$$
$$+ \mathrm{PBZ}(-, W, z + \mathcal{L}) - \mathrm{PBZ}(-, W, -z + \mathcal{L}) + \mathrm{PBZ}(+, W, -z + \mathcal{L})].$$

The following parameters and abbreviations are used:

$$W = \frac{(B_{11} - B_{22})^2 + 4B_{12}B_{21}}{(A_{22} - A_{11})(B_{22} - B_{11})},$$
$$Q = \sqrt{\lambda_2^2 - 4\lambda_3},$$
$$V_0 = \frac{\sqrt{(B_{11} - B_{22})^2 + 4B_{12}B_{21}}}{4A_{11}A_{22}|\lambda_{22}\lambda_{23}|},$$
$$a_{1,\pm} = \frac{A_{11} + A_{22}}{2} \pm \frac{2|\lambda_{22}\lambda_{23}|}{\sqrt{(B_{11} - B_{22})^2 + 4B_{12}B_{21}}},$$
$$a_{2,\pm} = \frac{B_{11} + B_{22}}{2} \pm \frac{\mathrm{sign}(\lambda_{22}\lambda_{23})}{2}\sqrt{(B_{11} - B_{22})^2 + 4B_{12}B_{21}}$$
$$\begin{aligned}
F_1(y,l) = {} & V_0 \{(3-2l) f_y(y,l)\lambda_{22}\lambda_{37} + [(3-2l)(f_1(y,l)\lambda_{23} + f_2(y,l)\lambda_{22}) \\
& + B_{l,3-l} f_1(y, 3-l)]\lambda_{40} + [(3-2l)(f_2(y,l)\lambda_{23} + f_3(y,l)\lambda_{22}) \\
& + B_{l,3-l} f_2(y, 3-l)]\lambda_{43} + [(3-2l) f_3(y,l)\lambda_{23} + B_{l,3-l} f_3(y, 3-l)]\,\lambda_{46}\} \\
& + \frac{1}{2a_{11}a_{22}Q}\left(\frac{f_1(y,l)}{2}(\lambda_2 + Q) - f_2(y,l) + \frac{f_3(y,l}{2\lambda_3}(\lambda_2 - Q)\right),
\end{aligned}$$
$$F_2(y,l) = F_1(y,l) - \frac{1}{A_{11}A_{22}Q}\left(\frac{f_1(y,l)}{2}(\lambda_2 + Q) - f_2(y,l) + \frac{f_3(y,l)}{2\lambda_3}(\lambda_2 - Q)\right),$$
$$\begin{aligned}
F_3(y,l) = {} & V_0 \Bigg\{(3-2l) f_1(y,l)\lambda_{22}\lambda_{38} + \lambda_{44}\Bigg(-W[(3-2l)(f_1(y,l)\lambda_{23} + f_2(y,l)\lambda_{22}) \\
& + B_{l,3-l} f_1(y, 3-l)] + [(3-2l)(f_2(y,l)\lambda_{23} + f_3(y,l)\lambda_{22}) + B_{l,3-l} f_2(y, 3-l)] \\
& - \frac{1}{W}[(3-2l) f_3(y,l)\lambda_{23} + B_{l,3-l} f_3(y, 3-l)]\Bigg)\Bigg\},
\end{aligned}$$
$$\begin{aligned}
F_4(y,l) = {} & -F_1(y,l) - F_3(y,l) + V_0 \left\{(3-2l) f_1(y,l)\lambda_{22} - \frac{1}{W\lambda_3}[(3-2l) f_3(y,l)\lambda_{23}\right. \\
& \left. + B_{l,3-l} f_3(y, 3-l)]\right\} + \frac{1}{2a_{11}a_{22}Q}\left(-2f_2(y,l) + f_3(y,l)\frac{\lambda_2}{\lambda_3} + f_1(y,l)\lambda_2\right),
\end{aligned}$$
$$\begin{aligned}
F_5(y,l) = {} & -F_1(y,l) - F_3(y,l) + V_0 \left\{(3-2l) f_1(y,l)\lambda_{22} - \frac{1}{W\lambda_3}[(3-2l) f_3(y,l)\lambda_{23}\right. \\
& \left. + B_{l,3-l} f_3(y, 3-l)]\right\} + \frac{1}{2A_{11}A_{22}}\left(f_1(y,l) - \frac{f_3(y,l)}{\lambda_3}\right),
\end{aligned}$$
$$\begin{aligned}
F_6(y,l) = {} & \frac{1}{A_{11}A_{22}\lambda_3}\left\{\frac{2}{\mathrm{sign}(\lambda_{22}\lambda_{23})\sqrt{(B_{11} - B_{22})^2 + 4B_{12}B_{21}}}\right. \\
& \left. \cdot[(3-2l) f_3(y,l)\lambda_{23} + B_{l,3-l} f_3(y, 3-l)] + f_3(y,l)\right\},
\end{aligned}$$
$$F_7(y,l) = F_6(y,l) - \frac{f_3(y,l}{A_{11}A_{22}\lambda_3},$$

$$\lambda_{44} = \frac{1}{\lambda_3 - \lambda_2 W + W^2}, \quad \lambda_{37} = \frac{(Q+\lambda_2)(\lambda_3 - \lambda_2 W) + 2W\lambda_3}{2Q}\lambda_{44},$$
$$\lambda_{38} = -\frac{\lambda_2(\lambda_3 - \lambda_2 W - W^2) + QW^2 + 2W^3}{\lambda_2 - Q - 2W}\lambda_{44}, \quad \lambda_{40} = \frac{-2\lambda_3 + \lambda_2 W + WQ}{2Q}\lambda_{44},$$
$$\lambda_{43} = \frac{\lambda_2 - Q - 2W}{2Q}\lambda_{44}, \quad \lambda_{46} = -\frac{(-\lambda_2 + Q)(-\lambda_2 + W) - \lambda_3}{2\lambda_3 Q}\lambda_{44}.$$

The solution for the subcase $(\hat{A} = 0 \wedge \hat{B} \neq 0) \vee (\hat{B} = 0)$ is

$$\begin{aligned} T(z,t) = T_{\infty,l} &+ X_1(l,1,1,1)P_1(0) - X_1(l,1,-1,1)P_2(0) + X_1(l,1,1,-1)P_3(0) \\ &- X_1(l,1,-1,-1)P_4(0) + X_2(l,1,1)P_5(0) - X_2(l,1,-1)P_6(0) \\ &- X_1(l,2,1,1)P_1(1) + X_1(l,2,-1,1)P_2(1) - X_1(l,2,1,-1)P_3(1) \\ &+ X_1(l,2,-1,-1)P_4(1) - X_2(l,2,1)P_5(1) + X_2(l,2,-1)P_6(1) \\ &+ X_3(l,1)\left(-\mathrm{Term}_{0,-}(z) + \mathrm{Term}_{0,+}(z) + \mathrm{Term}_{0,-}(-z+2\mathcal{L})\right. \\ &\left.-\mathrm{Term}_{0,+}(-z+2\mathcal{L})\right) + X_3(l,2)\left(\mathrm{Term}_{0,-}(z+\mathcal{L}) - \mathrm{Term}_{0,+}(z+\mathcal{L})\right. \\ &\left.-\mathrm{Term}_{0,-}(-z+\mathcal{L}) + \mathrm{Term}_{0,+}(-z+\mathcal{L})\right). \end{aligned}$$

The following parameters and abbreviations are used:

$$\mathrm{Term}_{0,\pm}(a_6) = \frac{a_6\sqrt{a_1}\exp\left(-\frac{a_6^2 a_1}{4t} - \frac{a_{2,\pm}t}{a_1}\right)}{2\sqrt{t^3\pi}},$$
$$a_{1,\pm} = \frac{A_{11}+A_{22}}{2}, \quad a_{2,\pm} = \frac{B_{11}+B_{22}}{2} \pm W_0,$$
$$\begin{aligned} X_1(l,y,v_1,v_2) = \frac{1}{2A_{11}A_{22}W_0\sqrt{\lambda_2^2-4\lambda_3}}&\left[\left(f_1(y,l)\left((3-2y)(3-2l)\lambda_{22}\lambda_2 + (3-2l)\lambda_{23}\right.\right.\right. \\ &\left.\left.\left.+v_1W_0\right) + f_2(y,l)(3-2l)\lambda_{22} + B_{l,3-l}f_1(y,3-l)\right)\frac{v_2\lambda_2 + \sqrt{\lambda_2^2-4\lambda_3}}{2} \right. \\ &- v_2\left((3-2y)f_1(y,l)(3-2l)\lambda_{22}\lambda_3 + f_2(y,l)\left((3-2l)\lambda_{23} + v_1W_0\right)\right. \\ &\left.+B_{l,3-l}f_3(y,3-l)\right)\frac{\lambda_2 - v_2\sqrt{\lambda_2^2-4\lambda_3}}{2\lambda_3} + f_3(y,l)(3-2l)\lambda_{22} \\ &\left.+B_{l,3-l}f_2(y,3-l)\right) + v_2\left(f_3(y,l)\left((3-2l)\lambda_{23} + v_1W_0\right)\right]. \end{aligned}$$
$$X_2(l,y,v_1) = \frac{1}{2A_{11}A_{22}W_0\lambda_3}\left(f_3(y,l)\left((3-2l)\lambda_{23} + v_1W_0\right) - b_{l,3-l}f_3(y,3-l)\right),$$
$$X_3(l,y) = \frac{f_1(y,l)(3-2l)\lambda_{22}}{2A_{11}A_{22}W_0}.$$

C Exemplary MATLAB code

At first, the solution approach for the single wire cable with constant excitations is implemented:

```
% temperature calculation for single wire cable

% define global parameters
global C_tot R R_i R_ref T_ref r_i I nu_T epsilon T_e sigma g T_0 T_1 T_2 % necessary
    for solution with pdepe

%% parameters
% geometrical and physical cable properties
L = 1.5; % cable length, in m

n_strand = 30; % number of strands of the inner conductor
d_strand = 0.25e-3; % strand diameter, in m
d_i = 0.7e-3; % insulation thickness, in m
r_i = 1.7e-3; % outer insulation radius, in m

k_i = 0.7; % correction factor for R_i

c_c = 3.4e6; % specific heat capacitance of conductor, in J/m^3K
c_i = 2.2450e6; % specific heat capacitance of insulation, in J/m^3K

lambda_c = 386; % thermal conductivity of conductor, in W/(m*K)
lambda_i = 0.21; % thermal conductivity of insulation, in W/(m*K)

R_ref = 13e-3; % electrical reference resistance at T_ref, in Ohm/m
T_ref = 24.9; % reference temperature, in degC

nu_T = 3.93e-3; % linear temperature coefficient of conductor, in 1/K
epsilon = 0.95; % emissivity of cable surface

% define time and spatial points for analytical calculations
z = linspace(0,L,151); % z for analytical calculations, in m
t_end = 490; % last calculated time, in s
t = linspace(0,t_end,99); % t for analytical calculations, in s

% define time and spatial points for numerical calculations
Delta_z_num = L/150; % Delta z for numerical calculations, in m
z_num = 0:Delta_z_num:L; % z for numerical calculations, in m
Delta_t_num = 1; % Delta t for numerical calculations, in s
t_num = 0:Delta_t_num:round(t_end); % t for numerical calculations, in s

% current
I = 30; % current that is switched on at t = 0 s, in A

% envirionmental, initial and termination temperatures
T_e = 25; % environmental temperature, in degC
T_0 = 25; % initial conductor temperature for all z, in degC
T_1 = 25; % conductor temperature at z = 0 m for all times, in degC
T_2 = 25; % conductor temperature at z = L for all times, in degC

% termination condition
Delta_Tlim = 0.001; % termination condition, if temperatures from two iterations
```

```
    deviate by less than this value, iteration is stopped, in K

% number of addends for Geen's functions solutions
n_max = 1; % number of addends for Green's functions solution (time domain)
m_max = 10; % number of addends for Green's functions solution (Laplace domain), for
    initial value and inhomogeneity
m_max_2 = 2000; % number of addends for Green's functions solution (Laplace domain),
    for termination conditions

%% constants
sigma = 5.67040e-8; % Stefan-Boltzmann constant, in W/(m^2K^4)
g = 9.81; % graviational acceleration, in m/s^2

%% precalculations
% effective and geometrical conductor radius
r_ceff = sqrt(n_strand)*d_strand/2; % effective conductor radius, in m
r_cgeom = r_i-d_i; % geometrical conductor radius, in m

% calculation heat capacitance
C_c = c_c*pi*r_ceff^2; % heat capacitance of conductor
C_i = c_i*pi*(r_i^2-r_cgeom^2); % heat capacitance of insulation
C_tot = C_i + C_c; % total cable heat capacitance

% characteristic cable length
l_alpha = 2*r_i;

% resistance for heat conduction through insulation
R_i = k_i*log(r_i/r_cgeom)/(2*pi*lambda_i);

% resistance for axial heat conduction in conductor
R = 1/(lambda_c*pi*r_ceff^2);

% initialization
R_alpha_initial = 3.5; % initial value for R_alpha

% output
disp('Precalculations done.');

%% iterative temperature calculation
tic % for time measurement

T = zeros(numel(z), numel(t)); % initialization cable temperature
T(:,1) = T_0*ones(size(T(:,1))); % use initial cable temperature for t = 0 s

A = R*C_tot; % parameter of the PDE

T_guess = T_e; % initialization value for cable temperature

for idx_z = 1 : numel(z)
    z_loc = z(idx_z); % local position
    % termination conditions, no calculation necessary:
    if z(idx_z) == 0
        T(idx_z,:) = T_1*ones(1,numel(t));
        continue
    elseif z(idx_z) == L
        T(idx_z,:) = T_2*ones(1,numel(t));
```

```
        continue
    end
    for idx_t = 2 : numel(t) % start with second time step, first one is t = 0 s (
        initial cable temperature)
        t_loc = t(idx_t); % local time
        % initializations
        R_alpha = R_alpha_initial;
        counter_loop_it = 0; % counter for loop for iterations
        T_last = -100;
        % iteration for temperature calcualation
        while counter_loop_it < 100 && (abs(T_last-T(idx_z,idx_t))>Delta_Tlim) %
            termination condition
            counter_loop_it = counter_loop_it + 1;
            if counter_loop_it > 1
                T_last = T(idx_z,idx_t); % update temperature
            else
                T_last = T_guess; % initialization temperature
            end
            % electrical losses
            P_el = I^2*R_ref*(1+nu_T*(T_last - T_ref)); % electrical losses = thermal
                power

            % surface temperature
            T_s = T_last-R_i/(R_i+R_alpha)*(T_last-T_e); % surface temperature

            % 4th order polynomials for parameters
            T_m = 0.5*(T_s+T_e); % mean temperature between surface and environement
            v_air = 1.77e-17*T_m^4-4.83e-14*T_m^3+1.14e-10*T_m^2+8.81e-8*T_m+1.35e-5;
                % kinematic viscosity of the air, in m^2/s
            Pr = 2.23e-13*T_m^4-6.27e-10*T_m^3+5.91e-7*T_m^2-1.58e-4*T_m+0.711; %
                Prandtl number
            lambda_air = -1.35e-14*T_m^4+3.64e-11*T_m^3-4.33e-8*T_m^2+7.7e-5*T_m+2.43e
                -2; % thermal conductivity of the air, in W/(m*K)

            % temperatures in Kelvin
            T_sK = T_s+273.15; % surface temperature in Kelvin
            T_eK = T_e+273.15; % environmental temperature in Kelvin

            % calculation of R_alpha
            alpha_rad = epsilon * sigma * (T_sK^2+T_eK^2)*(T_sK+T_eK); % heat transfer
                 coefficient for radiation
            Gr = g*l_alpha^3*abs(T_s-T_e)/(T_eK*v_air^2); % Grashof number
            Ra = Gr*Pr; % Rayleigh number
            Nu = (0.6+0.387*Ra^(1/6)/((1+(0.559/Pr)^(9/16))^(8/27)))^2; % Nusselt
                number
            alpha_conv = Nu*lambda_air/l_alpha; % heat transfer coefficient for
                convection
            R_alpha = 1/((alpha_conv + alpha_rad)*2*pi*r_i); % resistance for
                convection and radiation

            % coupling between conductor and environment
            G = 1/(R_i+R_alpha); % conductance for coupling between conductor and
                environment

            % PDE parameters
            B = R*G;
```

```
149             C = -R*(P_el+G*T_e);
150 
151             % temperature calculation for different solutions
152             T(idx_z,idx_t) = T_sw_La(A,B,C,L,T_0,T_1,T_2,z_loc,t_loc); % solution from
                    Laplace domain with approximation
153 %             T(idx_z,idx_t) = T_sw_G(A,B,C,L,T_0,T_1,T_2,z_loc,t_loc,n_max); %
    solution with Green's function in time domain
154 %             T(idx_z,idx_t) = T_sw_GL(A,B,C,L,T_0,T_1,T_2,z_loc,t_loc,m_max,m_max_2);
     % solution with Green's function in Laplace domain
155 
156         end
157         time = toc; % measure time
158     end
159 end
160 disp(['Analytical calculation done (' num2str(time) ' s).']) % print time
161 
162 %% numerical temperature calculation with pdepe
163 tic % for time measurement
164 m = 0;
165 sol = pdepe(m,@pde,@pdeic,@pdebc,z_num,t_num); % calculate solution
166 T_pdepe = transpose(sol(:,:,1));
167 time = toc; % measure time
168 disp(['Numerical calculation done (' num2str(time) ' s).']) % print time
169 
170 %% local functions for pdepe
171 function [c,f,s] = pde(~,~,u,dudz) % pde(z,t,u,dudz)
172 global C_tot R R_i R_ref T_ref r_i I nu_T epsilon T_e sigma g % global variables
173 
174 % characteristic cable length
175 l_alpha = 2*r_i;
176 
177 % electrical losses
178 P_el = @(T) -I^2*R_ref*(1+nu_T*(T - T_ref));
179 
180 % 4th order polynomials for parameters
181 v_air = @(T_s) 1.77e-17*(0.5*(T_s + T_e))^4-4.83e-14*(0.5*(T_s + T_e))^3+1.14e
    -10*(0.5*(T_s + T_e))^2+8.81e-8*(0.5*(T_s + T_e))+1.35e-5; % kinematic viscosity
    of the air, in m^2/s
182 Pr = @(T_s) 2.23e-13*(0.5*(T_s + T_e))^4-6.27e-10*(0.5*(T_s + T_e))^3+5.91e-7*(0.5*(
    T_s + T_e))^2-1.58e-4*(0.5*(T_s + T_e))+0.711; % Prandtl number
183 lambda_air = @(T_s) -1.35e-14*(0.5*(T_s + T_e))^4+3.64e-11*(0.5*(T_s + T_e))^3-4.33e
    -8*(0.5*(T_s + T_e))^2+7.7e-5*(0.5*(T_s + T_e))+2.43e-2; % thermal conductivity of
     the air, in W/(m*K)
184 
185 % temperatures in Kelvin
186 T_eK = T_e+273.15; % environmental temperature in Kelvin
187 
188 % calculation of R_alpha
189 alpha_rad = @(T_s) epsilon * sigma * ((T_s + 273.15).^2+T_eK^2)*(T_s + 273.15+T_eK); %
     heat transfer coefficient for radiation
190 Gr = @(T_s) g*l_alpha^3*abs(T_s-T_e)./(T_eK*v_air(T_s)^2); % Grashof number
191 Ra = @(T_s) Gr(T_s).*Pr(T_s); % Rayleigh number
192 Nu = @(T_s) (0.6+0.387*Ra(T_s)^(1/6)./((1+(0.559/Pr(T_s))^(9/16))^(8/27)))^2; %
    Nusselt number
193 alpha_conv = @(T_s) Nu(T_s)*lambda_air(T_s)/l_alpha; % heat transfer coefficient for
    convection
```

```
R_alpha = @(T_s) 1/((alpha_conv(T_s) + alpha_rad(T_s))*2*pi*r_i); % resistance for convection and radiation

% coupling between conductor and environment
G = @(T_s) 1./(R_i+R_alpha(T_s)); % conductance for coupling between conductor and environment

% code equations
c = [C_tot*R;0];
f = [1; 0] .* dudz;
s = [-R*G(u(2))*u(1)+R*(-P_el(u(1))+G(u(2))*T_e); u(1)-u(2)-R_i*(u(1)-T_e)*G(u(2))]; % u = [T; T_s]

end

function u0 = pdeic(~) % pdeic(z)
% code initial condition
global T_0
u0 = T_0 * [1;1];
end

function [pl,ql,pr,qr] = pdebc(~,ul,~,ur,~) % pdebc(zl,ul,zr,ur,t)
% code boundary condition
global T_1 T_2
pl = ul - T_1*[1;1];
ql = [0; 0];
pr = ur - T_2*[1;1];
qr = [0; 0];
end
```

For the solution in the Laplace domain with approximation, the following function is used:

```
function [T] = T_sw_La(A,B,C,L,T_0,T_1,T_2,z,t)

Lambda_1 = @(z) erf(z/2*sqrt(A/t));
theta_1 = @(z) -exp(-z*sqrt(B))*erfc((z*A-2*t*sqrt(B))/(2*sqrt(A*t)));
theta_2 = @(z) -exp( z*sqrt(B))*erfc((z*A+2*t*sqrt(B))/(2*sqrt(A*t)));
Lambda_2 = @(z) theta_1(z) + theta_2(z);
Lambda_3 = exp(-B/A*t);

T_ic_sw_La = @(T_0) -T_0*Lambda_3*(1-Lambda_1(z)-Lambda_1(L-z));
T_bc_sw_La = @(T_bc,z) -T_bc/2*Lambda_2(z);
T_inh_sw_La = -C/B + T_ic_sw_La(C/B) + T_bc_sw_La(C/B,z) + T_bc_sw_La(C/B,L-z);

T = T_ic_sw_La(T_0) + T_bc_sw_La(T_1,z) + T_bc_sw_La(T_2,L-z) + T_inh_sw_La;

end
```

For the solution via Green's functions in the time domain, the following function is used:

```
function [T] = T_sw_G(A,B,C,L,T_0,T_1,T_2,z,t,n_max)

Lambda_1 = @(z) erf(z/2*sqrt(A/t));
theta_1 = @(z) -exp(-z*sqrt(B))*erfc((z*A-2*t*sqrt(B))/(2*sqrt(A*t)));
theta_2 = @(z) -exp( z*sqrt(B))*erfc((z*A+2*t*sqrt(B))/(2*sqrt(A*t)));
Lambda_2 = @(z) theta_1(z) + theta_2(z);
Lambda_3 = exp(-B/A*t);
```

```
8
9  % expressions without sum
10 T_ic_sw_G = @(T_0) -T_0*Lambda_3*(1-Lambda_1(z)-Lambda_1(L-z));
11 T_bc_sw_G = @(T_bc,z) -T_bc/2*Lambda_2(z);
12
13 % additional terms in sum
14 for n = 1 : n_max
15     T_ic_sw_G = @(T_0) T_ic_sw_G(T_0) - T_0*Lambda_3*(Lambda_1(-(L-z)+2*n*L)-Lambda_1(
           z+2*n*L)+Lambda_1(-(L-z)-2*n*L)-Lambda_1(z-2*n*L));
16     T_bc_sw_G = @(T_bc,z) T_bc_sw_G(T_bc,z) - T_bc/2*(Lambda_2(z+2*n*L)-Lambda_2(-z+2*
           n*L));
17 end
18
19 % expression for inhomogeneities
20 T_inh_sw_G = -C/B + T_ic_sw_G(C/B) + T_bc_sw_G(C/B,z) + T_bc_sw_G(C/B,L-z);
21
22 % temperature calculation
23 T = T_ic_sw_G(T_0) + T_bc_sw_G(T_1,z) + T_bc_sw_G(T_2,L-z) + T_inh_sw_G;
24
25 end
```

For the solution via Green's functions in the Laplace domain, the following function is used:

```
1  function [T] = T_sw_GL(A,B,C,L,T_0,T_1,T_2,z,t,m_max,m_max_2)
2
3  % solution part for initial condition and inhomogeneity
4  T_ic_sw_GL = 0;
5  T_inh_sw_GL = 0;
6  for n = 0 : m_max
7      T_ic_sw_GL = T_ic_sw_GL + T_0*4/pi*exp(-t/A*(((2*n+1)*pi/L)^2+B))*sin((2*n+1)*pi/L
           *z)/(2*n+1);
8      T_inh_sw_GL = T_inh_sw_GL -C*4/pi*(1-exp(-t/A*(((2*n+1)*pi/L)^2+B)))/(B+((2*n+1)*
           pi/L)^2 )*sin((2*n+1)*pi/L*z)/(2*n+1);
9  end
10
11 % solution part for boundary conditions
12 T_bc_sw_GL_1 = 0;
13 T_bc_sw_GL_2 = 0;
14 for n = 1 : m_max_2
15     T_bc_sw_GL_1 = T_bc_sw_GL_1 + 2/L*T_1*(1-exp(-t/A*((n*pi/L)^2+B)))*(n*pi/L*sin(n*
           pi/L*z))/((n*pi/L)^2+B);
16     T_bc_sw_GL_2 = T_bc_sw_GL_2 + 2/L*T_2*(1-exp(-t/A*((n*pi/L)^2+B)))*(n*pi/L*sin(n*
           pi/L*(L-z)))/((n*pi/L)^2+B);
17 end
18
19 % temperature calculation
20 T = T_ic_sw_GL + T_bc_sw_GL_1 + T_bc_sw_GL_2 + T_inh_sw_GL;
21
22 end
```

The approach for a general cable arrangement is shown for an arrangement of three not identical cables with constant excitations:

```
1  % temperature calculation for three not identical single wire cables
2
3  % define global parameters
```

```
4  global G_coupling C_tot R R_i R_ref T_ref r_i I nu_T epsilon T_e sigma g k T_0 T_1 T_2
       n % necessary for solution with pdepe
5
6  %% parameters
7  % geometrical and physical cable properties
8  L = 1; % cable length, in m
9  n = 3; % number of cables
10
11 % cable 1
12 n_strand_1 = 39; % number of strands of the inner conductor
13 d_strand_1 = 0.25e-3; % strand diameter, in m
14 d_i_1 = 0.8e-3; % insulation thickness, in m
15 r_i_1 = 1.7e-3; % outer insulation radius, in m
16 k_i_1 = 0.7; % correction factor for R_i
17 k_1 = 1.55; % correction factor for G
18 R_ref_1 = 7.2e-3; % electrical reference resistance at T_ref, in Ohm/m
19 T_ref_1 = 22.7; % reference temperature, in degC
20 I_1 = 30; % current that is switched on at t = 0 s, in A
21
22 % cable 2
23 n_strand_2 = 16; % number of strands of the inner conductor
24 d_strand_2 = 0.17e-3; % strand diameter, in m
25 d_i_2 = 0.65e-3; % insulation thickness, in m
26 r_i_2 = 1.1e-3; % outer insulation radius, in m
27 k_i_2 = 0.7; % correction factor for R_i
28 k_2 = 2.01; % correction factor for G
29 R_ref_2 = 39e-3; % electrical reference resistance at T_ref, in Ohm/m
30 T_ref_2 = 22.8; % reference temperature, in degC
31 I_2 = 15; % current that is switched on at t = 0 s, in A
32
33 % cable 3
34 n_strand_3 = n_strand_2; % number of strands of the inner conductor
35 d_strand_3 = d_strand_2; % strand diameter, in m
36 d_i_3 = d_i_2; % insulation thickness, in m
37 r_i_3 = r_i_2; % outer insulation radius, in m
38 k_i_3 = k_i_2; % correction factor for R_i
39 k_3 = k_2; % correction factor for G
40 R_ref_3 = R_ref_2; % electrical reference resistance at T_ref, in Ohm/m
41 T_ref_3 = T_ref_2; % reference temperature, in degC
42 I_3 = 0; % current that is switched on at t = 0 s, in A
43
44 % coupling
45 G12 = 0.13; % coupling between cable 1 and cable 2
46 G23 = 0.17; % coupling between cable 2 and cable 3
47 G13 = G12; % coupling between cable 1 and cable 3
48
49 % parameters for all cables
50 nu_T = 3.93e-3; % linear temperature coefficient of conductor, in 1/K
51 epsilon = 0.95; % emissivity of cable surface
52
53 c_c = 3.4e6; % specific heat capacitance of conductor, in J/m^3K
54 c_i = 2.2450e6; % specific heat capacitance of insulation, in J/m^3K
55
56 lambda_c = 386; % thermal conductivity of conductor, in W/(m*K)
57 lambda_i = 0.21; % thermal conductivity of insulation, in W/(m*K)
58
```

```
% define time and spatial points for analytical calculations
z = linspace(0,L,11); % z for analytical calculations, in m
t_end = 1e3; % last calculated time, in s
t = linspace(0,t_end,11); % t for analytical calculations, in s

% define time and spatial points for numerical calculations
Delta_z_num = L/10; % Delta z for numerical calculations, in m
z_num = 0:Delta_z_num:L; % z for numerical calculations, in m
Delta_t_num = 100; % Delta t for numerical calculations, in s
t_num = 0:Delta_t_num:round(t_end); % t for numerical calculations, in s

% envirionmental, initial and termination temperatures
T_e = 25; % environmental temperature, in degC
T_0 = 25*[1; 1; 1]; % initial conductor temperatures for all z for all cables, in degC
T_1 = 10*[1; 1; 1]; % conductor temperatures at z = 0 m for all times for all cables,
    in degC
T_2 = 50*[1; 1; 1]; % conductor temperatures at z = L for all times for all cables, in
     degC

% termination condition
Delta_Tlim = 0.001; % termination condition, if temperatures from two iterations
    deviate by less than this value, iteration is stopped, in K

% number of addends for Geen's functions solutions
m_max = 10; % number of addends for Green's functions solution (Laplace domain), for
    initial value and inhomogeneity
m_max_2 = 500; % number of addends for Green's functions solution (Laplace domain),
    for termination conditions

%% constants
sigma = 5.67040e-8; % Stefan-Boltzmann constant, in W/(m^2K^4)
g = 9.81; % graviational acceleration, in m/s^2

%% precalculations
% change first and last z, if at cable termination
if z(1) == 0
    z(1) = z(1) + 5e-3; % to avoid unsteady behavior at boundary
end
if z(end) == L
    z(end) = z(end) - 5e-3; % to avoid unsteady behavior at boundary
end

% combine cable parameters to vectors
n_strand = [n_strand_1;n_strand_2;n_strand_3]; % number of strands of the inner
    conductor
d_strand = [d_strand_1;d_strand_2;d_strand_3]; % strand diameter, in m
d_i = [d_i_1;d_i_2;d_i_3]; % insulation thickness, in m
r_i = [r_i_1;r_i_2;r_i_3]; % outer insulation radius, in m
k_i = [k_i_1;k_i_2;k_i_3]; % correction factor for R_i
k = [k_1;k_2;k_3]; % correction factor for G
R_ref = [R_ref_1;R_ref_2;R_ref_3]; % electrical reference resistance at T_ref, in Ohm/
    m
T_ref = [T_ref_1;T_ref_2;T_ref_3]; % reference temperature, in degC
I = [I_1;I_2;I_3]; % current that is switched on at t = 0 s, in A

% matrix for coupling
```

```
108 G_coupling = [0, G12, G13; G12, 0, G23; G13, G23, 0];
109
110 % effective and geometrical conductor radius
111 r_ceff = sqrt(n_strand).*d_strand/2; % effective conductor radius, in m
112 r_cgeom = r_i-d_i; % geometrical conductor radius, in m
113
114 % calculation heat capacitance
115 C_c = c_c*pi*r_ceff.^2; % heat capacitance of conductor
116 C_i = c_i*pi*(r_i.^2-r_cgeom.^2); % heat capacitance of insulation
117 C_tot = C_i + C_c; % total cable heat capacitance
118
119 % characteristic cable length
120 l_alpha = 2*r_i;
121
122 % resistance for heat conduction through insulation
123 R_i = k_i.*log(r_i./r_cgeom)/(2*pi*lambda_i);
124
125 % resistance for axial heat conduction in conductor
126 R = 1./(lambda_c*pi*r_ceff.^2);
127
128 % initialization
129 R_alpha_initial = 3.5; % initial value for R_alpha
130
131 % output
132 disp('Precalculations done.');
133
134 %% iterative temperature calculation
135 tic % for time measurement
136
137 T = zeros(numel(z), numel(t), n); % initialization cable temperature
138 for ii = 1 : n
139     T(:,1,ii) = T_0(ii)*ones(size(T(:,1,ii))); % use initial cable temperature for t =
          0 s
140 end
141
142 A = diag(R.*C_tot); % parameter of the PDE
143
144 T_guess = T_e*ones(n,1); % initialization value for cable temperature
145
146 for idx_z = 1 : numel(z)
147     z_loc = z(idx_z); % local position
148     % termination conditions, no calculation necessary:
149     if z(idx_z) == 0
150         for ii = 1 : n
151             T(idx_z,:) = T_1(ii)*ones(1,numel(t),ii);
152         end
153         continue
154     elseif z(idx_z) == L
155         for ii = 1 : n
156             T(idx_z,:) = T_2(ii)*ones(1,numel(t),ii);
157         end
158         continue
159     end
160     for idx_t = 2 : numel(t) % start with second time step, first one is t = 0 s (
          initial cable temperature)
161         t_loc = t(idx_t); % local time
```

```
        % initializations
        T_ = zeros(n,1);
        R_alpha = R_alpha_initial;
        counter_loop_it = 0; % counter for loop for iterations
        T_last = -100*ones(n,1);
        % iteration for temperature calcualation
        while (counter_loop_it < 100 && sum(abs(T_last-T_))>Delta_Tlim) % termination
            condition
            counter_loop_it = counter_loop_it + 1;
            if counter_loop_it > 1
                T_last = T_; % update temperature
            else
                T_last = T_guess; % initialization temperature
            end
            % electrical losses
            P_el = I.^2.*R_ref.*(1+nu_T*(T_last - T_ref)); % electrical losses =
                thermal power

            % surface temperature
            T_s = T_last-R_i./(R_i+R_alpha).*(T_last-T_e); % surface temperature

            % 4th order polynomials for parameters
            T_m = 0.5*(T_s+T_e); % mean temperature between surface and environement
            v_air = 1.77e-17*T_m.^4-4.83e-14*T_m.^3+1.14e-10*T_m.^2+8.81e-8*T_m+1.35e
                -5; % kinematic viscosity of the air, in m^2/s
            Pr = 2.23e-13*T_m.^4-6.27e-10*T_m.^3+5.91e-7*T_m.^2-1.58e-4*T_m+0.711; %
                Prandtl number
            lambda_air = -1.35e-14*T_m.^4+3.64e-11*T_m.^3-4.33e-8*T_m.^2+7.7e-5*T_m
                +2.43e-2; % thermal conductivity of the air, in W/(m*K)

            % temperatures in Kelvin
            T_sK = T_s+273.15; % surface temperature in Kelvin
            T_eK = T_e+273.15; % environmental temperature in Kelvin

            % calculation of R_alpha
            alpha_rad = epsilon * sigma * (T_sK.^2+T_eK^2).*(T_sK+T_eK); % heat
                transfer coefficient for radiation
            Gr = g*l_alpha.^3.*abs(T_s-T_e)./(T_eK.*v_air.^2); % Grashof number
            Ra = Gr.*Pr; % Rayleigh number
            Nu = (0.6+0.387*Ra.^(1/6)./((1+(0.559./Pr).^(9/16)).^(8/27))).^2; %
                Nusselt number
            alpha_conv = Nu.*lambda_air./l_alpha; % heat transfer coefficient for
                convection
            R_alpha = 1./((alpha_conv + alpha_rad)*2*pi.*r_i); % resistance for
                convection and radiation

            % coupling between conductor and environment
            G = diag(1./(k.*(R_i+R_alpha))+sum(G_coupling,2))-G_coupling; %
                conductance for coupling between conductor and environment

            % PDE parameters
            B = diag(R)*G;
            C = -diag(R)*(T_e./(k.*(R_i+R_alpha))+P_el);

            % temperature calculation
            T_ = T_gen_GL(A, B, C, n, L, T_0, T_1, T_2, z_loc, t_loc, m_max, m_max_2);
```

```
                % solution with Green's function in Laplace domain
        end
        T(idx_z,idx_t,:) = T_; % write calculated temperature to variable
    end
end
time = toc; % measure time
disp(['Analytical calculation done (' num2str(time) ' s).']) % print time

%% numerical temperature calculation with pdepe
tic % for time measurement
m = 0;
sol = pdepe(m,@pde,@pdeic,@pdebc,z_num,t_num);
for ii = 1 : n
    T_pdepe(:,:,ii) = transpose(sol(:,:,ii));
end
time = toc; % measure time
disp(['Numerical calculation done (' num2str(time) ' s).']) % print time

%% local functions for pdepe
function [c_e,f,s] = pde(~,~,u,dudz) % pde(z,t,u,dudz)
global G_coupling C_tot R R_i R_ref T_ref r_i I nu_T epsilon T_e sigma g k n

% characteristic cable length
l_alpha = @(no) 2*r_i(no);

% electrical losses
P_el = @(no, T) —I(no)^2*R_ref(no)*(1+nu_T*(T — T_ref(no)));

% 4th order polynomials for parameters
v_air = @(T_s) 1.77e—17*(0.5*(T_s + T_e))^4—4.83e—14*(0.5*(T_s + T_e))^3+1.14e
    —10*(0.5*(T_s + T_e))^2+8.81e—8*(0.5*(T_s + T_e))+1.35e—5; % kinematic viscosity
    of the air, in m^2/s
Pr = @(T_s) 2.23e—13*(0.5*(T_s + T_e))^4—6.27e—10*(0.5*(T_s + T_e))^3+5.91e—7*(0.5*(
    T_s + T_e))^2—1.58e—4*(0.5*(T_s + T_e))+0.711; % Prandtl number
lambda_air = @(T_s) —1.35e—14*(0.5*(T_s + T_e))^4+3.64e—11*(0.5*(T_s + T_e))^3—4.33e
    —8*(0.5*(T_s + T_e))^2+7.7e—5*(0.5*(T_s + T_e))+2.43e—2; % thermal conductivity of
     the air, in W/(m*K)

% temperature in Kelvin
T_eK = T_e+273.15; % environmental temperature in Kelvin

% calculation of R_alpha
alpha_rad = @(T_s) epsilon * sigma * ((T_s + 273.15)^2+T_eK^2)*(T_s + 273.15+T_eK); %
    heat transfer coefficient for radiation
Gr = @(T_s, no) g*l_alpha(no)^3*abs(T_s—T_e)/(T_eK*v_air(T_s)^2); % Grashof number
Ra = @(T_s, no) Gr(T_s, no)*Pr(T_s); % Rayleigh number
Nu = @(T_s, no) (0.6+0.387*Ra(T_s,no)^(1/6)/((1+(0.559./Pr(T_s))^(9/16))^(8/27))).^2;
    % Nusselt number
alpha_conv = @(T_s, no) Nu(T_s, no)*lambda_air(T_s)/l_alpha(no); % heat transfer
    coefficient for convection
R_alpha = @(T_s, no) 1./((alpha_conv(T_s, no) + alpha_rad(T_s))*2*pi*r_i(no)); %
    resistance for convection and radiation

% coupling between conductor and environment
G = @(T_s, no) 1./(k(no).*(R_i(no)+R_alpha(T_s, no))); % conductance for coupling
    between conductor and environment
```

```
253
254 % code equations
255 c_e = [R.*C_tot;zeros(n,1)];
256 f = [ones(n,1);zeros(n,1)] .* dudz;
257 s = zeros(2*n,1);
258 for ii = 1 : n
259     s(ii) = R(ii)*(T_e*G(u(n+ii),ii)-P_el(ii,u(ii)));
260     for jj = 1 : n
261         if ii ~= jj
262             s(ii) = s(ii) + R(ii)*G_coupling(ii,jj)*u(jj);
263         else
264             G_ij = G(u(n+ii),ii)+sum(G_coupling(ii,:));
265             s(ii) = s(ii) - R(ii)*G_ij*u(jj);
266         end
267     end
268 end
269 for ii = n+1 : 2*n
270     s(ii) = u(ii-n)-u(ii)-k(ii-n)*R_i(ii-n)*(u(ii)-T_e)*G(u(ii),ii-n);
271 end
272 end
273
274 function u0 = pdeic(~) % pdeic(z)
275 % code initial condition
276 global T_0 n
277 u0 = zeros(n,1);
278 for ii = 1 : n
279     u0(ii) = T_0(ii);
280     u0(n+ii) = T_0(ii);
281 end
282 end
283
284 function [pl,ql,pr,qr] = pdebc(~,ul,~,ur,~) %pdebc(zl,ul,zr,ur,t)
285 global T_1 T_2 n
286 % code boundary condition
287 pl = ul;
288 for ii = 1 : n
289     pl(ii) = pl(ii)-T_1(ii);
290     pl(n+ii) = pl(n+ii)-T_1(ii);
291 end
292 ql = zeros(2*n,1);
293 pr = ur;
294 for ii = 1 : n
295     pr(ii) = pr(ii)-T_2(ii);
296     pr(n+ii) = pr(n+ii)-T_2(ii);
297 end
298 qr = zeros(2*n,1);
299 end
```

For the temperature calculation with the solution via Green's functions in the Laplace domain, the following function is used:

```
1 function [T] = T_gen_GL(A,B,C,n,L,T_0,T_1,T_2,z,t,m_max,m_max_2)
2
3 % solution part for initial condition and inhomogeneity
4 T_ic_GL = zeros(n,1);
5 T_inh_GL = zeros(n,1);
```

```
for m = 0 : m_max
    Lambda = -inv(A)*(B+(((2*m+1)*pi)/L)^2*eye(n));
    [v_i,D_i] = eig(Lambda);
    % part for initial conditions
    rs_ic = T_0;
    b_1_ic = v_i\rs_ic;
    x_1_ic = v_i*diag(exp(diag(D_i)*t))*b_1_ic;
    T_ic_GL = T_ic_GL + 4/pi*sin((2*m+1)*pi*z/L)/(2*m+1)*x_1_ic;
    % part for inhomogeneity
    rs_inh = inv(B+(((2*m+1)*pi)/L)^2*eye(n))*C;
    b_1_inh = v_i\rs_inh;
    x_1_inh = -inv(B+(((2*m+1)*pi)/L)^2*eye(n))*C + v_i*diag(exp(diag(D_i)*t))*b_1_inh
        ;
    T_inh_GL = T_inh_GL + 4/pi*sin((2*m+1)*pi*z/L)/(2*m+1)*x_1_inh;
end

% solution part for boundary conditions
T_bc_GL_T1 = zeros(n,1);
T_bc_GL_T2 = zeros(n,1);
if sum(abs(T_1)+abs(T_2)) ~= 0
    if m_max_2 > 0
        for m = 1 : m_max_2
            Gamma = -inv(A)*(B+((m*pi)/L)^2*eye(n));
            [v_i,D_i] = eig(Gamma);
            % boundary 1
            rs_T1 = -inv(B+((m*pi)/L)^2*eye(n))*T_1;
            b_2_T1 = v_i\rs_T1;
            x_2_T1 = inv(B+((m*pi)/L)^2*eye(n))*T_1 + v_i*diag(exp(diag(D_i)*t))*
                b_2_T1;
            T_bc_GL_T1 = T_bc_GL_T1 + 2*m*pi/L^2*sin(m*pi*z/L)*x_2_T1;
            % boundary 2
            rs_T2 = -inv(B+((m*pi)/L)^2*eye(n))*T_2;
            b_2_T2 = v_i\rs_T2;
            x_2_T2 = inv(B+((m*pi)/L)^2*eye(n))*T_2 + v_i*diag(exp(diag(D_i)*t))*
                b_2_T2;
            T_bc_GL_T2 = T_bc_GL_T2 + 2*m*pi/L^2*sin(m*pi*(L-z)/L)*x_2_T2;
        end
    end
end

% temperature calculation
T = T_ic_GL + T_bc_GL_T1 + T_bc_GL_T2 + T_inh_GL;

end
```

D Validation and Application

D.1 Cable Parameters and Load Cases

In this section, an overview of the cable data of the cables chosen for validation is given.

Table D.1: Cable parameters for flexible single wire cables with copper conductors and PVC insulation.

cable	n_{strand}	d_{strand}	d_{i}	r_{i}	R'_{ref}	T_{ref}
①	19	0.16	0.35	0.75	39	26.5
②	16	0.17	0.65	1.1	39	22.8
③	30	0.25	0.7	1.7	13	24.9
④	39	0.25	0.9	1.7	8.6	21.8
⑤	39	0.25	0.8	1.7	7.2	22.7

n_{strand}: number of strands
d_{strand}: strand diameter in mm
d_{i}: thickness of insulation in mm
r_{i}: outer diameter with insulation mm
R'_{ref}: resistance at T_{ref} in $\frac{\mathrm{m\Omega}}{\mathrm{m}}$

Table D.2: Load cases for the evaluation of the reproducibility of the indirect temperature measurement. Cable 1 (current I_1) is measured.

load case	1	2	3	4	5	6	7	8	9
I_1 in A	10	7.5	5	0	0	0	10	7.5	5
I_2 in A	0	0	0	10	7.5	5	10	7.5	5

Table D.3: Cable parameters for single wire cables with solid copper conductors and PVC insulation.

$\mathcal{A}_{\mathrm{c}}$	0.35	0.5	0.75	1	1.5	2.5	4	6
r_{i}	1.2	1.4	1.7	1.9	2.2	2.6	3.4	4
R'_{ref}	52	37.1	24.7	18.5	12.7	7.6	4.7	3.1
$\mathcal{A}_{\mathrm{c}}$	10	16	25	35	50	70	95	120
r_{i}	5.4	8.3	10.2	11.5	13.5	16	18	20.3
R'_{ref}	1.82	1.16	0.743	0.527	0.368	0.259	0.196	0.153

$\mathcal{A}_{\mathrm{c}}$: conductor cross-section area in mm^2
r_{i}: outer diameter with insulation mm
R'_{ref}: resistance at $T_{\mathrm{ref}} = 20\,^{\circ}\mathrm{C}$ in $\frac{\mathrm{m\Omega}}{\mathrm{m}}$

Table D.4: Cable parameters for the validation of the solution for a coaxial cable.

	n_{strand}	d_{strand}	d_{i}	r_{i}	R'_{ref}	T_{ref}
conductor, insulation	19	$0.18\,\mathrm{mm}$	$1\,\mathrm{mm}$	$1.5\,\mathrm{mm}$	$35\,\mathrm{m\Omega/m}$	$23.1\,^{\circ}\mathrm{C}$
shield, coating	111	$0.1\,\mathrm{mm}$	$0.8\,\mathrm{mm}$	$2.5\,\mathrm{mm}$	$16\,\mathrm{m\Omega/m}$	$23\,^{\circ}\mathrm{C}$
$\mathcal{L}$	$d_{\mathrm{vo,c}}$	$d_{\mathrm{vo,sh}}$				
$2.44\,\mathrm{m}$	$58\,\mathrm{cm}$	$61\,\mathrm{cm}$				

$\mathcal{L}$: total cable length
$d_{\mathrm{vo,c}}$: distance of voltage connections (inner conductor) from cable ends
$d_{\mathrm{vo,sh}}$: distance of voltage connections (shield) from cable ends

Table D.5: Parameters of the chosen $0.14\,\mathrm{mm}^2$ copper cable.

$r_{\mathrm{c,eff}}$ in mm	$r_{\mathrm{c,geom}}$ in mm	r_{i} in mm	k_{i}	R'_{ref} in $\mathrm{m\Omega/m}$	T_{ref} in $^{\circ}\mathrm{C}$
0.21	0.22	0.65	0.7	116	24.1

Table D.6: Geometrical parameters of the analyzed twisted pair cables.

cable	$d_{\mathrm{vo,1}}$ in cm	d_{vo} in cm	$d_{\mathrm{vo,2}}$ in cm	turns per length in turns/cm
loosely twisted	28.5	98.5	30	0.24
tightly twisted	26	88.5	27	1.40

$d_{\mathrm{vo,1}}$: distance of first voltage connection from first cable end (after twisting)
d_{vo}: distance between voltage connections (after twisting)
$d_{\mathrm{vo,2}}$: distance of second voltage connection from second cable end (after twisting)

D.2 33 Wire Example

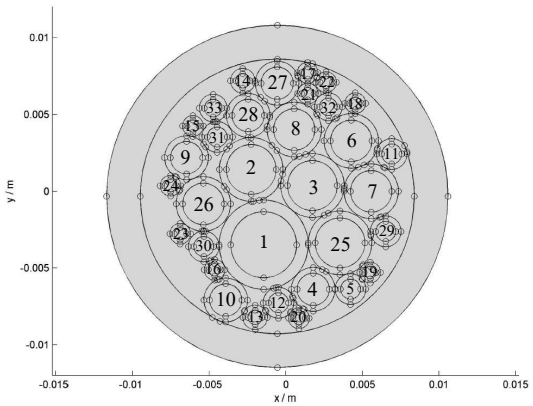

Figure D.1: Estimated conductor arrangement in the bundle. This figure is taken from [2] and has only been extended by the cable numbers.

Table D.7: Positioning of coupling conductances.

cable	1	2	3	4	5	6	7	8	9	10	11	12	13	14	15	16	17	18	19	20	21	22	23	24	25	26	27	28	29	30	31	32	33	sheath
1		G'_1	G'_1	G'_1						G'_1		G'_1				G'_1									G'_1	G'_1				G'_1				
2	G'_1		G'_1					G'_1																		G'_1		G'_1			G'_1			
3	G'_1	G'_1				G'_1	G'_1	G'_1																	G'_1									
4	G'_1				G'_1							G'_1								G'_1					G'_1									G'_3
5				G'_1															G'_1						G'_1									G'_3
6			G'_1				G'_1	G'_1			G'_1							G'_1													G'_1			G'_3
7			G'_1			G'_1					G'_1								G'_1									G'_1						G'_3
8		G'_1	G'_1			G'_1															G'_1						G'_1	G'_1			G'_1			
9															G'_1									G'_1		G'_1					G'_1			G'_3
10	G'_1												G'_1			G'_1																		G'_2
11						G'_1	G'_1						G'_1																						G'_2
12	G'_1			G'_1									G'_1							G'_1														G'_3
13										G'_1		G'_1															G'_1	G'_1						G'_3
14																															G'_1		G'_1	G'_3
15									G'_1																						G'_1		G'_1	G'_3
16	G'_1									G'_1																				G'_1				G'_3
17																					G'_1	G'_1					G'_1							G'_2
18						G'_1																										G'_1		G'_3
19					G'_1		G'_1																		G'_1									G'_3
20				G'_1								G'_1																						G'_3
21								G'_1									G'_1					G'_1					G'_1				G'_1		G'_2
22																	G'_1				G'_1										G'_1		
23									G'_1																	G'_1				G'_1				G'_3
24									G'_1																	G'_1								
25	G'_1		G'_1	G'_1	G'_1														G'_1										G'_1					G'_3
26	G'_1	G'_1							G'_1														G'_1							G'_1				G'_3
27								G'_1					G'_1				G'_1				G'_1							G'_1					G'_2
28		G'_1						G'_1					G'_1													G'_1					G'_1	G'_1		
29							G'_1																	G'_1										G'_3
30	G'_1															G'_1							G'_1		G'_1									G'_3
31		G'_1							G'_1					G'_1	G'_1												G'_1						G'_1		
32						G'_1		G'_1										G'_1			G'_1	G'_1					G'_1							
33														G'_1	G'_1															G'_1				G'_3
sheath				G'_3	G'_3	G'_3	G'_3		G'_3	G'_2	G'_2	G'_3	G'_3	G'_3	G'_3	G'_3	G'_2	G'_3	G'_3	G'_3	G'_2		G'_3		G'_3	G'_3	G'_2		G'_3	G'_3			G'_3		

E Spatial and Time Characteristic Cable Quantities

In some cases, measuring the temperature distribution of a cable is challenging. For example, particularly large cables are often difficult to handle, as very long sections and a correspondingly large measurement environment with controlled ambient conditions are required. In addition, large conductor cross-sections are associated with smaller resistances, so indirect temperature measurement also has to be performed over comparatively long cable sections to keep measurement inaccuracies within acceptable limits. Another disadvantage is that large solid cables only slowly heat up, which means that measurements have to be carried out over a long time.

Difficulties can also arise with cables with particularly small cross-sections. Here, the length-related conductor resistance is higher and the cables heat up more quickly, but they are particularly vulnerable to fluctuations in ambient conditions. Also, the cable temperature changes due to contacted measurement equipment (for example a thermocouple) gain importance.

So, for cables with particularly small or particularly large copper cross-sections, measurements can be challenging. Therefore, in this section, it is investigated whether the temperature development of cables can be approximated from the known curves for other cables using a rescaling approach and characteristic quantities to describe the cables.

E.1 Axial Steady State

For large conductor cross-sections, the influence of the cable terminations on the cable temperature lasts over a longer distance. This behavior is now quantified. For this purpose, the single wire cables from table D.3 are considered. It is assumed that the terminations cool the cable. The current is chosen in each case in a way that the temperatures $T_{\mathrm{rs}} = 50\,^{\circ}\mathrm{C}$, $85\,^{\circ}\mathrm{C}$, $105\,^{\circ}\mathrm{C}$, and $155\,^{\circ}\mathrm{C}$ are reached for the steady state in the middle of a long cable. The coordinate z is discretized with a step size of $1\,\mathrm{mm}$. The following values are used as temperatures at the beginning of the cable: $0\,^{\circ}\mathrm{C}$, $20\,^{\circ}\mathrm{C}$, $50\,^{\circ}\mathrm{C}$, $85\,^{\circ}\mathrm{C}$. However, only combinations are used where the termination temperature is lower than the temperature T_{rs}. For the ambient temperature, the values $20\,^{\circ}\mathrm{C}$ and $85\,^{\circ}\mathrm{C}$ are used. Altogether, this results in different ambient conditions for each cable (characterized by its conductor radius). The distance $\mathcal{L}_{\mathrm{char}}$ from the cable termination is calculated at which the temperature

$$T_{\mathrm{lim},z} = T_1 + (T_{\mathrm{rs}} - T_1)\left(1 - \frac{1}{\mathrm{e}}\right) \tag{E.1}$$

is exceeded. The calculation results are presented in figure E.1(a). A linear function is fitted to these data:

$$\frac{\mathcal{L}_{\mathrm{char}}}{1\,\mathrm{m}} = a_{\mathcal{L},\mathrm{char}}\hat{r}_{\mathrm{c}} + b_{\mathcal{L},\mathrm{char}}, \quad a_{\mathcal{L},\mathrm{char}} = 38.12, \quad b_{\mathcal{L},\mathrm{char}} = 0.03788, \quad \hat{r}_{\mathrm{c}} = \frac{r_{\mathrm{c}}}{1\,\mathrm{m}}. \tag{E.2}$$

To reproduce the curvature behavior more accurately, the following fourth-order polynomial (black curve in figure E.1) can also be used as a fitting function instead:

$$\frac{\mathcal{L}_{\mathrm{char}}}{1\,\mathrm{m}} = a_{4,\mathcal{L}}\hat{r}_{\mathrm{c}}^4 + a_{3,\mathcal{L}}\hat{r}_{\mathrm{c}}^3 + a_{2,\mathcal{L}}\hat{r}_{\mathrm{c}}^2 + a_{1,\mathcal{L}}\hat{r}_{\mathrm{c}} + a_{0,\mathcal{L}}, \tag{E.3}$$

$$a_{0,\mathcal{L}} = 0.01108, a_{1,\mathcal{L}} = 80.54, a_{2,\mathcal{L}} = -1.812 \cdot 10^4, a_{3,\mathcal{L}} = 3.161 \cdot 10^6, a_{4,\mathcal{L}} = -2.049 \cdot 10^8.$$

The quantity $\mathcal{L}_{\mathrm{char}}$ is interpreted as the characteristic length for the cable, which can be used to rescale the temperature developments along the cables. As an example, two cables are compared. The steady-state temperature of the first cable is calculated normally. For the second cable, the length

$$\mathcal{L}_2 = \mathcal{L}_1 \cdot \frac{\mathcal{L}_{\mathrm{char},2}}{\mathcal{L}_{\mathrm{char},1}} \tag{E.4}$$

is chosen and the current is changed, so both cables reach the same steady-state radial temperature. Rescaling the temperature development along the second cable via

$$z_{\mathrm{plot},2} = z_2 \cdot \frac{\mathcal{L}_{\mathrm{char},1}}{\mathcal{L}_{\mathrm{char},2}} \tag{E.5}$$

leads to comparable results for both calculations. In figure E.1(b), exemplary results are presented for a $1\,\mathrm{mm}^2$ cable and a $120\,\mathrm{mm}^2$ cable using the fit from equation (E.3) (4th order polynomial). The results are in good accordance, so by introducing this characteristic length, information about the temperature profile along one cable can be approximated from the known profile of another cable.

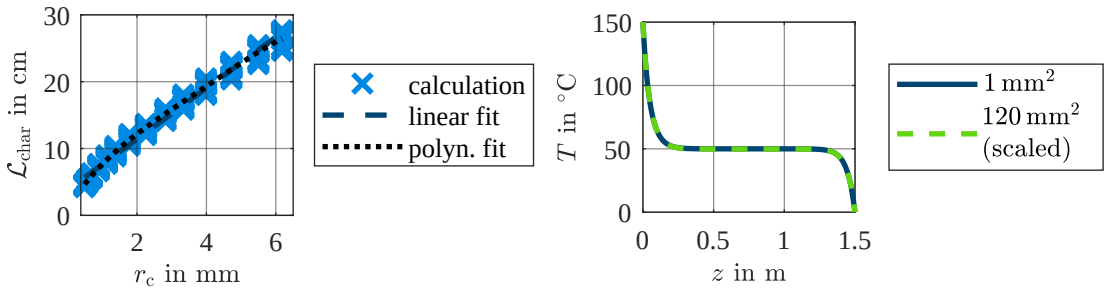

Figure E.1: (a) Characteristic cable length depending on the conductor radius. (b) Scaling with characteristic length to compare temperatures of different cables.

E.2 Radial Transient Case

For the radial transient case, a similar procedure as in the previous section is used. For long cables, the time t_{char} is searched, after which the temperature

$$T_{\mathrm{lim},t} = T_0 + (T_{\mathrm{rs}} - T_0)\left(1 - \frac{1}{\mathrm{e}}\right) \tag{E.6}$$

is exceeded assuming $T_0 < T_{\mathrm{rs}}$. The time t is discretized with a step size of $1\,\mathrm{s}$. For the ambient and radial steady-state temperatures known from the previous section and the initial temperatures $T_0 = 0\,^{\circ}\mathrm{C}$, $20\,^{\circ}\mathrm{C}$, $50\,^{\circ}\mathrm{C}$, and $85\,^{\circ}\mathrm{C}$, the results are presented in figure E.2(a). A fourth-order polynomial fit is applied:

$$\frac{t_{\mathrm{char}}}{1\,\mathrm{s}} = a_{4,t}\hat{r}_{\mathrm{c}}^4 + a_{3,t}\hat{r}_{\mathrm{c}}^3 + a_{2,t}\hat{r}_{\mathrm{c}}^2 + a_{1,t}\hat{r}_{\mathrm{c}} + a_{0,t}, \quad a_{0,t} = 55.33, \tag{E.7}$$
$$a_{1,t} = -9.025 \cdot 10^4,\ a_{2,t} = 1.546 \cdot 10^8,\ a_{3,t} = -3.177 \cdot 10^{10},\ a_{4,t} = 2.264 \cdot 10^{12}.$$

The relative deviations of the data points from the mean values

$$\Delta t_{\mathrm{rel}} = \frac{t_{\mathrm{char}} - t_{\mathrm{char,mean}}}{t_{\mathrm{char,mean}}} \tag{E.8}$$

are given in figure E.2(b). Changes of up to about $\pm 15\,\%$ for the time t_{char} occur induced by the variation of the environmental conditions. t_{char} is interpreted as the characteristic time of the cable. Again, two cables are compared. The radial temperature development of the first

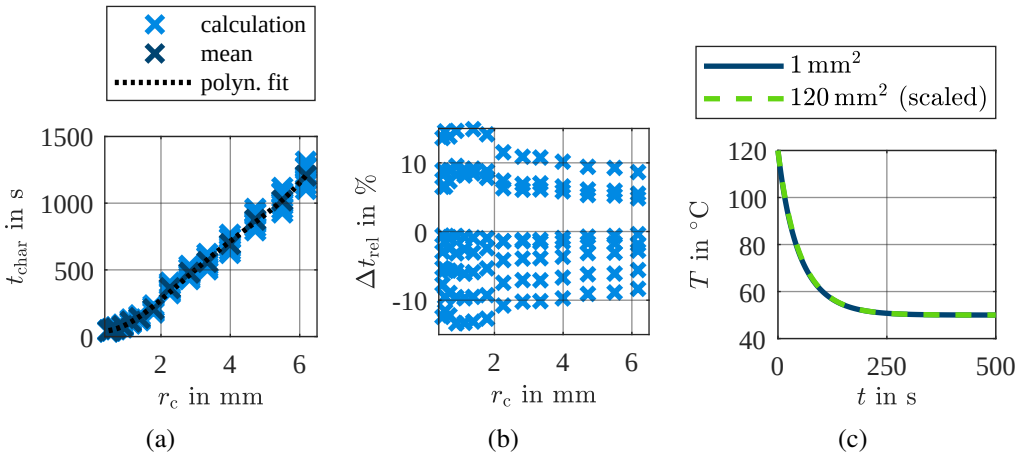

Figure E.2: (a) Characteristic time depending on the conductor radius. (b) Relative deviation between the data points and the mean value. (c) Scaling with characteristic time to compare temperatures of different cables.

cable is calculated normally. For the second cable, the end time

$$t_{\mathrm{end},2} = t_{\mathrm{end},1} \cdot \frac{t_{\mathrm{char},2}}{t_{\mathrm{char},1}} \tag{E.9}$$

is chosen and the current is selected to result in the same radial steady-state temperature as for the first cable. For plotting, the time values for the second cable are corrected again for comparability:

$$t_{\mathrm{plot},2} = t_2 \cdot \frac{t_{\mathrm{char},1}}{t_{\mathrm{char},2}}. \tag{E.10}$$

In figure E.2(c), results for a $1\,\mathrm{mm}^2$ cable and a $120\,\mathrm{mm}^2$ cable are shown exemplarily. The results agree well.

E.3 Axial Transient Case

In the general axial transient case, the results of the previous analysis are superimposed, so both the characteristic time and the characteristic length of the cable are considered. For an examplary application case (ambient temperature $25\,^{\circ}\mathrm{C}$, initial temperature $25\,^{\circ}\mathrm{C}$, left termination at $85\,^{\circ}\mathrm{C}$, right termination at $125\,^{\circ}\mathrm{C}$, radial steady-state temperature: $105\,^{\circ}\mathrm{C}$, cable 1: $1\,\mathrm{mm}^2$, current $I_1 = 22.96\,\mathrm{A}$, length $\mathcal{L}_1 = 0.4\,\mathrm{m}$, end time $t_{\mathrm{end},1} = 500\,\mathrm{s}$; cable 2: $120\,\mathrm{mm}^2$, current $I_1 = 534.52\,\mathrm{A}$), the absolute deviation between the cable temperature of the first cable and the rescaled temperature of the second cable is shown in figure E.3. Overall, there is a good agreement (deviations lower than $2.5\,\mathrm{K}$). So, a known temperature profile of one cable can be used to find a first approximation for the temperature profile along another cable.

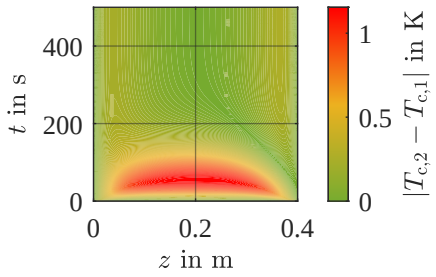

Figure E.3: Deviation between temperature for cable 1 and rescaled temperature for cable 2.